

Isomeric Olefinic Periodic Mesoporous Organosilicas: An Emerging Class of Versatile Nano-materials

Carl Vercaemst

Promotor: Prof. Dr. P. Van Der Voort
Co-promotor: Prof. Dr. F. Verpoort

Proefschrift ingediend tot het behalen van de graad van
Doctor in de Wetenschappen: Scheikunde

Vakgroep Anorganische en Fysische Chemie
Vakgroepvoorzitter: prof. dr. I. Van Driessche
Faculteit Wetenschappen
2009



Members of the Jury:

Prof. dr. A. Adriaens (Chairman)
Prof. dr. P. Van Der Voort (Promoter)
Prof. dr. F. Verpoort (Co-Promoter)
Prof. dr. Y. Khimyak
Prof. dr. ir. B. Sels
Prof. dr. J. Martins
dr. ir. A. Verberckmoes

This research was funded by the Fund for Scientific Research - Flanders (F.W.O.-Vlaanderen) and the Special Research Fund of the University of Ghent (BOF).

“What we observe is not nature itself, but nature exposed to our method of questioning.”

Werner Karl Heisenberg

Dankwoord - Acknowledgements

Hier is het dan, mijn boekske,... het resultaat van intensief onderzoek, een afsluiting van een hoofdstuk, en een begin van een nieuw. Het was een geweldige rit, één die me voor de rest van mijn leven zal bijblijven. Het was een uitdagende en vaak intense periode, maar bovenal een unieke ervaring. Dankzij de onvoorwaardelijke steun, het vertrouwen, de inzet en de vriendschap van vele mensen, sta ik hier nu... met mijn boekske. Dankbaarheid valt moeilijk onder woorden te brengen, maar ik doe alvast een poging. Hier komen jullie dankbetuigingen,... op de pagina die het meest wordt gelezen.

Het spreekt voor zich dat ik mijn eerste dankwoorden richt aan de mensen die doctoreren voor mij hebben mogelijk gemaakt. In mijn geval zijn dit twee personen, mijn twee promotoren. Professor Francis Verpoort wil ik bedanken voor het vertrouwen die hij in mij heeft gesteld. Dankzij u ben ik op “den S3” terecht gekomen, en is de bal aan het rollen gegaan. Tevens heeft u me geïntroduceerd in de boeiende wereld van katalyse en olefine metathese, waarvoor dank. Professor Pascal Van Der Voort wil ik in eerste plaats bedanken om mij te inspireren en aan te zetten om nieuwe wegen te bewandelen en “out of the box” te denken. U heeft me geïntroduceerd tot de intrigerende wereld van de nanoporeuze materialen, dank u daarvoor. Tevens wil ik u bedanken voor de team spirit die u heeft gecreëerd in de COMOC groep. Dankzij u hebben we niet enkel leren werken als individuele wetenschappers, maar ook als één team met hetzelfde doel: vooruitstrevend onderzoek verrichten. U heeft me tevens de mogelijkheid geboden om onderzoek te verrichten in een internationale omgeving. Het was een unieke ervaring om te kunnen samenwerken met verschillende universiteiten. U heeft me tevens de mogelijkheid geboden om naar buitenlandse congressen te gaan. De international zeolite conference in Beijing, de nanoporous materials symposium in Vancouver en de international mesostructured materials symposium in Namen, zullen mij altijd bijblijven. Dank u voor alles!

Er zijn een aantal mensen die een grote bijdrage hebben geleverd in dit onderzoeks werk, een aantal hiervan komen uit buitenlandse universiteiten. Daarom richt ik mij nu tot deze mensen in het Engels. I would like to thank some people who have made a large contribution to this research work, and who have helped me with the

characterization of materials and the interpretation of data. First of all I would like to thank professor Yaroslav Khimyak and his group for performing advanced NMR measurements. The obtained results have been essential in this research work and have contributed to some nice papers. I would also like to thank professor Krijn de Jong, Petra de Jongh, Heiner Friedrich and Johannes Meeldijk from the university of Utrecht for performing both TEM and ET measurements. They have also helped with the interpretation of the obtained data, and have contributed in some exciting papers. These results have had an enormous impact on this research work and have helped with the understanding of many features of the studied materials. I would especially like to thank Heiner Friedrich for the tremendous effort he has put into the characterization of our complex materials with TEM and ET. Also, thank you for the many e-mail discussions, it was a real pleasure to have worked with you. I also would like to thank professor Alex Neimark from Rutgers, the state university of New Jersey for NLDFT calculations and Bart Goderis from the catholic university of Leuven for SAXS measurements. Also thank you for the help with the interpretation of the complex data. Your work has helped me significantly and has also contributed to some fine papers.

De volgende mensen die ik wil bedanken zijn deze die mijn doctoraatsonderzoek hebben verlicht door hun aanwezigheid en vriendschap. In het bijzonder wil ik Bart, Nele en Hans bedanken. Jullie waren fantastische collega's en hebben de sfeer in het labo gemaakt. Ik heb jullie tijdens de laatste jaren van mijn doctoraat gemist, maar hoewel onze band als collega's is gebroken, heeft deze plaats gemaakt voor een mooie vriendschap! Uiteraard mag ik Fu, Jeroen, Stijn, Steven, David en Siegfried niet vergeten. Dankzij jullie was de sfeer in het labo altijd levendig.

Met het vertrek van vele goede collega's mocht ik gelukkig ook een reeks nieuwe collega's verwelkomen: Matthias, Ilke, Frederik, Els en Karen. Jullie waren een frisse wind in het labo en de leeszaal. Ik heb genoten van de coffee breaks en de leuke babbels. Jullie vormen nu het hart van de COMOC-team, ik wens jullie alvast veel succes in het verder verloop van jullie doctoraat. In het bijzonder wil ik ook Matthias bedanken. Je bent bij mij begonnen als thesis student, maar onze band is gegroeid tot collega's en intussen tot vrienden. Ik heb genoten van de vele losse babbels, tussen de worstenbroodjes en de pizza's. Bovendien wil ik je bedanken om mij de knepen van Photoshop te leren kennen. De vele illustraties die ik voor dit doctoraat heb getekend, had ik anders nooit kunnen maken,... bedankt!

Verder wil ik natuurlijk ook mijn dank betuigen aan de "vaste stoffers", Veerle, Klaartje en Jonas en alle andere collega's die ik niet persoonlijk heb vermeld. Een welverdiende dank gaat ook uit naar alle ATP'ers die hebben bijgedragen tot dit onderzoek. In het bijzonder Cindy, Danny, Pat, en Els,... dank u!

And last, but not least de mensen die mij het dichtst bij het hart liggen. Dear mom, I want to thank you for everything. You have always stimulated me to be the best at what I do. Thank you for your love and support. Valerie, zonder u was ik niet wie ik vandaag ben. Jij bent mijn inspiratie, the ying to my yang, mijn liefdevolle vrouw, mijn beste vriendin. Dank u om steeds aan mijn zijde te staan, en om mij door de moeilijke momenten heen te duwen. Bedankt om altijd in mij te geloven. Bedankt om me te blijven steunen, vooral tijdens de zware en lange laatste

maanden. Bedankt voor mijn twee kleine schatjes, mijn boellekes Mathias en Lucas. Jullie hebben mij, zonder het te beseffen, enorm geholpen tijdens de moeilijkere momenten. Het thuis komen naar jullie glimlach deed me al mijn zorgen vergeten. Jullie hebben mij geholpen om te relativeren, . . . dank u.

Preface

Porous materials appear widely in nature and are the subject of intense study in many research areas owing to their unique properties. They have been employed since ancient Egyptian times and have helped shape modern society as we know it today. Their ability to interact with atoms, ions and molecules has lead to the wide spread applicability of these materials in sorption, catalysis, separation (chromatography), ion exchange, controlled drug release, micro-electronics, environmental technology, . . .

In the field of porous materials, scientists aim to control the size, shape, uniformity and periodicity of porous space and the atoms and molecules that define it. By controlling and fine-tuning these properties, materials can be engineered to meet the desired function and behavior in a particular application.

The infatuation of researchers to design materials with uniform pore sizes and shapes has lead to superior application properties. An example illustrating the need for materials with uniform pore sizes and shapes is the widespread industrial application of zeolites as selective catalysts for various reactions. Their selectivity is based on the narrow pore size distributions, allowing only specific molecules, depending on their size and shape, to enter or leave the pores. In petrochemical processing, zeolites are used as catalysts for Fluid Catalytic Cracking, a process which transforms long-chain alkanes (crude oil) into shorter ones (petrol). For this specific industrial application it is quite clear that a wide distribution of pore sizes and shapes would limit the ability of the solid to separate molecules of various dimensions.

Although essential in many applications, the small pore apertures of zeolites make them useless in reactions involving large molecules. In a way the shape selective nature of zeolites excludes many reactions by prohibiting molecules which are larger than their pores. For this reason scientists have been keen to develop materials with uniformly sized mesopores, that is pores which exhibit diameters in the range between 2 to 50 nm.

With the discovery of a new class of aluminosilicates, designated M41S, by researchers of the Mobil Research and Development Corporation in 1992, a new era in ordered porous materials commenced. The novelty of the work described by the researchers of Mobil Oil was in the use of assemblies of ionic surfactant molecules as framework templates, instead of using single organic cationic species such as the ones used in zeolite synthesis. However, this method also comes with some limitations. A serious drawback of M41S type materials in terms of stability, is the wall thickness, which ranges between 0.8 and 1.3 nm. A second drawback of using

molecular surfactants as templates is the limited pore size of the resulting mesostructures (≈ 4 nm when no swelling agents are added). The next step in designing ordered mesostructured materials with larger pores and thicker pore walls was the implementation of more versatile supramolecular templates. Using commercially available non-ionic triblock copolymers as templates, ordered silica materials with larger mesopores (4 to 30 nm) and thicker pore walls (3 to 7 nm) can be developed, leading to materials with enhanced hydrothermal stability.

Beyond the pore space, the atoms or molecules of the structure embracing this space can be of great importance. For instance, for the effective binding or adsorption of heavy metals or organic components in environmental technological applications, the molecular composition of the porous architecture is decisive, both in terms of selectivity as capacity. It is evident that for the adsorption of hydrophobic organic molecules from waste water, a molecular sieve comprised of a hydrophobic surface will be more effective than one comprising of a hydrophilic surface, while for the adsorption of certain heavy metals the inclusion of specific organic entities with high affinity for these metals will increase both the selectivity as the capacity of the solid material.

These two material features which have been briefly discussed, being pore size and framework composition, play a central part throughout this dissertation. With the aim of developing materials with controllable chemical, physical and structural properties, which can be implemented in catalysis, environmental technology and chromatography, a relatively novel generation of mesoporous materials has been investigated: Periodic Mesoporous Organosilicas (PMOs).

PMOs are very unique in their compositional structure. The organic groups are covalently bonded within the siliceous network and hence are an intrinsic constituent of the mesoporous framework. The high loading and uniform distribution of organic groups in the pore walls of these open porous structures is a distinctive feature which allows for the easy tailoring of both the chemical and physical properties while preserving the structural stability of the porous framework.

While having a very high organic loading these materials can have very narrow pore size distributions, high specific surface areas, large pores, thick pore walls and large pore volumes. Furthermore, as the organic units are embedded in the channel walls, the pores remain completely open and fully accessible for eventual further modification of the surface functionalities.

From this perspective ethylene-bridged PMOs are very appealing, as they offer plenty of opportunities for further surface modification based on olefin chemistry. To date, only limited research has been done on these very promising type of organic-inorganic hybrid materials and their potential in various applications has not been explored yet.

The main goal of this research work is to develop a novel class of versatile olefinic PMOs, which consist of diastereoisomerically configured organic bridges in their pore walls. The aim is to investigate new synthesis strategies which enable the synthesis of highly stable hybrid materials with controllable properties. With the intent of expanding the scope of olefinic PMOs, both the synthesis of new materials and the application thereof in catalysis has been studied.

Outline

This dissertation consists of two main sections. Chapters 1 and 2 are informative, covering various aspects and developments in the field of ordered mesoporous materials. The following chapters 3 to 8 describe research and developments made during this PhD work. The results represented in chapters 3 to 7 have been published (or are in press) as peer review articles. Chapter 8 is devoted to recent research results which have not been published yet.

Chapter 1 gives a brief insight into porous materials that exhibit ordered pore structures. It describes the historical evolution from microporous zeolites to periodic mesoporous organosilicas, and reveals the reasoning behind this evolution and behind this PhD work.

Chapter 2 provides a general introduction to periodic mesoporous organosilicas. It gives a brief overview of the developments made in this relatively novel field, describing both pioneering work as well as recent discoveries. This chapter helps the reader to comprehend the presented research work and reveals the possibilities, limitations, and potential applications of periodic mesoporous organosilicas.

Chapter 3 initially gives an introduction on olefin metathesis, the reaction which is used to prepare olefinic periodic mesoporous organosilica precursors. The rest of the chapter deals with the synthesis of 1,2-bis(trimethoxysilyl)ethene and 1,4-bis(trimethoxysilyl)butene *via* the self-metathesis of vinyltrimethoxysilane and allyltrimethoxysilane, respectively. It reveals that through careful use of the right catalyst under the right reaction conditions, diastereoisomeric olefinic precursors can be developed which can be employed in the synthesis of diastereoisomeric olefinic periodic mesoporous organosilicas.

Chapter 4 surveys the synthesis of ethenylene-bridged periodic mesoporous organosilicas with different isomeric configurations. It addresses the impact of the diastereoisomeric configuration of the ethenylene-bridges in periodic mesoporous organosilica pore walls on the overall structural properties and hydrothermal stability. By means of solid-state NMR, the local structure of these materials is described. Chapter 4 also investigates the surface group accessibility and modifiability of ethenylene-bridged periodic mesoporous organosilicas.

Chapter 5 deals with the synthesis of diastereoisomeric ethenylene-bridged periodic mesoporous organosilicas with various pore structures. It addresses the complexity of both mesostructure formation and material characterization. By means of nitrogen gas physisorption, NLDFT, SAXS, TEM and electron-tomography the detailed structures of these complex periodic mesoporous organosilica materials is disclosed.

Chapter 6 focuses on synthesis strategies to control the properties of ethenylene-bridged periodic mesoporous organosilicas. The porosity of these materials can be controlled by fine-tuning the reaction conditions and by selecting adequate solvents for efficient template removal. Other than porosity, the particle morphology and the the pore size, structure, and connectivity of the described ethenylene-bridged periodic mesoporous organosilicas can be controlled. In addition, post-thermal treatment of these materials and the thermally induced generation of multifunctional periodic mesoporous organosilicas is investigated by means of DRIFT, FT-Raman and solid-state NMR spectroscopy.

Chapter 7 surveys the synthesis of ethenylene-bridged periodic mesoporous organosilicas with ultra-large mesopores. The impact of various swelling agents on the properties of these materials is described. The synthesis of periodic mesoporous organosilicas with bimodal pore size distributions is also addressed.

Chapter 8 illustrates the potential of olefinic periodic mesoporous organosilicas and reveals how the scope of these appealing materials can be expanded. A first topic which is addressed is the synthesis of butenylene-bridged periodic mesoporous organosilicas, a novel type of hybrid material. A second topic deals with the synthesis of ethenylene-bridged periodic mesoporous organosilicas under basic conditions with a gemini surfactant template. A third topic is the synthesis and application of sulfonic acid ethenylene-bridged periodic mesoporous organosilicas. A last topic is the use of periodic mesoporous organosilicas as catalysts in olefin metathesis, and illustrates how these catalysts can be prepared.

Chapter 9 summarizes the most important conclusions made throughout this thesis and gives a future outlook.

Chapter 10 gives experimental details on the synthesis procedures used in this work.

Chapter 11 provides a Dutch summary of this PhD research work.

List of Abbreviations

A

ATMS Allyltrimethoxysilane

B

BET Brunauer Emmett Teller
BJH Barrett Joyner Halenda
BTSB 1,4-bis(trimethoxysilyl)butene
BTSE 1,2-bis(triethoxysilyl)ethene

C

CBU Composite Building Unit
COD 1,5-cyclooctadiene
CP MAS Cross Polarization Magic Angle Spinning
CTAB Cetyltrimethylammonium bromide
CTAC Cetyltrimethylammonium chloride

D

DRIFT Diffuse Reflectance Infrared Fourier Transform

E

EBP-x *E*-configured ethenylene-bridged PMO, x = sample number
E-BTSE *E*-isomer of 1,2-bis(triethoxysilyl)ethene
E-EBP *E*-configured ethenylene-bridged PMO
50(*E,Z*)-BTSE diastereoisomeric mixture of 1,2-bis(triethoxysilyl)ethene,
50 % *E*- and *Z*-isomers

80(<i>E,Z</i>)-BTSE	diastereoisomeric mixture of 1,2-bis(triethoxysilyl)ethene, 80 % <i>E</i> - and 20 % <i>Z</i> -isomers
50(<i>E,Z</i>)-EBP	Ethenylene-bridged PMO consisting of both isomers, 50 % <i>E</i> - and <i>Z</i> -isomers
80(<i>E,Z</i>)-EBP	Ethenylene-bridged PMO consisting of both isomers, 80 % <i>E</i> - and 20 % <i>Z</i> -isomers
ee	Enantiomeric excess
EISA	Evaporation induced self-assembly
EO	Ethylene oxide
ET	Electron Tomography

F

FCC	Fluid Catalytic Cracking
FE-SEM	Field-Emission Electron Microscopy

H

HETCOR	Heteronuclear Correlation
HLB	Hydrophylic-Lipophylic Balance
HMDS	Hexamethyldisilazane

M

MCM	Mobil Composition of Matter
-----	-----------------------------

N

NLDFT	Nonlocal Density Functional Theory
NHC	Nitrogen-Heterocyclic Carbene
NMR	Nuclear Magnetic Resonance

O

OTAC	Octadecyltrimethylammonium chloride
------	-------------------------------------

P

PEO	Poly(ethylene oxide)
PHTS	Plugged Hexagonal Templated Silica
PILC	Pillared Interlayered Clay

PMO	Periodic Mesoporous Organosilica
PO	Propylene oxide
PPO	Poly(propylene oxide)
PSD	Pore Size Distribution

S

SAXS	Small Angle X-ray Scattering
SBA	Santa Barbara Amorphous material
SBU	Secondary Building Unit
SDA	Structure Directing Agent
SEBP-x	Sulfonated ethenylene-bridged PMO, x = sample number
SEM	Scanning Electron Microscopy
SETS	styrylethyltrimethoxysilane

T

TEM	Transmission Electron Microscopy
TEOS	Tetraethyl orthosilicate
TGA	Thermo Gravimetric Analysis
TMB	1,3,5-trimethylbenzene
TMOS	Tetramethyl orthosilicate
TON	Turn-Over Number

V

VTES	Vinyltriethoxysilane
------	----------------------

W

WISE	Wideline Separation
------	---------------------

X

XRD	X-ray Diffraction
-----	-------------------

Z

Z-BTSE	Z-isomer of 1,2-bis(triethoxysilyl)ethene
Z-EBO	Z-configured ethenylene-bridged organosilica (non-periodic)
Z-EBP	Z-configured ethenylene-bridged PMO

Table of Contents

Dankwoord	v
Preface	ix
Outline	xi
List of Abbreviations	xiii
Table of Contents	xvii
1 The Road to Periodic Mesoporous Organosilicas	1
1.1 Introduction to nanoporous materials	1
1.1.1 A brief history lesson	1
1.1.2 The importance of porous materials	2
1.2 Zeolites and Zeotypes: The Ancestors of Ordered Mesoporous Materials	3
1.2.1 What are zeolites?	3
1.2.2 Synthetic zeolites and their historical evolution	5
1.2.3 Zeolites in catalysis: The significance of their shape selective nature and their boundaries	8
1.3 Pillared Interlayered Clays	10
1.3.1 Clay minerals	10
1.3.2 Concept of Pillaring	11
1.4 M41S: The First True Ordered Mesoporous Materials	13
1.4.1 Surfactants as Framework Templates	13
1.4.2 Sol-gel Chemistry of Metal Oxides	16
1.4.3 The Mobil Hypotheses	18
1.4.4 Interactions Involved in Mesostructure Formation	20
1.4.5 The Complexity of Mesostructure Formation	22
1.5 SBA Materials: Combined Micro- and Mesoporous Solids	23
1.5.1 Introduction to SBA materials	23
1.5.2 Block copolymers as organic templates	24
1.5.3 Introducing Micropores in a Mesoporous System	29
1.6 Ordered Mesoporous Organic-Inorganic Hybrid Materials	32
1.6.1 Post-synthetic modification of siliceous materials	32
1.6.2 Functionalized silicas by the co-condensation method	34

1.6.3	Periodic Mesoporous Organosilicas	36
2	Periodic Mesoporous Organosilicas: Versatile Hybrid Materials	39
2.1	Constructing walls at a molecular level	39
2.1.1	Aliphatic Periodic Mesoporous Organosilicas	41
2.1.2	Aromatic Periodic Mesoporous Organosilicas	45
2.2	Expanding the scope of PMOs	48
2.3	Applications of PMO materials	52
2.3.1	PMOs as supports and catalysts	52
2.3.2	PMOs for chromatographic applications	54
2.3.3	PMOs as adsorbents in environmental technological applications	56
2.3.4	PMOs as biosensors	57
2.3.5	PMOs as low- <i>k</i> dielectric films	58
3	Olefinic PMO precursors: Exploring Novel Synthesis Strategies	61
3.1	Introduction to olefin metathesis	61
3.1.1	Unraveling the olefin metathesis mechanism	62
3.1.2	Olefin metathesis catalysts	63
3.2	Typical synthesis of ethene-PMO precursors	67
3.3	Diastereoisomeric ethene-PMO precursors	68
3.3.1	Synthesis of the <i>E</i> -isomer: Role of catalyst	68
3.3.2	Synthesis of the <i>Z</i> -isomer	72
3.4	Synthesis of an entirely novel olefinic PMO precursor	73
3.4.1	Preliminary investigation	73
3.4.2	Probing novel catalysts: circumventing isomerization reactions	78
3.4.3	Diastereoisomeric butenylene-bridged PMO precursor	81
3.5	Conclusions on the synthesis of olefinic PMO precursors	83
4	Ethenylene-bridged PMOs: From <i>E</i> to <i>Z</i>	85
4.1	Ethenylene-bridged PMOs with different isomeric configurations	85
4.1.1	Synthesis procedure	85
4.1.2	Nitrogen physisorption properties of PMOs	86
4.1.3	Isomeric configuration of ethenylene-bridged PMOs	88
4.2	Influence diastereoisomeric configuration on PMO structural properties	89
4.3	Understanding the local structure of ethenylene-bridged PMOs	93
4.3.1	^1H - ^{13}C CP/MAS NMR of ethenylene-bridged PMOs	93
4.3.2	Structure of PMO pore walls: an NMR investigation	94
4.3.3	Template-framework interactions	96
4.4	Hydrothermal stability of ethenylene-bridged PMOs	99
4.5	Chemical accessibility of the ethene functions: bromination	102
4.6	Conclusions on the synthesis of diastereoisomeric PMOs	103

5 Understanding Mesostructure Formation	105
5.1 Influence of pH on N ₂ -physisorption properties of ethene-PMOs	105
5.2 Investigation of PMO structures with SAXS, TEM and ET	111
5.2.1 Ethenylene-bridged PMO with open cylindrical mesopores	111
5.2.2 Ethenylene-bridged PMOs with open and confined mesopores	113
5.2.3 Ethenylene-bridged PMO with globular and blocked mesopores	115
5.2.4 The pore-blocking effect: Hypothesis	118
5.3 Conclusions on ethene-PMO structure formation	119
6 Ethenylene-bridged PMOs with Controllable Properties	121
6.1 Controlling the porosity of ethenylene-bridged PMOs	121
6.1.1 Enhancing the efficiency of template removal	121
6.1.2 Influence of synthesis pH on porosity of ethenylene-bridged PMOs	123
6.1.3 Influence of the <i>n</i> -butanol concentration on porosity of ethenylene-bridged PMOs	129
6.1.4 Role of synthesis temperature in controlling the pore size, structure, connectivity and volume	130
6.2 The role of cosolvent in controlling the morphology of ethene-PMOs	132
6.3 Thermally induced metamorphosis in ethene-PMOs	134
6.3.1 Thermal properties of ethene-PMOs	134
6.3.2 PMO metamorphism: Ethene-bridge, where art thou?	136
6.4 Conclusions on ethenylene-bridged PMOs with controllable properties	143
7 Isomeric Ethenylene-bridged PMOs with Ultra-Large Mesopores	145
7.1 Principal of pore expansion	145
7.2 Ethene-PMOs with ultra-large mesopores	146
7.2.1 Influence of TMB on mesostructure formation	146
7.2.2 Role of TMB in the self-assembly process	153
7.2.3 Bimodal ethene-PMOs with ultra-large mesopores	157
7.2.4 There is nothing so stable as change	157
7.3 Conclusions on ethene-PMOs with ultra-large mesopores	160
8 Expanding the Scope of Olefinic PMOs	163
8.1 Perspective	163
8.2 One builds too many walls and not enough bridges	164
8.2.1 The challenges	164
8.2.2 Butenylene-bridged hybrid materials: a first step	164
8.3 A place for everything, everything in its place	168
8.3.1 Gemini surfactants	168
8.3.2 Using gemini surfactants in PMO synthesis	169
8.3.3 A well-ordered system: Organizing bridges at a molecular level	174
8.4 PMOs in practice: novel solid acid catalysts	175
8.4.1 Sulfonic acid ethene-PMOs	176
8.4.2 PMOs put to the test: A model esterification reaction	178
8.5 Closing the cycle: PMO catalysts for olefin metathesis	183
8.5.1 The challenges in olefin metathesis	183
8.5.2 Ethene-PMOs with anchor points for olefin metathesis catalysts	184

8.5.3 Styrene-ethene PMOs as supports for olefin metathesis catalysts: prospect	185
8.6 Conclusions on expanding the scope of olefinic PMOs	188
9 General Conclusions and Outlook	191
9.1 Conclusions	191
9.2 Outlook	197
10 Experimental	199
10.1 General information	199
10.1.1 Chemical compounds and synthesis	199
10.1.2 Characterization techniques and procedures	199
10.2 Synthesis of ethene-PMO precursors	202
10.2.1 Classic synthesis of 1,2-bis(trimethoxysilyl)ethene (80(<i>E,Z</i>)-BTSE)	202
10.2.2 Direct synthesis of the diastereoisomerically pure <i>E</i> -isomer of 1,2-bis(trimethoxysilyl)ethene (<i>E</i> -BTSE)	202
10.2.3 Synthesis of 1,2-bis(trimethoxysilyl)ethene with catalysts 2 , 4 , 5 , and 6	202
10.2.4 Indirect synthesis of the diastereoisomerically pure <i>Z</i> -isomer of 1,2-bis(trimethoxysilyl)ethene (<i>Z</i> -BTSE)	203
10.2.5 Indirect synthesis of 1,2-bis(trimethoxysilyl)ethene with 50 % <i>E</i> - and <i>Z</i> -isomers (50(<i>E,Z</i>)-BTSE)	203
10.3 Synthesis of butene-PMO precursor	203
10.3.1 Monitoring the self-metathesis of allyltrimethoxysilane with ^1H NMR	203
10.3.2 Direct synthesis of the diastereoisomerically pure <i>E</i> -isomer of 1,4-bis(trimethoxysilyl)butene	204
10.4 Synthesis of ethylene-bridged PMOs	204
10.4.1 Synthesis of <i>E</i> -EBP, 80(<i>E,Z</i>)-EBP, 50(<i>E,Z</i>)-EBP, and <i>Z</i> -EBO204	204
10.4.2 Synthesis of <i>Z</i> -EBP	204
10.4.3 Synthesis of EBP-1 to EBP-9	205
10.4.4 Synthesis of EBP-10 to EBP-33	205
10.4.5 Synthesis of EBP-AT and EBP-PT	205
10.4.6 Hydrophobization of ethene-PMOs with HMDS	206
10.4.7 Synthesis of ultra-large pore ethene-PMOs: EBP-34 to EBP-47206	206
10.4.8 Synthesis of bimodal ethene-PMO EBP-48	206
10.4.9 Synthesis of ethene-PMOs with gemini surfactant 16-12-16: EBP-49 to EBP-62	206
10.5 Synthesis of a butenylene-bridged PMO	207
10.6 Synthesis of sulfonic acid ethene-PMOs: SEBP-42 and SEBP-63	207
10.7 Synthesis of styrylethyl-modified ethene-PMO: Styrene-Ethene-PMO	208
10.8 Syntheses without surfactants: disordered amorphous materials	208
10.8.1 Synthesis of vinylsilica	208

10.8.2 Synthesis of styrylethylsilica	208
10.9 Synthesis of SBA-15 and extraction investigation	208
10.10Bromination of ethylene-bridged PMOs	209
10.11Synthesis gemini surfactant 16-12-16	210
10.12Esterification of <i>n</i> -propanol with acetic acid	210
11 Nederlandse samenvatting	211
11.1 Inleiding	211
11.2 Ontwikkeling van diastereoisomere olefinsche PMO precursoren	212
11.2.1 Etheen-PMO precursoren	212
11.2.2 Buteen-PMO precursoren	213
11.3 Etheen-PMOs: Van <i>E</i> tot <i>Z</i>	215
11.3.1 Invloed diastereoisomere configuratie op structurele PMO eigenschappen	215
11.3.2 Templaat-PMO interacties	216
11.3.3 Hydrothermale stabiliteit	216
11.3.4 Chemische toegankelijkheid van de etheenfuncties	217
11.4 Doorgronden van mesostructuur vorming	217
11.4.1 Stikstof fysisorptie analyse	217
11.4.2 Opheldering van PMO structuren met SAXS, TEM en ET	218
11.5 PMOs met controleerbare eigenschappen	220
11.5.1 Controle van de porositeit	220
11.5.2 Controle van de externe morfologie	221
11.5.3 Thermische geïnduceerde vorming van multifunctionele PMOs	221
11.6 Etheen-PMOs met ultra-large mesoporiën	223
11.7 Olefinische PMOs: het uitbreiden van hun draagwijdte	224
11.7.1 Buteen-PMOs	224
11.7.2 Etheen-PMOs met semi-kristallijne wanden	225
11.7.3 Sulfonzure etheen-PMOs	225
11.7.4 Styreen-Etheen-PMOs: dragermaterialen voor olefine metathese katalysatoren	226
References	229
Scientific Publications	255

Chapter 1

The Road to Periodic Mesoporous Organosilicas

1.1 Introduction to nanoporous materials

1.1.1 A brief history lesson

In our daily life we are surrounded by porous materials. Sponges, cleaning tissues, disposable diapers, cat litter, filters and washing powders are just a few examples. Although porous materials are integrated in our modern day society, the importance of these materials has already been recognized since antiquity. In fact, charcoal has been applied as a folk remedy since ancient Egyptian times. Adsorption on porous charcoal was first described in an ancient Egyptian papyrus, dated 1550 B.C.¹ It was applied both for the adsorption of odorous vapours from putrefying wounds as for the purification of water. There is even an Old Testament reference (Numbers 19:9) to the ritual purification of water using the charred remains of a heifer. In those days, charcoal may have seemed to possess mystical powers. It was only until the 18th century that the adsorptive nature of charcoal was scientifically studied. The first quantitative observations were made by the Swedish chemist Carl Wilhelm Scheele, who described his work in a letter to his friend Gahn in 1773, and published his findings in a book in 1777.² Around the same period the Italian physicist Felice Fontana reported some experiments on the uptake of gases by charcoal.³ These experiments were conducted with the aid of, what later was called, an Eudiometer. Fontana found out that plunging red-hot charcoal under mercury and allowing it to rise into an inverted tube containing gas, the charcoal, upon cooling down, absorbs most of the gas, causing the mercury to rise in the tube. He also discovered that by extinguishing red-hot charcoal in a glass bell full of water, inflammable air (hydrogen) was liberated. The significance of his work, which was also translated in French by Louis Bernard Guyton de Morveau in 1783,⁴⁻⁶ is unquestionable as his methods were enthusiastically adopted by many scientists, including Joseph Priestley^{7,8} and Antoine Laurent Lavoisier⁹.



Soon after, scientists showed that charcoal not only adsorbs gases but also liquids. The first report of the adsorptive ability of charcoal in the liquid phase was that of the Russian chemist Johann Tobias Lowitz in 1786.^{10,11} A nice anecdote illustrating the effectiveness of charcoal in the adsorption of liquids is the bold demonstration of the pharmacist Pierre-Fleurus Touery. At a meeting at the French Academy of Medicine in 1831, he ingested ten times the lethal dose of strychnine with an equal amount of charcoal, and survived.¹² A similar incidence is the equally bold, yet crazy demonstration of the French chemist Michel Bertrand, who ingested 150 times the lethal dosage of arsenic trioxide (one teaspoon) and survived by immediately thereafter consuming an amount of charcoal.¹³ Risking their lives in the name of science, a good thing the poisons these scientists consumed had an affinity for carbon. The outcome would have been less heroic if they had ingested cyanide. Although the adsorptive nature of porous materials was widely studied throughout the 18th century, it was only in the 19th century that the term “adsorption” was first introduced in the literature and that scientists started to realize that porosity played a key role, although they had no means to measure this feature.¹⁴ It was the Swiss chemist Nicolas Théodore de Saussure, son of Horace-Bénédict de Saussure (the first scientist who climbed the Mont Blanc in 1787), who first came to the conclusion that the size of the exposed surface area of a solid material correlates with the volume of adsorbed gas, and that the adsorption process is accompanied by the evolution of heat.¹⁵ Later, a German chemist named Eilhardt Alfred Mistscherlich (best known for his work on isomorphism) claimed that the uptake of gas was caused by pores within the charcoal.¹⁶

Although the importance of surface area and porosity was first anticipated in the 19th century, to this date, these two features of a solid material are recognized to play a decisive role in many processes in various applications.

1.1.2 The importance of porous materials

Porosity is a measure of the void spaces (pores) in a solid material. The word pore comes from the Greek word “πόρος” (poros), which means passage. This indicates the role of a pore acting as a passage between the external and the internal surfaces of a solid, allowing material, such as gases and vapours, to pass into, through or out of the solid. The pores of porous solids are classified by the IUPAC according to their size: pore sizes in the range of 2 nm and below are called micropores, those in the range of 2 nm to 50 nm are denoted as mesopores, and those above 50 nm are referred to as macropores.

As ancient civilizations found out, porous solids are of great interest and importance due to their unique properties. Their ability to interact with atoms, ions and molecules has resulted in the wide spread applicability of these materials in sorption, catalysis, separation (chromatography), ion exchange, controlled drug release, micro-electronics, environmental technology, . . .

In the field of porous materials, scientists aim to control the size, shape, uniformity and periodicity of porous space and the atoms and molecules that define it. By controlling and fine-tuning these properties, materials can be engineered to meet the desired function and behavior in a particular application.

The infatuation of researchers to design materials with uniform pore sizes and

shapes has lead to superior application properties. An example illustrating the need for materials with uniform pore sizes and shapes is the widespread industrial application of zeolites as selective catalysts for various reactions. Their selectivity is based on the narrow pore size distributions, allowing only specific molecules, depending on their size and shape, to enter the pores (educt selectivity) or to leave the pores (product selectivity). In petrochemical processing, zeolites are used as catalysts for Fluid Catalytic Cracking (FCC process), a process which transforms long-chain alkanes (crude oil) into shorter ones (petrol). They are also used to enhance the octane number of the petrol by producing branched species. For this specific industrial application it is quite clear that a wide distribution of pore sizes and shapes would limit the ability of the solid to separate molecules of various dimensions.

Beyond the pore space, the atoms or molecules of the structure embracing this space can be of great importance. For instance, for the effective binding or adsorption of heavy metals or organic components in environmental technological applications, the molecular composition of the porous architecture is decisive, both in terms of selectivity as capacity. It is evident that for the adsorption of hydrophobic organic molecules from waste water, a molecular sieve comprising of a hydrophobic surface will be more effective than one comprising of a hydrophilic surface, while for the adsorption of certain heavy metals the inclusion of specific organic entities with high affinity for these metals will increase both the selectivity as the capacity of the solid material.

Probably the most important application where both the void space as the molecular constitution of porous materials is of vital importance is catalysis. Dependent on the catalytic reaction, the pore size and shape will determine the reaction selectivity and yield, while the functionalities comprised in the material (catalytic sites) will determine the catalyst activity. The research work presented in this thesis is focused on the development of novel mesoporous materials and their implementation in catalysis. Therefore, Chapter 1 gives a brief insight on ordered porous materials with the main emphasis on catalysis. Its intent is twofold, covering various porous materials and recent developments. It is informative, giving the necessary background information, but it is presented in a constructive way, leading to the reasoning behind this research work.

1.2 Zeolites and Zeotypes: The Ancestors of Ordered Mesoporous Materials

1.2.1 What are zeolites?

The term zeolite was first adopted in 1756 by the Swedish mineralogist Axel Fredrik Cronstedt, who, upon rapidly heating a natural mineral (Stilbite) in a blow-pipe flame, observed that the stones began to froth and dance about as the water evaporated; the stones appeared to boil. Using the Greek words “zeo” (to boil) and “lithos” (stone), he published a paper titled: “Observation and description of an unknown mineral species, called zeolite”.¹⁷ Today, the term zeolite is used to denote rigid crystalline hydrated aluminosilicates of natural or synthetic origin,

with the following empirical formula: $M_x^{n+}[(AlO_2)_x(SiO_2)_y] \cdot zH_2O$

Herein, M is an exchangeable cation with valency n. Zeolites are mainly distinguished according to the geometry of the cavities and channels formed by the rigid framework. The primary building unit is composed of corner-sharing, symmetrically stacked SiO_4^{4-} and AlO_4^{5-} tetrahedra, each consisting of four oxygen atoms (see Figure 1.1). The tetrahedra are linked by secondary building units (SBUs), which are generally depicted schematically as polygons. Such a polygon is generated by connecting the centers of neighboring tetrahedra with a line. Herein, each vertex represents a silicon or aluminum atom, while the midpoint of each edge represents an oxygen atom. A series of SBUs can also be combined into tertiary or composite building units (CBUs). An example of a CBU is the sodalite cage, which consists of 24 tetrahedra (see Figure 1.1). These secondary or composite building units are linked, forming an open, three-dimensional cage-like structure consisting of a complex network of cavities and interconnecting channels which are usually occupied by H_2O molecules and mobile alkali metal ions. These interchannel cations, which can be exchanged with other cations, neutralize the negative charge of the zeolite structure resulting from the aluminum content. The entrances to the zeolite cavities are formed by 6-, 8-, 10- and 12-ring apertures (small-, medium-, and large pore zeolites).

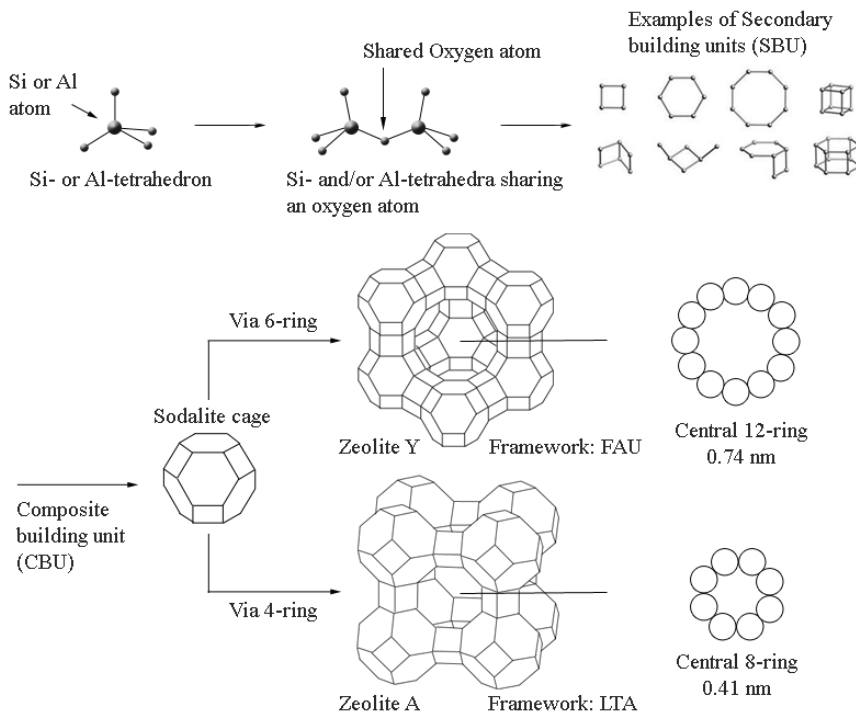


Figure 1.1: Composition of zeolites: from primary building unit to zeolite cage-like frameworks

As an example, the frameworks of zeolite Y and A are given in Figure 1.1. The

structure of the large pore zeolite Y (Faujasite) is formed when the sodalite cages are linked together by hexagonal prisms. When the sodalite cages are linked to each other by the square faces via intermediate cubic units, zeolite A is formed. Zeolites are able to both lose and gain water reversibly as exchange extraframework cations without change of the crystal structure. After thermal activation (water removal), small molecules can pass through the channels while larger molecules are excluded, giving rise to the “molecular sieving” property of zeolites.

In 2007, over 48 naturally occurring zeolites were known, and about 186 zeolite framework types had been developed (approved by the Structure Commission of the IZA).¹⁸ Natural zeolites are volcanic minerals, that came about after volcanic ash, immersed in saline water, solidified and mineralized over thousands of years. Different depositional environments during the formation of the zeolite, such as temperature, location and ash/water composition, differentiates the chemical constitution and physical structure of each unique natural zeolite. Although these low-cost natural materials are used on a large scale in low-tech applications such as agriculture, householding, environmental clean-up and construction (in fact they have been used in construction since Roman times)¹⁹, they are rarely phase-pure and are often contaminated by other minerals. For this reason these type of zeolites are excluded from many commercial applications where purity is essential. Other advantages of synthetic zeolites are: uniformity, ease of synthesis, the ability to synthesize (design) zeolites with structures which do not occur in nature and low-cost production, due to the natural abundants of the zeolite raw materials, silica and alumina.

1.2.2 Synthetic zeolites and their historical evolution

The Founding Fathers of synthetic zeolites

The first claim to a synthetic zeolite (levnrite) is that of Saint-Claire Deville in 1862.²⁰ The absence of reliable characterization methods however, made it impossible to verify his success. The scientists, who can be regarded as the “Founding Fathers” of zeolites, are Richard Maling Barrer and Robert Mitchell Milton. Inspired by McBain’s work “Sorption of gases and vapours by solids”,²¹ Richard Barrer’s interest in zeolites grew during the 1930s and early 1940s. Ultimately his infatuation with zeolites led to one of the most significant new fields of research in the 20th century. In 1948, Barrer reported the first definitive synthesis of a zeolite which had no natural counterpart.²² He used strong salt solutions under high temperatures and pressures, mimicking the conditions under which he believed zeolites are formed in nature. Of course, the one condition which could and can not be duplicated is crystallization time. His method of zeolite synthesis, using hot alkaline aqueous solutions, became known as the hydrothermal method, and it is still the main method used today. At the time, Milton was exploring sorption as a potential method for separation of gases at the Linde Division of the Union Carbide Corporation. Inspired by Barrer, who had already indicated the potential of zeolites, Milton began to explore the synthesis of zeolites in 1949. Ultimately he developed a new synthesis method which led Milton to a major breakthrough in zeolite synthesis. The use of soluble reactants in strongly basic solutions, led to the precipitation of highly reactive gels. Using these freshly precipitated aluminosilicate gels, he

enabled reactions to be carried out under milder conditions. Incredibly, using this new method, within the first year of his research, Milton discovered zeolites A, B and X, two of which (A and X), were new, and above all formed the basis of a worldwide industry in gas and liquid separation and purification in the following decades.^{23–25} By 1953, the Union Carbide Corporation developed 20 zeolites, 14 of which were unknown as natural minerals.²⁶ The following year they announced entering the business of manufacturing and selling molecular sieves as a novel class of industrial adsorbents.

Introducing templates in the zeolite synthesis

The next breakthrough in the synthesis of zeolites was once more achieved by Barrer. In 1961, he described the affect of introducing quaternary ammonium cations into zeolite synthesis.²⁷ The addition of such cationic templates led to the production of silica-rich zeolites (e.g. zeolite β), the discovery of which was only appreciated in the next decade.²⁸ The key to the increasing interest in silica-rich zeolites, was the discovery of ZSM-5 by researchers of Mobil Oil.²⁹ This zeolite exhibited a new tetrahedral framework enclosing two sets of perpendicular intersecting channels, defined by 10-membered rings (MFI framework topology). By substituting Si^{4+} for Al^{3+} in the framework, a M^+ ion is required to maintain the overall neutrality of the zeolite. When the framework is neutralized by protons, a highly acidic zeolite is obtained, giving rise to solid acid catalysts. Mobil's patented ZSM-5 is used commercially in synthetic fuels (conversion of methanol to gasoline), petroleum refining (dewaxing of distillates) and petrochemicals (xylene isomerization, toluene disproportionation).³⁰ It has been successfully employed in many FCC units worldwide as an additive to boost the octane rating of gasoline and improve light olefin yields by both isomerizing low-octane linear olefins to high-octane branched olefins and by upgrading low-octane components (C7 to C10) into light olefins (C3 to C5). Herein, the Bronsted acid sites are necessary for cracking hydrocarbons, while the shape selectivity allows preferential cracking of long-chain, low-octane normal paraffins, as well as some olefins.

Zeotypes: breaking the 12 T-ring barrier

The most important limitation of zeolites is unquestionably, their small pore apertures. Their microporous frameworks frequently cause intracrystalline diffusion limitations due to the difficult transport of reactants to the active sites in the channels, or back-diffusion of the generated products. Therefore, during the 1980s and the decades that followed, one of the main goals in the synthesis of zeolites and related crystalline materials, was the development of more open structures containing larger pores. Hereby, by improving the diffusional properties of zeolites, scientists aimed to create new applications in catalysis, adsorption and ion exchange. Up to this point, the largest rings found in the frameworks of either natural or synthetic zeolites, consisted of 12 T-atoms (T = tetrahedral).^{25,31–38} This limited applications in both catalysis and sorption, to molecules no larger than about 8.5 Å. It became clear that novel materials with greater flexibility in bond lengths and bond angles could lead to large pore zeolites. Not surprisingly,

the 1980s were characterized by the discovery of a completely new family of zeolites, the zeotypes. These novel microporous materials contain elements other than Si and Al. The first in line were the aluminophosphates (AlPO), consisting of Al and P.^{39,40} Other zeotypes discovered shortly later were, silico-aluminophosphates (SAPO)⁴¹ and metal-aluminophosphates (MeAPO)^{42–44}. The development of the aluminophosphate VPI-5 (Virginia Polytechnic Institute) in 1988, provided the first microporous material containing rings of 18 T-atoms and an average pore size of about 13 Å.^{45,46} Although these zeotype materials did lead to the first crystalline materials containing rings larger than 12 T-atoms, the increase in pore size can be considered as rather modest. For applications involving molecules larger than 11 Å, even these “large-pore” zeolite materials proved to be insufficient. Figure 1.2 compares the pore apertures of some zeolites with the kinetic molecular diameters of some molecules.

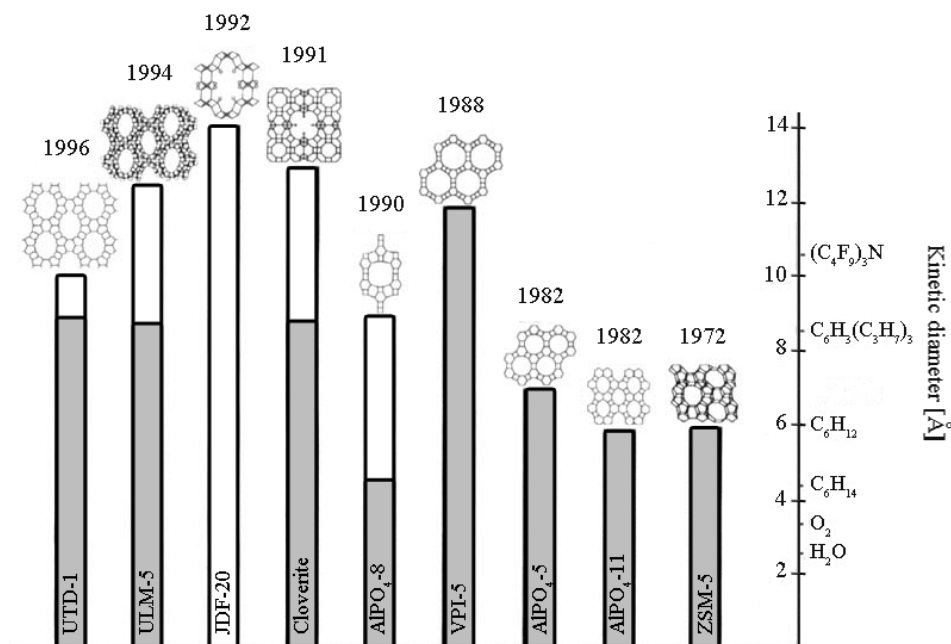


Figure 1.2: Correlation between the pore size of some zeolites and zeotypes (top of the bar) and adsorption studies (top of shaded region in each bar) and the kinetic diameter of various molecules.⁴⁷

Besides the modest pore size, the practical value of phosphate-based large pore materials is limited by their relatively poor hydrothermal and thermal stabilities, compared to those of silica-based molecular sieves.⁴⁸ In fact, concern was raised over whether the lack in stability was a direct result of the large pore size. In the mean time, the relatively poor stability of VPI-5 has been attributed to the nature of the structural units, rather than to the presence of large pores.^{47,48} Features such as mixed metal-ion coordination (such as tetrahedral and octahedral aluminum), terminal OH groups, and the presence of other non-tetrahedral

framework species (such as OH, F or H₂O) lower the framework stability relative to that of fully tetrahedrally coordinated materials such as zeolites. More direct evidence that the instability of these large pore materials is not related to their ring sizes, was provided with the discovery of the silica rich large pore aluminosilicates UTD-1 (University of Texas at Dallas)^{49–51} and CIT-5 (California Institute of Technology)^{52,53}. The hydrothermal and thermal stabilities of these crystalline silicas, containing 14-membered pore rings, are comparable to the stabilities of other zeolites consisting of smaller rings.

1.2.3 Zeolites in catalysis: The significance of their shape selective nature and their boundaries

Although the application of zeolites is often limited by their small pore apertures, they are still the most widely applied catalysts in industry. The considerable success of zeolites is partly due to their shape selectivity. Their ability to accommodate only molecules of a particular shape and size within the pores of their framework has led to significant progress in numerous applications. The shape selectivity of zeolites is a result of the very uniform and regular pores present in their structure. Access to the pores is controlled by the size of the apertures of the zeolite channels, which themselves depend on the zeolite structure considered. Zeolites also have the ability to confine high concentrations of molecules in the restricted pore space of their structure. This property can be applied both in adsorption as catalysis. The shape selectivity of zeolites may arise in three ways: reactant selectivity, product selectivity and transition state selectivity. A schematic representation of these different types of shape selectivity is depicted in Figure 1.3.

Reactant selectivity

Reactant selectivity arises from the ability of only certain molecules to enter the zeolite cavities and undergo reaction at the catalytically active sites. An important commercial process that exploits this type of selectivity is catalytic dewaxing. Compared to the branched isomers, the straight chain alkanes have low octane numbers and contribute to wax formation in diesel fuel. By applying shape selective zeolites, the dewaxing of the diesel fuel is promoted by removing the alkanes with low octane numbers.

Product selectivity

Product selectivity occurs when, among all the product species formed within the pores of the zeolite, only those with certain dimensions can diffuse out of the pores. This way, bulky products are either converted to less bulky molecules or eventually deactivate the catalyst by blocking the pores. Well known examples of product selectivity are the methylation and disproportionation of toluene on ZSM-5. In both reactions the three isomers *o*-, *m*- and *p*-xylene are formed. Although the thermodynamic equilibrium to the desired product *p*-xylene is only 24 %, this isomer can be obtained with a selectivity of over 90 %. Because *p*-xylene is slimmer than the other isomers, its rate of diffusion is faster by a factor 10000.

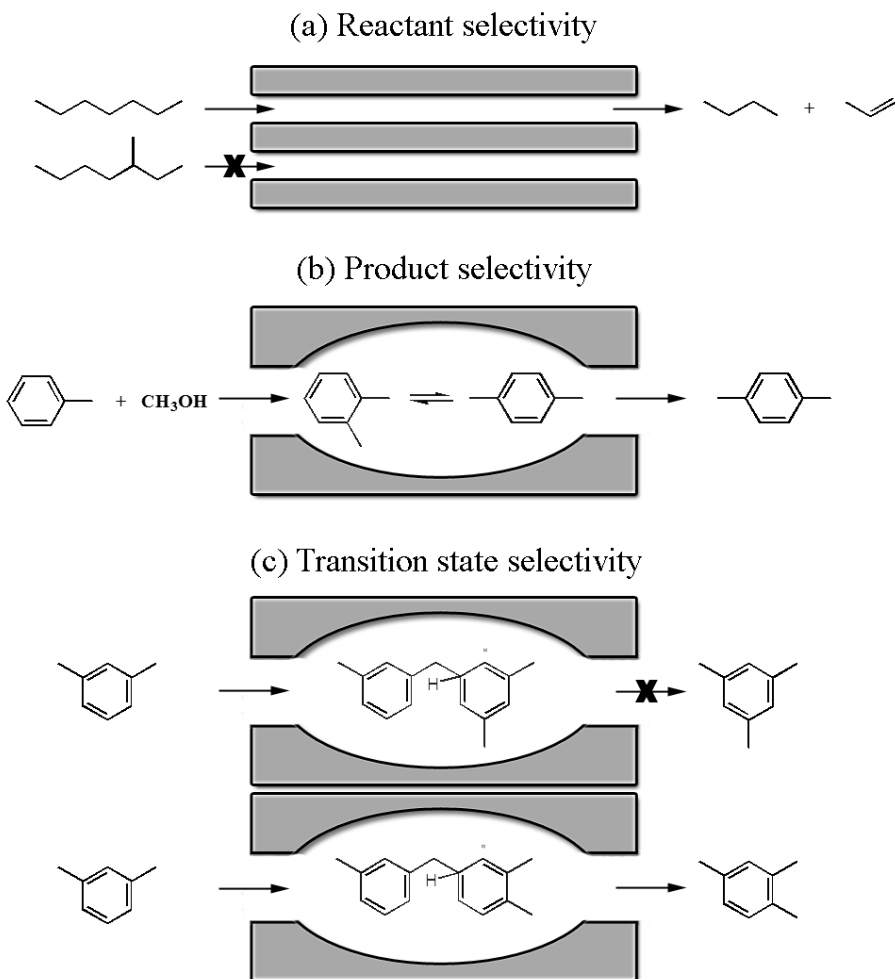


Figure 1.3: Shape selectivity of zeolites. (a) Reactant selectivity: cleavage of linear hydrocarbons, (b) Product selectivity: methylation of toluene, (c) Transition state selectivity: disproportionation of *m*-xylene.

Transition state selectivity

Restricted transition-state selectivity takes place when certain reactions are prevented because the corresponding transition state would require more space than available in the cavities. An example is the disproportionation of *m*-xylene to toluene and trimethylbenzenes in zeolite Y. In the large zeolite cavity, bulky diphenylmethane carbenium ion transition states can be formed as precursors for methyl group rearrangement, whereby the less bulky carbenium ion is favored. Thus the reaction product consists mainly of the unsymmetrical 1,2,4-trimethylbenzene rather than mesitylene. In contrast, in ZSM-5, with its medium sized pores, monomolecular xylene isomerization dominates, and the disproportionation reaction is not observed as a side reaction.

The boundaries of zeolites

Although essential in many applications, the small pore apertures of zeolites make them useless in reactions involving large molecules. In a way the shape selective nature of zeolites excludes many reactions by prohibiting molecules which are larger than their pores. For this reason scientists not only explored the synthesis of large pore zeolites, but also started investigating new synthesis strategies, involving different solid materials. At the beginning of the 1990s, the ability to synthesize well ordered true mesoporous materials was about to be announced. A group of aluminosilicates with relatively large pores, which are certainly worth mentioning, but are often overlooked, are the pillared interlayered clays.

1.3 Pillared Interlayered Clays

1.3.1 Clay minerals

Clay is usually not associated with zeolites, but rather with pottery. Not surprising, as people have been making pottery out of clay as far back as 10000 B.C., near the beginning of the Neolithic period.⁵⁴ Historically, the term clay refers to small inorganic particles of a soil fraction without regarding its composition, while clay minerals refer to phyllosilicates (sheet silicate structures), which are layered, hydrous, magnesium or aluminum silicates in such a fraction.

Every clay mineral is characterized by oxygen sharing interconnected six membered rings of $[\text{SiO}_4]^{4-}$ tetrahedra that extend outward in infinite two-dimensional sheets, as illustrated in Figure 1.4. Herein, each tetrahedron shares its three vertex oxygen atoms with other tetrahedra. Usually, phyllosilicates contain hydroxyl ions, which are located at the center of the six membered rings. Via the unshared apical oxygens or hydroxyl ions, the tetrahedral sheets are connected to octahedral sheets consisting of small cations (e.g. Al^{3+} or Mg^{2+}) which are coordinated by six oxygens or hydroxyls.

Today, clay minerals are important materials which can be used in the synthesis of polymer nanocomposites.^{55–59} Furthermore, they can be applied as adsorbents^{60–63}, ion exchangers^{64–67} and molecular sieve catalysts^{68–72}. For the latter application, a group of clays known as smectites (derived from the Greek word smectos, which means soap) are used. In the mid 1930s, acid modified smectites

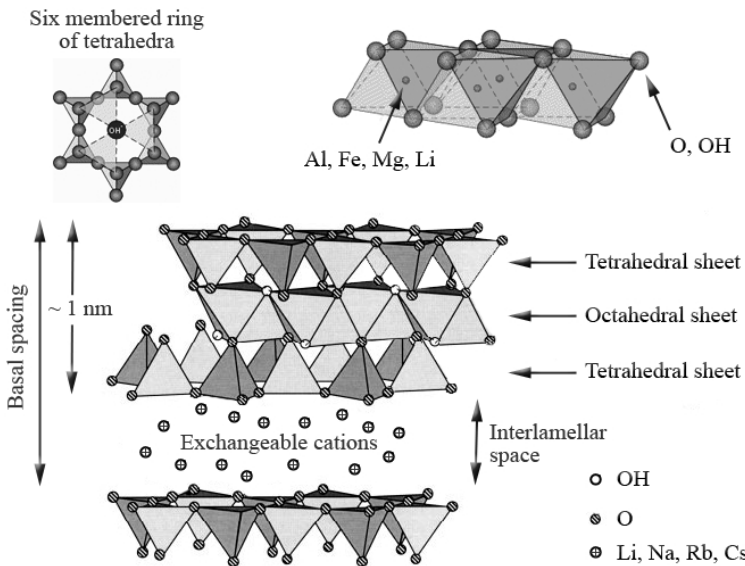


Figure 1.4: Crystal constitution of a smectite lamella. Redrawn from reference⁵⁵.

were employed as commercial catalysts in petroleum-cracking reactions (Houdry process).^{73–75} However, with the discovery of thermally more stable and shape selective zeolites, such as zeolite Y, these clay mineral catalysts were suppressed in the mid 1960s. Clay minerals did not disappear from the scene for very long though. With the escalation of the oil prices in 1973, the oil industry was confronted with the desperate need to maximize the processing of crude oil to gasoline.⁷⁶ Due to the limited pore sizes of zeolites and the rapid poisoning of zeolites by metals, the heavy fractions of the crude oil were especially hard to process.⁷⁵ In a way, the oil crisis stimulated researchers to search for alternatives for zeolites and resulted in a renewed interest in pillared clay minerals.

1.3.2 Concept of Pillaring

Research into the synthesis of Pillared Interlayered Clays (PILC) is based on the pioneering work of Richard Maling Barrer in 1955.⁷⁷ He obtained microporous materials by replacing the interlayer exchangeable cations in the smectite Montmorillonite with tetraalkylammonium ions. However, organic pillared clay minerals of this type are thermally unstable. At temperatures above 250 °C the interlayers collapse. When used below the decomposition temperature, these clays can however still be applied as catalysts⁷¹ or adsorbents^{78,79}. In the late 1970s, scientists, still in search for an answer to the need for large-pore nanoporous materials, started investigating the possibility of creating porosity in the interlayer space of layered clay hosts by inserting inorganic polymers.^{80–84} These PILCs are prepared by exchanging the charge-compensating cations (e.g. Na^+ , K^+ and Ca^{2+}) between the swelling phyllosilicate clay layers with larger polymeric or oligomeric hydroxy

metal cations. Upon heating, these metal hydroxy cations undergo dehydration and dehydroxylation, whereby stable metal oxide clusters are formed (e.g. Al_2O_3 , TiO_2 , Fe_2O_3 , . . .). These metal oxide clusters act as pillars, keeping the silicate layers permanently separated and creating an interlayer space. In Figure 1.5 a schematic overview is given, illustrating the concept of pillaring. With these novel two-dimensional aluminosilicates, an easy method to develop materials with pores ranging from 0.5 to 2.0 nm and surface areas up to $500 \text{ m}^2/\text{g}$, was introduced. Moreover, clay minerals intercalated with inorganic species retain their porosity above 300 °C.

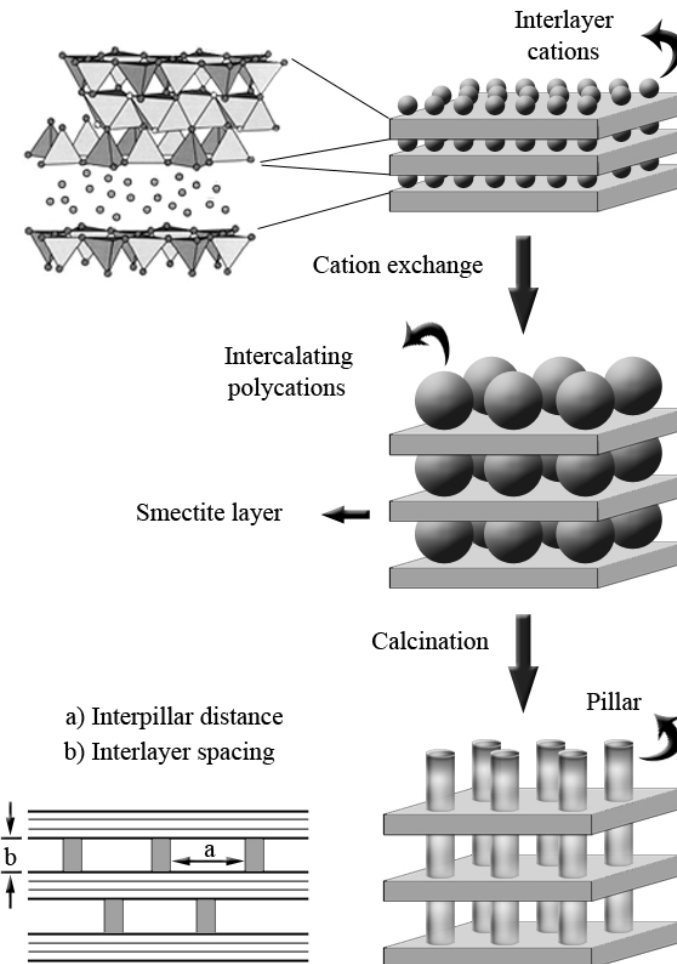


Figure 1.5: Concept of pillaring.

Ever since the first announcement of the commercial availability of PILC in 1979,⁸² their use in petroleum cracking alone has exceeded that of other catalysts. With an acidity as strong as zeolite Y, PILCs demonstrate a high activity in cracking, while displaying a selectivity for larger product molecules. However, due to their low

hydrothermal stability, the original objective of using these materials as catalysts for FCC was not achieved.⁸⁵ Nevertheless, PILCs have proved to be very interesting acid catalysts in various organic reactions.⁸⁶

However, with the discovery of a new class of aluminosilicates in 1992, namely M41S,⁸⁷ a new era in ordered porous materials commenced and much interest on PILCs faded away.

1.4 M41S: The First True Ordered Mesoporous Materials

Actually, ordered mesoporous materials were reported for the first time in 1990 by Kato *et al.*⁸⁸ Herein, a hydrothermal synthesis is described wherein sodium ions in the interlayer space of Kanemite are exchanged with alkyltrimethylammonium chloride ions. By means of ²⁹Si-MAS NMR and X-ray powder diffraction they observed condensation of the silicate layers of Kanemite. This was ascribed to the partial exchange of sodium ions with protons whereby Si–OH groups are formed, which under the given reaction conditions, polycondense into an ordered SiO₂ network. By increasing the alkyl chain in the alkyltrimethylammonium ions, mesopores between 2 - 4 nm and surface areas of about 900 m²/g were attained. In a subsequent report by Inagaki *et al.*, optimization of the reaction conditions led to a highly ordered mesoporous material with a hexagonal unit cell.⁸⁹ The hexagonal honeycomb structure was clearly visible by TEM. However, in the mean time the Mobil Research and Development Corporation reported their breakthrough research on a new family of ordered mesoporous materials, designated M41S.⁸⁷ Most likely inspired by the development of large pore crystalline materials like zeotype VPI-5, Kresge *et al.* prepared mesoporous silicas with both hexagonal (MCM-41) and cubic (MCM-48) symmetry with pore sizes ranging between 2 and 10 nm, by employing surfactants. After the first patents on these materials appeared,⁹⁰⁻⁹² a publication in Nature⁹³ and one in JACS⁸⁷ followed. With over 12000 citations (1992 - 2008), these two papers form the foundation of the field of ordered mesoporous materials.

1.4.1 Surfactants as Framework Templates

The novelty of the work described by the researchers of Mobil Oil was in the use of assemblies of surfactant molecules as framework templates, instead of using single organic cationic species such as the ones used in zeolite synthesis. Knowledge of surfactant behavior in aqueous solution is fundamental to understand the relation between surfactant and mesostructure formation. For this reason, before describing the mechanism postulated by the researchers of Mobil Oil, a brief description of conventional surfactant-water systems is given.

Conventional Surfactant-Water Systems

The development of mesostructured materials is based on the ability of surfactants to form spherical or cylindrical micelles or higher-order phases in aqueous solution. Surfactants, or surface-active agents, are large, organic molecules which con-

sist of hydrophilic (water soluble) and hydrophobic (water insoluble) components. Alkyltrimethyl ammonium surfactants with the formula $C_nH_{2n+1}(CH_3)_3N^+$, such as those employed by researchers of Mobil Oil, consist of hydrophilic head groups and long hydrophobic tails of variable length. In order to reduce the unfavorable contact between the hydrophobic hydrocarbon tails of the surfactant and the surrounding water, the hydrophobic tails gather together in the center forming the micelle cores, while the polar groups are arrayed on the surface, in contact with the surrounding water. This way the the minimum energy configuration is reached, and the generated micelles are in dynamic equilibrium with the soluble surfactant molecules, as illustrated by Figure 1.6

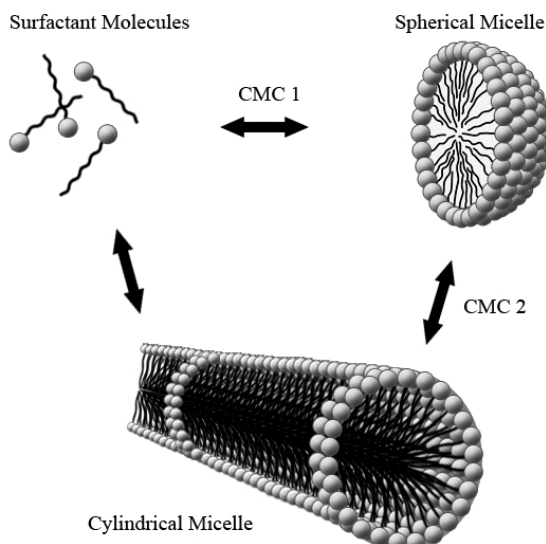


Figure 1.6: Dynamic equilibria in a surfactant-water system.

The first critical micelle concentration (CMC-1), is defined as the lowest concentration at which spherical micelle formation can be observed. The second critical micelle concentration (CMC-2), is the concentration at which spherical micelles start to transform into rodlike micelles. The concentration required for both the formation of spherical and rodlike micelles strongly depends on the synthesis conditions such as type of surfactant and temperature. For instance, with increasing temperature, the required concentration of surfactant for a sphere-to-rod transformation to occur, increases.

The Packing Parameter

Molecular organization, also referred to as self-assembly, is determined by the equilibrium among three forces: 1) the tendency of the hydrophobic tails to minimize their contact with water and maximize their organic interactions, 2) the Coulombic interactions between the hydrophilic head groups, and 3) the solvation energies. A theoretical model predicting the shape-structure relationship between monomeric

units and their aggregates was developed by Israelachvili and was based on statistical mechanics of phospholipids.⁹⁴ This model predicts the type of aggregate formed on the basis of the packing parameter (g), which relates the volume of the molecule (V) to its length (l) and to the mean cross-sectional (effective) head group surface area (a_0):

$$g = \frac{V}{(a_0 \cdot l)} \quad (1.1)$$

As illustrated in Figure 1.7, the packing parameter provides a simple geometric characterization of the surfactant molecules employed, which is useful to predict the structure of the aggregate that will be formed in solution.

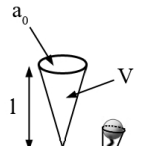
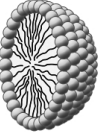
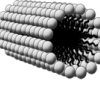
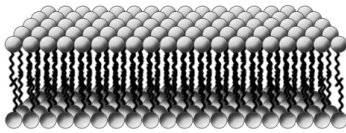
Packing Shape	Micellar Structure
 $g < 1/3$	 Spherical
 $1/3 < g < 1/2$	 Rodlike
 $g \sim 1$	 Lamellar

Figure 1.7: Relation between the packing parameter and micellar aggregate structures.

If the value of the packing parameter changes, phase transition is expected to occur. This transition reflects a change in surface curvature of the amphiphile. Thus knowledge of the packing parameter of a particular surfactant can be a powerful tool in determining the micellar structure and can be helpful in the molecular design of novel mesoporous materials.

1.4.2 Sol-gel Chemistry of Metal Oxides

The so-called sol-gel process which is involved in the synthesis of ordered inorganic mesostructures, is based on the hydrolysis and polycondensation of metal alkoxide precursors $M(OR)_n$, (with R an alkyl group, most commonly methyl or ethyl). In the case of ordered mesostructured silicas such as MCM-41, the most commonly employed precursors are $Si(OCH_3)_4$ (tetramethoxysilane, TMOS) and $Si(OCH_2CH_3)_4$ (tetraethoxysilane, TEOS). Because water and alkoxy silanes are immiscible, a mutual solvent such as an alcohol is typically used as a homogenizing agent. However, since the alcohol, which is produced as a byproduct during the hydrolysis reaction of alkoxy silanes, is sufficient to homogenize the initially phase separated system, the addition of alcohols is not essential. What is required though for a rapid and complete hydrolysis is a base or acid catalyst. In both cases the reaction occurs by a nucleophilic attack of the oxygen atom of a water molecule, to the silicon atom, as illustrated in Figures 1.8 and 1.9, respectively.⁹⁵

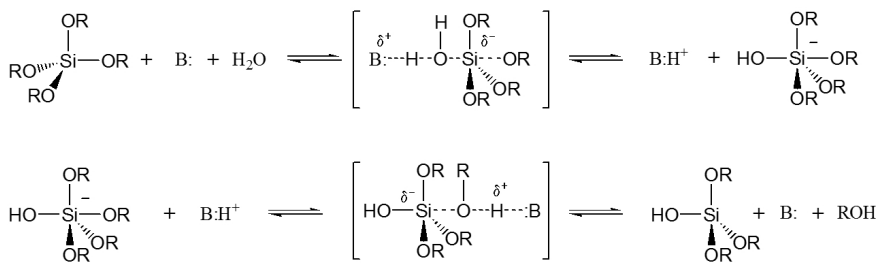


Figure 1.8: Base catalyzed hydrolysis of alkoxy silanes.

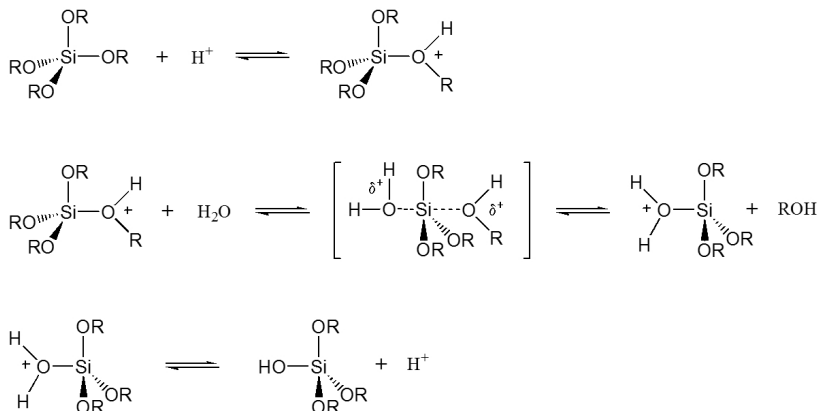


Figure 1.9: Acid catalyzed hydrolysis of alkoxy silanes.

The base catalyzed hydrolysis of alkoxy silanes (Figure 1.8) is a two-step process in which a pentacoordinated intermediate is formed. According to an S_{N^2} -type mechanism, an alkoxy group is replaced by a hydroxyl group with inversion of the silicon tetrahedron.⁹⁵ The acid catalyzed hydrolysis also likely proceeds via

an S_{N^2} -type mechanism (Figure 1.9). Herein, the leaving alkoxy group is rapidly protonated in a first step whereby the electron density is withdrawn from the silicon atom, making it more electrophilic and thus more susceptible to a nucleophilic attack from water.⁹⁵

In a next stage, the hydrolyzed silane molecules condense and form siloxane bonds, as illustrated in Figure 1.10A. The condensation may also proceed *via* a reaction between an alkoxy silane molecule and a silanol group (Figure 1.10B).

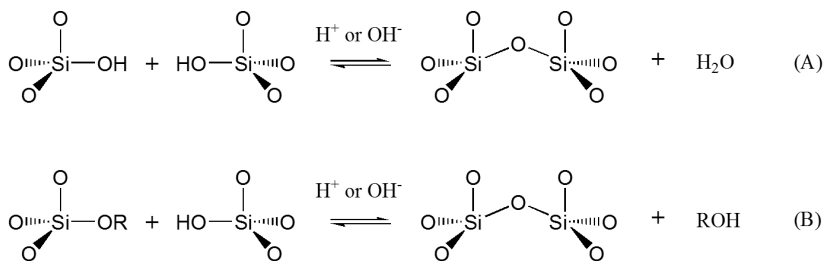


Figure 1.10: Condensation of silane molecules leading to the formation of siloxane bonds.

The condensation is also acid or base catalyzed and presumably proceeds *via* an S_{N^2} -type mechanism.⁹⁵

Although the hydrolysis and condensation steps are depicted as separate reactions, in reality they occur simultaneously. Moreover, the relative rate of both processes has a different pH dependence, as illustrated in Figure 1.11, and determines the structure of the silica network.^{96,97}

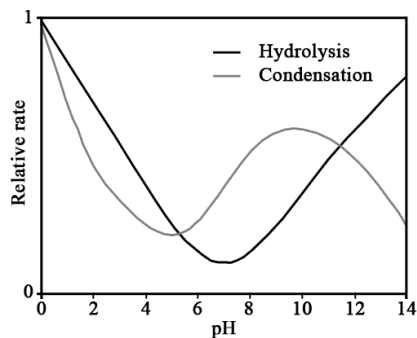


Figure 1.11: The relative rates of hydrolysis and condensation of $\text{Si}(\text{OR})_4$ as a function of pH.⁹⁶

Under acidic conditions, hydrolysis is favored and condensation is the rate determining step. Additionally, as the number of siloxane bonds around a central silicon atom increase, the rate of condensation slows down. This leads to weakly branched long polymeric networks. On the other hand, under basic conditions, condensation is favored and hydrolysis is the rate determining step. In this case, the rate of condensation increases with increasing number of siloxane bonds. Thus, highly branched networks are formed.⁹⁷

1.4.3 The Mobil Hypotheses

The synthesis of MCM-41 (Mobil Composition of Matter) described by Kresge *et al.*⁹³ and Beck *et al.*⁸⁷, involves the use of aluminosilicate gels in the presence of the surfactant hexadecyltrimethylammonium chloride ($C_{16}H_{33}(CH_3)_3N^+Cl^-$), also abbreviated as CTAC. The postulated mechanism whereby ordered mesostructures are attained is designated as the liquid-crystal templating mechanism. Herein, the quaternary ammonium ion, which acts as a structure directing agent (SDA), forms micelles that aggregate into a liquid-crystal. The term template is associated with the liquid-crystal because it determines the mesostructure of the solid material. Depending on the synthesis conditions, such as synthesis temperature and the molar ratio of surfactant/aluminosilicate, the liquid-crystal phase can have a hexagonal (MCM-41), cubic (MCM-48) or lamellar structure (MCM-50), as depicted in Figure 1.12.

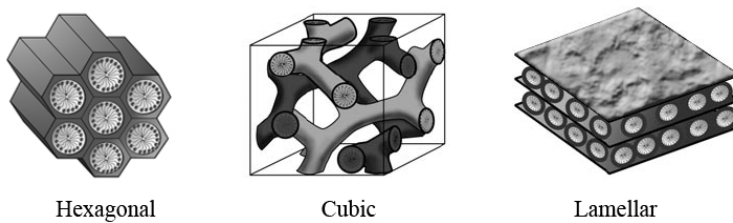


Figure 1.12: Structures of ordered mesoporous M41S type materials: MCM-41 (hexagonal, $P6/m\bar{m}$), MCM-48 (cubic, $Ia\bar{3}d$), and MCM-50 (lamellar, $p2$).

In the case of MCM-41, the liquid-crystal template consists of a hexagonal array of cylindrical micelles in which the hydrophobic hydrocarbon chains are gathered in the center forming the micelle core, while the polar groups are arrayed on the surface, in contact with the surrounding water. Upon addition, the inorganic precursor interacts with the micelle surface and occupies the water medium between the surfactant micelles, creating inorganic walls between the hexagonal array of cylindrically aggregated micelles. Upon calcination, the surfactant template is removed out of the pores, leaving a mesoporous material consisting of hollow cylinders in a hexagonal arrangement. At that time, no conclusions were drawn as to whether or not the walls of these channels had precise atomic ordering. In fact, MCM-41 was speculated to be a larger-pore version of VPI-5. In the mean time proof for the lack of atomic ordering in the pore walls of M41S type materials has been reported.⁹⁸ Fourier transform infrared, ²⁹Si-MAS NMR, and Raman studies support the idea that MCM-41 materials are amorphous in terms of local atomic arrangement and bonding. Mid-infrared spectra of Si and Al MCM-41 show framework vibrations similar to that of amorphous silicas and amorphous aluminosilicates. Together with the absence of reflection lines at high angles in the corresponding x-ray diffractograms, these results suggest that the pore walls of MCM-41 resemble amorphous silicas and aluminosilicates rather than zeolites in terms of local structure and bonding.⁹⁸

Another matter which still remains a topic of interest, is the manner in which the micelles aggregate into a liquid-crystal. At the time, the researchers of Mo-

bil proposed two synthesis mechanisms to explain the formation of M41S type materials.^{87,93} These two mechanisms are illustrated in Figure 1.13. In the first mechanism, the surfactant liquid-crystal phase is formed prior to the addition of the inorganic species, and directs the growth of the inorganic mesostructures. However, this mechanism did not meet much support in the literature.^{99,100} In 1995, Cheng *et al.* pointed out that the liquid-crystal phase in a CTAC-water system only forms when the concentration of CTAC is higher than 40 wt%.¹⁰⁰ In the conventional synthesis procedure of MCM-41, the CTAC concentration is much lower than 40 wt%, and only micelles can exist in solution. Because MCM-41 could be formed at surfactant concentrations as low as 1 wt%, while *in situ*¹⁴NMR spectra of CTAC-water systems revealed no hexagonal liquid-crystal phase, it was very doubtful that this first mechanism occurred.⁹⁹

In the second mechanism proposed by the researchers of Mobil, the presence of the inorganic species in the synthesis mixture initiates the formation of the liquid-crystal phase and facilitates in the formation of the inorganic mesostructures.^{87,93} Under the reaction conditions described by the researchers of Mobil, this mechanism is more realistic and therefore encountered more acceptance in the literature.¹⁰⁰ Davis *et al.* found that randomly distributed rod-shaped surfactant micelles form initially and as such interact with inorganic oligomers to form randomly oriented surfactant encapsulated inorganic rods.⁹⁹ Upon heating, a base-catalyzed condensation between inorganic species on adjacent rods occurs. This condensation initiates the long-range hexagonal ordering which corresponds to the minimum energy configuration for the packing of the rods.

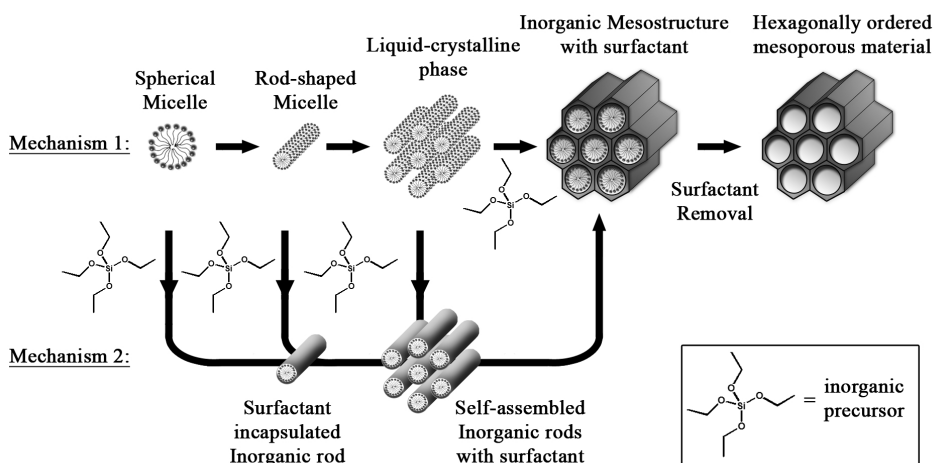


Figure 1.13: Possible mechanisms involved in mesostructure formation. Path 1 is denoted as the true liquid-crystal templating mechanism and path 2 is designated as the cooperative liquid-crystal templating mechanism.

In general, depending on the reaction conditions, two mechanisms can be involved: 1) When the concentration of the surfactant is sufficiently high, the liquid-

crystalline phase is formed without requiring the presence of the inorganic precursor. This is described as the true liquid-crystal templating mechanism (mechanism 1 in Figure 1.13). 2) When the concentration of the surfactant is insufficient, the formation of the liquid-crystalline phase can be mediated by the inorganic precursor. In this case the mechanism is a cooperative self-assembly (mechanism 2 in Figure 1.13). Either way, ordered materials can only be obtained when the template and the inorganic precursor interact. This interaction ensures the inclusion of the template by the condensing Si-species and excludes phase separation. Under the basic reaction conditions used by Mobil's researchers, this attractive interaction is ensured by the negative charge of the inorganic species and the positive charge of the ammonium head groups of the surfactant, as depicted in Figure 1.14.

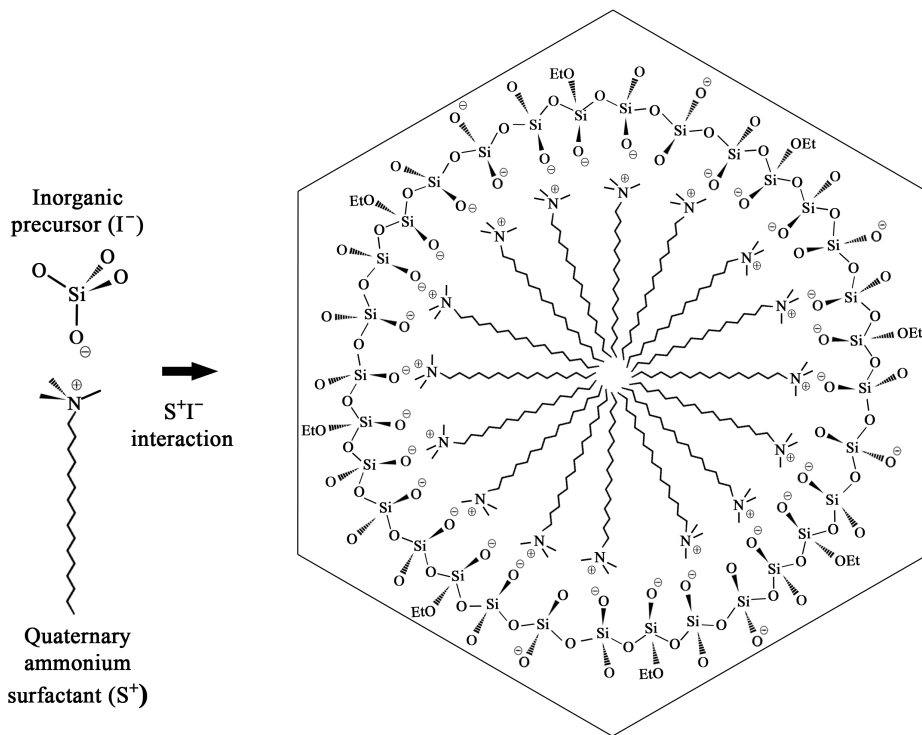


Figure 1.14: Cooperative self-assembly through ionic interactions between inorganic species and quaternary ammonium surfactant molecules under basic conditions.

1.4.4 Interactions Involved in Mesostructure Formation

The attractive interactions between the surfactant and the inorganic precursor are critical to the formation of ordered mesostructures. A convenient way to classify the different types of interactions is to consider how the surfactant head group binds to the inorganic precursor. A generalized mechanism of mesostructure formation based on the specific type of interaction between an inorganic precursor

(I) and a surfactant head group (S) was proposed by Huo *et al.*^{101,102} They identified three criteria for the formation of inorganic mesoporous frameworks. The inorganic precursor should be capable of forming flexible polyionic species and should undergo extensive polymerization. Furthermore, charge density matching between the surfactant and the inorganic species should be possible. Based on these concepts, four different categories of surfactant-precursor interactions were proposed, as illustrated in Figure 1.15 (a-d). The first category (a) involves the charge density matching between cationic surfactants and anionic inorganic species (S^+I^-). Considering the conventional basic ($pH > 10$) synthesis procedure described by the researchers of Mobil, the inorganic precursor is anionic (I^-), while the surfactant is a cationic quaternary ammonium ion (S^+).^{87,93} In this case, the ionic interaction is termed S^+I^- . The second category (b) involves the charge density matching between anionic surfactants and cationic inorganic species (S^-I^+). Huo *et al.* reported both the synthesis of iron and lead oxide mesoporous materials using anionic sulfonate surfactants.^{101,102} The third (c) and fourth (d) categories are counterion-mediated interactions which allow the assembly of cationic or anionic inorganic species via halide ($S^+X^-I^+$) or alkali metal ($S^-M^+I^-$) ions, respectively. This way, the synthesis of M41S type materials is feasible both under basic and acidic conditions. By operating under acidic conditions, below the isoelectric point of silica ($pH \approx 2$), the silicate species are cationic (I^+). The same ammonium surfactant (S^+) can be employed as templating agent, but in this case the halide counteranion (X^-) is involved in the interaction between the silicate species and the surfactant.¹⁰¹ The halide counteranion serves to buffer the repulsion between the cationic silicate (I^+) and surfactant (S^+) molecules by means of weak hydrogen bonding forces. On the other hand, negatively charged surfactants such as long-chain alkyl phosphates or sulfonates (S^-), can be used as templates in basic media if the interaction with the negatively charged silica species (I^-) involves a metal counterion (M^+).¹⁰¹

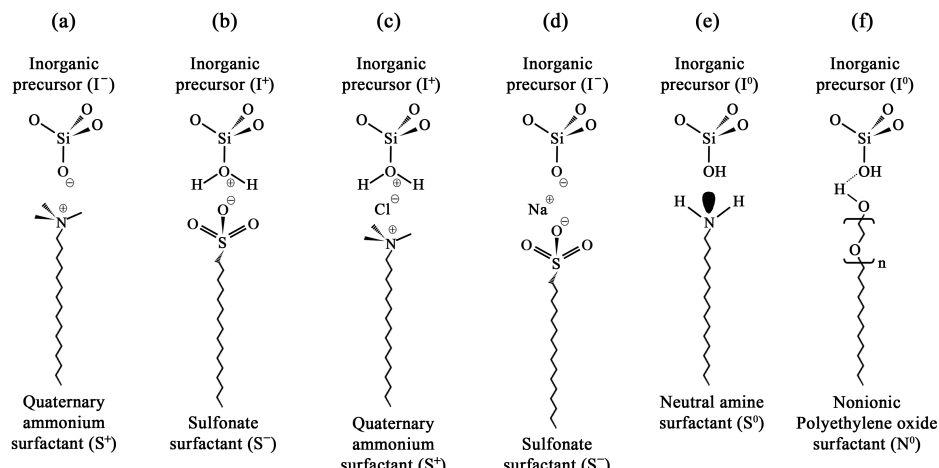


Figure 1.15: Possible interactions between inorganic species and surfactant molecules under basic and acidic conditions.

Soon after Huo *et al.* reported on the generalized liquid-crystal templating mechanism based on electrostatic interactions between inorganic precursors and surfactants, Pinnavaia *et al.* proposed a fifth category to synthesize inorganic mesoporous materials (Figure 1.15 e).¹⁰³ This synthesis involves a neutral templating mechanism based on hydrogen-bonding between neutral primary amines and neutral inorganic precursor molecules (S^0I^0). The materials lacked long-range ordering of pores due to the absence of electrostatic interactions which would normally control the packing of micellar rods and ensure long-range ordering. Though, the neutral templating synthesis method produced mesoporous silicates with thicker pore walls and consequently higher thermal stability when compared to the conventionally prepared inorganic mesostructures. Another hydrogen-bonding synthesis method (f), also reported by Pinnavaia *et al.*, involves surfactants with poly(ethylene oxide) head groups.¹⁰⁴ Due to the adjustable length of the surfactant tail and head group, pores in the range of 2.0 - 5.8 nm could be attained. The poly(ethylene oxide) head group is non-ionic (N^0), unlike the amine head group (S^0) which is uncharged. The non-ionic route (N^0I^0) seemed to provide greater pore ordering than the neutral route (S^0I^0), but still lacked long-range hexagonal ordering of the pores. However, this synthesis procedure presents the advantage of using low-cost, nontoxic, and biodegradable surfactants.

1.4.5 The Complexity of Mesostructure Formation

While all of the above described mechanisms of mesostructure formation have been supported by some form of experimental data, they are neither exclusive nor definitive. The actual formation mechanism depends on the synthesis conditions which forms a very complex system in which numerous parameters affect the outcome. The smallest shift of one of these parameters such as temperature, molar composition, reaction time, pressure, stirring rate, presence of additives, humidity, ... can have a tremendous affect on the structure formation. Nevertheless, the above described mechanisms can be used as a guidance through this complex maze. Correlations, such as the affect of the surfactant concentration on the liquid-crystal templating mechanism, are very useful in predicting the required molar composition of a reaction mixture for the formation of ordered mesostructures. However, as with all parameters, the surfactant concentration has to be evaluated together with other parameters, such as temperature. Another helpful tool, as described above, is the packing parameter of a surfactant. Knowledge of the hydrophobic/hydrophilic volume ratio of a surfactant is important to predict its nature in aqueous media. Though, once more it has to be evaluated in combination with other parameters. For instance, the presence of additives such as salts can have a large affect on the curvature of the surfactant surface and thus influence its nature in water.

Finally, for the synthesis of non-silica materials, the flexibility of the inorganic species has to be taken into account. Also important with non-silica materials, is the tendency of the employed metal oxide to change oxidation state. For instance, ordered mesoporous tungsten frameworks have shown to collapse after surfactant removal due to changes in the oxidation state of the material, even though the tungsten species were originally fully condensed in the walls.^{101,102}

In short, an in-depth understanding of the formation mechanism of ordered meso-

structured materials is essential in developing successful strategies for the synthesis of novel materials, but still requires extensive empirical research. A fine example of this is the early research of Zhao *et al.* on the synthesis of large-pore ordered mesoporous silica materials using non-ionic copolymers as surfactant templates.¹⁰⁵

1.5 SBA Materials: Combined Micro- and Mesoporous Solids

The next breakthrough in the development of ordered mesoporous silica materials is that of Zhao *et al.* in 1998.¹⁰⁵⁻¹⁰⁷ Using commercially available non-ionic triblock copolymers as templates, they succeeded in developing ordered silica materials with larger mesopores (4.5 - 30 nm) and thicker pore walls (3.0 - 7.0 nm). These new mesostructured solids were designated as SBA materials, which is the acronym for Santa Barbara, the University where they were developed for the first time by the group of Stucky.

1.5.1 Introduction to SBA materials

As mentioned in section 1.4.4, the first reports on inorganic mesostructures described the use of ionic surfactants as supramolecular templates. This strategy yielded materials with controllable, and often very uniform pore sizes in the range of 1.5 - 10 nm. However, this method also renders some limitations. A serious drawback of MCM-type materials in terms of stability, is the wall thickness, which ranges between 0.8 and 1.3 nm. A second drawback of using molecular surfactants as templates is the limited pore size of the resulting mesostructures. The only way to develop MCM-type materials with pores beyond 5.0 nm is by employing swelling agents (which often results in reduced pore ordering). Not surprising, the next step in designing ordered mesostructured materials with larger pores and thicker pore walls was the implementation of more versatile supramolecular templates. As a template, amphiphilic block copolymers are a very good alternative to molecular surfactants as their self-assembly characteristics permit control of mesostructure formation.

As mentioned in section 1.4.4, the first report which describes the use of oligomeric alkyl-poly(ethylene oxide) surfactants as mesostructure templates, was that of Pinnavaia *et al.*¹⁰⁴ This synthesis procedure had some advantages such as thicker pore walls (1.5 - 4.0 nm), easy pore diameter tuning by varying both the type and concentration of surfactant, and easier surfactant removal by solvent extraction. However, these materials displayed only modest structural ordering. Therefore, with over 4685 citations (1998 - 2008), the reports of Zhao *et al.* are considered as the first contributions to a new family of highly organized large-pore mesostructured silica materials using non-ionic triblock copolymers ($\text{EO}_n\text{PO}_m\text{EO}_n$) with large poly(ethylene oxide) (EO_n) and poly(propylene oxide) (PO_m) blocks (see Figure 1.16).^{105,106}

The most widely studied SBA material is SBA-15. Having a 2D-hexagonal pore structure ($\text{P}6/\text{mm}$), it is the large-pore equivalent to MCM-41. It is synthesized under strongly acidic conditions by using the commercially available tri-

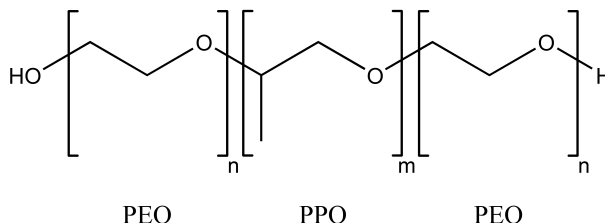


Figure 1.16: Non-ionic triblock copolymer with large poly(ethylene oxide) (PEO) and poly(propylene oxide) (PPO) blocks.

block copolymer Pluronic® P123 ($\text{EO}_{20}\text{PO}_{70}\text{EO}_{20}$) as the structure directing agent. Another important SBA material is SBA-16, which has a cubic cage structure ($\text{Im}\bar{3}m$).¹⁰⁶ It is usually synthesized with the commercially available triblock copolymer Pluronic® F127 ($\text{EO}_{106}\text{PO}_{70}\text{EO}_{106}$). Other, but less studied, SBA materials are SBA-11 (cubic, $\text{Pm}\bar{3}m$) and SBA-12 (3D-hexagonal, $\text{P}6_3/mmc$).¹⁰⁶ These are usually synthesized using the commercially available surfactants Brij 56 ($\text{C}_{16}\text{EO}_{10}$) and Brij 76 ($\text{C}_{18}\text{EO}_{10}$), respectively.

As non-ionic oligomeric and polymeric surfactants are available in a wide variety of different chemical structures, it is not surprising that these materials are attractive templates for the synthesis of novel mesostructured inorganic materials. However, a good understanding of the formation mechanisms of these mesostructures is required to effectively utilize these non-ionic surfactants.

1.5.2 Block copolymers as organic templates

The main classes of non-ionic surfactants for the synthesis of ordered mesostructured materials are amphiphilic block copolymers, oligomeric alkyl ethylene oxides, oligomeric alkylphenol ethylene oxides and sorbitan ester surfactants. Commercial non-ionic surfactants are frequently used and are listed in Figure 1.17.

With SBA-15 and SBA-16 being two of the most widely studied large-pore ordered silica materials, the $\text{EO}_n\text{PO}_m\text{EO}_n$ triblock copolymers can be considered as the most important non-ionic surfactants for mesostructure formation. An important advantage of block copolymers compared to molecular surfactants is that the hydrophilic-lipophilic balance (HLB) can be easily tuned by changing the polymerization degree. Moreover, the intrinsic chemistry of each block can be varied, modulating the interactions with the inorganic units that build up the mesostructured framework. This way, block copolymers can serve as very versatile templates leading to a variety of novel mesostructures.

To obtain an inorganic solid with a certain desired mesostructure, the nature of a non-ionic polymeric surfactant can give a guidance as to which surfactant should be employed. In particular the hydrophilic/hydrophobic volume ratio (V_H/V_L) of a surfactant is suggested to account for the formation of different mesophases.¹⁰⁸ With the PEO groups in PEO-PPO-PEO triblock copolymers being the hydrophilic headgroups and the PPO groups being the hydrophobic tails, the increase in the number of ethylene oxide units relative to the number of propylene oxide units, corresponds to an increase in the curvature of the surfactant layer toward water.

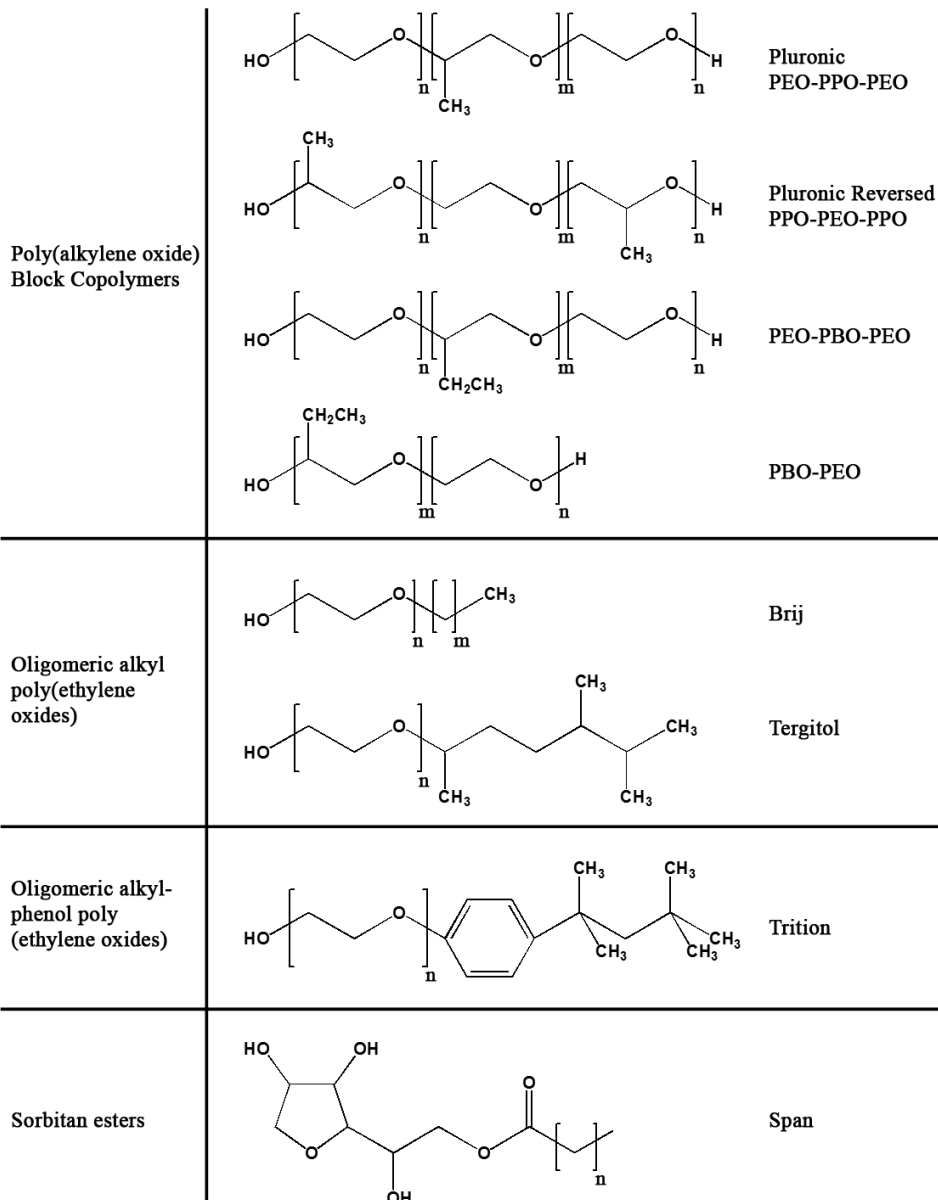


Figure 1.17: Some typical commercially available non-ionic surfactants.

Herein, the hydrophilic ethylene oxide groups tend to dissolve in water, while the hydrophobic propylene oxide moieties gather together to form the micelle cores. The change in surfactant surface curvature with varying hydrophilic/hydrophobic volume ratio can be related to an alteration in the surfactant packing parameter, g . With increasing number of ethylene oxide chains, the headgroup, a_0 , increases and consequently the packing parameter, g , diminishes. Thus the number of ethylene oxide groups in a PEO-PPO-PEO surfactant, is essential in determining which mesophase can be obtained. Amphiphilic surfactants with high V_H/V_L ratios, such as Pluronic® F127, favor the formation of cubic caged-like mesostructures whose topological curvatures are rather high.¹⁰⁶ On the other hand, block copolymers with medium V_H/V_L ratios, such as Pluronic® P123, favor the formation of mesostructures with medium curvatures such as 2D-hexagonal structures.¹⁰⁶ Besides the V_H/V_L ratio, the concentration of block copolymers can also change the mesostructure.¹⁰⁹ Usually, higher concentrations lead to structures with lower mesophase curvature.

As with molecular surfactants, the surfactant-silica interaction is of particular importance in systems involving non-ionic polymeric templates. Depending on the reaction conditions different interactions can be involved leading to both ordered or disordered mesostructured materials. Especially the pH can have a tremendous affect on the type of surfactant-silica interaction and is a decisive parameter in mesostructure formation.

Synthesis below the isoelectric point of silica

When considering poly(alkylene oxide) block copolymers such as those employed in the synthesis of SBA-15 and SBA-16, the different possible interactions at the surfactant-inorganic interface are characterized by hydrogen bonding, as depicted in Figure 1.18.

By operating under acidic conditions, below the isoelectric point of silica ($\text{pH} < 2$), the silicate species are cationic (I^+) and preferentially interact with the hydrophilic PEO blocks of the template. Under these conditions, the mechanism is most likely occurring *via* a $(\text{N}^0\text{H}^+\text{X}^-\text{I}^+)$ double-layer hydrogen bonding interaction. It is not clear yet whether the PEO headgroups actually get protonated during the self-assembly, but the acid induced increase in pore ordering of SBA-15 and SBA-16 strongly suggests that the anion mediated interactions between cationic silica species and PEO headgroups occur *via* H_3O^+ ions or *via* protonated terminal OH groups of the PEO-chains.

Synthesis around the isoelectric point of silica

When the synthesis is performed around the isoelectric point of silica ($\text{pH} \approx 2$), the silicate species are neutral and the self-assembly is characterized by a (N^0I^0) or a $(\text{N}^0\text{H}^+\text{X}^-\text{I}^0)$ hydrogen bonding interaction (see Figure 1.18). Stucky *et al.* showed that up to a $\text{pH} \approx 4$ highly ordered mesoporous silica materials can be obtained.¹¹⁰ Above the isoelectric point of silica ($\text{pH} > 4$) the silica species are partially ionized ($\text{N}^0\text{H}^+\text{I}^-$) and disordered silica framework structures with worm-like channel motifs are obtained.^{104,110,111} Results reported by Stucky *et al.* suggest that oligomeric silica species, formed from fully hydrolyzed monomeric silica molecules, are required

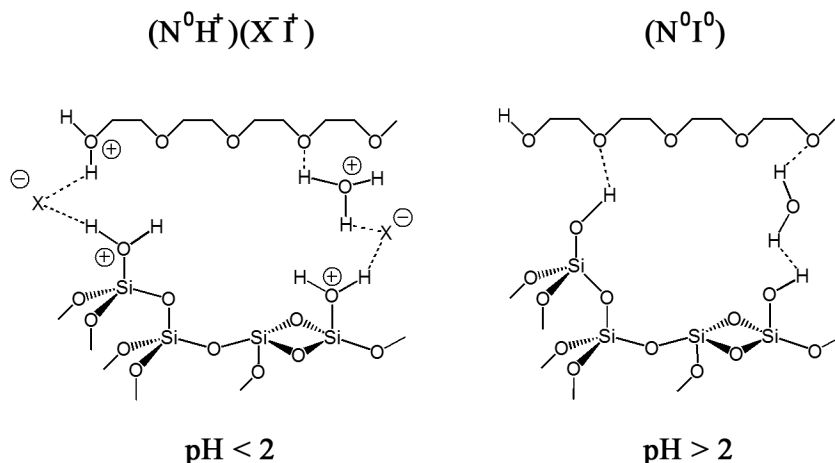


Figure 1.18: Possible interactions between poly(alkylene oxide) block copolymers and silica species under different reaction conditions.

for suitable interactions with the polymeric surfactant and hence to obtain ordered mesostructures.¹¹⁰ This is due to competition between the condensation of partially hydrolyzed silica species and the hydrolysis of alkoxy silane molecules.¹¹² Above a pH of 4, the condensation reaction of silica species is relatively fast compared to the hydrolysis reaction (see Figure 1.11, p17). This can cause incomplete hydrolysis of the silica oligomers, which thus contain alkoxy groups. The presence of such residual alkoxy groups leads to weaker interactions between the hydrophilic ethylene oxide blocks of the surfactant and the condensing silica oligomers, resulting in poorly organized mesostructures.¹¹⁰

Synthesis above the isoelectric point of silica

A way to obtain ordered mesostructured silica materials at a pH above 4 is to increase the hydrolysis rate relative to the condensation rate by another means than lowering the pH. Fluoride is a well known catalyst for hydrolysis and has been used by the group of Stucky in order to improve structural ordering of silica materials.¹¹⁰ They showed that by employing fluoride as a hydrolysis catalyst well ordered mesostructures could be obtained up to a pH of 9 when using TMOS as a precursor.¹¹⁰ However, Stucky *et al.* also pointed out that the catalytic activity of fluoride depends on the nature of the silica precursor. When TEOS is used as silica source instead of TMOS, disordered mesostructures are obtained above a pH of 2.7. This is not so surprising as TEOS hydrolyzes much slower than TMOS because of the steric hindrance of the ethoxy moieties.⁹⁶ This implies that the hydrolysis reaction has to compete more with the condensation reaction. The higher hydrolysis rate of TMOS thus makes it a more suitable precursor than TEOS for producing ordered mesostructures at higher pH values.

Another method to improve template-silica interactions at a pH above 4, is through

complex formation of the non-ionic surfactant with metal ions.^{113,114} This way mesoporous silica materials, denoted as MSU (Michigan State University), can be obtained even under neutral conditions. Although the mechanism is not fully understood yet, Bagshaw showed that electrolytes can increase the degree of silica cross-linking, indicating that electrolytes can increase the hydrolysis rate of the silica precursor.¹¹⁴ Interestingly Bagshaw also found that, to obtain ordered mesostructures, the electrolytes should not be added prior to the addition of the silica source. Spectroscopic investigations of the PEO-based surfactant, showed that the metal cations interact with the ethylene oxide functions. This complexation, prior to silicate addition, seemed to cause the H-bonding sites to become unavailable for templating or silica hydrolysis. Therefore, in the absence of a hydrolysis catalyst, the silica precursor hydrolyzes slowly and will not be directed into an ordered mesostructure during the condensation.¹¹⁴ On the other hand, when the electrolytes are added after the silica source has reacted for some time with the surfactant, the addition of metal cations renders rapidly condensed ordered mesostructures. A possible explanation is that the cations affect the packing parameter, g , of the surfactant. Another possibility is that the electrolytes do not modify the template microstructure, but induce bridging interactions between terminal hydroxyl groups of adjacent templating micelles, as illustrated in Figure 1.19.¹¹⁴

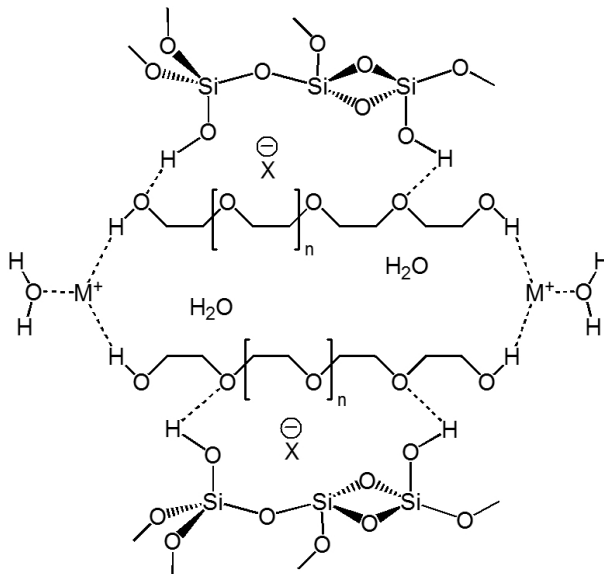


Figure 1.19: Possible interaction between metal cations M^+ and terminal hydroxyl groups of adjacent templating PEO-based surfactant micelles.

Naturally, the addition of electrolytes means that both cations and anions will be introduced to the synthesis system. Various anions are known to influence the rate and extent of hydrolysis and condensation of silica precursors.¹¹⁵ Other than the previously mentioned F^- anion, which is the most well known anion to catalyze the silicate hydrolysis, Cl^- , Br^- , I^- , SO_4^{2-} , NO_3^- and OAc^- seem to affect the hydrolysis rate of silica precursors, of which strongly ionising hard

anions, such as F^- and Cl^- , have the largest effect.¹¹⁵ It has been proposed that strong nucleophilic attack of the F^- anion on the hydrolyzing silica precursor leads to the formation of an unstable reactive penta-coordinate Si complex.¹¹⁶ The strongly electron donating ligand causes the Si atom to be more susceptible to nucleophilic attack of water at the Si–OR bond. Poorly ionising anions, such as acetate, only have little influence on the hydrolysis of silica precursors and thus disordered materials are obtained under neutral conditions.¹¹⁴

1.5.3 Introducing Micropores in a Mesoporous System

As mentioned before, SBA-15 and MCM-41, both having 2D-hexagonal mesostructures with $\text{P}6/\text{mm}$ space groups, are similar silica materials. However, besides SBA-15 having larger pores and thicker pore walls than MCM-41, the wall structures of these two solids are also quite different. More explicitly, the pore walls of SBA-15 consist of a large amount of disordered intraframework micropores and even small mesopores, while this is not the case for MCM-41. The presence of micropores in the pore walls of SBA-15 was first indicated by the group of Stucky¹¹⁷ and was shortly after confirmed by several research groups^{118–122} that performed systematic studies based on nitrogen physisorption and X-ray powder diffraction. Moreover, it was also suggested that a significant fraction of these disordered complementary pores in the walls of SBA-15 provide connectivity between the ordered primary mesopore channels, as illustrated in Figure 1.20.

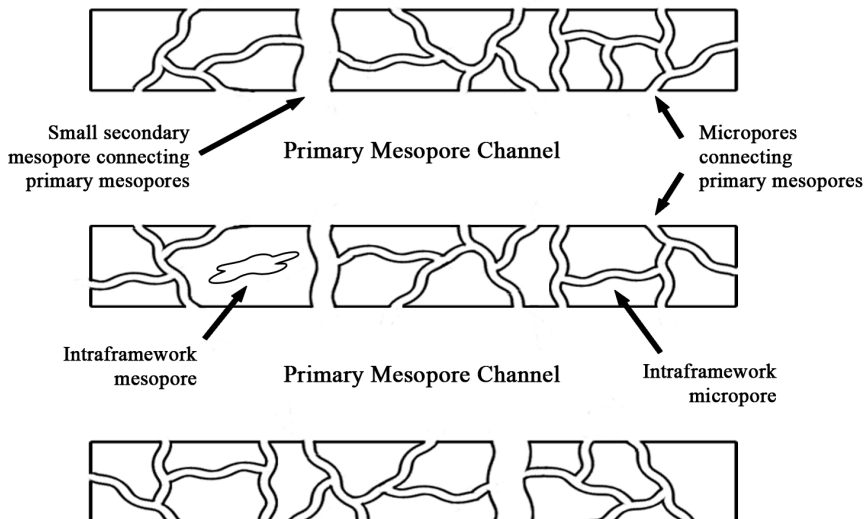


Figure 1.20: Schematic representation of SBA-15 pore walls, illustrating the connectivity between the mesopore channels.

This structural feature of SBA-15 was unambiguously supported by the successful synthesis of hexagonally ordered mesoporous carbon (CMK-3) by using SBA-15 as a hard template.^{123–126} This technique, often referred to as exotemplating or

nanocasting, involves the filling of the pores of mesostructured silica materials with carbon precursors. After calcination and subsequent removal of the hard silica template (e.g. with HF or NaOH) an inverse carbon replica of the ordered mesoporous silica material is obtained (see Figure 1.21). Such carbon replicas can only be synthesized if the hard silica template has a 3D-structure, consisting of interconnected pore channels. When the hard silica template is a 2D-hexagonally ordered material which lacks pore connectivity, such as MCM-41, the carbon replica collapses into loose carbon rods (see Figure 1.21).^{127,128} Similar studies, supporting these results, have been conducted involving the synthesis of inverse platinum replicas of SBA-15.^{129–131}

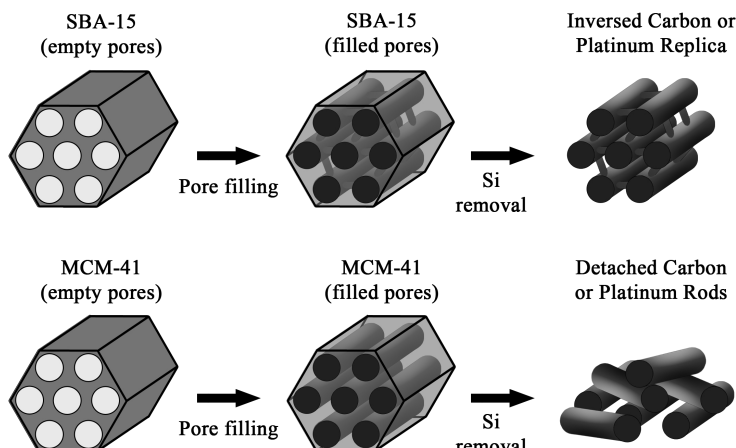


Figure 1.21: Nanocasting of SBA-15 and MCM-41. After removal of the silica framework, an inverted metal oxide or carbon replica is obtained when using SBA-15 as a mold, while detached metal oxide or carbon rods are attained when MCM-41 is used.

With the fact that platinum or carbon rods, grown inside the SBA-15 pore structure, form ordered bundles, as evidenced by transmission electron microscopy (TEM), unambiguous evidence is given that the large ordered mesopores of SBA-15 are interconnected by smaller disordered pores which are located in the pore walls. The intraframework bridges between mesopore channels have even been observed by high resolution transmission electron microscopy (HRTEM) of inverse platinum replicas of SBA-15.¹³⁰

These interconnecting pores are suggested to be related to the micellar behavior of non-ionic amphiphilic PEO-PPO-PEO triblock copolymers.^{118,131} In water, the surfactant micelles consist of a hydrophobic poly(propylene oxide) core and a corona of hydrated hydrophilic poly(ethylene oxide) chains which protrude from the micelle surface.^{132–134} As a result of the penetration of these poly(ethylene oxide) chains in the silica framework of SBA-15, micropore connections between the mesopores are generated after template removal, as illustrated in Figure 1.22.^{118,119} However, the tendency of the PEO-chains to extend from the micelle surface and penetrate the silica walls is strongly temperature dependent. With increasing temperature,

dehydration of the PEO-chains causes them to be more hydrophobic and draw back from the silica walls into the hydrophobic PPO micelle cores. As a result, the extracted SBA-15 material is characterized by larger mesopores combined with a reduced micropore volume.^{118,119,121}

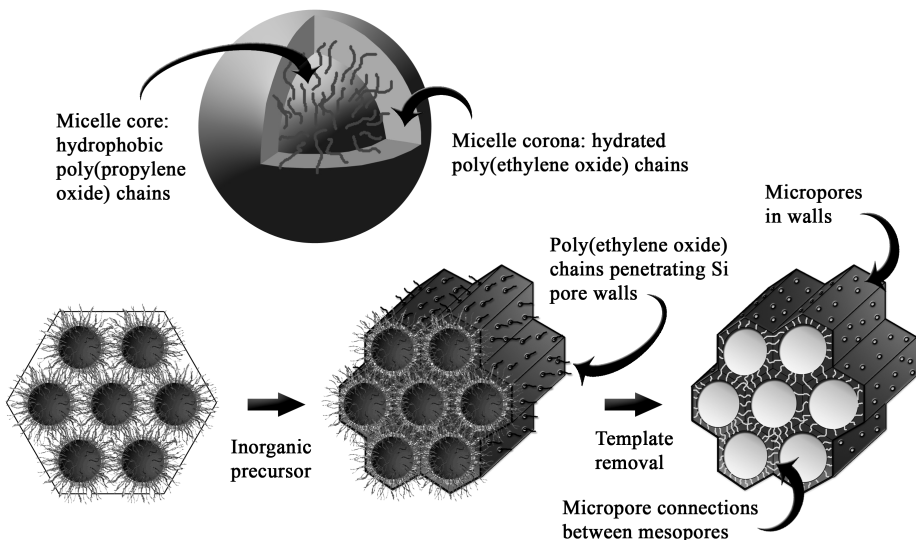


Figure 1.22: Micelle structure of PEO-PPO-PEO triblock copolymers. The micelle core consists of hydrophobic PPO-chains surrounded by a hydrated corona of PEO-chains. The PEO-chains penetrate the Si pore walls and generate connectivity between the mesopores.

These results were supported by Galarneau *et al.* who found that the temperature at which the mesopores enlarge and the micropores in the pore walls of SBA-15 disappear, is very close to the cloud point of the surfactant (85 °C in the case of Pluronic® P123), indicating a lower solvation of the PEO-chains.¹³¹ The similar behavior of micelle-encapsulated silica and silica-free micelles towards temperature variations suggests an enhanced interaction between solvated PEO-chains and the silica matrix at relatively low temperatures and a decreased interaction between dehydrated PEO-chains and the silica matrix at elevated temperatures. This is supported by the easier extraction of the surfactant out of SBA-15 materials that were synthesized at higher temperatures.¹³¹

Imaging of platinum replicas and analysis of low-pressure argon adsorption of SBA-15 enabled Galarneau *et al.* to elucidate the temperature dependent pore structure of SBA-15 more adequately.¹³¹ When synthesized below 80 °C they found that SBA-15 features microporous silica walls of about 4 nm, corresponding to the minimum distance between hydrated micelles in water. If these silica walls reproduce the topology of the hydration shells of the PEO chains in water, no microporous bridges should be expected between adjacent mesopores, as the protruding PEO-chains only extend about 1 nm from the micelle surface. However, when the synthesis temperature is higher than 80 °C, near the cloud point of Pluronic® P123, the

PEO-chains withdraw to the micelle surface and a net intermicellar attraction arises from PEO-PEO interactions between adjacent micelles, causing them to aggregate. As a result, more dense silica walls consisting of pore bridges (1.5 to 4 nm) between enlarged adjacent mesopores are generated. Further elevation of the synthesis temperature coincides with a further decrease of the micropore volume, an increase in pore size and larger pore bridges (1.5 to 5 nm) between the mesopores.

1.6 Ordered Mesoporous Organic-Inorganic Hybrid Materials

The integration of organic functional groups into inorganic frameworks has led to the discovery of organic-inorganic hybrid materials with well defined pore structures and unique properties. These materials combine the structural characteristics of ordered mesoporous silica with the chemical functionality of organic groups. By fusing the properties of organic and inorganic building units within the same network, an extremely versatile, robust and hydrothermally stable composite material is obtained. Moreover, the integration of functional groups in or on mesostructured materials broadens the applicability of these solids, making them potentially interesting for applications in catalysis,^{135–155} sorption,^{156–165} environmental technology,^{166–185} chromatography,^{186–192} nanoelectronics,^{193–200} sensing^{201–210} and drug delivery^{211–228}.

The synthesis of organic-inorganic materials based on organosilica building blocks, is feasible *via* three pathways: (1) post-synthetic functionalization, also referred to as grafting, (2) co-condensation of silica- and organosilica precursors and (3) direct condensation of bissilanes. These three pathways result in organic-inorganic hybrid ordered mesoporous materials, though with different properties.

1.6.1 Post-synthetic modification of silicious materials

Early organic functionalized mesoporous silicas were synthesized *via* post-synthetic modification (grafting) of the inner surfaces of ordered mesostructured silica materials. This procedure generally implies the condensation of organosilanes, most frequently of the type $(R'O)_3SiR$ (R = organic group), with free surface silanol groups of mesostructured silicas, as illustrated in Figure 1.23. These materials are ultimately composed of an inorganic framework with an organic layer grafted onto its surface. This functionalization procedure implies that the loading of organic groups is limited by the number of surface silanols.

This method of modification has several advantages. First of all, depending on the amount of grafted organosilane, the initial mesostructure of the silica material is generally preserved. Second, due to the vast number suitable organosilanes, a wide range of organic functionalized silicas can be developed with different chemical and physical properties, simply by varying the organic group R . Third, by using bulky organosilanes, these groups can selectively be grafted at the pore openings, leading to complete closure of the pores and sealing the air within, potentially leading to low- k materials.¹

¹Low- k materials are those which are characterized by small dielectric constants. These insu-

An issue which should be taken into consideration when grafting functional groups to the surface of mesostructured silica materials, is the homogeneity of this post-synthetic modification process. The homogeneous immobilization of organic groups on the surface of a silica material is controlled both by the accessibility of the pore system (diffusion properties), and the difference in reactivity between the surface silanol groups and the organosilane species. While the diffusion properties are determined by the pore system architecture (size, shape, symmetry, orientation and pore interconnections), the tendency of organosilane species to react with the surface or with each other (clustering) depends on the chemistry of the organosilane and on the synthesis conditions.

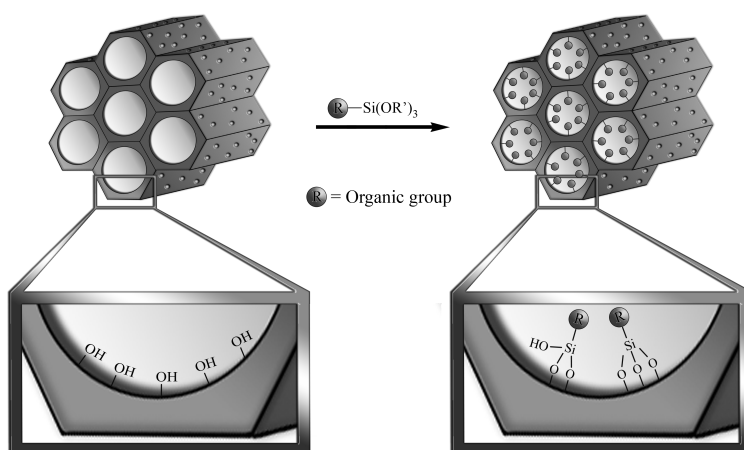


Figure 1.23: Post-synthetic functionalization of ordered mesoporous silica materials.

The possible competition between the diffusion of organosilanes in the pores of a mesostructured material and the reaction between organosilanes and silanols could lead to a more dense functionalization of the external surface and the pore openings than the pore interior. Moreover, accumulation of functional groups at the pore entrances can hinder diffusion of organosilane entities in the pores and can thus prohibit functionalization inside the pore channels.

As mentioned above, the diffusion properties of a silica material strongly depend on the pore system architecture. For instance, Kaliaguine *et al.* showed that the diffusion of *n*-heptane in SBA-15 is significantly controlled by the relative amount of micropores and secondary mesopores.²²⁹ If the micropore content is high, the diffusion is low and the process is similar to that of microporous materials such as zeolites. With decreasing micropore content, the diffusion becomes faster and is controlled more by secondary mesopores.

Other than a good knowledge of the diffusion properties of mesostructured materials in a grafting process, it is important that the condensation of organosilanes is controlled in order to avoid them reacting with each other instead of with the surface silanols. Self-condensation can lead to the formation of organosilane oligomers,

lating dielectrics are implemented in microelectronic devices in which they separate conducting parts.

which can block the pore channels. Parameters which influence the competition between self-condensation and grafting are type of organosilane, choice of solvent, reaction temperature, and amount of adsorbed water on the surface.^{230–233} As self-condensation of organosilanes is moisture sensitive, grafting is usually performed in dry non-protic solvents such as toluene.^{148,151,152} Another means to increase the tendency of organosilanes to react with the silica surface instead of with itself, is to catalyze the grafting process by preadsorbing amines to the silica surface.^{234,235} This amine-catalyzed grafting process can be performed at room temperature without the presence of water. The self-condensation of organosilane molecules can be avoided if a two-step process is followed in which the amine is preadsorbed on the surface and the excess amine is removed before the addition of the organosilane. Amines adsorb strongly to the acidic silanol groups making them more nucleophilic and thus more reactive towards silanes.²³⁵ Upon adsorption of the organosilane, nucleophilic attack occurs and a pentacoordinate intermediate is probably formed, as illustrated in Figure 1.24. If ammonia is used as a catalyst, the leaving group (usually alkoxy group) abstracts a proton from the amine, producing an alcohol, ammonia, and a functionalized silica surface. If a tertiary amine is used as a catalyst, the leaving group must abstract a proton from the silanol group.

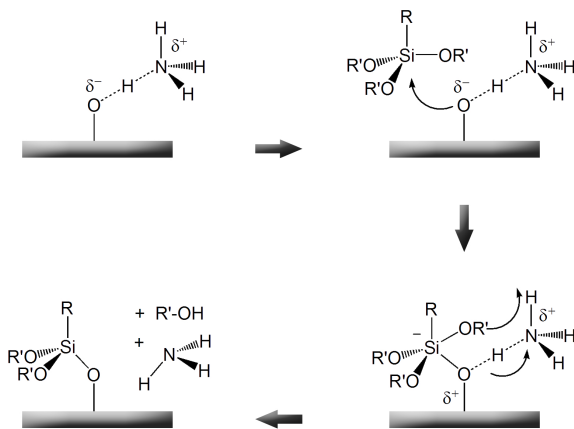


Figure 1.24: Amine-catalyzed grafting of organosilanes onto mesoporous silicas.

For the reasons described above, post-synthetic functionalization of silica materials is a very powerful technique to require organic-inorganic hybrid materials, but clearly has to be executed in a controlled manner.

1.6.2 Functionalized silicas by the co-condensation method

In contrast to the grafting technique, the co-condensation method is a one-pot synthesis procedure. Here, the organic-inorganic hybrid material is typically prepared through co-condensation of tetra-alkoxysilanes ($R'O$)₄Si with terminal tri-alkoxyorganosilanes ($R'O$)₃Si–R in the presence of a structure-directing organic template, as illustrated in Figure 1.25. This direct functionalization process can

occur under basic^{236–238}, acidic^{239–241} or neutral conditions^{242–244} in which the organosilane participates in the cooperative self-assembly process, making it very different from the grafting method. The involvement of the organosilane in the mesostructure formation implies that the chemistry of the functional group has to be taken into account when designing a synthesis procedure. If not, the organosilane can interfere in the formation of micellar aggregates, leading to disordered amorphous materials. For instance, if the organosilane consists of an amine group, working under acidic conditions implies protonation of the this functional group which may interact with silanol groups and prevent direct interaction of the surfactant with the condensating silicate species.

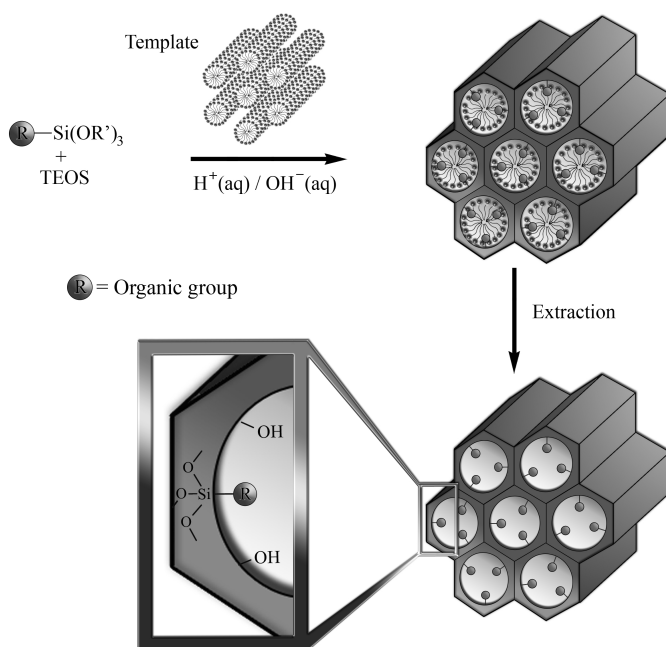


Figure 1.25: Synthesis of functionalized ordered mesoporous silica by means of the co-condensation method.

As the organic functionalities of these materials are incorporated into the framework during the formation of the mesostructure, they are usually more homogeneously distributed throughout the network compared to the organic groups of hybrid materials synthesized *via* the grafting method.²⁴⁵ However, the homogeneous distribution of the organic units is strongly dependent on the hydrolysis and condensation rates of the silica- and organosilica precursors. Rate differences for the hydrolysis and/or condensation of mixed precursors can lead to self-condensation and phase separation.

The main disadvantage of this method however, is the affect of organic content on the degree of mesoscopic order of the obtained hybrid materials. As the concentration of organosilane increases, the structural ordering of the material decreases and will ultimately lead to a completely disordered solid. Generally, the amount of

functional groups introduced by the co-condensation method cannot exceed 25 % surface coverage without complete loss of structural ordering.^{246–248} This limitation can be attributed to several aspects. Possibly the organic functions disrupt the formation of the silica network and interfere with the micelle formation. Especially when the organosilane constitutes very large organic groups, will the cross-linking of the silica units be compromised. The hydrophobic nature of the organic groups may also cause phase separation from more hydrophilic species.

1.6.3 Periodic Mesoporous Organosilicas

While both grafting and co-condensation procedures can produce various organic-inorganic hybrid materials, both methods have their advantages and disadvantages. The grafting method provides functionalized mesostructures without loss of mesostructural ordering while suffering from a relatively low density and uniformity of organic groups. On the other hand, the co-condensation method can lead to more homogeneously distributed organic groups in the mesostructure of the hybrid material, though, high organic loading can only be acquired at the expense of structural ordering.

Periodic mesoporous organosilicas (PMOs) are developed as an answer to the need for ordered organic-inorganic hybrid mesoporous materials with high organic content in which the organic and inorganic building units are homogeneously dispersed throughout the network. These hybrid materials are synthesized *via* the direct condensation of bridged organosilanes, typically $(R'O)_3Si-R-Si(OR')_3$ with R a bridging organic group, in the presence of a structure-directing agent, as illustrated in Figure 1.26.

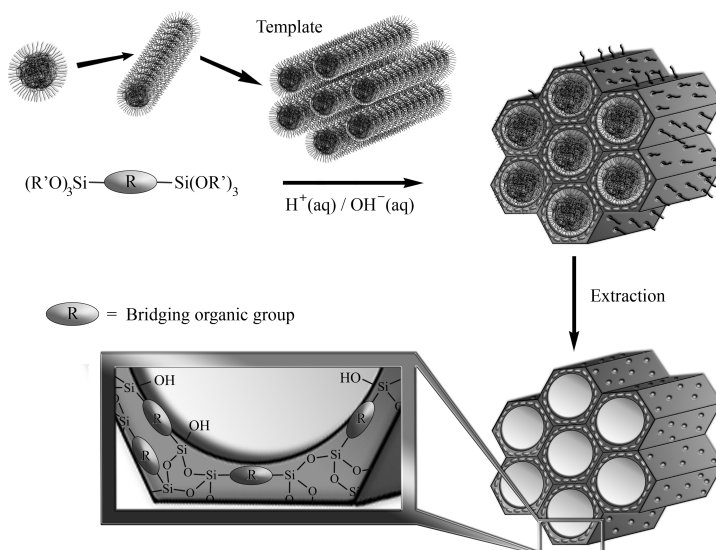


Figure 1.26: Synthesis of periodic mesoporous organosilicas in the presence of non-ionic poly(alkylene oxide) block copolymers.

Periodic mesoporous organosilicas are very unique in their compositional struc-

ture. The organic groups are covalently bonded within the siliceous network and hence are an intrinsic constituent of the mesoporous framework. The high loading and uniform distribution of organic groups in the pore walls of these open porous structures is a distinctive feature which allows for the easy tailoring of both the chemical and physical properties while preserving the structural stability of the porous framework.

While having a very high organic loading these materials can have very narrow pore size distributions, high specific surface areas, large pores, thick pore walls and large pore volumes. Furthermore, as the organic units are embedded in the channel walls, the pores remain completely open and fully accessible for eventual further modification of the surface functionalities.

In short, the disadvantages associated with the early organic functionalized mesoporous materials syntheses are nonexistent. Problems such as inhomogeneity of the functional groups, low organic loading, influence of organic content on structural ordering, pore narrowing, different reaction kinetics between mixed precursors, phase separation, ... are eliminated by using single precursors which contain bridging organic functions between polymerizable entities.

Being the focus of this PhD research work, the following chapter gives a more comprehensive discussion on PMOs, including historical evolution, synthesis strategies, PMO features, limitations and applications.

A comprehensive review on mesoporous materials, including detailed information on PMOs, has been published as a peer review article.²⁴⁹

Chapter 2

Periodic Mesoporous Organosilicas: Versatile Hybrid Materials

2.1 Constructing walls at a molecular level

Periodic mesoporous organosilicas were first introduced in the literature in 1999 by two separate research groups.^{250–252} The English chemist Geoffrey Alan Ozin, a professor at the university of Toronto, is considered as the founding father of PMOs. In his first paper on this novel class of porous solids, he describes the synthesis of an organic-inorganic hybrid material containing bridge-bonded ethene groups directly integrated into the silica framework, and designated these novel hybrids as periodic mesoporous organosilicas.²⁵⁰ Since their introduction, PMOs with various bridging organic groups have been synthesized.^{250–265} Figure 2.1 gives an overview of the organosilica precursors which have been employed in the development of these PMOs.

Built from organosilica building units, PMOs can be designed by molecular-scale tailoring of their functionalities. However, only a limited range of bridged organosilanes are suitable for developing ordered mesoporous hybrid frameworks. The required rigidity of the PMO pore walls implies that the organic functionality of the PMO precursor has to consist of a rigid structure, either as a short chain or a conjugated system. To avoid collapse of the pore walls it is important that the organic bridge is not too large. To assure sufficient cross-linking in the PMO pore walls, the bridging distance between two hydrolyzable inorganic species needs to be limited. Also, besides the required stability of the PMO precursors under the employed synthesis conditions, phase separation from the organic template has to be eliminated. To assure a strong template-precursor interaction, various reaction parameters can be adjusted: nature of template, pH, concentrations, temperature, aging conditions and the presence of certain additives. By tailoring these reaction conditions and matching them to the nature of the PMO precursor, the thermodynamics of mesostructure formation can strongly be enhanced while assisting the

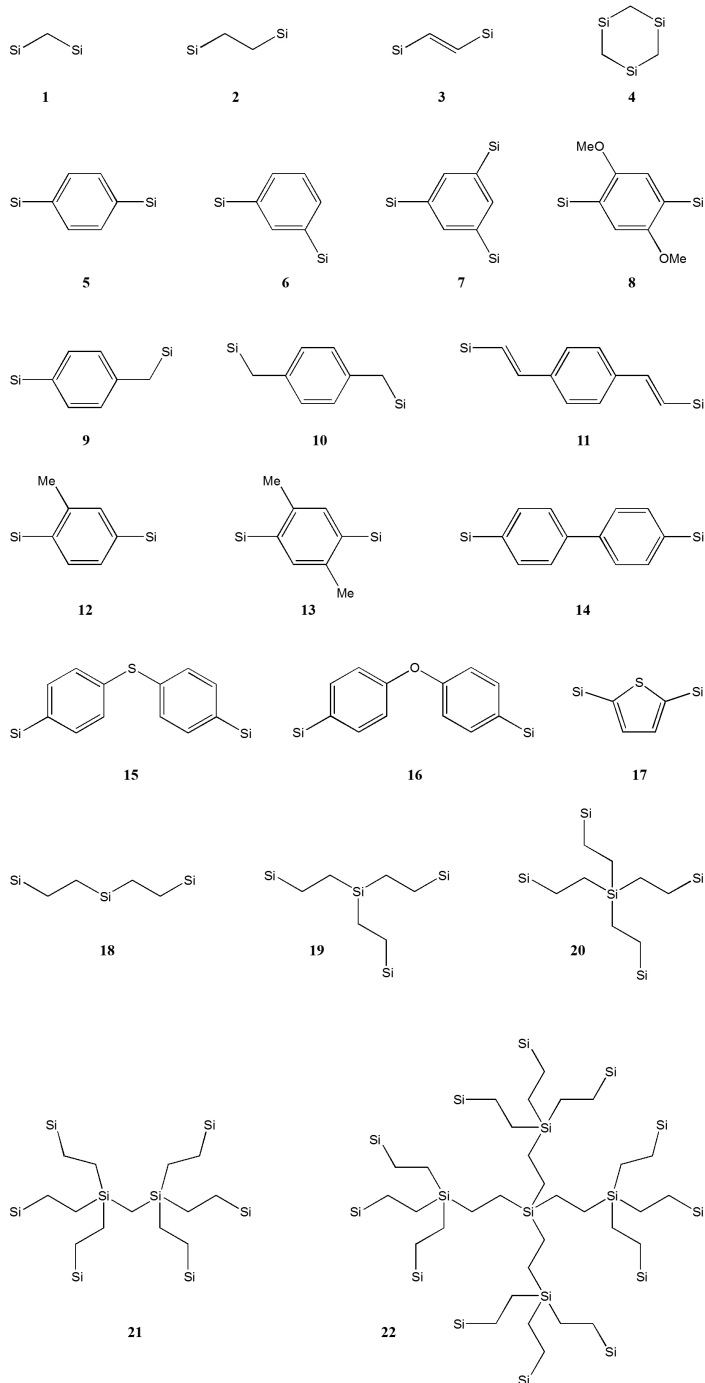
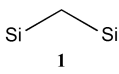


Figure 2.1: Organosilica precursors employed in the synthesis of PMOs. The terminal alkoxygroups on the silicon atoms have been omitted for reasons of clarity.

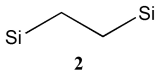
aggregation of the growing organosilica particles into an ordered porous framework.

2.1.1 Aliphatic Periodic Mesoporous Organosilicas



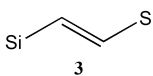
The simplest PMOs, in terms of functionality, are those composed of methylene-bridging organic groups (**1**). The first report on these methane PMOs comes from the group of Ozin.²⁶⁶

As is usually the case, these initial PMOs were prepared in basic medium with an ionic surfactant. The materials revealed hexagonally ordered mesopores of about 3 nm diameter. Most intriguing is the very high thermal stability of these materials, which can withstand temperatures as high as 600 °C under nitrogen (in an air atmosphere gradual decomposition of the material is observed above 400 °C). The synthesis of methane PMOs with larger mesopores (\approx 8.8 nm) was first reported by Holmes *et al.* who used Pluronic P123 as a template under acidic conditions with the aid of NaCl as an additive.²⁶⁷ The obtained PMOs were subsequently modified by grafting thiol groups onto the surface, leading to host materials for Ge nanocrystals. The authors found that methane PMOs were better hosts than mesoporous silicas, probably due to the hydrophobicity of the PMO, making it easier for the Ge precursor to diffuse into, nucleate, and grow inside the PMO pores. This study highlights the benefits of relatively thermally stable PMOs as hosts for the encapsulation of semiconductor nanomaterials. Other than these two reports, for unclear reasons, methane PMOs have not been studied in more detail. Maybe the costly price of the precursor or the limited pH range in which these materials can be synthesized (vide infra) has played a part in discouraging further advancement in the development of methane PMOs.



The majority of the literature reports on PMOs have been focused on the synthesis of ordered mesoporous ethane silicas, probably due to the wide commercial availability of its precursor 1,2-bis(triethoxysilyl)ethane (**2**). The first report was that of Inagaki *et al.*, who developed ethane PMOs with both 2D and 3D hexagonal pore arrangements under basic conditions.²⁵² Shortly after, Guan *et al.*²⁶⁸ and Sayari *et al.*²⁶⁹ reported on the synthesis of ethane PMOs with cubic symmetry ($Pm\bar{3}n$) by using ionic surfactants as templates under basic conditions. Interestingly, both groups obtained PMO particles with crystal-like external morphology. Since these first reports, numerous other publications on the synthesis of ethane PMOs with various framework structures, properties and external morphologies have been published.^{270–297} These studies describe different synthesis strategies involving various types of surfactant templates under diverse reaction conditions. After the initial reports on the synthesis of PMOs with ionic surfactants, considerable effort has been made to enlarge the pore diameters of these hybrid materials. As with traditional pure inorganic materials, researchers started employing nonionic block copolymers as templates for the synthesis of PMOs with relatively large mesopores. The first report on large pore PMOs was that of Fröba *et al.* in 2001.²⁷² By using Pluronic P123 as supramolecular template under acidic conditions, they developed ethane PMOs with pores of 6.5 nm. However, the obtained materials did not exhibit highly ordered pore structures. Zhu *et al.* however succeeded in preparing well

ordered ethane PMOs with 2D hexagonal pore structures with pore diameters of about 7.7 nm, also using P123 as a template.²⁷⁰ Although at first glance the syntheses procedures described by both groups seem very similar, they used different precursors, which may explain the difference in pore ordering. While the group of Fröba used 1,2-bis(trimethoxysilyl)ethane as precursor, Zhu *et al.* employed 1,2-bis(triethoxysilyl)ethane. This is an illustrative example of how small variations in reactions conditions may have tremendous effects on material properties. Though both precursors lead to the same material in terms of composition, they have completely different reactivities. The hydrolysis rate of organosilanes consisting of trimethoxy groups is faster than related organosilanes with triethoxy groups and thus implies a required optimization of the synthesis conditions. The degree of pore ordering can also be enhanced by adding inorganic salts to the synthesis mixture, as illustrated by Guo *et al.*²⁷⁹ Using NaCl as an additive, Pluronic P123 as a template and 1,2-bis(trimethoxysilyl)ethane as a precursor, they were able to synthesize highly ordered ethane PMOs with 2D hexagonal pore structures. Other than with large pore 2D hexagonal mesostructures, ethane PMOs have also been prepared with cubic pore structures by employing surfactant templates with higher hydrophilic/hydrophobic volume ratios. Using the poly(butylene oxide) containing triblock copolymer (EO₃₉BO₄₇EO₃₉) under acidic conditions, Jaroniec *et al.* developed well-ordered ethane PMOs with very large cage-like pores of about 10 nm.²⁷⁷ By employing K₂SO₄ as an additive and Pluronic F127 as a template under acidic conditions, Guo *et al.* were able to prepare ethane PMOs with cubic pore structures ($Im\bar{3}m$).²⁷⁸ Without the addition of K₂SO₄, only amorphous gel-like substances were obtained, indicating that the additive increases the organosilica-template interaction. Ethane PMOs with large cage-like pores with $Fm\bar{3}m$ symmetry have also been prepared by using F127 as a template under acidic conditions with the aid of KCl.²⁹²



Although most of the literature reports on PMOs are of ethylene-bridged materials, the saturated organic groups of these PMOs unfortunately offer limited possibilities for further chemical modification. In this respect, ethene PMOs with ethenylene-bridging groups (**3**) are far more interesting as these functionalities are easily modified by means of olefin chemistry. Since the first publication on ethene PMOs by the group of Ozin in 1999,²⁵⁰ only limited research has been done on these very promising materials, which is quite incomprehensible.^{298–305} Most of these reports involve ionic surfactants under basic conditions and lead to PMOs with relatively small mesopores (≤ 4 nm). A substantial part of the research on ethene PMOs with small mesopores has been done by the group of Mokaya.^{302–305} Their most important finding was the ability to prepare ethene PMOs which exhibit partial ordering in the pore walls. The first report of large pore ethene PMOs, synthesized with non-ionic block copolymers as surfactants, is that of Sayari *et al.* in 2004.³⁰⁰ Depending on the synthesis conditions, and in particular the employed surfactant, materials with medium (4 to 5 nm) and large (8 to 9 nm) mesopores could be developed. They also found that by adding butanol to the synthesis mixture, materials with much narrower pore size distributions were attained.

Several of these research groups also illustrated the potential of ethenylene-bridged

PMOs by modifying the ethene groups *via* a bromination reaction.^{250,300,301,304} Depending on the material and the reaction conditions, up to 30 % of the ethene groups could be modified.³⁰⁰ By chemically modifying ethene PMOs, these hybrid materials can be potentially interesting for catalytic or sorption properties as illustrated by the groups of Kondo³⁰⁶ and Yoshitake³⁰⁷, respectively. Kondo *et al.* prepared solid acid catalysts by modifying ethenylene-bridged PMOs *via* a two-step chemical modification, involving a Diels-Alder and a sulfonation reaction, as illustrated in Figure 2.2. The resulting solid acids showed high activity for various acid-catalyzed reactions and could be used repeatedly without deactivation.

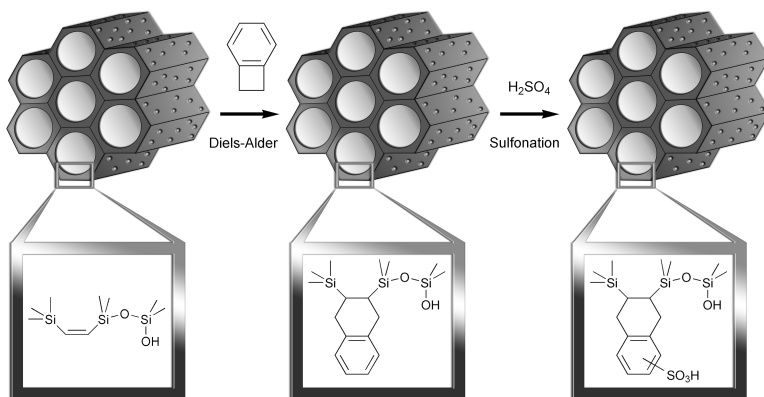


Figure 2.2: Synthesis of a solid acid PMO *via* a two-step chemical modification of an ethenylene-bridged PMO. (Redrawn from reference³⁰⁶)

Yoshitake *et al.* prepared ethylenediamine functionalized ethene PMOs by bromine addition of the accessible ethene groups and subsequent substitution with ethylenediamine.³⁰⁷ The obtained materials were screened for the adsorption of arsenate out of water, the results of which were compared to those of ethylenediamine functionalized ethane PMOs prepared by the direct co-condensation of 1,2-bis(trimethoxysilyl)ethane and 3-chloropropyl-trimethoxysilane and subsequent substitution with ethylenediamine. They found that the adsorption capacity of both materials were similar, but that the adsorption of arsenate was stronger on the ethylenediamine functionalized ethene PMOs. Moreover, when compared to MCM-41 type analogues, the adsorption capacity of the PMOs is almost two-fold, which can be ascribed to the nature of the pore wall surface.

Before moving on to more complex aliphatic PMOs, it is important to realize that although methane, ethane and ethene PMOs consist of relatively simple functional groups, it is crucial to tailor the synthesis conditions and match them to the nature of the PMO precursor so that ordered mesostructures may be obtained. Generally, the larger the precursor molecule the more difficult it is to synthesize a PMO material. However, when considering the organosilanes with methylene (**1**), ethylene (**2**) and ethenylene (**3**) bridges, this is not the case. By far, methylene-bridged PMOs are the most difficult to synthesize. The synthesis chemistry of these PMOs requests not only a controlled acid environment to slow down the hydrolysis and condensation rates of the precursor, but also requires the aid of inorganic salts to

increase the organosilane-template interaction. An enlightening report which deals with this issue is that of Zhao *et al.*³⁰⁸ They describe different synthesis strategies to develop methane, ethane and ethene PMOs and come to the conclusion that methylene-bridged PMOs require more rigorous synthesis conditions than the other two PMOs. As mentioned earlier, different precursors require different synthesis conditions, and in particular different acid concentrations, to allow precipitation and regular mesostructure formation. The acid concentration limits, within which Zhao *et al.* found that precipitation, irregular mesostructure formation, and regular mesostructure formation occurred for the different PMOs and for SBA-15, is shown in Figure 2.3

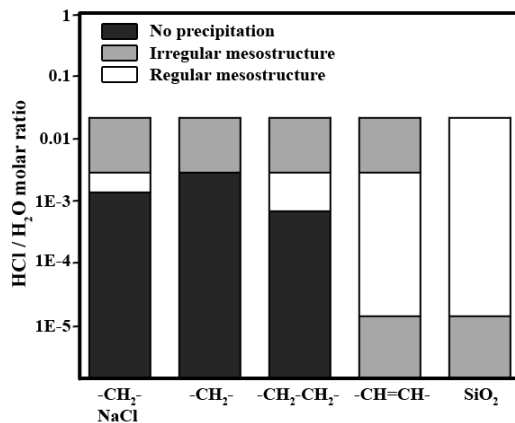


Figure 2.3: Schematic illustration of the HCl/H₂O ranges where no precipitation, irregular mesostructure formation, and regular mesostructure formation occurred for SBA-15, methylene-, ethylene-, and ethenylene-bridged PMOs.³⁰⁸

This figure shows that the acid concentration range in which methylene-bridged PMOs can be prepared, is very small and that the synthesis of these PMOs requires the aid of salts to allow mesostructure formation. The authors proposed that the difficulty in which methylene-bridged PMOs are obtained in acidic medium, is largely due to the conformation effect of the Si—CH₂—Si bond. The rigidity of the Si atoms due to the tetracoordinated C atom leads to weak organosilane-template interactions and delays the precipitation of the mesostructure despite the rapid hydrolysis and condensation rates of its precursor. With the aid of salts, the organosilane-template interaction can be enhanced and ordered mesostructures can be obtained.

Other than the above described methane, ethane and ethene PMOs, of which the precursors are bisilylated organosilanes, there are a few reports on aliphatic PMOs which have been prepared from multisilylated or branched precursors (see Figure 2.1, 4, **18-22**). In contrast to the other described PMOs, which have been studied independently by different research groups, these more complex PMOs have not been widely studied. In fact, all of them have been prepared by the group of Ozin. A first report on these types of aliphatic PMOs appeared in 2003 in *Science* and described the synthesis of organosilicas containing interconnected [Si(CH₂)₃]

rings.³⁰⁹ These cyclic PMOs represent a previously unknown class of nanocomposites in which two bridging organic groups are bound to each silicon atom. These hybrid materials could be synthesized both as powders and oriented films with mesopores of about 2.2 nm. The films revealed low dielectric constants and good mechanical and thermal stability, making them potentially interesting for micro-electronic applications. A second report on PMOs synthesized from multisilylated precursors also appeared in science in 2004 and described the synthesis of so-called periodic mesoporous dendrisilicas.²⁶⁴ They are prepared from dendrimers with terminal trialkoxysilyl groups (**20-22**), both under basic and acidic conditions, using ionic and nonionic surfactants, respectively. Under these conditions, materials with hexagonally ordered pore channels with diameters of about 2.5 nm and 8 nm could be attained. A third and as yet last report on these branched type PMOs describes the synthesis of bifunctional PMOs from single-source precursors (**18** and **19**), using Pluronic P123 as a template.²⁶³ Hexagonally ordered materials with mesopores in the range of 6 to 7 nm could be attained. It was found though that the ordering of these PMOs decreased as siloxane bridges were replaced by carbosilane bridges. Also, despite these materials revealing very thick pore walls (up to 6.8 nm), their thermal stability is only average (up to 250 °C).

2.1.2 Aromatic Periodic Mesoporous Organosilicas

The above described aliphatic PMOs synthesized from single-source precursors (**1-4** and **18-22**) are built up from hydrocarbon chains consisting of no more than two carbon atoms. This fact suggests that the flexibility of the bridging organic group should not be too high if ordered mesoporous materials are to be attained. Moreover, with increasing distance between two polymerizable inorganic species, the relative amount of silanol groups reduces. This implicates both a reduced organosilica-template interaction, and a decrease in cross-linking. For these reasons, much effort has gone into the development of rigid aromatic PMOs.

The first report of an aromatic PMO was (once more) of Ozin's group.²⁵¹ They used 1,4-bis(triethoxysilyl)benzene (**5**) and 2,5-bis(triethoxysilyl)thiophene (**17**) as precursors in the presence of an ionic surfactant as organic template. Strangely enough, when they followed the same procedure as previously reported by their group for ethenylene-bridged PMOs, almost all the organic moieties were cleaved from Si. Therefore, they adopted a mild acidic synthesis procedure involving hexadecylpyridinium chloride as organic template which led to hexagonally ordered materials of which most of the benzene and thiophene organic moieties stayed intact. The next report on aromatic PMOs was also published by the group of Ozin and described the synthesis of PMOs with tolylene (**12**), xylylene (**13**) and dimethoxyphenylene (**8**) bridging organic groups in acidic medium using ionic surfactants.²⁵⁴ These materials revealed hexagonally ordered mesopores of about 2.3 nm. Interestingly, this is the first report on PMOs in which the authors mention observing some degree of ordering in the pore walls, likely through $\pi - \pi$ stacking of the aromatic groups. Soon after, Inagaki *et al.* reported the synthesis of phenylene-bridged PMOs with crystal-like organization of organic bridges within the pore walls.²⁵⁵ These hexagonally ordered PMOs with mesopores of about 3.8 nm were synthesized in basic medium using octadecyltrimethylammonium chlo-

ride (OTAC) as a SDA. Besides low-angle peaks in the X-ray diffraction pattern, which could be assigned to the hexagonal ordering of the mesopores, the described benzene PMO also displayed distinctive sharp reflections in the wide-angle range, which revealed the existence of a periodicity of 0.76 nm on a molecular level. The crystal-like organization of the phenylene bridges within the pore walls was confirmed by high resolution TEM images, which revealed lattice fringes stacked along the pore channel axes with a uniform spacing of 0.76 nm. A model of the pore walls is illustrated in Figure 2.4. These materials exhibit high thermal and hydrothermal stability. Thermogravimetric analysis showed that benzene groups were kept in the walls up to 500 °C, while meso- and molecular scale periodicity was completely preserved even after boiling the material in water for 8 hours.

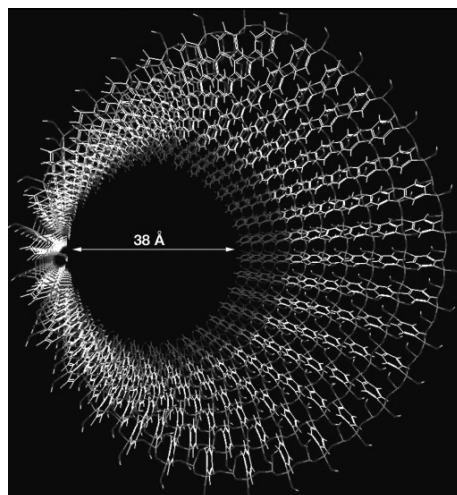


Figure 2.4: Model showing the pore wall structure of phenylene-bridged PMOs with crystal-like organization of benzene groups.²⁵⁵

A similar report on phenylene-bridged PMOs with crystal-like arrangement of organic groups in the pore walls, is that of Rocha *et al.*³¹⁰ They used different alkyltrimethylammonium surfactants with alkyl chain lengths from 14 to 18 carbons and this way managed to tune the mesopore size of these materials between 3.2 and 3.9 nm. Inagaki *et al.* also developed aromatic PMOs with molecular ordering in the pore walls by using 4,4'-bis(triethoxysilyl)biphenyl (**14**) as an organosilica precursor and OTAC as a SDA under basic conditions.²⁵⁶ The obtained PMO material with mesopores of about 3.5 nm, revealed five reflections in the wide-angle region of its XRD pattern. These reflections could be attributed to a crystal-like arrangement of biphenyl groups within the pore walls with a spacing of 1.16 nm. The periodicity of the biphenyl bridges was confirmed by high resolution TEM, which revealed lattice fringes on the pore walls with a spacing of 1.16 nm. The larger periodicity of 1.16 nm for these biphenylene-bridged PMOs when compared to the periodicity of 0.76 nm observed in phenylene-bridged PMOs, is due to the larger length of the biphenylene groups compared to the phenylene groups. In a subsequent report, Inagaki *et al.* also illustrated that the synthesis of aromatic PMOs

with crystal-like arrangement of organic groups in the pore walls, is not limited to linearly shaped organic bridges.²⁵⁹ In this report they describe the synthesis of phenylene-bridged PMOs with hexagonally ordered mesopores of about 4 nm and 0.76 nm periodicity in the pore walls, by using 1,3-bis(triethoxysilyl)benzene (**6**) as a precursor and OTAC as a template under basic conditions. Interestingly, the symmetry of the phenylene bridge had very little effect on the molecular scale periodicities in the pore walls. This was attributed to the tilted conformation of the nonlinear phenylene bridges.

The number of aromatic organosilica precursors that can produce PMOs with pore wall periodicity was further extended independently by Sayari *et al.*²⁶¹ and Fröba *et al.*²⁶² They used 1,4-divinylphenylene-bridged precursors (**11**) and OTAC as a SDA under basic conditions to obtain hexagonally ordered mesopores of about 3 nm with a periodicity in the pore walls of 1.19 nm. Surprisingly, Sayari *et al.* also found that without the presence of a surfactant template, the obtained materials still revealed periodicity in the pore walls.

Phenylene-bridged PMOs have also been synthesized with 3D cage-like pore structures.³¹¹ These PMO materials with pores no larger than 3.7 nm, could be obtained by using 1,4-bis(triethoxysilyl)benzene (**5**) as a precursor in the presence of either ionic or nonionic surfactants under acidic conditions. Unlike the above described aromatic PMOs which were synthesized under basic conditions, the cubic phenylene-bridged PMOs did not display any molecular periodicity in the pore walls, which can be attributed to the acidic environment in which they were prepared.

Other aromatic PMOs which have been synthesized under acidic conditions in the presence of nonionic surfactants are those with benzylene (**9**) and xylylene (**10**) bridging groups.²⁵⁸ These PMOs revealed 2D hexagonal pore structures with small mesopores (2-3 nm). However, the described PMOs clearly lack long-range pore ordering. Moreover, the xylylene-bridged PMO reveals a small pore volume (0.47 cm³/g) and a very weak capillary condensation step in the nitrogen physisorption isotherm. This probably can be explained by the large size and flexibility of the organic bridging groups which reduce the organosilica-template interaction. Similar to the results in this report, the 4-phenyl ether (**15**) and 4-phenyl sulfide (**16**) PMOs synthesized by the group of Ozin also exhibit weak to no structural ordering of pores which are on the meso-micro borderline.²⁶⁰ The authors attributed the poor pore ordering of the sulfur containing PMO to a less efficient packing of the sterically more demanding and rotationally restricted sulfur hinge group.

A last type of PMOs which has not been discussed yet are those synthesized from multisilylated aromatic precursors. However, so far there has only been one report on these type of PMOs. In 2002 Ozin *et al.* reported on the synthesis of a phenylene-bridged PMO with three point attachments synthesized from 1,3,5-tris(triethoxysilyl)benzene (**7**).²⁵⁷ However, the nitrogen physisorption measurements indicate that the materials are in fact microporous rather than mesoporous. Having high thermal stabilities (up to 600 °C), further research to obtain multisilylated aromatic PMOs is of interest and will most probably lead to future reports. Thus far all the above described aromatic PMOs reveal relatively small mesopores (≤ 4 nm). The first report of a phenylene-bridged PMO with relatively large mesopores was of Inagaki *et al.*³¹² PMOs with 2D hexagonally ordered mesopores of

7.4 nm could be attained under acidic conditions by employing Pluronic P123 as a SDA. However, these materials did not exhibit any crystal-like pore walls, once more due to the acidic environment in which they were synthesized. Nonetheless, thermogravimetric analysis showed that the PMO materials were stable up to 550 °C, which is even slightly higher than that of phenylene-bridged PMOs with crystal-like pore walls. The next report on large pore aromatic PMOs was of Fröba *et al.* in 2005.³¹³ They reported highly ordered PMOs synthesized from a thiophene-bridged precursor (**17**) using Pluronic P123 as a SDA under acidic conditions. According to this method, materials with 2D hexagonally ordered mesopores of about 6 nm could be obtained. While previous reports on thiophene-bridged PMOs showed significant Si-C cleavage, ²⁹Si MAS NMR and Raman measurements revealed the preservation of the Si-C bond under the acidic synthesis conditions employed by the group of Fröba. Having relatively high thermal stabilities (up to 400 °C) these PMO materials may be potentially interesting in applications at elevated temperatures. In a subsequent report of Fröba *et al.*, bifunctional PMOs containing different amounts of thiophene (**17**) and benzene (**5**) bridging groups have also been described.³¹⁴ For the bifunctional PMOs synthesized with the surfactant Pluronic P123, the specific surface areas decreased from 800 to 440 m² g⁻¹, whereas the pore diameters increased from 4.8 to 5.4 nm with increasing amount of thiophene groups in the materials. By employing Brij 76 as a surfactant, smaller mesopores (3.3 nm) and higher surface areas (\approx 1100 m² g⁻¹) were obtained for all the bifunctional PMO materials.

The preparation of large pore aromatic PMOs with well defined pore structures is a challenging task. In fact, only very recently have large pore aromatic PMOs with cubic pore structures been reported. In 2009, Jaroniec *et al.* described the synthesis of both phenylene- and thiophene-bridged PMOs with 3D cubic ($I\bar{m}\bar{3}m$) highly ordered mesopores in the range of 6.7 and 8.4 nm by employing Pluronic F127 as a surfactant template under acidic conditions.³¹⁵

2.2 Expanding the scope of PMOs

As can be deduced from Figure 2.1, the number of precursors which are suitable for PMO synthesis is quite limited. As mentioned above, this is due to the structural requirements of the bridged organosilanes (rigidity, size, reactivity). Besides these limitations it is not always easy to synthesize novel pure precursors. However, the scope of PMOs can be extended by co-condensation of precursors, which by themselves are structurally not suitable to synthesize PMOs, with precursors that are suitable for either PMO or pure silicious ordered mesostructured materials synthesis. In Figure 2.5 the possible co-condensation reactions which can lead to PMO materials from dual-source precursors, is illustrated.

This section will mainly focus on co-condensation reactions (1) and (2), which involve large and often flexible bridged organosilanes. In reaction (1) the organic functionalities in the PMO pore walls are diluted with inorganic species. This way, the framework structure can be preserved by assuring sufficient cross-linking of pure silicious species in the pore walls while incorporating large organic groups. Of course, as with the co-condensation method discussed in 1.6.2, the degree of mesoscopic order of the obtained PMO material depends on the organic content.

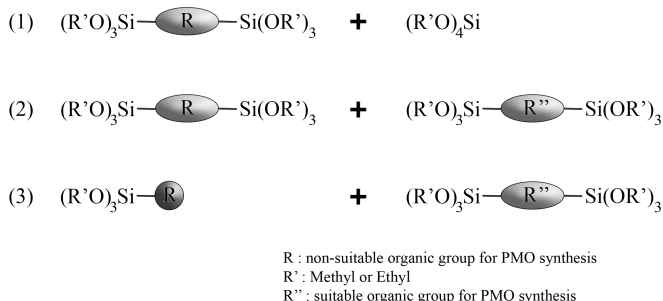


Figure 2.5: Possible co-condensation reactions which can lead to PMO materials from dual-source precursors.

If the organosilane consists of a very large organic group, the mesoporous framework structure will possibly only be preserved if small amounts of the bridged organosilane are used.

An illustrative example of co-condensation reaction (1) is that reported by Corma *et al.* in 2003.³¹⁶ They describe the synthesis of a PMO material with large chiral metal complexes integrated into the framework *via* co-condensation of TEOS with the bridged chiral vanadyl salen complex shown in Figure 2.6. From chemical vanadium analysis and ²⁹Si-MAS NMR, the authors estimated that 2.5 % of the Si present in the PMO material correspond to the silane groups of the salen complex. The obtained PMO material was active for the room temperature cyanosilylation of benzaldehyde with trimethylsilyl cyanide with an enantiomeric excess (ee) of 30 %. It was also found to be very stable and didn't display any leaching.

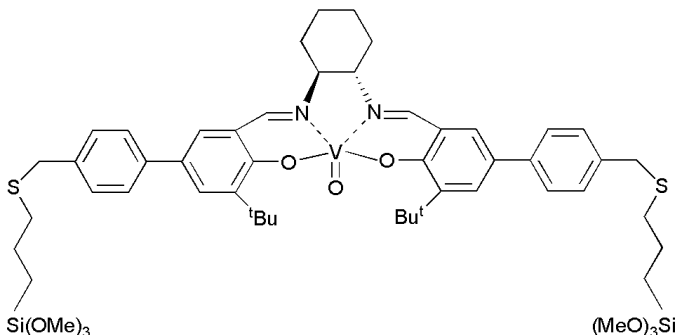


Figure 2.6: Bridged chiral vanadyl salen complex used by Corma *et al.* for the synthesis of enantioselective PMO catalysts.³¹⁶

Another fine example in which PMOs are synthesized *via* co-condensation of bridged organosilanes with tetra-alkoxysilanes was reported by Li *et al.* in 2006.³¹⁷ Enantioselective PMO catalysts could be obtained by co-condensating either one of the bridged organosilanes represented in Figure 2.7 (≈ 20 mol%) with TMOS and subsequently complexating them with $[\text{Rh}(\text{cod})\text{Cl}]_2$. These chiral catalysts exhibit higher conversions (up to 97 %) and ee values (up to 30 %) than their homoge-

neous counterparts (45 % conversion and 21 % ee) for the asymmetric transfer hydrogenation of ketones. For the asymmetric reduction of 2-acetylnaphthalene by 2-propanol, up to 61 % ee was obtained. These results illustrate that PMO materials are promising candidates for enantioselective catalysis. Co-condensation reaction (1) can however also lead to interesting PMOs for environmental applications, as will be illustrated in 2.3.

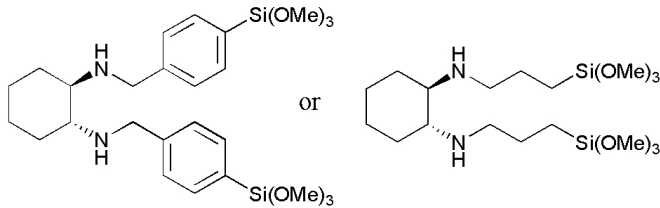


Figure 2.7: Bridged chiral ligands used by Li *et al.* for the synthesis of enantioselective PMO catalysts.³¹⁷

Co-condensation reaction (1) has also led to the development of photochemically responsive PMO materials. *Via* co-condensation of TEOS with the bridged organosilane *trans*-1,2-bis(4-pyridyl)ethylene (1.5 to 18 mol%), Garcia *et al.* synthesized a PMO which undergoes photochemical isomerization of the *trans*-configured bridges in the PMO pore walls to *cis*-configured bis(4-pyridyl)ethylene bridges, as illustrated in Figure 2.8.³¹⁸

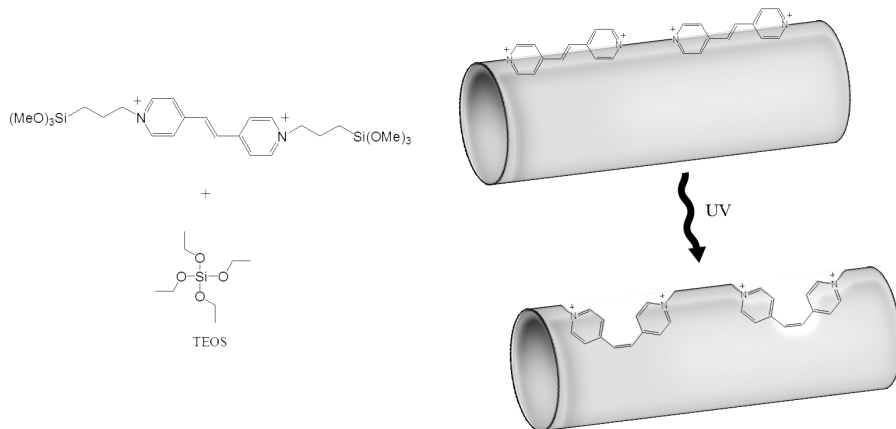


Figure 2.8: Photochemically responsive PMO reported by Garcia *et al.* in which *trans*-configured bridges in the PMO pore walls switch to *cis*-configured bridges upon radiation. (Redrawn from reference³¹⁸)

Via co-condensation reactions (2) and (3), illustrated in Figure 2.5, bifunctional PMOs can be synthesized with the aid of surfactant templates. When both precursors consist of bridged organic groups, PMOs with two different organic bridges that are covalently bonded within the PMO framework, are obtained. A nice ex-

ample in which bifunctional PMOs are synthesized through co-condensation of 1,2-bis(triethoxysilyl)ethane and 1,2-bis(triethoxysilyl)ethene in the presence of Pluronic P123 as a SDA, was reported by Khimyak *et al.*³¹⁹ The authors demonstrated that the distribution of the ethylene and ethenylene groups in the PMO pore walls can be controlled by prehydrolyzing the precursors. When both precursors are prehydrolyzed together, a homogeneous distribution of the two organic functionalities is observed, while separate prehydrolysis conditions lead to segregated regions of ethylene and ethenylene bridges. Besides co-condensating two rigid bridged organosilanes, large flexible bridged organosilane precursors can be co-condensed with rigid PMO precursors. For instance, Zhu *et al.* reported the synthesis of a bifunctional PMO through co-condensation of Cu^{II}-complexed *N,N'*-bis[(3-trimethoxysilyl)propyl]ethylenediamine with 1,2-bis(triethoxysilyl)ethane in the presence of Pluronic P123 (see Figure 2.9).³²⁰ Very interestingly, the authors were able to incorporate relatively large amounts of the bulky bridged organosilane ($\approx 23\%$) which is attributed to the complexation of the ligands to Cu ions whereby the flexibility of the bridged organic groups is reduced. The embedded Cu ions could subsequently be removed from the framework by acid leaching, giving rise to large pore bifunctional PMO materials with both small rigid and large flexible organic entities.

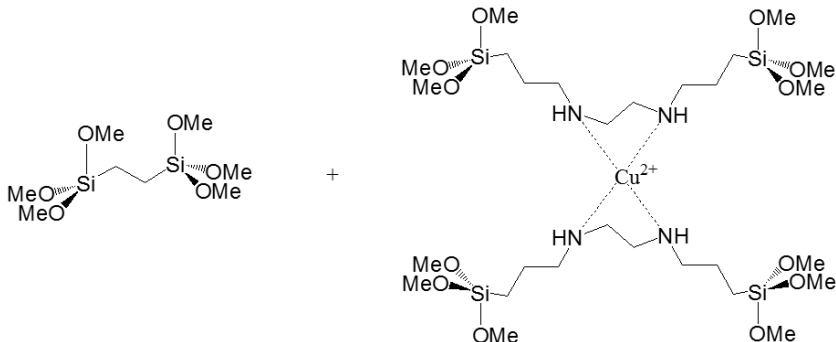


Figure 2.9: PMO precursors used by Zhu *et al.* for the synthesis of bifunctional PMOs.³²⁰

Co-condensation reaction (3) (Figure 2.5) involves co-condensation of bridged organosilanes, suitable for PMO synthesis, with terminal organosilanes. The resulting bifunctional PMOs consist of organic bridges in the pore walls and terminal organic groups in the pores interior. The synthesis of these types of bifunctional PMOs has been established and described by several groups. A series of bifunctional PMOs consisting of aliphatic or aromatic bridged organic groups in combination with pendant organic functionalities such as vinyl, amino, thiol, cyano, aromatic and heteroaromatic groups have been reported.^{298,321–332} Naturally, in order to obtain well ordered PMO materials, the bridged organic group has to be a rigid structure such as those depicted in Figure 2.1.

2.3 Applications of PMO materials

The ability to control the chemistry within the channel walls as well as the typical material characteristics such as pore structure and external morphology, offers scientists unlimited possibilities in developing materials with tailored properties. Depending on the application, different demands will be made on PMOs. These can range from mechanical and hydrothermal stability to insulating properties.

2.3.1 PMOs as supports and catalysts

PMOs are very promising materials for applications in catalysis, either directly as heterogeneous catalysts or indirectly as supports for homogeneous catalysts. Although the number of reports on catalytic applications is limited, these materials offer plenty of advantages over the common industrially applied microporous zeolites. The most obvious advantage is their pore sizes, which can be engineered from 2 to 30 nm, while retaining narrow pore size distributions. This broadens the applicability of PMOs as they can be potentially employed both by petrochemical or refining companies as by pharmaceutical companies. Another important aspect in catalysis is the stability of the catalyst or the support. The hydrothermal stability of ordered mesoporous silicas, such as MCM-41 and MCM-48, is poor due to the hydrolysis of their thin pore walls (1-2 nm).³³³⁻³³⁵ A great breakthrough in the development of ordered mesoporous materials with thick pore walls and large pores, has been the use of non-ionic triblock copolymers, like Pluronic P123 and F127, as SDAs. SBA-15, with typical wall thicknesses of 5 nm and more, can withstand a hydrothermal treatment in boiling water for 48 h without any sign of structural degradation.^{105,106,336} Moreover, the hydrothermal stability of PMO materials is greatly enhanced due to the presence of organic units in the framework. Ethylene-bridged PMOs have been reported to withstand a 60-day boiling treatment, without any significant degradation.^{279,282,337}

PMOs have proven to be suitable solid acid catalysts. As PMOs do not exhibit intrinsic Brønsted acid centers such as zeolites, acid functional groups have to be incorporated into the framework. Yang *et al.* synthesized well-ordered mesoporous PMOs functionalized with sulfonic acid groups *via* the co-condensation of ethylene- or phenylene-bridged organosilanes with 3-mercaptopropyltrimethoxysilane in the presence of H₂O₂ using Brij-76 as a SDA in acidic medium.³³⁸ These PMOs proved to be efficient catalysts for the condensation of phenol with acetone, forming Bisphenol A. The authors found that the PMOs prepared according to a grafting method showed a higher catalytic activity than those prepared *via* a co-condensation procedure. They attributed this finding to the higher accessibility of the acid sites since these are located mainly on the outer surface of the material. This phenomenon emphasizes the importance of controlling diffusion problems in heterogeneous catalysis.

Molnár *et al.* developed several sulfonic acid functionalized PMOs and evaluated their catalytic behavior.³³⁹ The authors illustrated that the catalytic performance of PMO-based materials noticeably exceed those of functionalized ordered mesoporous materials such as MCM-41 and SBA-15. The PMO materials also exhibited a higher stability in the flow reactor studies (alkylation of phenol in the gas phase),

which was attributed to the higher stability of the phenylene-bridged framework under the employed reaction conditions.

Recently, Alauzun *et al.* illustrated that bifunctional PMOs consisting of both acidic and basic groups can be synthesized.³⁴⁰ Obviously the simultaneous incorporation of antagonistic functionalities in a PMO framework is not possible. Therefore, in a first step the authors synthesized a bifunctional PMO through co-condensation of a disulfide-bridged organosilane with a protected terminal aminopropylsilane and tetra-alkoxysilane in the presence of Pluronic P123. Subsequently, reduction of the disulfide bridges to thiol groups, followed by their oxidation in sulfonic acid groups and deprotection of the amino groups gave rise to a PMO material containing two antagonist functionalities (see Figure 2.10). Although these materials were not tested for catalytic reactions, they are potentially of great interest and are ideally suited for acid-base catalysis.

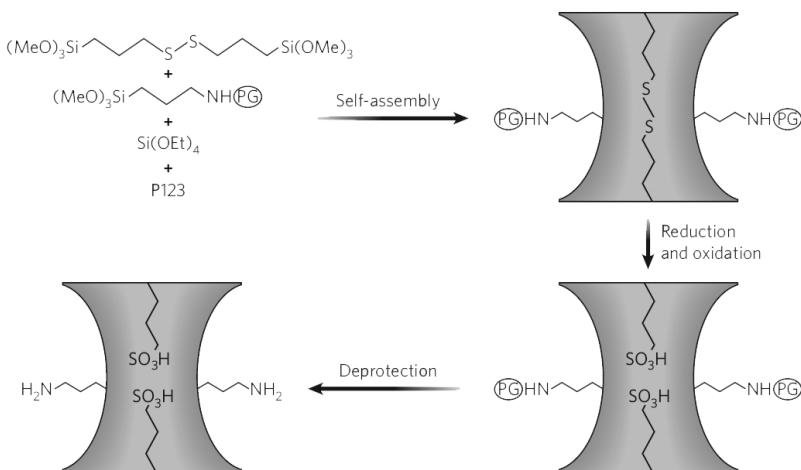


Figure 2.10: Synthesis strategy reported by Alauzun *et al.* for the preparation of PMOs which consist of both acidic and basic functional groups.³⁴⁰

Besides PMOs being used as solid-acid catalysts, they can also be applied in epoxidation- and selective oxidation reactions. By introducing heteroatoms in the framework, catalytic sites can be created within the channel walls of PMOs. Recently, Singh *et al.* synthesized vanadium-containing ethane-PMOs *via* the direct condensation of 1,4-bis(triethoxysilyl)ethane in the presence of vanadyl sulfate, under basic conditions.³⁴¹ These hybrid materials exhibit a high activity and stability for the liquid-phase epoxidation reaction of styrene with peroxides as oxidants. The authors attributed the high catalytic activity and improved epoxide selectivity of the vanadium-containing PMOs, when compared to vanadium-containing MCM-41, to the more hydrophobic environment inside the pore channels. Also, spectroscopic data confirm the absence of crystalline V₂O₅ species and show the existence of isolated and highly dispersed vanadium sites in the framework of the PMO materials. The same group also developed chromium-containing ethane-PMOs *via* the direct condensation of 1,4-bis(triethoxysilyl)ethane, under basic conditions, in the presence of chromium nitrate.³⁴² The catalytic activity in the liquid-phase oxidation of

cyclohexane, was tested. When compared to conventional chromium-containing MCM-41, the PMOs demonstrate better catalytic activities while exhibiting a higher stability. The higher catalytic activity is attributed to the textural and morphological features of the PMO materials, next to the improved hydrophobicity.

Another report on metal-containing PMOs is that of Melero *et al.*³⁴³ They describe the synthesis of titanium-functionalized mesostructured materials with different organic contents, using titanocene dichloride in the presence of non-ionic surfactants in acidic media. The catalytic activity of the obtained materials, with different hydrophobic properties, was evaluated for the epoxidation of 1-octene with hydroperoxides. The authors showed that surface hydrophobization through post-synthetic silylation, enhances the catalytic activity of the titanium-containing hybrid materials. Titanium-containing PMO materials, while exhibiting low metal content, showed a higher catalytic activity per titanium site than silica-based hybrid materials. Moreover, the removal of hydrophilic silanol groups in titanium-containing PMOs causes a great improvement of the catalytic activity. This contribution further emphasizes the importance of the ability to control the chemistry within the channel walls of PMO-materials. As the hydrophobicity, among other characteristics, can easily be controlled, PMOs can be tuned aiming to fulfill the necessary demands.

2.3.2 PMOs for chromatographic applications

Conventional syntheses of PMO materials generally lead to non-uniform particles with irregular external structures. For their use in chromatography however, it is highly desirable to obtain spherical particles with very narrow pore size distributions. Usually, the synthesis of monodispersed spherical particles is based on the Stöber method.³⁴⁴ Herein, mild basic synthesis conditions are used by employing ammonia solutions in ethanol, rather than the commonly applied sodium hydroxide solutions.

Inagaki *et al.* reported on the synthesis of phenylene-bridged PMO particles ($\approx 0.8 \mu\text{m}$) with spherical morphology.³⁴⁵ Investigation of the particle growth *via* electron microscopy lead the authors to the conclusion that mild basicity and very low hydrolysis and condensation rates are required for the formation of spherical particles. However, ethylene-bridged PMOs with spherical morphology (between 1.5 and 2.5 μm) and narrow pore size distributions have also been synthesized in sodium hydroxide solutions in the presence of CTAC as SDA.³⁴⁶ These PMOs were synthesized both under conventional hydrothermal, and non-conventional microwave heating procedures. The former method produced octadecahedral shaped particles of about 8.0 μm , while the latter produced spherical particles of about 2.2 μm . The separation performance of these materials in HPLC was investigated for a mixture of eight aromatic substances with medium to high hydrophobic character. Separation of all substances was achieved with both PMOs, although, as a consequence of the morphology, the spherical PMO particles demonstrated clear separation improvement.

Fröba *et al.* also developed spherical phenylene-bridged PMO particles with average diameters tunable between 3 and 15 μm (see Figure 2.11).³⁴⁷ However, these

were not synthesized according to the Stöber method. Instead, the PMO materials were synthesized under acidic conditions with Pluronic P123 and CTAB as SDAs and ethanol as a co-solvent. The obtained materials, which revealed narrow pore size distributions, proved to be suitable for HPLC and were successfully implemented for the separation of three different mixtures with a wide range of polarities. Through the combination of silanol groups and organic bridges in the framework of the PMOs, the properties of a normal and a reversed phase are merged into one material.

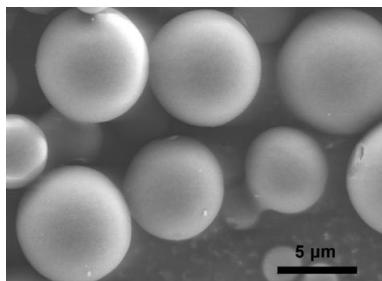


Figure 2.11: SEM image of phenylene-bridged PMO with spherical morphology, prepared by Fröba *et al.*³⁴⁷

The development of mesoporous organosilica spheres for HPLC has also been investigated by Li *et al.* In a first report they describe the synthesis of a bifunctionalized mesoporous organosilica through co-condensation of phenyltrimethoxysilane with 1,2-bis(trimethoxysilyl)ethane using ethanol as a co-solvent and Pluronic P123 in combination with CTAB as SDAs in an acidic medium.³⁴⁸ These materials, which exhibit wormhole-like mesostructures, can however not be considered as PMO materials as the pores are not periodically arranged. Nonetheless, their compositional and morphological nature make them interesting as packing material for HPLC columns. These bifunctional materials demonstrated to be promising stationary phases to separate polycyclic aromatic hydrocarbons. They exhibit relatively large retention factors and offer significant column stability at high pH.

In a second report, Li *et al.* described the synthesis of another bifunctional mesoporous organosilica with spherical morphology through co-condensation of a chiral organosilane (see Figure 2.12) with 1,2-bis(trimethoxysilyl)ethane in a basic medium using OTAC as a SDA and ethanol as a co-solvent.³⁴⁹



Figure 2.12: Precursors used by Li *et al.* for the synthesis of spherical bifunctional mesoporous organosilicas for HPLC.³⁴⁸

The authors found that, by slowing down the condensation rate of hydrolyzed silane species, higher concentrations of ethanol and the chiral precursor are favorable for

the formation of perfect microspheres of about $5\text{ }\mu\text{m}$ with smooth surfaces. These bifunctionalized mesoporous organosilica spheres were used as a chiral stationary phase in HPLC for the separation of racemic amino acids. When compared to a commercial silica onto which the same chiral organosilane was grafted, the bifunctional material exhibited higher retention, better selectivity and resolution for the amino acids, clearly illustrating the potential of PMO and related materials for chromatography.

2.3.3 PMOs as adsorbents in environmental technological applications

The ability to control the functionality within the channel walls in combination with the large surface areas and the high pore surface accessibilities which PMOs can exhibit, make these materials ideal to be used in the field of sorption, such as in waste water purification. Shi *et al.* synthesized a thioether functionalized PMO material *via* co-condensation of 1,4-bis(trimethoxysilyl)propane tetrasulfide (see Figure 2.13) with TEOS.³⁵⁰ This novel ordered mesoporous material is suitable for selectively removing high quantities of Hg^{2+} from aqueous solutions containing cations Pb^{2+} , Cd^{2+} , Zn^{2+} and Cu^{2+} . A PMO containing 15 % of tetrasulfide showed an exceptional Hg^{2+} adsorption capacity of up to 2700 mg g^{-1} , which is about one order higher than that of ordinary polythioether chelating resins.

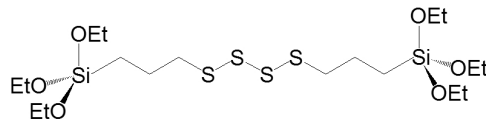


Figure 2.13: Precursor used by Shi *et al.* for the synthesis of PMOs for the adsorption of Hg^{2+} out of water.³⁵⁰

Jaroniec *et al.* synthesized a PMO with tris[3-(trimethoxysilyl)propyl]isocyanurate groups *via* co-condensation with TEOS in the presence of Pluronic P123.³⁵¹ Surprisingly, they were able to incorporate 25 % of these very large organic groups in the PMO pore walls while preserving an ordered mesostructure. The materials revealed a high affinity and high adsorption capacity for mercury. In a subsequent report, the same authors reported the synthesis of a bifunctional PMO containing the same heterocyclic rings as in their previous report, in combination with mercaptotripropyl ligands which are located on the surface of the mesopore walls (see Figure 2.14).³⁵² These bifunctional materials were prepared by direct co-condensation of 3-mercaptopropylsilane with tris[3-(trimethoxysilyl)propyl]isocyanurate and TEOS under acidic conditions in the presence of Pluronic P123. The obtained PMOs showed metal-chelating properties due the presence of nitrogen, oxygen and sulfur elements in the incorporated functional groups. As a result the PMOs revealed high mercury adsorption capacities (4 to $6\text{ mmol g}^{-1}\text{ Hg}^{2+}$). Moreover, these were greater than the combined adsorption capacities reported for thiol-functionalized mesoporous silicas and isocyanurate-containing PMOs with comparable amounts of incorporated ligands.³⁵²

Another report on PMOs used for the adsorption of Hg^{2+} is that of Yang *et al.*³⁵³

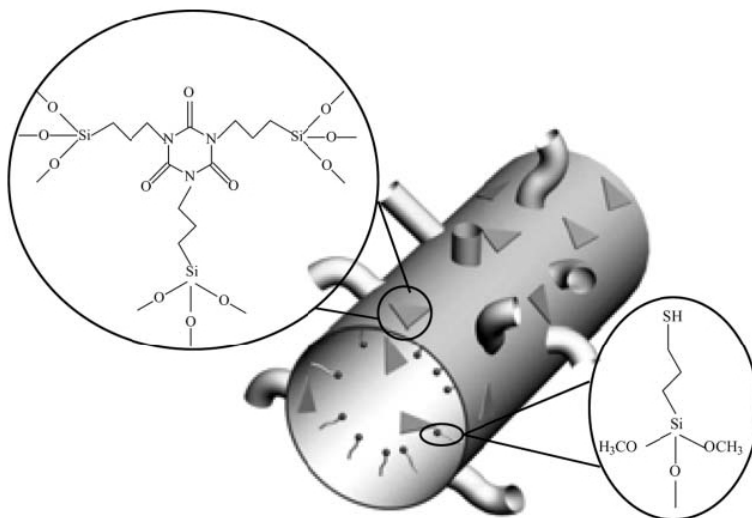


Figure 2.14: Bifunctional PMO synthesized by Jaroniec *et al.* for the adsorption of Hg^{2+} out of water.³⁵²

They describe the synthesis of thiol-functionalized ethylene-bridged PMOs by co-condensation of 1,2-bis(triethoxysilyl)ethane with 3-(mercaptopropyl)trimethoxysilane using nonionic surfactants in acidic medium. The obtained materials revealed hexagonally ordered mesopores of 1-3 and 4-6 nm by using the surfactants Brij-76 and Pluronic P123, respectively. The authors found that while the Hg^{2+} adsorption capacities of the materials increase in proportion to the amount of thiol groups incorporated, the Hg/S ratios decrease. The Hg/S ratio can give an indication of the amount of thiol groups accessible to Hg^{2+} . In the light of this relationship, the authors found that almost all thiol groups are accessible to Hg^{2+} when the PMOs exhibit large mesopores. For the materials with large quantities of thiol groups (40 %), lower Hg/S ratios are observed due to their disordered microporous nature, which does not allow all the Hg^{2+} ions to diffuse through the pores and reach the thiol functions. The ability of the thiol-functionalized mesoporous ethylene-bridged PMOs to remove other heavy metal ions in the presence of Hg^{2+} was also investigated. The presence of Cd^{2+} , Cu^{2+} , Zn^{2+} and Cr^{3+} , did not affect the adsorption of Hg^{2+} in PMOs synthesized with Brij-76. However, the PMOs synthesized with Pluronic P123 also revealed an affinity for the other heavy metal ions, probably due to the larger pore sizes. This phenomenon illustrates that the mesoscopic structure of a material plays a significant role in its adsorption behavior.

2.3.4 PMOs as biosensors

Owing to the stability, selectivity, high density of binding sites and ease of modification, PMOs are suitable candidates to be employed as optical indicators of target binding. Recently porphyrin-embedded diethylbenzenebridged PMOs were prepared and used for the detection of volatile organic compounds without any aid of lasers or highly sensitive spectrophotometric equipment.³⁵⁴ The authors showed

that these PMOs containing porphyrins, of which their spectrophotometric characteristics are extremely sensitive to changes in their immediate environment, exhibit binding of TNT (2,4,6-trinitrotoluene), RDX (cyclotrimethylenetrinitramine), *p*-nitrophenol and *p*-cresol, with selective adsorption of TNT over the other analytes. These materials prove to be very interesting and, after further optimization, could be employed in the detection of low level concentrations of explosives.

2.3.5 PMOs as low-*k* dielectric films

The most important property requirements for materials to be suitable for low-*k* applications are thermal stability, mechanical stability and moisture resistance. Therefore, due to their high organic content, easily controllable hydrophobicity and large pore volumes, PMO materials, under the form of thin films, are very suitable as low-*k* dielectrics. Besides the typical spin- and dip-coating methods, the EISA (Evaporation Induced Self-Assembly) technique is especially suitable for the development of such PMO films. In the EISA approach, an excess of a volatile solvent is used to ensure that the initial concentration of the SDA remains below the critical micellar concentration. Upon addition of the reaction solution to the substrate, the rapid evaporation of the solvent induces self-assembly of the bridged silanes.

Brinker *et al.*, the first group to apply the EISA approach, prepared ethane-PMO films, co-condensed with varying concentrations of TEOS and further hydrophobized with hexamethyldisilazane.³⁵⁵ Capacitance measurements indicated a decrease in dielectric value with increasing organic content, illustrating the potential of PMOs as low-*k* dielectrics.

To increase the organic content beyond the stoichiometry $\text{SiO}_{1.5}\text{R}_{0.5}$, PMOs in which each Si atom is bound to two or more bridging organic groups have been developed. As mentioned in 2.1 (p 45) Ozin *et al.* developed PMOs as oriented thin films consisting of interconnected $[\text{Si}(\text{CH}_2)]_3$ rings, by spin coating onto glass plates.³⁰⁹ These PMO films, exhibiting high mechanical stabilities, were synthesized with various organic content from mixtures of TMOS and $[(\text{EtO})_2\text{Si}(\text{CH}_2)]_3$. Also here, the films displayed a linear decrease in dielectric value with increasing organic content.

PMOs exhibit polar silanol groups on the channel walls. Further hydrophobization can be achieved by a post-synthetic modification with, for example, hexamethyl-disilazane. Another possibility is thermally-induced self-hydrophobization. Ozin *et al.* reported a silanol-consuming transformation of methylene bridges to terminal methyl groups in methylene-bridged PMOs, which plays an important role in silanol-elimination.²⁶⁶ This reaction, illustrated in Figure 2.15, involves the transfer of a proton from a silanol to a bridging group, leading to the cleavage of one Si–R–Si bridge and the simultaneous formation of one new Si–O–Si bridge. This transformation consumes silanol groups and creates a hydrophobic surface with terminal organic groups, resulting in materials with lower *k* values.

In a subsequent report, Ozin *et al.* illustrated that PMO thin films with methylene, ethylene, ethenylene and phenylene bridges can be synthesized *via* the EISA approach.³⁵⁶ Moreover, they describe the influence of organic content and self-hydrophobization on the dielectric constant of methylene- an ethenylene-bridged

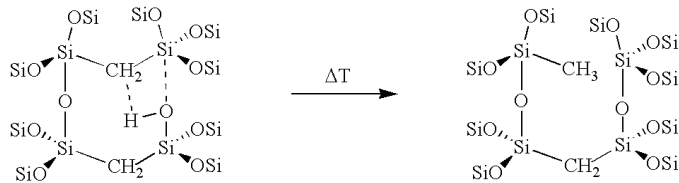


Figure 2.15: Schematic representation of the thermally-induced self-hydrophobization reported by Ozin *et al.*²⁶⁶

PMOs. To investigate the effect of organic content a series of methylene- and ethenylene-bridged PMOs was synthesized through co-condensation with different amounts of TMOS. For both types of PMOs (calcined at 300 °C), the dielectric constant decreased from > 4 (pure silica) to ≈ 2.9 (pure PMO). When the methylene-bridged PMO films were further heated to 400 °C and 500 °C, the dielectric constant further decreased to 2.2 and 1.9, respectively. In the case of the ethenylene-bridged PMOs, the dielectric constant also decreased to about 1.9, however little difference in the measured k value was observed above 400 °C. When the films were heated to 600 °C, the k value increased dramatically to > 8, probably due to mesostructure deterioration. The moisture resistance of the PMO films, treated at different temperatures and consisting of different amounts of organic content, was also investigated by exposing the films to 60 and 80 % relative humidity environments. The authors found that, due to water adsorption, the films with low organic content showed dramatic increases in dielectric constants upon exposing them to the humid environments. On the other hand, the dielectric constants of the films with higher organic content were effected significantly less, which indicates an increase in hydrophobicity compared to pure silica. Moreover, the k value of the PMO films that were thermally treated at 550 °C were unaffected by the exposure to moisture, indicating a material with extremely high resistance to humid environments. Other important approaches in developing low- k PMOs are increasing the porosity and pore sealing. The latter approach refers to air-trapping ($\varepsilon_R \approx 1$) by blocking the pore openings.³⁵⁷ By combining these different techniques: PMO synthesis with high organic content, thermally-induced self-hydrophobization and air-trapping, ultra-low- k materials are obtained which can be applied in the microelectronics industry.

Chapter 3

Olefinic PMO precursors: Exploring Novel Synthesis Strategies

The first step in designing PMO materials with exceptional properties, is the synthesis of a pure PMO precursor. In the case of ethylene-bridged PMOs, this first step has been somewhat neglected in the literature. As the synthesis of PMO materials is commonly conducted by materials chemists, whose knowledge of organometallic chemistry and olefin metathesis may be limited, this scientific neglect in PMO synthesis is probably due to the lack in understanding the catalytic reaction involved in the synthesis of 1,2-bis(triethoxysilyl)ethene. On the other hand, since the initial report on the synthesis of this precursor, organometallic chemists have made no real efforts in synthesizing it as a pure diastereoisomer. Furthermore, to date no other olefinic PMO precursors have been developed. Therefore, trying to combine the knowledge of olefin metathesis and materials chemistry, the initial part of this research work has been focused on the synthesis of both diastereoisomeric ethene-PMO precursors, and a completely novel butene PMO precursor.

3.1 Introduction to olefin metathesis

Derived from the Greek words *meta* (change) and *thesis* (position), metathesis is the exchange of segments of two substances. In the case of olefin metathesis, two new olefins are formed through carbene (alkylidene) exchange between two starting olefins, as shown in Figure 3.1.

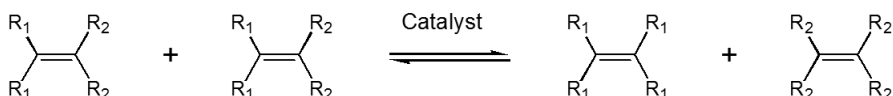


Figure 3.1: The exchange (*meta*) in position (*thesis*) of segments of two olefins leading to the formation of two new olefins.

3.1.1 Unraveling the olefin metathesis mechanism

Being a carbon-carbon coupling reaction, olefin metathesis is a very important and powerful catalytic reaction which has been and is still being studied extensively worldwide. Essentially, the development of olefin metathesis was driven by the petrochemical industry. While investigating the polymerization of norbornene, researchers at Dupont unexpectedly produced a highly unsaturated polymer *via* opening of the strained norbornene ring.³⁵⁸ In a similar way, while studying the polymerization of propene, Eleuterio *et al.* unexpectedly found the formation of an ethylene-propylene copolymer.³⁵⁹ Moreover, besides propene, the off-gas of this reaction also contained ethene and butene as byproducts. Other than these findings, the group of Natta found that cyclopentene could be polymerized *via* a ring opening metathesis polymerization reaction, illustrating that highly strained olefins are not necessarily required for polymerization.^{360,361} In the late 1960s, the group of Calderon at Goodyear was the first to realize that the above described findings were related by recognizing that the chemistry of both cyclic and acyclic olefins was the same.^{362–364} Using labeling studies, they also discovered that the reactions leading to these unexpected products involve the cleavage and reformation of carbon-carbon double bonds. Accordingly, they named the reaction olefin metathesis. However, the structure of the active catalytic species and the mechanism of olefin metathesis were still unknown. In fact, the elucidation of the reaction mechanism has been a subject of intense debate in the literature.^{362–374} As chemists started to realize that metathesis could offer great potential in organic synthesis, many researchers made proposals as to how olefin metathesis could take place. After all, without a clear understanding of the reaction mechanism, the development of novel and better catalysts would be a matter of trial and error.

It was not until 1971, with the revolutionary report of Yves Chauvin and his student Jean-Louis Hérisson of the Institut Français du Pétrole, that some light was shed on the true olefin metathesis mechanism.³⁷⁵ They proposed that the catalyst that initiated the olefin metathesis reaction was a metal carbene (a complex in which the metal is bound to a carbon *via* a double bond). In a first stage, the metal carbene (also referred to as alkylidene) reacts with an olefin *via* a [2+2]-cycloaddition to form a metallocyclobutane intermediate (see Figure 3.2). This intermediate cleaves *via* a [2+2]-cycloreversion to form an ethene and a new metal carbene. While the liberated ethene molecule contains one carbon from the catalyst and one carbon from the starting olefin, the metal center of the catalyst is attached to an alkylidene from the substrate alkene. In a next step this metal alkylidene reacts with a new substrate alkene molecule to yield another metallocyclobutane intermediate which, upon cleavage in the forward direction, yields a new olefin and a metal methylidene. This metal methylidene enters another catalytic cycle and propagates the olefin metathesis reaction in which alkylidene species are exchanged.

While previously proposed mechanisms could not be reconciled with experimental observations, the mechanism of Chauvin and Hérisson proved to be consistent with earlier results. Their mechanism received strong support from experimental investigations by Robert H. Grubbs, Thomas J. Katz and Richard R. Schrock, and is now generally accepted.

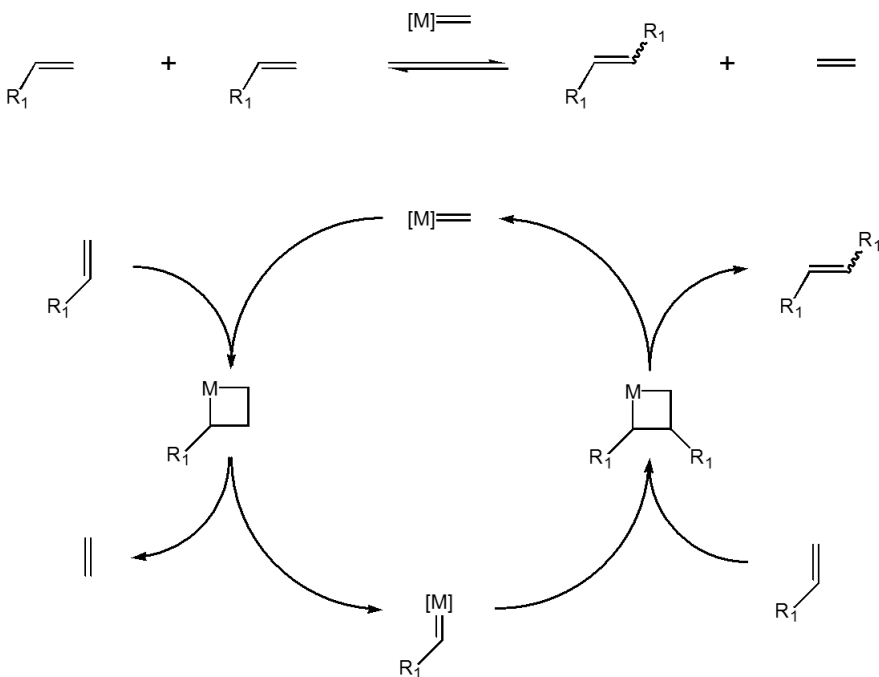


Figure 3.2: Olefin metathesis mechanism reported by Chauvin and Hérisson.

3.1.2 Olefin metathesis catalysts

Early metathesis catalysts were ill-defined (unknown propagating species), sensitive to air and moisture and revealed short life times. However, with the report of Chauvin and Hérisson, scientists acquired knowledge of the active catalyst structure and a good understanding of its nature in the olefin metathesis mechanism, providing them with an essential starting point to design novel well-defined efficient metathesis catalysts. Metal carbenes are the smallest fragments that allow olefins to exchange one carbon atom at a time and, therefore, became the best candidates for use as catalysts in the olefin metathesis reaction.

Numerous chemists made large contributions to the development of olefin metathesis catalysts and their applications. However, the most pioneering work has been done by Robert H. Grubbs and Richard R. Schrock. In fact, their work has had such a large impact on academic research, the development of polymeric materials, new drugs and industrial syntheses, that, together with Yves Chauvin, they were rewarded with the Nobel Prize in Chemistry in 2005.³⁷⁶

An important aspect in olefin metathesis catalyst development is functional group tolerance. As Tsuji stated, in order to exploit the metathesis reaction as a truly useful synthetic methodology, it is essential to discover a new catalyst system which can tolerate the presence of functional groups in olefin molecules.³⁷⁷ A first breakthrough in the development of well-defined and very active olefin metathesis catalysts which exhibited some functional group tolerance was that of Schrock *et al.* in 1990.³⁷⁸ They reported the synthesis of a very active molybdenum catalyst,

which became widely known as the Schrock catalyst (see Figure 3.3). Despite revealing somewhat higher stability than previously reported tungsten catalysts, the Schrock catalyst is quite sensitive to ambient conditions and decomposes when it is exposed to air, moisture or protic compounds. The instability of this catalyst can be attributed to the highly oxophilic nature of the early transition metal center.

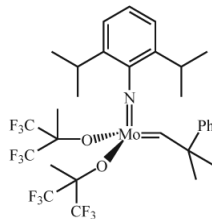


Figure 3.3: The Schrock catalyst.

With the synthesis of novel catalysts, it was soon found that the functional group tolerance of a catalyst increases when it consists of late transition metal (especially from group VIII and IX).³⁷⁹ This is illustrated in Table 3.1, in which the reactivity of some transition metals toward typical functional groups is given. When concerning these transition metals, titanium is the least suitable to develop olefin metathesis catalysts as it is highly reactive toward oxygen-containing compounds. Ruthenium on the other hand exhibits a preference for soft Lewis bases and acids, such as olefins, over hard bases, such as oxygen-containing compounds, which explains its high tolerance to air and water. Of course, other late transition metals also allow the formation of metal-carbon double bonds, however, ruthenium appears to be the optimum metal. Iron, cobalt and rhodium alkylidene complexes are less suitable than ruthenium as they tend to catalyze cyclopropanation reactions.^{380–388} On the other hand, osmium and iridium complexes are generally less active metathesis catalysts than corresponding ruthenium analogues. Moreover, since they are much more expensive, they have not been subject to much research.^{389–391}

Table 3.1: Reactivity of transition metals toward functional groups

Reactivity	Titanium	Tungsten	Molybdenum	Ruthenium
High	Acids	Acids	Acids	Olefins
	Alcohols, Water	Alcohols, Water	Alcohols, Water	Acids
	Aldehydes	Aldehydes	Aldehydes	Alcohols, Water
	Ketones	Ketones	Olefins	Aldehydes
	Esters, Amides	Olefins	Ketones	Ketones
Low	Olefins	Esters, Amides	Esters, Amides	Esters, Amides

One of the most pioneering discoveries in olefin metathesis was the development of well-defined, very stable and very active ruthenium alkylidene complexes by the group of Grubbs. A first in the series, $(\text{PPh}_3)_2\text{Ru}=\text{CH}-\text{CH}=\text{CPh}_2$, was prepared in 1992.³⁹² Although it revealed good functional group tolerance, its metath-

sis activity was limited to strained olefins. An improvement on this system was made by replacing the PPh_3 (Ph = phenyl) with the PCy_3 (Cy = cyclohexyl) ligands.^{393,394} With this finding, researchers also realized that ruthenium catalysts are fundamentally different from titanium, tungsten and molybdenum catalysts. Where the latter require electron-withdrawing ligands, ruthenium catalysts require electron-donating ligands for high catalyst activity. Despite the promising nature of $(\text{PCy}_3)_2\text{Ru}=\text{CH}-\text{CH}=\text{CPh}_2$, both the catalyst activity and the time-consuming synthesis procedure needed to be improved for it to meet commercial needs.³⁷⁹ The first truly large-scale synthesis of a ruthenium alkylidene catalyst was that of $(\text{PCy}_3)_2\text{Cl}_2\text{Ru}=\text{CHPh}$, which is now known as the Grubbs first generation catalyst (see Figure 3.4).^{395,396} The relative ease of its synthesis, allowing kilogram scale production, combined with its high catalytic activity and its broad functional group tolerance, have made the Grubbs first generation catalyst the “workhorse” in olefin metathesis applications.³⁷⁹

Convinced that the activity and efficiency of the Grubbs first generation catalyst could be improved, Grubbs and his group continued their research in developing novel and better olefin metathesis catalysts. However, improving the activity of the Grubbs first generation catalyst proved to be not that straightforward. After all, high catalytic activity is often accompanied by low catalyst stability, and vice versa. A design motif and starting point to develop more active catalysts could be established by studying the reaction mechanism. Mechanistic studies of several research groups namely indicated that during the catalytic cycle, $(\text{PCy}_3)_2\text{Cl}_2\text{Ru}=\text{CHPh}$ forms a highly active 14-electron intermediate by dissociating one phosphine ligand (see Figure 3.4).^{397–405} Subsequently, an olefin substrate coordinates to this unstable intermediate to give a reactive 16-electron complex, referred to here as the design motif.

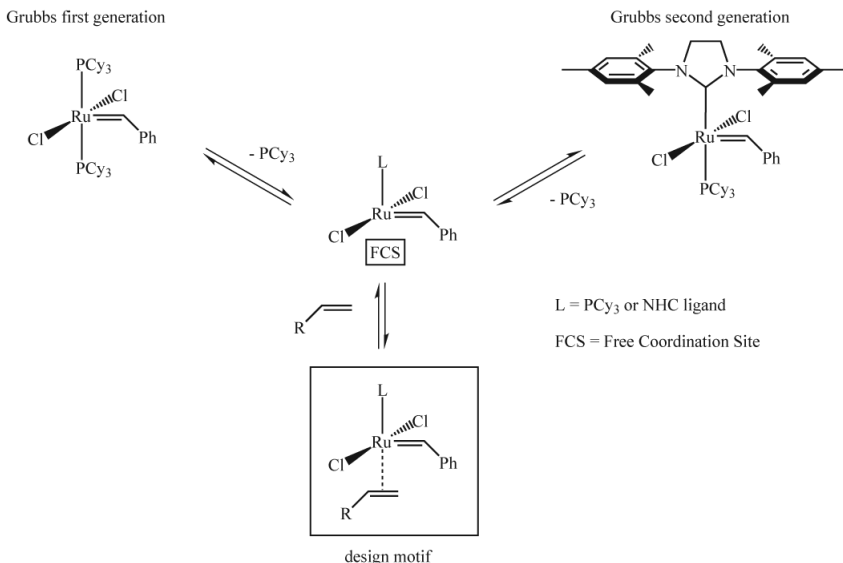


Figure 3.4: Generation of design motif for ideal metathesis-active ruthenium alkylidene catalysts, through phosphine ligand-dissociation of Grubbs type catalysts.

As a result, scientists attempted to synthesize catalysts with single phosphine ligands which exhibit this design motif. Simply removing a phosphine ligand, for instance with CuCl or HCl, enhances the catalytic activity, but severely increases the decomposition rate of the catalyst.^{398,405} Therefore, an ideal catalyst consists of ligands that can both stabilize the design motif during the catalytic cycle, and prevents decomposition of the active ruthenium species. The group of Grubbs ultimately succeeded in their attempts to develop superior olefin metathesis catalysts by substituting one phosphine ligand of the Grubbs first generation catalyst by saturated or unsaturated N-heterocyclic carbene (NHC) ligands.^{406,407} These catalysts, which are now widely known as the Grubbs second generation catalysts (see Figure 3.4), display remarkable catalytic performance and functional group tolerance, and for the first time enabled metathesis of tri- and tetra-substituted olefins.^{406–408} Having the same intent as Grubbs, the groups of Herrmann^{409–412} and Nolan⁴¹³ developed very similar catalysts in the same period.

The improved catalytic properties of the second generation Grubbs type catalyst was initially attributed to increased phosphine exchange rates. However, investigation of degenerative phosphine exchange showed that phosphine dissociation of this catalyst is two orders of magnitude slower than from the Grubbs first generation catalyst. Despite the slower initiation of the Grubbs second generation catalyst, it reveals a higher catalytic activity than the first generation catalyst, which may seem contradictory. However, the increased donor strength of NHC ligands,⁴¹⁴ when compared to PCy₃, enhances coordination of olefin substrates relative to phosphine. As a result, the Grubbs second generation catalyst remains longer in the catalytic cyclic without decomposing, leading to overall faster rates of catalysis.^{415–417} However, the positive influence of the NHC ligand on the activity of the second generation Grubbs catalyst is not only related to its basicity, but can also be ascribed to steric effects.^{417–422} For instance, it has been reported that the strong steric hindrance of the bulky mesidine (2,4,6-trimethylphenyl) NHC-substituents of the second generation Grubbs catalyst, destabilize the 14-elektron intermediate in the catalytic cycle. As a result, phosphine dissociation slows down and olefin coordination improves.⁴¹⁹ In another report, by Ledoux *et al.*, the influence of the NHC ligand environment on the catalyst stability and activity was clearly illustrated.⁴²³ For example, the authors showed that catalysts with symmetrical NHC ligands with aliphatic substituents could not be isolated due to their instability. On the other hand, ruthenium complexes with unsymmetrical NHC ligands consisting of one planar mesidine substituent, were stable enough to be isolated. They also found that when the second substituent of the latter NHC ligand is very small and sterically undemanding, the corresponding catalyst reveals very high catalytic activity.

The slow initiation step of the Grubbs second generation catalyst has been improved by replacing the PCy₃ ligand with more labile heterocyclic ligands such as pyridine.^{424–426} This system, which is often referred to as the Grubbs third generation catalyst, is depicted in Figure 3.5.

The developments in olefin metathesis, both in terms of catalyst synthesis and applications, is never ending. Olefin metathesis is a vast expanding research field, making it both impossible to describe everything and redundant to go into more detail on the subject. Nevertheless, one other type of catalyst which is interesting

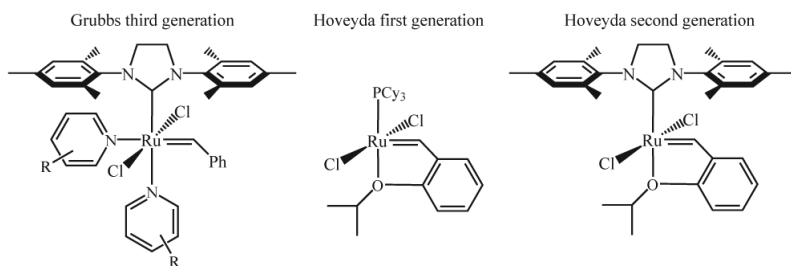


Figure 3.5: Grubbs third ($R = H, Br, Ph, NO_2$), Hoveyda first and Hoveyda second generation catalysts.

to mention (as it will be discussed later on in this work) is the Hoveyda catalyst (see Figure 3.5). This type of catalyst is characterized by an isopropoxystyrene chelating ligand which renders these systems robust and recyclable.^{427–429} Especially the Hoveyda second generation catalyst (see Figure 3.5) is very interesting as it combines good metathesis activity and selectivity with good stability. The enhanced stability of these systems, which implies long life times during reaction, is a result of the release and return mechanism of the isopropoxystyrene ligand. I.e. this ligand, which decoordinates during the metathesis reaction, can recoordinate with the metal center.⁴³⁰ As a result these catalysts are so stable that they can be recovered (*via* column chromatography) after finishing the reaction, and subsequently reused in a following metathesis reaction. Moreover, recently a recyclable and stable Hoveyda type catalyst immobilized onto a silica support has been reported.⁴³¹ Variants of the Hoveyda type catalyst, were also reported by Blechert^{432,433} and Grela^{434,435}.

3.2 Typical synthesis of ethene-PMO precursors

To date, ethenylene-bridged PMOs have been synthesized using 1,2-bis(triethoxysilyl)ethene that was either obtained commercially or synthesized according to a method described by Marciniec *et al.*⁴³⁶ In either case, the PMO precursor consists of a mixture of two isomers (*E* and *Z* diastereoisomers). The method of Marciniec *et al.* involves the self-metathesis of vinylsilanes using $(PPh_3)_3RuCl_2$ as a catalyst, as illustrated in Figure 3.6.

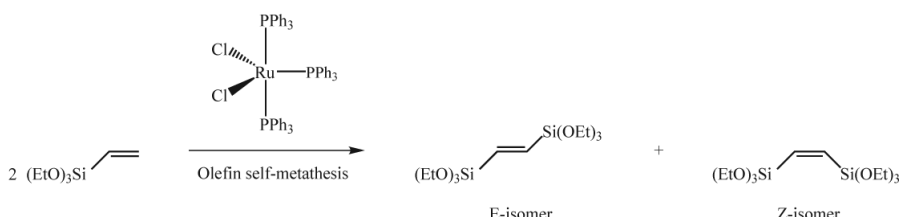


Figure 3.6: Self-metathesis of vinyltriethoxysilane using $(PPh_3)_3RuCl_2$ as a catalyst.

Using this method Marciniec *et al.* obtained a diastereoisomeric mixture with an *E/Z*-ratio of 86/14 and a reaction yield of 82 %. When employing vinyltrimethoxysilane instead of vinyltriethoxysilane an *E/Z*-ratio close to 1/1 was found, which could not be explained by the authors. At the time the use of these type of ruthenium catalysts for the metathesis of vinyl-substituted olefins was a good step in the right direction. Prior to this report, these olefins were prepared in low yields by utilizing either heterogeneous catalysts based on Re_2O_7 and MoO_3 ,⁴³⁷ or homogeneous catalysts based on WCl_6 .⁴³⁸

Though olefin metathesis is a very good method to obtain 1,2-bis(triethoxysilyl)ethene, the so far employed catalyst may not be ideal. In fact, at the time that Marciniec *et al.* reported on the metathesis of silicon containing olefins in 1989, the now commonly used metathesis catalysts had not been discovered yet. Strangely enough, since this initial report, there has been no other report on the synthesis of 1,2-bis(triethoxysilyl)ethene. Therefore, with the aim of developing isomerically pure ethylene-bridged PMO precursors, several metathesis catalysts were screened for the self-metathesis of vinyltriethoxysilane, which will be described in the following section.

3.3 Diastereoisomeric ethene-PMO precursors

3.3.1 Synthesis of the *E*-isomer: Role of catalyst

As mentioned above, the synthesis of 1,2-bis(triethoxysilyl)ethene (BTSE) proceeds by means of an olefin self-metathesis reaction of vinyltriethoxysilane (VTES). In our effort to catalytically obtain the pure *E*-isomer of 1,2-bis(triethoxysilyl)ethene (*E*-BTSE), several catalysts, illustrated in Figure 3.7, were probed.

To compare with the literature report of Marciniec *et al.*,⁴³⁶ the self-metathesis reaction of VTES was initially examined with catalyst **1**. BTSE was identified by ^1H and ^{13}C NMR and GC analysis as a diastereoisomeric mixture with an *E/Z* ratio of about 80/20, which is equal to that of the commercially available silane and comparable to that reported by Marciniec. Subsequently, the other catalysts represented in Figure 3.7 were investigated, and the resulting silane BTSE was also analyzed by ^1H and ^{13}C NMR and GC analysis. In Table 3.2 the investigated catalysts and their selectivity in the metathesis of VTES are given.

Table 3.2: Diastereoselectivity of the investigated catalysts in the self-metathesis reaction of VTES

Catalyst	<i>E</i> -isomer [%] ^[a]	<i>Z</i> -isomer [%] ^[a]
Grubbs' 2 nd generation, 4	79.3	20.7
$\text{RuCl}_2(\text{PPh}_3)_3$, 1	79.7	20.3
$[\text{Ru}(p\text{-cymene})\text{Cl}_2]_2$, 2	89.2	10.8
Hoveyda-Grubbs' 2 nd generation, 6	92.1	7.9
Hoveyda-Grubbs' 1 st generation, 5	94.6	5.4
Grubbs' 1 st generation, 3	≈ 100	< 0.1

^[a] Determined via GC-analysis.

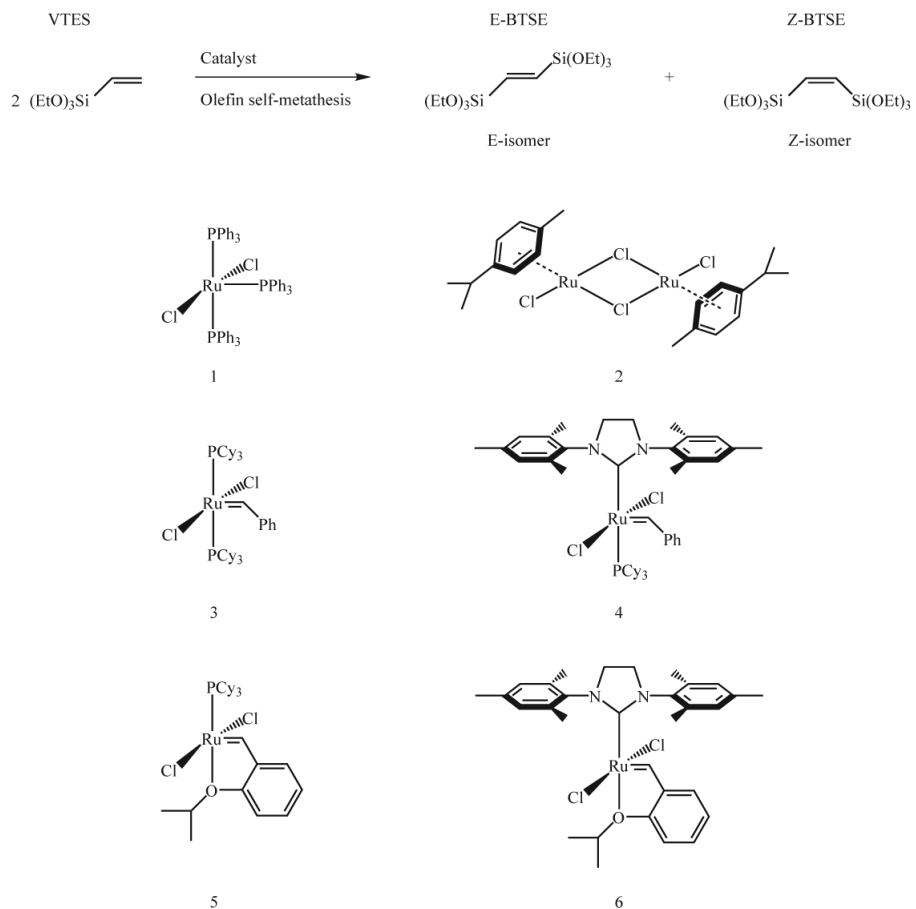


Figure 3.7: Investigated catalysts for the self-metathesis of VTES.

The commercially available first generation Grubbs catalyst **3** is the most selective catalyst in the metathesis reaction of VTES. Surprisingly, the latter produced the pure *E*-diastereoisomer of 1,2-bis(triethoxysilyl)ethene, without further purification being required. In Figure 3.8 the ^1H NMR spectra are given of the resulting silanes, obtained with catalysts **1** and **3**.

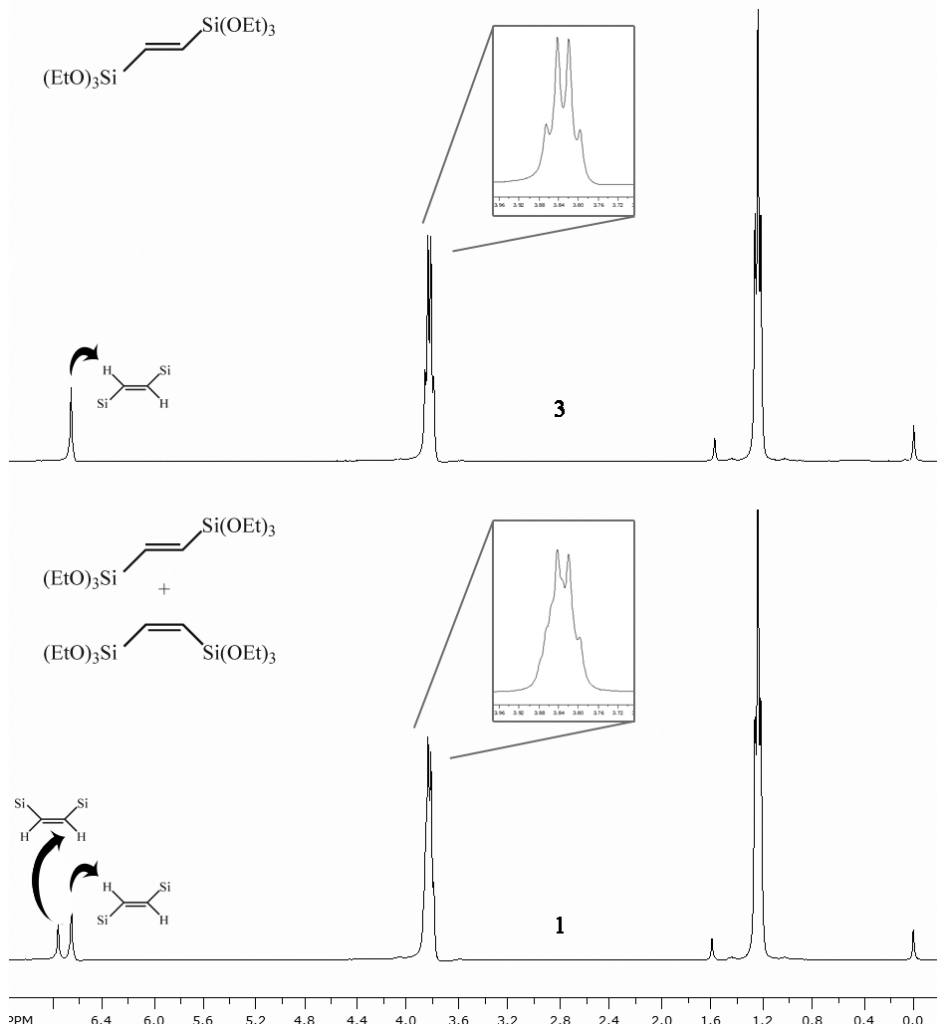


Figure 3.8: ^1H NMR spectra of 1,2-bis(triethoxysilyl)ethene, obtained with catalyst **1** and **3**. While catalyst **3** produces a mixture of two diastereoisomers, catalyst **1** produces the pure *E*-diastereoisomer

The spectrum of the reaction product obtained with catalyst **1** *via* the method of Marciniec *et al.*, clearly exhibits two well-resolved resonances at 6.77 and 6.66 ppm, which can be assigned to the *Z*- and *E*-configured CH=CH bridging organic groups, respectively. The assignment of these peaks to both isomers is based on the

analysis of the ^{13}C NMR spectra of the respective organosilanes (vide infra) and comparison to literature data.⁴³⁶ On the other hand, the spectrum of the reaction product obtained with catalyst **3** clearly only exhibits one resonance at 6.66 ppm, which can be assigned to the *E*-configured CH=CH bridging organic groups.

These results were confirmed by GC. The chromatogram of the reaction product obtained with catalyst **1** displays two peaks, which can be assigned to the two diastereoisomers. The chromatogram of the product produced with catalyst **3** on the other hand only displays one peak, indicating a highly pure diastereoisomeric compound. The relative amounts of both isomers for each catalytic system are given in Table 3.2.

Overall, the high *E/Z* ratios of 1,2-bis(triethoxysilyl)ethene, produced by the investigated catalysts, indicate that the catalytic reaction is under thermodynamic control. A possible explanation is that the formation of *E*-configured species with relatively unhindered triethoxy groups is favored above *Z*-configured species with sterically more hindered triethoxy groups. This rationalizes the high selectivity of the described catalysts for the *E*-isomer.

As to why specifically the first generation Grubbs catalyst is the most selective, an exact explanation can't be given. The catalyst does not consist of any ligands which would lead us to predict it to induce stereoselectivity. However, both electronic and steric properties of the active catalytic species will most definitely play a role in the reaction selectivity. The problem with relating the catalyst structure to its selectivity is the fact that the structure of the active catalytic species is unknown. At the elevated temperatures required for the olefin self-metathesis of VTES to occur (around its boiling point, 160 °C), the mechanism is hard to predict.

As the *E/Z* diastereoselectivity of an olefin metathesis reaction is often controlled by the thermodynamic stability of the olefin isomers rather than the selectivity of the catalyst, the possibility of secondary metathesis was investigated. In this case, the product *E/Z* ratio is influenced by a metathesis reaction between *Z*-configured silanes, formed in a primary olefin metathesis reaction, and the ruthenium alkylidene catalyst. Although secondary metathesis could account for the formation of the thermodynamically favorable *E*-isomer, no evidence was found that it occurred. When investigating the initial stage of the olefin metathesis reaction of VTES with catalyst **3**, no *Z*-isomer was apparent, indicating that the self-metathesis of VTES selectively leads to *E*-BTSE. Furthermore, when investigating the *E/Z* ratio of the reaction product during the metathesis reaction catalyzed by **1**, no isomerization was found to occur. Both at the very beginning and at the end of the reaction, the *E/Z* ratio was about 80/20, indicating no secondary metathesis. These results suggest that the enhanced selectivity toward *E*-BTSE is a result of the sterically demanding bulky triethoxysilyl groups attached to the olefin.

Other than a high selectivity, the first generation Grubbs catalyst exhibits a high turnover number (TON) in the metathesis reaction of VTES. With a catalyst loading of 0.03 %, a maximum yield of 95 % is observed, giving a TON of 3167. Compared to RuCl₂(PPh₃)₃ (TON = 670), the first generation Grubbs catalyst is superior in the described metathesis reaction, both in terms of selectivity as activity. Therefore, this catalyst can be considered as an ideal candidate for the synthesis of diastereoisomeric pure *E*-configured ethene-PMO precursors.

3.3.2 Synthesis of the Z-isomer

There is no general catalyst solution for the formation of *Z*-configured olefins in a self- or cross-metathesis reaction. For thermodynamic reasons, as stated above, the formation of *E*-isomers will always be favored above *Z*-isomers. In other words, to obtain a lower E/Z ratio, a different synthesis approach is required. The most obvious approach is separation of the two isomers. However, these type of hygroscopic compounds are some of the most difficult and most challenging compounds to separate.

GC-analysis of the reaction product obtained with catalyst **1** gave us the idea that it may be possible to separate the two isomers based on their slightly different boiling points. By carefully performing multiple successive fractionated vacuum distillations, the *E/Z* ratio could be drastically lowered. Ultimately, the 100 % pure *Z*-isomer of 1,2-bis(triethoxysilyl)ethene (*Z*-BTSE) could be prepared. In Figure 3.9 some ^{13}C NMR spectra are given of distillates with different *E/Z* ratios.

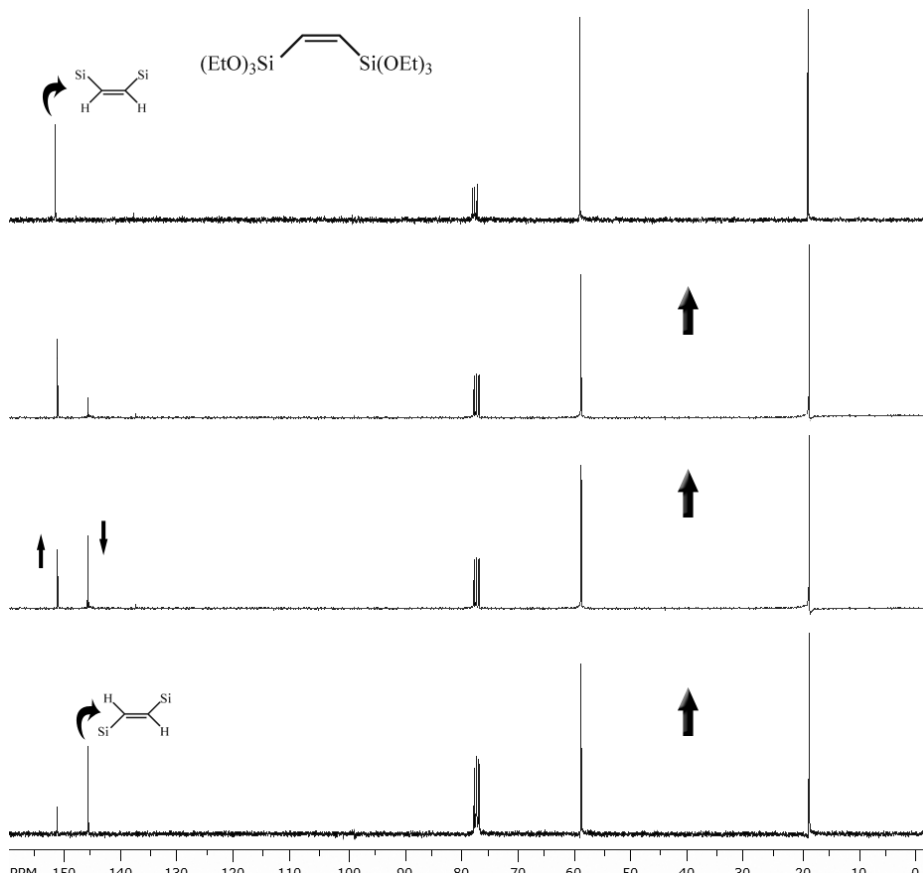


Figure 3.9: ^{13}C NMR spectra of distillates with different *E/Z* ratios. Via multiple successive fractionated vacuum distillations, the fraction of *E*-isomer can be reduced relative to the fraction of *Z*-isomer.

The bottom spectrum is that of the reaction product obtained with catalyst **1**. By performing multiple distillations, the fraction of *E*-isomer clearly reduces while the fraction of the *Z*-isomer increases, as illustrated in Figure 3.9. The purity of *Z*-BTSE was further confirmed by GC-analysis, the chromatogram of which only revealed one peak that could be assigned to *Z*-BTSE.

3.4 Synthesis of an entirely novel olefinic PMO precursor

3.4.1 Preliminary investigation

With the aim of extending the scope of olefin metathesis in the development of novel PMO precursors, several catalysts were screened for the metathesis of allyltrimethoxysilane (ATMS), as illustrated in Figure 3.10.

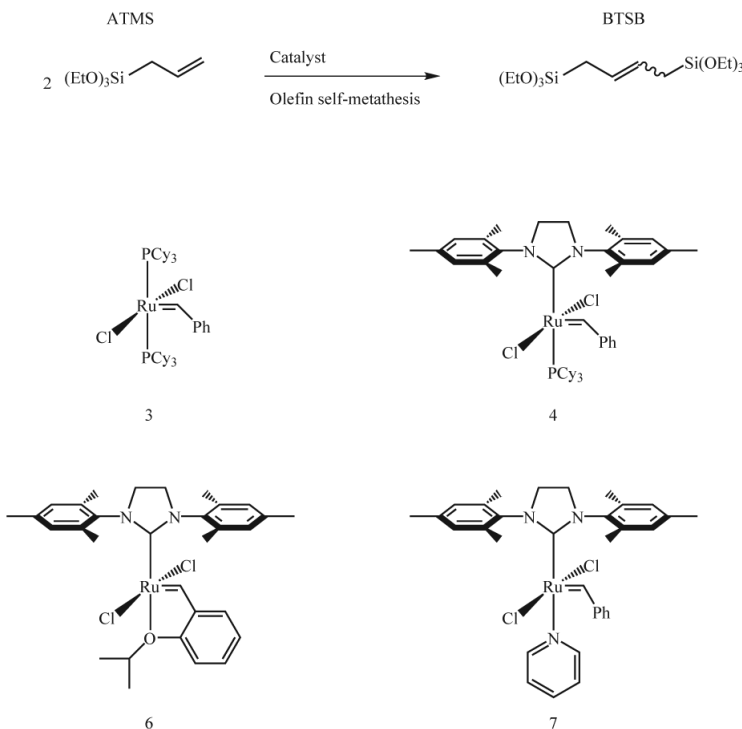


Figure 3.10: Investigated catalysts for the self-metathesis of ATMS.

Preliminary catalytic test reactions in the synthesis of 1,4-bis(trimethoxysilyl)butene (BTSB) revealed that the reactivity of ATMS is quite different from VTES. While the metathesis of the vinylic silane required very high temperatures (≈ 160 °C), the metathesis of the allylic silane can be carried out at relatively low temperatures (≤ 50 °C). This can be a result of the sterically less hindered alkene bond. A more detailed investigation was performed by monitoring the metathesis

reaction of ATMS, catalyzed by the complexes represented in Figure 3.10, as a function of time with ^1H NMR (see Figure 3.11).

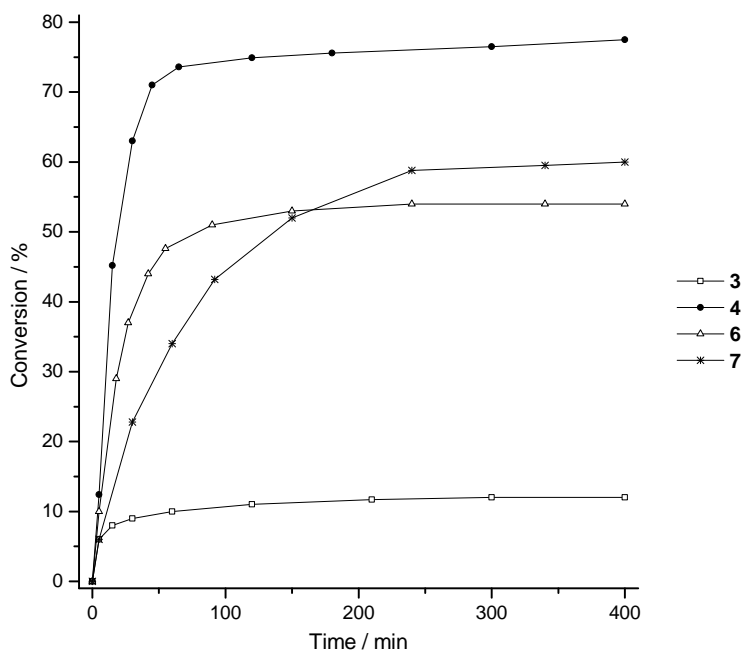


Figure 3.11: Monitoring the self-metathesis of ATMS as a function of time *via* ^1H NMR.
ATMS/Cat. = 1000, 50 °C.

In strong contrast to the self-metathesis reaction of VTES, the first generation Grubbs catalyst **3** was not effective in the metathesis of ATMS. With a molar ATMS/Cat ratio of 1000, only 12 % conversion was obtained when performing the reaction at 50 °C. On the other hand, the second generation Grubbs catalyst **4** was quite active giving about 74 % conversion within one hour. Quite surprising, the third generation Grubbs catalyst **7** revealed a slower initiation than catalyst **4**. This is unexpected as the dissociation of pyridine is faster than that of the phosphine ligand PCy_3 .

Though some of these catalysts are good candidates for the synthesis of BTSP, there is another matter which has to be taken into account. Unlike the self-metathesis reaction of VTES, the metathesis of ATMS can be accompanied by an isomerization reaction, i.e. migration of the double bond along the alkyl chain by 1,3-H shifts.^{439,439–445} This side reaction, which can be competitive with the metathesis reaction, is typical for allylic substrates. It is not clear whether olefin isomerization is promoted by the metathesis catalyst itself, decomposition products, or impurities from the catalyst synthesis. However, two pathways are accepted for transition metal catalyzed isomerization of olefins. Herein, the isomerization either occurs *via* a hydrometalation-dehydrometalation (hydride mechanism) or *via* a π -allyl metal mechanism, as illustrated in Figure 3.12. In the most common pathway, the hydride mechanism, a free olefin coordinates to a metal hydride. Subsequent

insertion of the hydride produces a metal alkyl which itself dissociates, yielding either the original olefin or an isomer thereof. In the π -allyl metal mechanism, a free olefin coordinates to the metal center of the catalyst followed by an oxidative addition of the activated allylic C–H bond, yielding a metal hydride. Insertion of the hydride subsequently yields an olefin, similar as in the hydride mechanism.

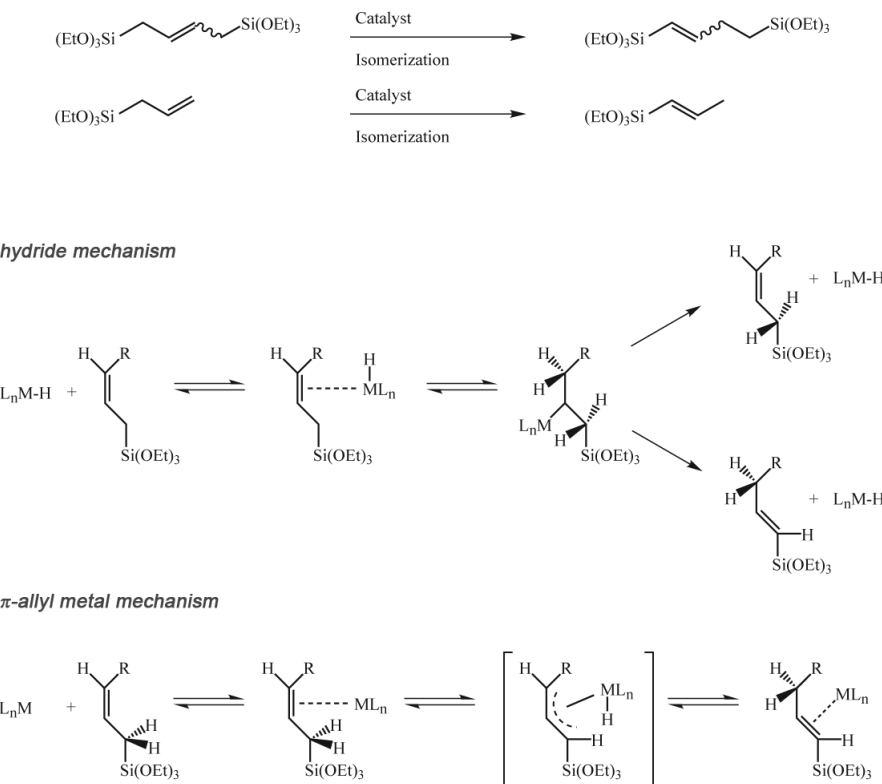


Figure 3.12: Isomerization of BTSB as a side reaction in the self-metathesis of ATMS. The isomerization can either occur *via* the hydride mechanism or *via* the π -allyl metal mechanism.

The isomerization reaction, induced by the complexes represented in Figure 3.10, was monitored as a function of time with ^1H NMR (see Figure 3.13). In this catalyst series, the first generation Grubbs catalyst **3** is the only catalyst which does not induce isomerization. As the latter catalyst reveals a very low activity in the metathesis of ATMS, the absence of isomerization products indicates that isomerization of the substrate ATMS does not occur. Interestingly, isomerization generally occurs when the metathesis activity starts to reduce. This indicates that isomerization is induced by decomposition products of the catalyst. When concerning the most active catalyst in the metathesis of ATMS, the second generation Grubbs catalyst **4**, the isomerization reaction starts competing with the metathesis reaction after about 45 minutes. With other words, when employing catalyst **4** in the self-metathesis reaction of ATMS, the reaction should be terminated before

isomerization starts, at which point 71 % conversion is obtained. Another catalyst which may be a good candidate for the metathesis of ATMS, when concerning the competing isomerization reaction, is the third generation Grubbs catalyst **7**. If the reaction is terminated after one hour, only 4 % isomerization products are produced. However, after this period of time, only 34 % conversion is obtained. Thus in this catalyst series, catalyst **4** can be considered as the best candidate for the metathesis of ATMS.

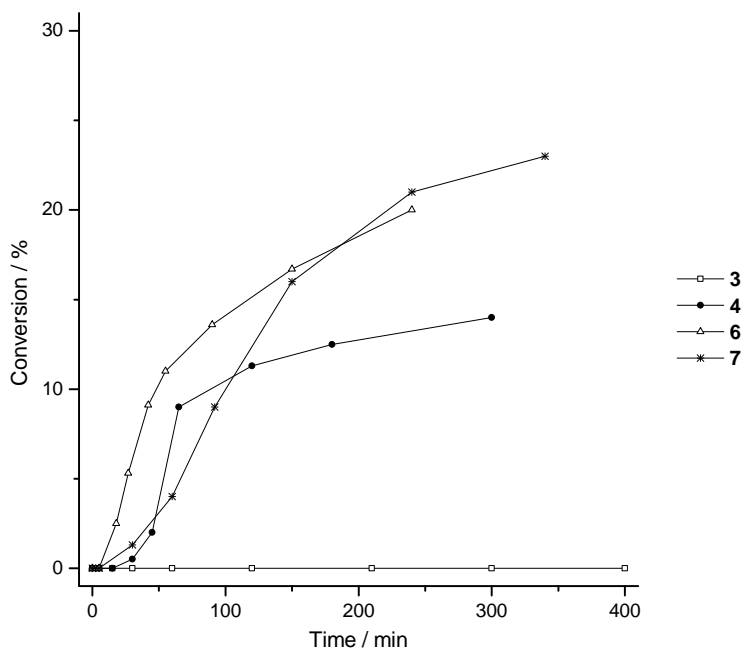


Figure 3.13: Monitoring the isomerization reaction as a function of time *via* ^1H NMR.
ATMS/Cat. = 1000, 50 °C.

A good method to reduce isomerization is to limit catalyst decomposition by lowering the reaction temperature. However, by doing so, the metathesis of ATMS can also be effected. In Figure 3.14 A, both the metathesis conversion and the isomerization catalyzed by **4** at different temperatures, are given as a function of time. Though the isomerization reaction is repressed by lowering the temperature, this is accompanied with a lower metathesis conversion.

A better method to increase the metathesis conversion relative to the isomerization reaction is to lower the ATMS/Cat. ratio. In Figure 3.14 B, both the metathesis conversion and the isomerization reaction catalyzed by **4**, are given as a function of time. When lowering the ATMS/Cat. ratio from 1000 to 800, the conversion increases considerably from about 77 % to 96 %. Moreover, the isomerization side reaction is also suppressed. Terminating the reaction after 65 minutes, reveals 94 % metathesis conversion and 6 % isomerization. The downside of this method is of course the required higher amount of catalyst. Therefore, a new set of non-commercial catalysts were probed for the metathesis of ATMS.

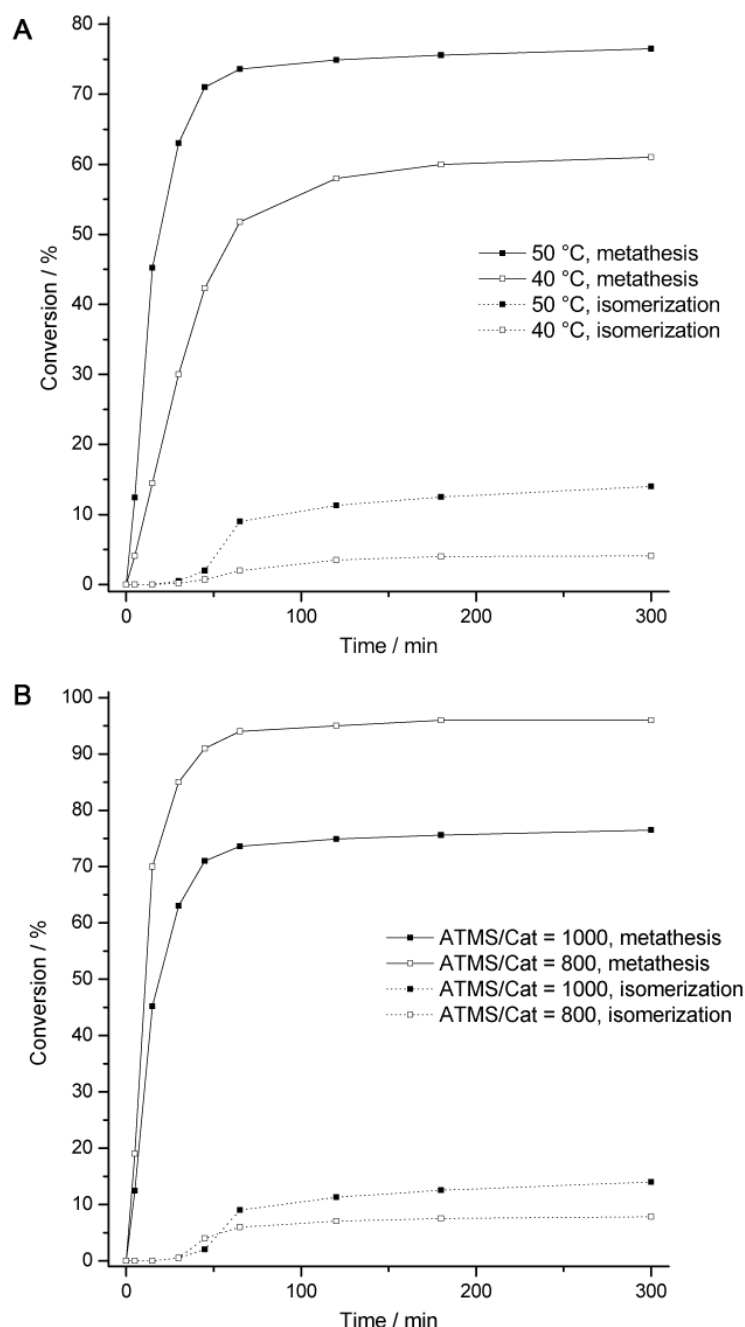


Figure 3.14: Influence of A) the reaction temperature and B) the ATMS/Cat. ratio, on the metathesis conversion of ATMS and on the isomerization reaction, catalyzed by **4**. Reactions monitored with ^1H NMR.

3.4.2 Probing novel catalysts: circumventing isomerization reactions

The second series of catalysts which were screened for the metathesis of ATMS, is represented in Figure 3.15. These catalysts which were prepared by the Ghent University spin-off company ViaCatt, are so-called latent catalysts, i.e. catalysts which are very stable and which reveal no metathesis activity at room temperature. The latent character of these complexes is introduced by the chelating Schiff base ligands. Being inactive in the self-metathesis of ATMS under the above described reaction conditions, latent catalysts, as such, may not seem very interesting. However, when activated by an external force (high temperature, addition of activator, light), these systems represent a very powerful tool in olefin metathesis. They enable precise control of the catalyst activity. For instance, latent catalysts are very interesting in applications involving reaction injection molding (RIM).⁴⁴⁶ This is a technique which enables the development of polymer parts by direct polymerization in the mold through mixing monomeric feeds. In this case, one monomer feed contains the inactive catalyst, while a second monomer feed contains an activator. After mixing the feeds, an active catalyst species is generated *in situ*, allowing polymerization of the introduced monomer. An important advantage of latent catalysts is that they can be mixed with olefinic substrates and stored for long periods of time without inducing reaction. However, for the self-metathesis of ATMS, these systems were initially investigated as alternatives for the Grubbs and Hoveyda type catalysts, with the main goal being: preventing isomerization.

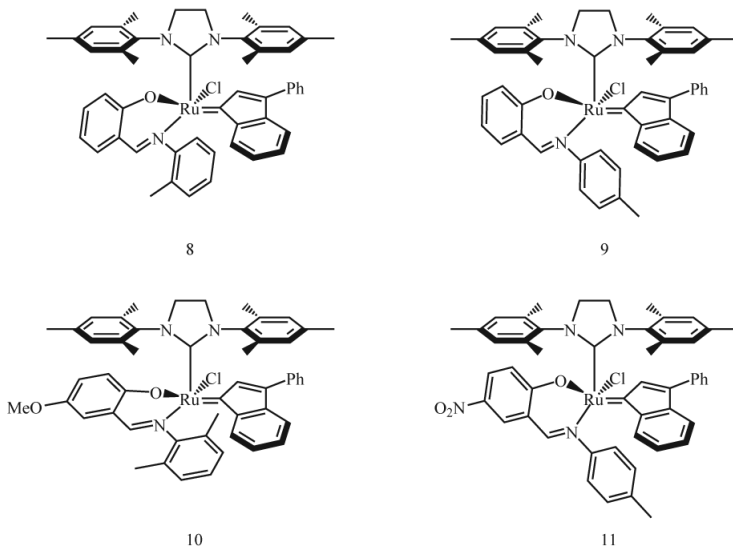


Figure 3.15: Investigated latent indenylidene catalysts for the self-metathesis of ATMS.

As the catalysts represented in Figure 3.15 are inactive in the metathesis of ATMS, an activator (co-catalyst) was added to the reaction mixture to trigger the self-metathesis reaction. Herein, the co-catalyst is expected to react with the Schiff

base ligand in such a manner that nitrogen decoordinates from the metal center, producing a highly active 14-electron complex. Good co-catalysts are Brönsted and Lewis acids. However, addition of excessive amounts of strong acids causes fast catalyst decomposition. Therefore, it is important to find an optimal catalyst/acid ratio.

Preliminary investigations revealed that HCl is too strong an acid to be used as a co-catalyst. The catalyst decomposes before self-metathesis occurs. A very good alternative to Brönsted acids are chlorosilanes. Small amounts of the latter induce quick activation of the described catalysts, allowing fast self-metathesis of ATMS. In particular phenyltrichlorosilane and ethyltrichlorosilane are good co-catalysts in this metathesis reaction (see Table 3.3). As to how these silanes act as co-catalysts, it has been proposed that they form an adduct with the electron pair from the imine nitrogen atom of the Schiff base ligand, as illustrated in Figure 3.16.^{447,448} Formation of a silane-Schiff base complex implies that the electron donation from the basic nitrogen toward the ruthenium center is prevented, rendering an active 14-electron species which enables olefin coordination and fast self-metathesis of ATMS. Important though is to avoid hydrolysis of the chlorosilanes in order to prevent the generation of HCl which would induce catalyst decomposition. Therefore, the reactions should be performed under inert atmosphere.

Besides phenyltrichlorosilane being the most interesting co-catalyst, these preliminary results also indicate that catalyst **10** is superior to catalyst **8** in the metathesis of ATMS and that a reaction temperature of 50 °C is required in order to obtain high conversions (see Table 3.3).

Table 3.3: Preliminary investigation of acid-activated catalysts in the self-metathesis reaction of ATMS

Catalyst	Co-catalyst ^[a]	Temp. [°C]	Time [min]	Conv. [%] ^[b]	Isomeriz. [%] ^[b]
8	-	25	100	0	0
8	-	50	100	11	0
8	HCl	50	100	0	0
8	SiCl ₄	50	100	64	0
8	HSiCl ₃	50	100	70	0
8	EtSiCl ₃	50	100	79	0
8	PhSiCl ₃	50	100	86	0
8	PhSiCl ₃	17	100	47	0
8	PhSiCl ₃	25	100	57	0
10	EtSiCl ₃	50	120	94	0
10	PhSiCl ₃	50	120	97	0
10	PhSiCl ₃	50	160	100	0

[a] Catalyst/Co-catalyst/ATMS = 1/30/1000. [b] Determined via ¹H NMR.

Based on these preliminary investigations, phenyltrichlorosilane was chosen as a co-catalyst in the metathesis reaction of ATMS at 50 °C, catalyzed by complexes **8** to **11**. The reactions were monitored as a function of time with ¹H NMR and the conversion curves are illustrated in Figure 3.17.

In terms of activity, catalysts **10** and **11** are the best candidates for the self-metathesis reaction of ATMS. While catalyst **10** gave 98 % conversion, catalyst

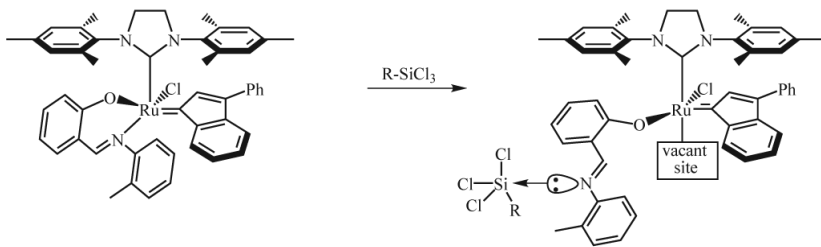


Figure 3.16: Schematic representation of the activation of Schiff base containing catalysts with trichlorosilanes.

11 gave full conversion after 100 minutes. With a catalyst loading of 0.1 %, these catalysts reveal TONs of 980 and 1000, respectively. Though catalyst **9** is the fastest initiating catalyst (42 % conversion after 5 minutes), it revealed a lower TON (760) than catalysts **8** (TON of 850), **10** and **11**.

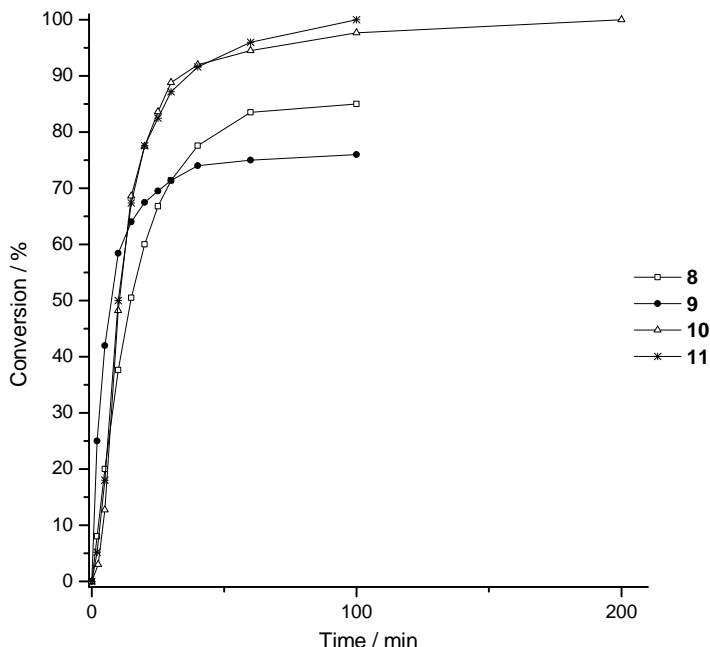


Figure 3.17: Monitoring the self-metathesis of ATMS as a function of time *via* ¹H NMR. Catalyst/Co-catalyst/ATMS = 1/30/1000, Reaction temperature = 50 °C.

Although these catalysts, especially **10** and **11**, are very good candidates for the metathesis of ATMS, GC-analysis of the reaction products revealed some byproducts which could not be identified. Also, a diastereoisomeric mixture (*E*- and *Z*-isomers) is obtained. Therefore, additional efforts were made to further optimize the synthesis and develop purer and diastereoisomeric butenylene-bridged PMO precursors.

3.4.3 Diastereoisomeric butenylene-bridged PMO precursor

Revealing high TONs and producing low to no isomerization products, some of the above described catalysts are interesting for the self-metathesis reaction of ATMS. However, when employing these catalytic systems, further purification of the reaction products is required in order for these to be implemented in PMO synthesis. For these reasons it would be more appealing to develop a catalytic system which produces pure products, requiring no further purification.

At the time, in our group much research was done in the field of olefin metathesis, both in developing novel catalysts and testing these catalytic systems in RCM (Ring Closing Metathesis) and ROMP (Ring Opening Metathesis Polymerization) reactions.^{423,449–452} Having a chiral ligand, one of these systems in particular struck our attention (catalyst **12** in Figure 3.18) and was synthesized and investigated for the metathesis of ATMS. The synthesis of this highly stable second generation Hoveyda type catalyst is based on that reported by Ledoux *et al.* and is illustrated in Figure 3.18.⁴²³

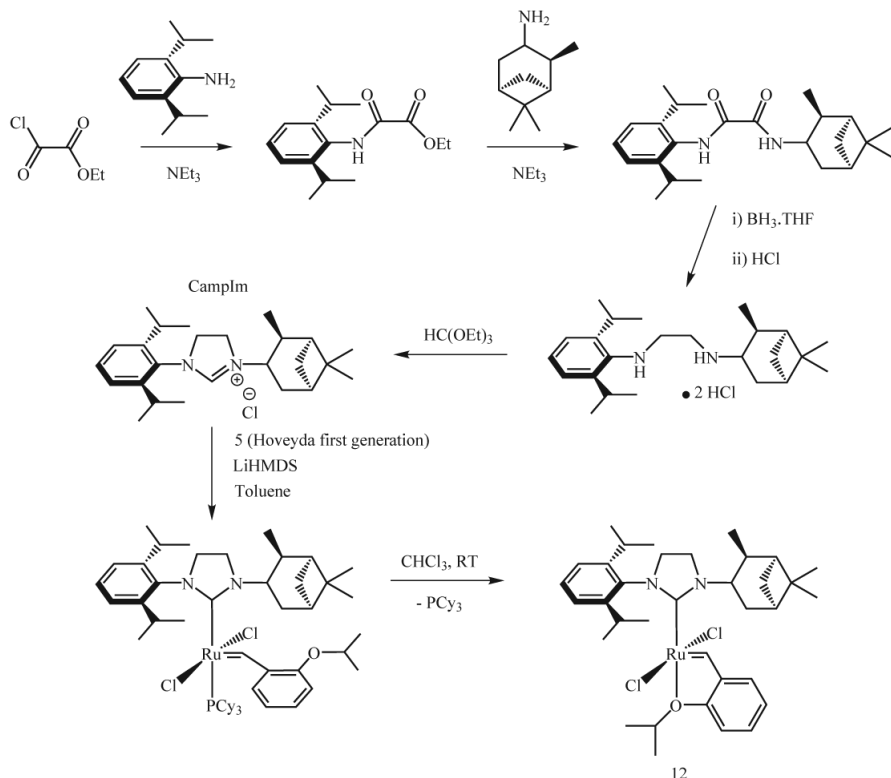


Figure 3.18: Synthesis of a second generation Hoveyda type catalyst bearing a chiral ligand. Synthesis is based on a report by Ledoux *et al.*⁴²³

Synthesis of the asymmetric NHC-ligand 1-(2,6-diisopropylphenyl)-3-isopinocamphoryl-4,5-dihydroimidazolium (CampIm) is conducted by subsequent condensa-

tion of ethyl chlorooxooacetate with 2,6-diisopropylaniline and (*1R,2R,3R,5S*)-(*-*)-isopinocampheylamine, followed by reduction, precipitation with HCl and cyclization with triethyl orthoformate. Addition of CampIm to the first generation Hoveyda catalyst **5** (see Figure 3.7, page 69) in the presence of the strong base LiHMDS afforded catalyst **12**, after liberation of the phosphine ligand by stirring in chloroform.

Catalyst **12** was tested in the self-metathesis reaction of ATMS and monitored with ^1H NMR. Figure 3.19 gives both the metathesis conversion and the isomerization catalyzed by **12** and **4** as a function of time. When compared to the second generation Grubbs catalyst **4**, catalyst **12** reveals a slower initiation in the metathesis reaction of ATMS. However, this is compensated by the high stability of the complex, which enables longer reaction times without catalyst decomposition. With a catalyst loading of 0.1 %, these catalysts both revealed a TON of 780 after 400 minutes. While in the presence of catalyst **4**, no further increase in conversion took place after 400 minutes, catalyst **12** remained active over a longer period of time, and gave a maximum conversion of 83 % after 15 hours. The slower initiation and the robustness of catalyst **12**, when compared to **4**, results from the chelating nature of the 2-isopropoxystyrene ligand, which dissociates reluctantly from the metal center.

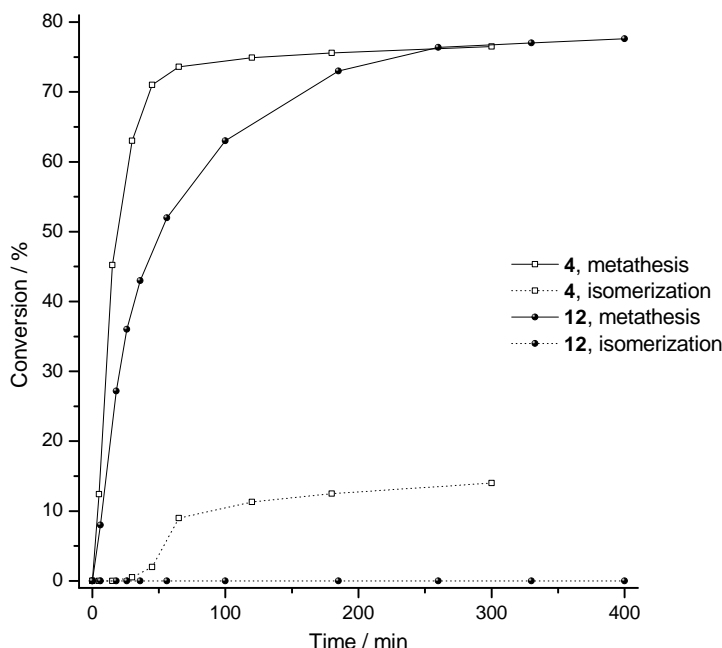


Figure 3.19: Monitoring the self-metathesis of ATMS, catalyzed by **4** and **12**, as a function of time *via* ^1H NMR. ATMS/Catalyst = 1000, Temp. = 50 °C.

More importantly, while the metathesis reaction with catalyst **4** is competitive with the previously described isomerization reaction, no isomerization products are formed with catalyst **12**. Moreover, analysis of the reaction product (after

removing non-reacted ATMS *via* vacuum distillation), revealed only one peak in the chromatogram, which could be ascribed to the pure *E*-diastereoisomer of 1,4-bis(trimethoxysilyl)butene (see Figure 3.20). Thus catalyst **12** may be considered as the perfect candidate for the synthesis of a pure and isomeric butenylene-bridged PMO precursor.

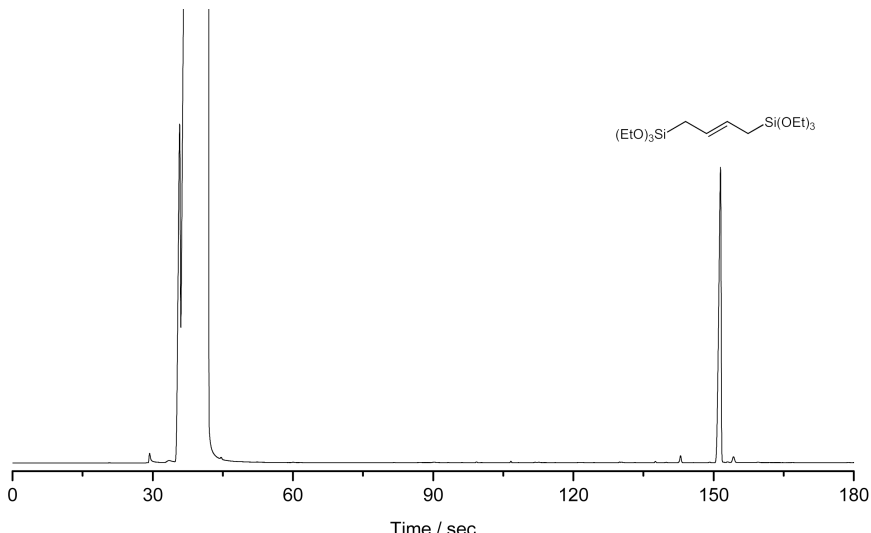


Figure 3.20: Chromatogram of 1,4-bis(trimethoxysilyl)buteen, obtained via the self-metathesis of ATMS with catalyst **12**.

3.5 Conclusions on the synthesis of olefinic PMO precursors

For the first time, diastereoisomeric ethenylene-bridged PMO precursors have been synthesized *via* the self-metathesis of vinyltriethoxysilane. Use of the commercially available first generation Grubbs catalyst rendered the ($\approx 100\%$) pure *E*-diastereoisomer of 1,2-bis(triethoxysilyl)ethene with a TON of 3167, which may be considered as a great improvement when compared to the commonly used synthesis procedure, involving the catalyst $(\text{PPh}_3)_3\text{RuCl}_2$ which produces a diastereoisomeric mixture ($\approx 80\%$ *E*-isomer) with a TON of 670. These results have been published as a peer review article.⁴⁵³

From a thermodynamic point of view, the synthesis of pure *Z*-isomers is a difficult objective to achieve. For steric reasons, the *E*-isomer of 1,2-bis(triethoxysilyl)-ethene will always be favored above the less stable *Z*-isomer, when a catalytic approach is considered. Nevertheless, for the first time, a ($\approx 100\%$) pure *Z*-isomer of 1,2-bis(triethoxysilyl)ethene has been developed by carefully performing multiple successive vacuum distillations of a diastereoisomeric mixture containing 20 % of the desired *Z*-isomer. The synthesis and application of *Z*-BTSE is described in a peer review article.⁴⁵⁴

With the aim of extending the scope of olefin metathesis in the development of novel PMO precursors, several catalysts were screened for the self-metathesis of allyltrimethoxysilane. However, the synthesis of 1,4-bis(trimethoxysilyl)butene is somewhat more complicated than that of 1,2-bis(triethoxysilyl)ethene. Unlike the self-metathesis reaction of vinyltriethoxysilane, the metathesis of allyltrimethoxysilane can be accompanied by an isomerization reaction, i.e. migration of the double bond along the alkyl chain by 1,3-H shifts. All tested commercial catalysts which revealed good activity in the metathesis of allyltrimethoxysilane also produced isomerization products. Therefore, alternative catalysts were investigated. Latent Schiff base containing catalysts, required from the University of Ghent spin-off Vi-acatt, revealed very good activity in the metathesis of allyltrimethoxysilane, when activated with phenyltrichlorosilane. Moreover, no isomerization products were produced with these complexes. However, GC-analysis of the reaction products revealed some impurities which could not be identified. More importantly, in all cases, diastereoisomeric mixtures were obtained. Based on previous synthesis procedure reported by researchers of our group, a second generation Hoveyda type catalyst bearing a chiral ligand was synthesized and successfully implemented in the synthesis of a diastereoisomeric butenylene-bridged PMO precursor.⁴²³ This chiral catalyst revealed a relatively high TON of 780 and produced no isomerization products. Moreover, the ($\approx 100\%$) pure *E*-isomer of 1,4-bis(trimethoxysilyl)butene could be attained. These results show that olefin metathesis is a powerful tool which can be exploited in the synthesis of novel olefinic PMO precursors. In a next stage, these pure diastereoisomeric precursors can be employed in the synthesis of PMO materials with exceptional properties.

Chapter 4

Ethenylene-bridged PMOs: From *E* to *Z*

Periodic mesoporous organosilicas are a promising class of ordered materials that combine the structural features of ordered mesoporous silicas with the chemical functionality of organic groups. Doing so, they open up a wide range of new opportunities in designing materials with novel organic functionalities and controlled morphological, structural and surface properties. The majority of the literature reports on PMOs have been focused on the synthesis of ordered mesoporous ethane silicas, probably due to the wide commercial availability of its precursor 1,2-bis(triethoxysilyl)ethane. As the functional groups of PMOs are homogeneously embedded inside the channel walls, the pore channels are easily accessible for further modification. From this perspective ethenylene-bridged PMOs are more interesting than ethane PMOs, as they offer plenty of opportunities for further surface modification based on olefin chemistry. However, to date, ethenylene-bridged PMOs have been synthesized using precursors that consist of a mixture of *E*- and *Z*-isomers, without considering the effect this may have on the PMO properties. Having developed ethene-PMO precursors with varying isomeric configuration, from the ($\approx 100\%$) pure *E*-isomer to the ($\approx 100\%$) pure *Z*-isomer, the influence of the diastereoisomeric configuration of the PMO pore walls on the overall structural properties, hydrothermal stability and surface group accessibility was investigated.

4.1 Ethenylene-bridged PMOs with different isomeric configurations

4.1.1 Synthesis procedure

A series of PMOs was synthesized by varying the precursor and keeping all other reaction parameters constant. Throughout this chapter, the precursor 1,2-bis(triethoxysilyl)ethene is abbreviated as BTSE, preceded by the diastereoisomeric configuration. I.e., *E*-BTSE, 80(*E,Z*)-BTSE and 50(*E,Z*)-BTSE consist *ca.* 100, 80

and 50 % of the *E*-isomer, while *Z*-BTSE is the 100 % pure *Z*-isomer. In a typical synthesis procedure, 1.00 g of Pluronic P123 is diluted in an acidified solution containing 47.80 ml of H₂O, 3.42 ml of concentrated HCl and 2.45 ml of n-butanol. The solution is stirred at room temperature for 1.5 hours upon which 1.86 ml of *E*-BTSE, 80(*E,Z*)-BTSE, 50(*E,Z*)-BTSE or *Z*-BTSE, is added. The final reactant molar composition is: P123 : BTSE : HCl : H₂O : n-butanol = 1 : 29 : 238 : 16097 : 155. This solution is stirred for 4 hours at 35 °C upon which 18.0 ml of n-butanol is added. The PMO material is successively aged for an additional 23 hours at 90 °C under static conditions. The mixture is left to cool down to room temperature after which the precipitated PMO is filtrated and washed with distilled water. The surfactant is removed by means of Soxhlet extraction using acetone over a period of 5 hours. This PMO synthesis procedure leads to ethenylene-bridged hybrid materials with different isomeric configurations. Throughout the text, the diastereoisomerically pure *E*-configured and *Z*-configured ethenylene-bridged PMOs are denoted as *E*-EBP and *Z*-EBP respectively, while 80(*E,Z*)-EBP and 50(*E,Z*)-EBP refer to PMOs consisting of 80 % *E*-isomer (20 % *Z*-isomer) and 50 % *E*-isomer (50 % *Z*-isomer), respectively. Disordered *Z*-configured ethenylene-bridged organosilicas are abbreviated as *Z*-EBO instead of *Z*-EBP, as these materials are not periodic. For the synthesis of *Z*-EBP, 8.9 ml of concentrated HCl was used, while keeping all other reaction parameters constant.

4.1.2 Nitrogen physisorption properties of PMOs

Typical nitrogen adsorption-desorption isotherms of ethenylene-bridged PMOs are illustrated in Figure 4.1 (a).

Based on their shape, the isotherms are of type IV according to the IUPAC classification and the hysteresis loop resembles that of type H1. Characteristic features which can be derived from the adsorption isotherms are: (1) nitrogen adsorption in the intrawall micropores at very low relative pressures, (2) multilayer adsorption in the mesopores and (3) a one-step capillary condensation, indicating uniform mesopores. This nitrogen adsorption process is schematically illustrated in Figure 4.1 (b). The presence of micropores is related to poly(ethylene oxide) chains of the surfactant template which penetrate the pore walls during the self-assembly process.

In Figure 4.1, the isotherms are divided in four relative pressure areas. These areas can be used to determine different characteristic properties of the porous material. At relatively low pressures, a first monolayer of nitrogen molecules is adsorbed on the surface. Subsequently, nitrogen molecules start to adsorb on top of each other. During the formation of these multilayers (area between A and B), the amount of adsorbed nitrogen is more or less linearly related to the increase of the relative pressure. This is the part of the adsorption isotherm which is used to calculate the specific surface area by the BET method. When the adsorbed nitrogen molecules on opposite pore walls start to “feel” each others potential, capillary condensation in the pores takes place which is accompanied with a strong increase in the amount of adsorbed gas (area between B and C). As the relative pressure at which capillary condensation occurs correlates with the pore radius by the Kelvin equation, the area between B and C is used to calculate the pore size

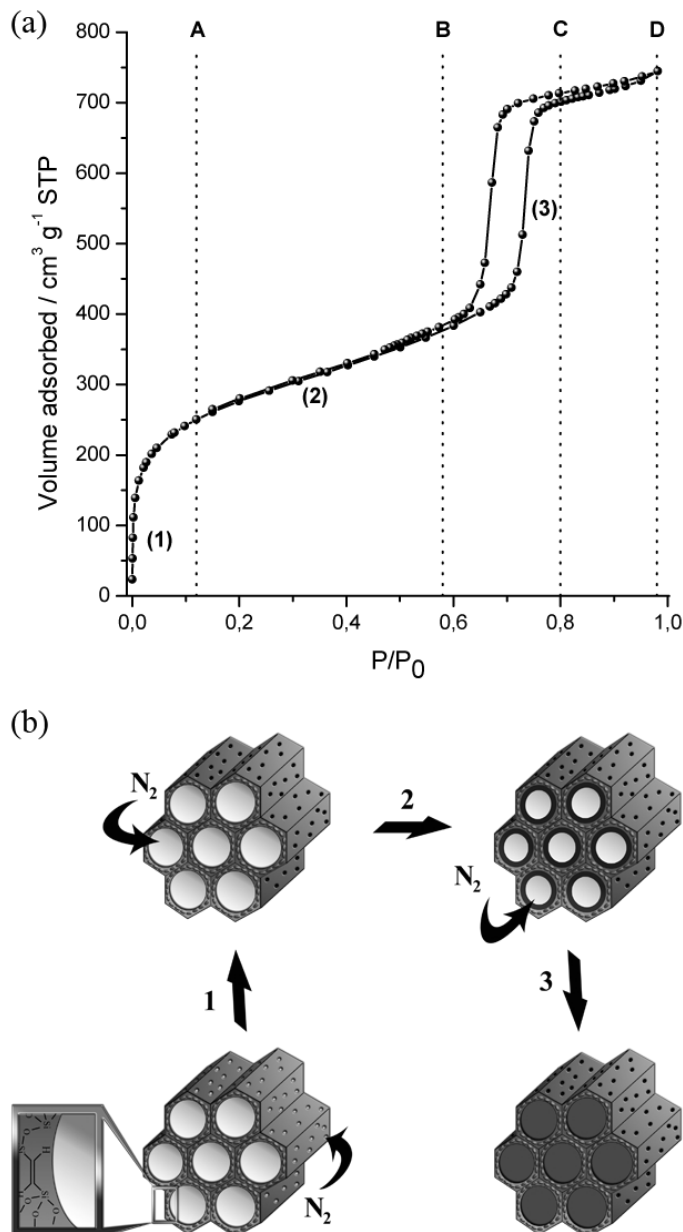


Figure 4.1: (a) Typical nitrogen adsorption-desorption isotherms of ethenylene-bridged PMOs. (b) Adsorption process of nitrogen in open cylindrical pores: 1) filling of the micropores, 2) multilayer adsorption in the mesopores and 3) capillary condensation of nitrogen in the mesopores.

distribution. Herein, the slope of the capillary condensation step is related to the pore size uniformity: the steeper the slope, the narrower the pore size distribution will be. When the capillary condensation is completed, the pores are completely filled with liquid nitrogen, so that no further adsorption is possible, and a plateau in the isotherm is apparent (area between C and D). This area is used to calculate the total pore volume of the porous system.

The desorption of nitrogen occurs at lower relative pressures than the adsorption, thus a hysteresis is formed. The shape of the hysteresis is important to predict the shape of the pores. This will be discussed in more detail later on in the text.

4.1.3 Isomeric configuration of ethenylene-bridged PMOs

To establish whether the isomeric configuration of the precursor is maintained in the corresponding PMO materials, these were analyzed with FT-Raman and ^1H - ^{13}C CP/MAS NMR spectroscopy. In Figure 4.2 the FT-Raman spectra of (a) *E*-EBP, (b) 80(*E,Z*)-EBP, (c) 50(*E,Z*)-EBP and (d) *Z*-EBP are given.

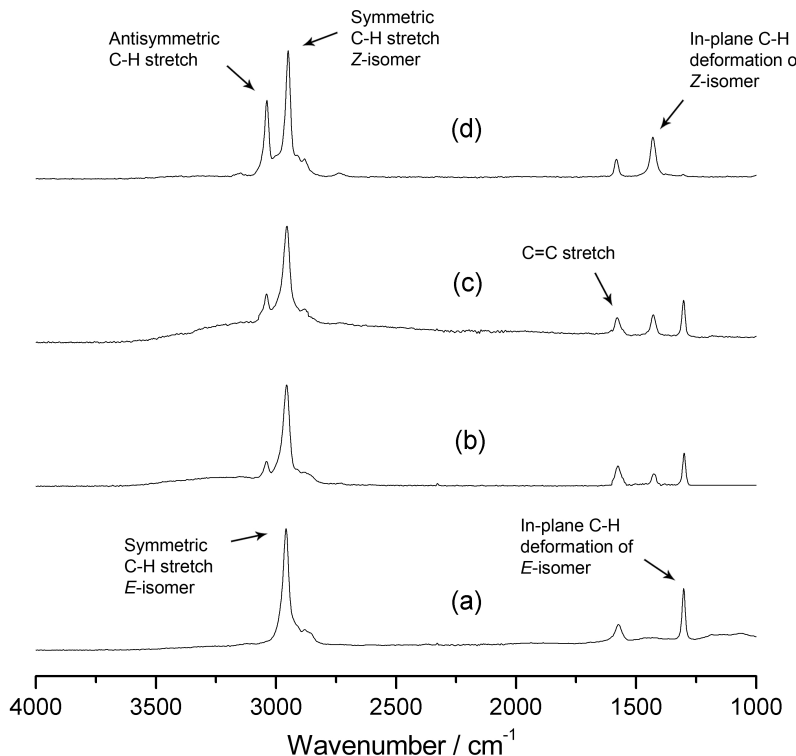


Figure 4.2: FT-Raman spectra of (a) *E*-EBP, (b) 80(*E,Z*)-EBP, (c) 50(*E,Z*)-EBP and (d) *Z*-EBP.

The FT-Raman spectrum of *E*-EBP (a) exhibits intense peaks at 2956, 1575 and 1301 cm^{-1} . These peaks can be assigned to the C–H stretch vibration, the C=C stretch vibration and the in-plane C–H deformation of the *E*-configured CH=CH

bridges, respectively. The FT-Raman spectrum of *Z*-EBO (d) exhibits intense peaks at 3038, 2949, 1582 and 1430 cm⁻¹. These peaks can be assigned to the antisymmetric and symmetric C–H stretch, the C=C stretch and the in-plane C–H deformation of the *Z*-configured CH=CH bridges, respectively. Comparison of spectrum (a) and (d) suggests that the C–H and the C=C stretch vibrations of both isomers have almost identical wavenumbers. Therefore, the peaks at 2956 and 1575 cm⁻¹ in spectrum (b) and (c) are superpositions of two peaks which can be assigned to the C–H and the C=C stretch vibrations of both isomers, respectively. Comparison of the four spectra also clearly shows that *E*-EBP, only consists of *E*-configured ethylene bridges, while *Z*-EBO only consists of *Z*-configured ethylene bridges. On the other hand, 80(*E,Z*)-EBP and 50(*E,Z*)-EBP clearly consist of both isomers.

The ¹H-¹³C CP/MAS NMR spectra of the above discussed PMO materials will be presented and discussed in detail further on in the text, at which point the PMO properties will be correlated with the structure of the pore walls at the molecular level.

4.2 Influence diastereoisomeric configuration on PMO structural properties

The isomeric purity of 1,2-bis(triethoxysilyl)ethene plays a significant role in the ordering of the ethylene-bridged PMOs, as illustrated by the XRD-patterns in Figure 4.3.

E-EBP has a much better ordering than 80(*E,Z*)-EBP and 50(*E,Z*)-EBP. *E*-EBP reveals three well-resolved peaks which can be attributed to the (100), (110) and (200) reflections. These assignments are consistent with a hexagonally ordered material with a *P6mm* space group. 80(*E,Z*)-EBP on the other hand, only reveals one peak which can be attributed to the (100) reflection of the 2D hexagonal unit cell. The intensity of the (100) reflection further decreases with increasing amount of *Z*-isomer.

In Figure 4.4, the nitrogen adsorption-desorption isotherms of *E*-EBP, 80(*E,Z*)-EBP, 50(*E,Z*)-EBP and *Z*-EBO are given. Distinctive features of these organosilicas are the capillary condensation and evaporation steps in the nitrogen isotherms. These are almost vertical in the case of *E*-EBP, while for 80(*E,Z*)-EBP these are far less steep. In fact, with increasing amount of *Z*-isomer, the inclinations of the capillary condensation and evaporation steps decrease. This reflects the much narrower pore size distribution of *E*-EBP when compared to that of 80(*E,Z*)-EBP and 50(*E,Z*)-EBP (see Figure 4.5).

When *Z*-BTSE is used as a precursor under the given reaction conditions, a microporous material is obtained. These results suggest that the *Z*-isomer of 1,2-bis(triethoxysilyl)ethene has a different reactivity than the *E*-isomer, which has to be taken into account when employing diastereoisomeric mixtures for the synthesis of ethylene-bridged PMOs.

The enhanced pore ordering and pore size uniformity of *E*-EBP is most probably a result of the homogeneous polycondensation of *E*-BTSE and in particular the more regular cross-linking and stacking of the *E*-configured ethylene-bridges.

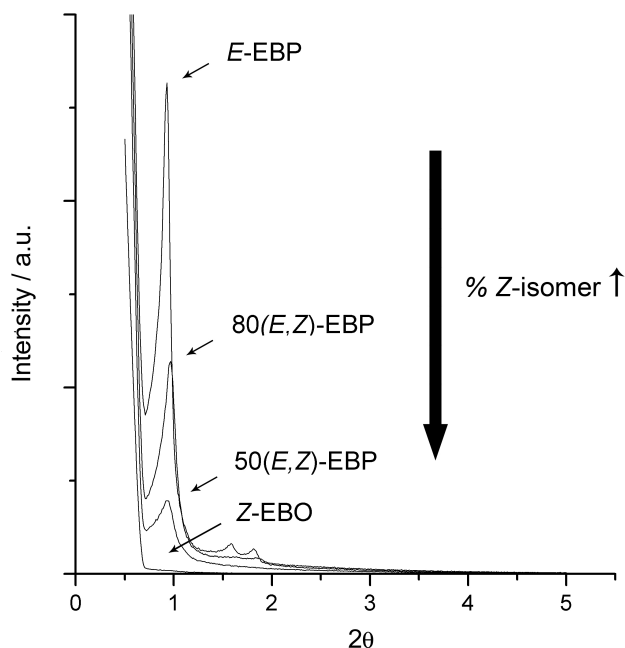


Figure 4.3: XRD-plots of *E*-EBP, 80(*E,Z*)-EBP, 50(*E,Z*)-EBP and *Z*-EBO.

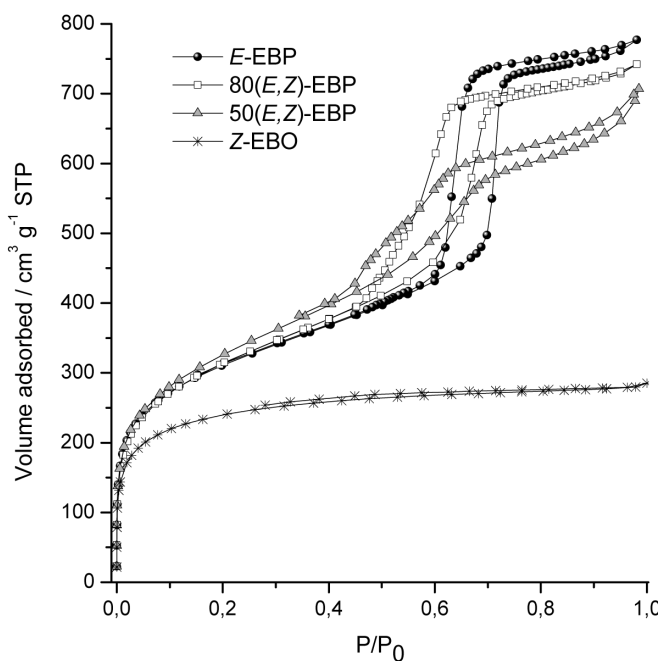


Figure 4.4: Nitrogen isotherms of *E*-EBP, 80(*E,Z*)-EBP, 50(*E,Z*)-EBP and *Z*-EBO.

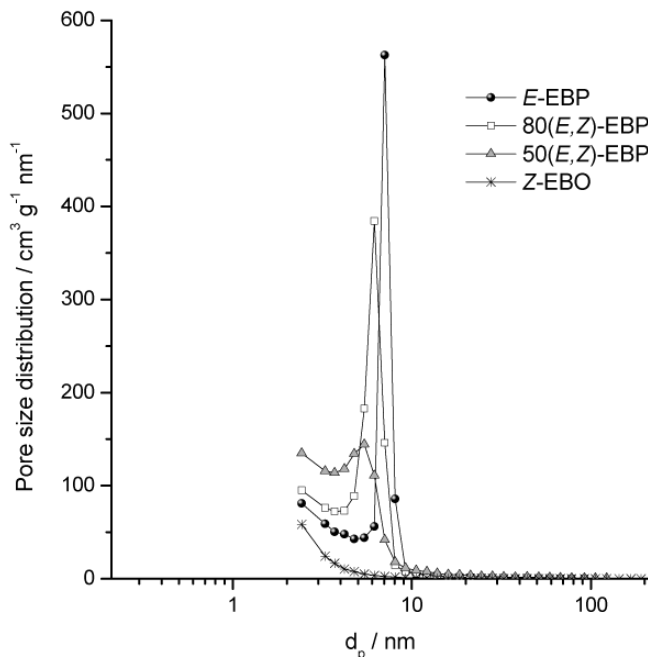


Figure 4.5: BJH pore size distributions of *E*-EBP, 80(*E,Z*)-EBP, 50(*E,Z*)-EBP and *Z*-EBO, calculated from the adsorption isotherms.

In the case of 80(*E,Z*)-BTSE and 50(*E,Z*)-BTSE, the polycondensation rates of the two isomers are different and the cross-linking and stacking of the ethylene bridges will proceed at random. Because the described synthesis procedure is optimized for the *E*-isomer of 1,2-bis(triethoxysilyl)ethene, the presence of the *Z*-isomer disturbs the self-assembly which results in an inferior structural ordering and pore size uniformity. This hypothesis is supported by the complete loss of structural ordering when employing *Z*-BTSE as a precursor. The structural ordering and pore uniformity of *Z*-configured ethylene-bridged PMOs (*Z*-EBP) can be enhanced by altering the reaction conditions. In particular, lowering the pH of the reaction mixture enhances the template/*Z*-BTSE interaction and favors the formation of *Z*-EBP with uniform pores instead of disordered *Z*-EBO. Further on in the text, the template/framework interaction will be discussed from an NMR perspective. In Figure 4.6 the pore size distributions of both *Z*-EBO and *Z*-EBP are given, illustrating the impact of the reaction mixture pH on the mesostructure formation. The required high acidity for the formation of *Z*-EBP (≈ 2.1 mol/l) when compared to that needed for *E*-EBP (≈ 0.8 mol/l), verifies the significant difference in reactivity between *Z*-BTSE and *E*-BTSE, and rationalizes the reduced pore ordering and uniformity of ethylene-bridged PMOs synthesized from diastereoisomeric mixtures.

In Table 4.1, the properties of the discussed hybrid materials are given. Besides having a drastic effect on the pore ordering and pore uniformity, the isomeric configuration clearly also has a significant effect on the micropore volume, the pore

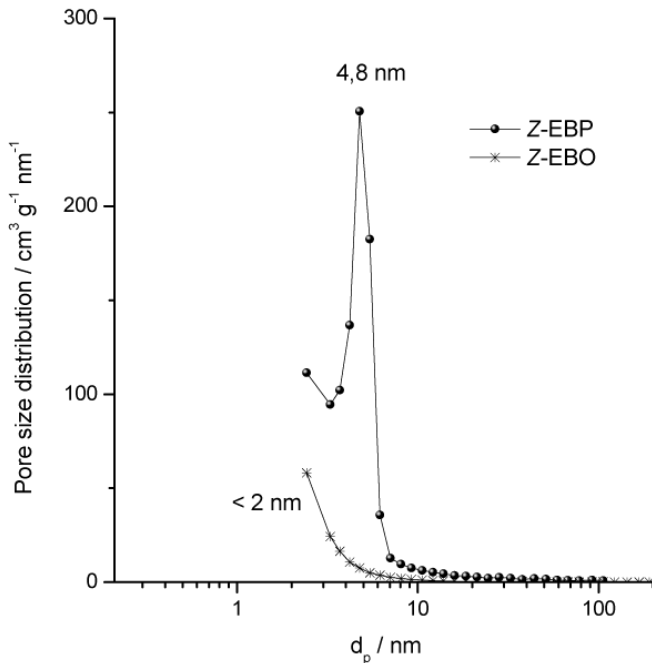


Figure 4.6: BJH pore size distributions of *Z*-EBO and *Z*-EBP, illustrating the impact of the reaction mixture pH on the mesostructure formation.

size and the pore wall thickness. The isomeric configuration has little effect on the unit cell dimension of the PMOs. Consequently, the decrease in pore size with the increasing contribution of *Z*-isomer is related to the increase of the pore wall thickness. The closer stacking of *E*-isomers in comparison to *Z*-isomers is a known fact which is related to their more linear shape, and rationalizes the increasing pore wall thickness with increasing content of *Z*-configured ethenylene groups.

Table 4.1: Properties of ethenylene-bridged PMOs with different isomeric configurations

Sample	% <i>E</i> -isomer	% <i>Z</i> -isomer	$S^{[a]}$ / $\text{m}^2 \text{g}^{-1}$	$V_t^{[b]}$ / $\text{m}^3 \text{g}^{-1}$	$V_\mu^{[c]}$ / $\text{m}^3 \text{g}^{-1}$	$D_p^{[d]}$ / nm	$a_0^{[e]}$ / nm	$t_w^{[f]}$ / nm
<i>E</i> -EBP	100	0	1133	1.20	0.18	7.1	11.0	3.9
80(<i>E,Z</i>)-EBP	80	20	1144	1.15	0.12	6.2	10.5	4.3
50(<i>E,Z</i>)-EBP	50	50	1187	1.09	0.06	5.4	10.8	5.4
<i>Z</i> -EBO	0	100	1143	0.44	0.44	< 2	-	-
<i>Z</i> -EBP	0	100	1160	1.03	0.14	4.8	10.7	6.0

[a] Surface area, [b] Total pore volume, [c] Micropore volume, [d] Pore diameter, [e] Unit cell dimension, [f] Pore wall thickness.

4.3 Understanding the local structure of ethenylene-bridged PMOs

4.3.1 ^1H - ^{13}C CP/MAS NMR of ethenylene-bridged PMOs

The ^1H - ^{13}C CP/MAS NMR spectrum of *E*-EBP, represented in Figure 4.7, clearly exhibits a single resonance at 146.7 ppm corresponding to the *E*-configured $\text{CH}=\text{CH}$ bridging organic groups. The spectrum of *Z*-EBO shows two lines at 150.0 and 138.8 ppm. The spectra of 80(*E,Z*)-EBP and 50(*E,Z*)-EBP result from the superposition of the lines detected for pure *E*- and *Z*-isomers. Though the line at 138.8 ppm in the spectra of ethene-PMOs consisting of the *Z*-isomer is unexpected, very careful examination of the reported solid-state NMR data for typical ethene-PMOs (i.e. consisting of both isomers), also indicate the presence of this line, while the expected peak at 150 ppm is usually masked by a more intense line from the *E*-isomer at *ca.* 147 ppm.^{300,301,306} However, so far this unexpected line has either been overlooked, or has not been further investigated, as there is no mention of its existence. Therefore, with the aim to explain the line at 138.8 ppm, additional NMR-investigations were performed.

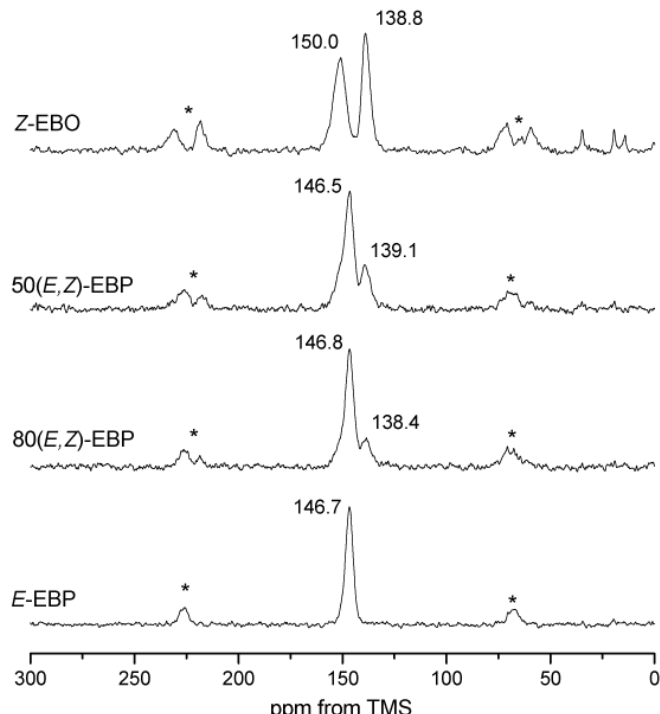


Figure 4.7: ^1H - ^{13}C CP/MAS NMR spectra of *E*-EBP, 80(*E,Z*)-EBP, 50(*E,Z*)-EBP and *Z*-EBO, acquired at an MAS rate of 8 kHz using a contact time of 2 ms. Asterisks denote spinning sidebands.

4.3.2 Structure of PMO pore walls: an NMR investigation

To examine the origin of the second resonance at 138.8 ppm, which is associated with the presence of the *Z*-diastereoisomer in the PMO framework, ^1H - ^{13}C CP/MAS NMR kinetic and Heteronuclear Correlation (HETCOR) experiments were performed at the university of Liverpool by the group of prof. Y. Khimyak. The obtained results, which were interpreted by prof. Khimyak, are summarized below.

VCT (Variable Contact Time) measurements are helpful for studying structure and dynamics of complex materials and have been widely employed to examine mesoporous silica materials⁴⁵⁵ and PMOs^{319,456}. CP kinetics are measured by recording dependencies of signal intensity versus contact time. In Figure 4.8, the ^1H - ^{13}C CP/MAS kinetic curves for *E*-EBP, *Z*-EBP and *Z*-EBO are given and compared to that of vinyl-functionalized silica.

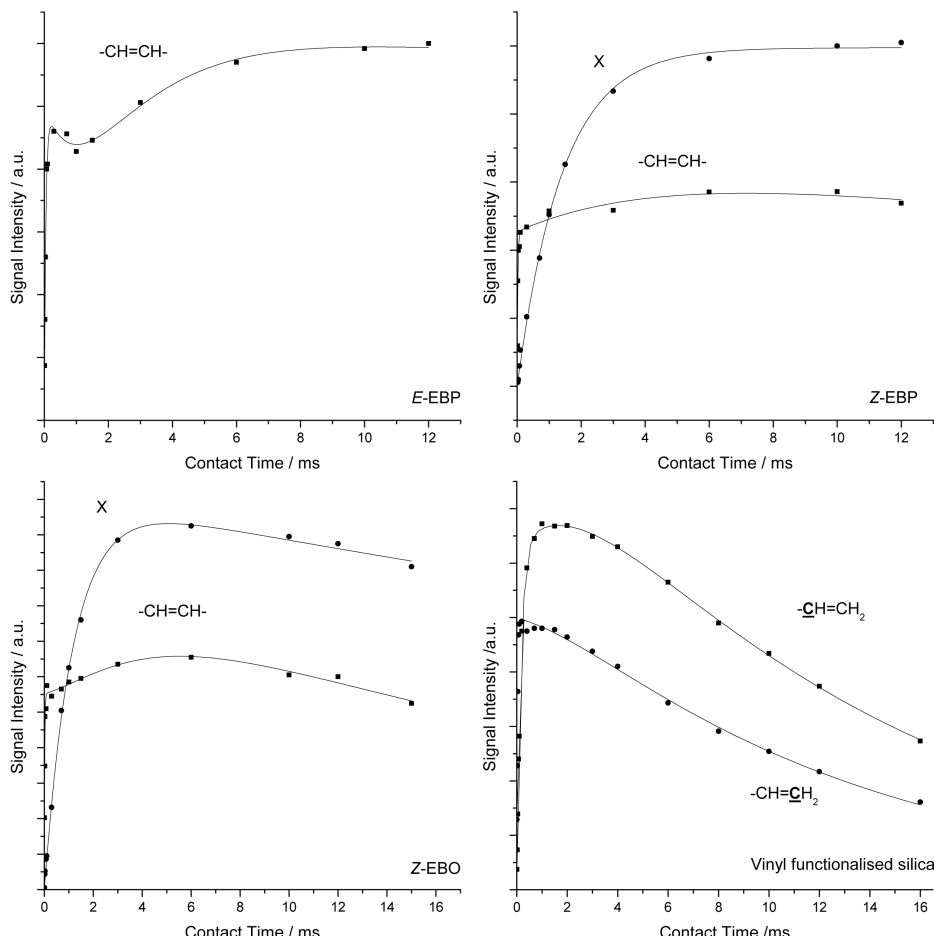


Figure 4.8: ^1H - ^{13}C CP/MAS kinetic curves for *E*-EBP, *Z*-EBP, *Z*-EBO and vinyl-functionalized silica.

Similarly to the recently reported mono- and bifunctional $\text{CH}_2\text{CH}_2/\text{CH}=\text{CH}$ PMOs, the $^1\text{H}-^{13}\text{C}$ CP/MAS kinetics curves give unsatisfactory results when fitted using the typical I-S or the more complex I-I*-S models.³¹⁹

The unusual CP kinetics curves can only be explained using a model where two components with different T_{IS} (CP time constant) and $T_{1\rho}^H$ (proton relaxation time in the rotating frame) times are identified depending on the mobility of the CP-determining ^1H source spins. The “rigid” component displays extremely short T_{CP} (time constant describing the cross-polarization transfer) and $T_{1\rho}^H$ times and the “mobile” component shows much longer T_{CP} and $T_{1\rho}^H$. The fast CP of the rigid components is a result of directly attached protons with reduced mobility and is indicative of a strong $^1\text{H}-^{13}\text{C}$ heteronuclear dipolar coupled network, thus representing organic bridges embedded in the bulk of hybrid pore walls. The mobile component with slow CP kinetics can be attributed to organic bridges located at the pore wall interface.

Looking at the kinetic curves in Figure 4.8, *E*-EBP exhibits short and long T_{IS} times, indicative of bulk and surface bound $\text{CH}=\text{CH}$ bridges respectively. Though *Z*-EBO and *Z*-EBP were fitted using different models, both display similar T_{IS} times for the unknown environment at 138.8 ppm. Due to the similarity in chemical shifts, a vinyl-functionalized silica was also examined. Clearly, no similarity exists between that of the end $=\text{CH}_2$ group and the resonance at 138.8 ppm. It is important to note that the peak at 138.8 ppm displays much slower CP-kinetics, indicative of ^{13}C sites with no directly attached protons. The CP for such sites relies on ^1H spin-diffusion.

Further information concerning the peak at 138.8 ppm can be attained with $^1\text{H}-^{13}\text{C}$ HETCOR. $^1\text{H}-^{13}\text{C}$ HETCOR experiments provide detailed information on the spatial proximity of the organic functionalities. The HETCOR spectrum correlates ^{13}C resonances to ^1H sites in their close proximity.

The $^1\text{H}-^{13}\text{C}$ HETCOR spectrum of *Z*-EBO, represented in Figure 4.9, shows the same cross-peak pattern for the lines at 150 and 138.8 ppm. This is indicative that two types of ^{13}C species represented by respective lines in the ^{13}C spectra are in close proximity to the same ^1H source, i.e. sp^2 hydrogen atoms, and belong to the same porous network.

Based on these advanced NMR experiments, valuable information has been gathered and some conclusions have been drawn on the chemical nature of the species. The assignment of the additional resonance at 139 ppm in the $^1\text{H}-^{13}\text{C}$ CP/MAS NMR spectra presented a significant challenge. Aiming at the identification of the chemical nature of the species represented by these peaks, CP/MAS NMR kinetic and HETCOR experiments were performed. These experiments are appropriate for such mainly amorphous materials and reveal several details about their identity.

It is important to point out, that the exact nature of the species represented by the peak at ca. 139 ppm in the $^1\text{H}-^{13}\text{C}$ CP/MAS NMR spectra is not clear at this point in time. However, the absence of any impurities in the precursors (see chapter 3) support the idea that the species represented by the line at 139 ppm are formed during the supramolecular self-assembly of the mesostructured solids.

A complete, unambiguous assignment of the peak at ca. 139 ppm in the $^1\text{H}-^{13}\text{C}$ CP/MAS NMR spectra would require triple resonance experiments and possibly

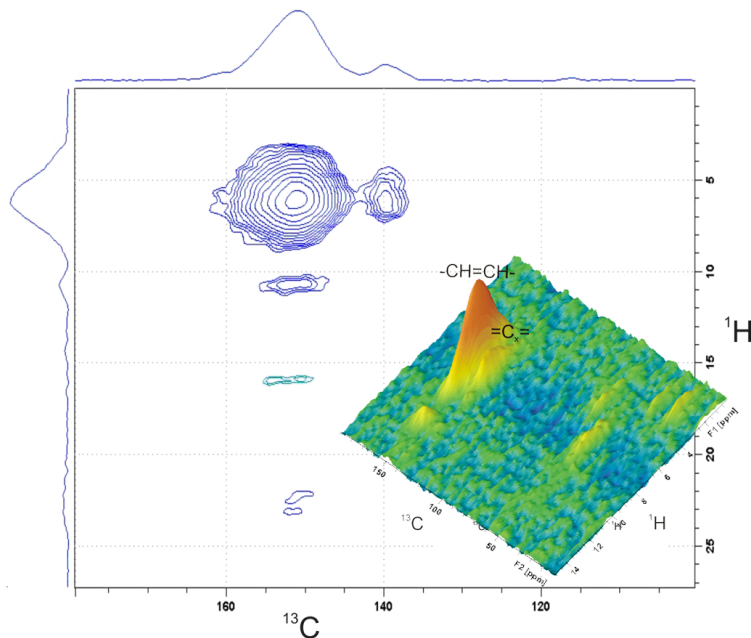


Figure 4.9: ^1H - ^{13}C HETCOR NMR experiment of *Z*-EBO. The figure clearly illustrates that both carbon environments are coupled to the $\text{CH}=\text{CH}$ protons. Low intensity cross-peaks correlate to residual template and OCH_3 environments.

isotopic enrichment of the precursors. The cost and time required for these experiments are prohibitive and the outcomes, while potentially interesting, are not essential in this research work.

4.3.3 Template-framework interactions

In Figure 4.10 the ^1H - ^{13}C CP/MAS NMR spectra of as-synthesized (i.e. surfactant containing) *E*- and *Z*-configured ethenylene-bridged PMOs are given. Besides the typical resonances that can be assigned to the $\text{CH}=\text{CH}$ bridging organic groups, the spectra reveal resonances at *ca.* 76, 71 and 17 ppm which can be ascribed to the surfactant template.

To elucidate template-framework interactions, ^1H - ^{13}C VCT CP/MAS NMR of as-synthesized PMOs was performed by the group of Khimyak (see Figure 4.11). *E*-EBP and *Z*-EBP share similar T_{1S} and $T_{1\rho}^H$ times indicating that the template is held in a rigid geometry regardless of the isomeric configurations. The framework-forming organic moieties at 146.8 ppm (*E*-isomer) and 149.6 ppm (*Z*-isomer) show the presence of two components with significantly different CP-kinetics. Since the ^1H pool is now dominated by the organic template, the $T_{1\rho}^H$ times for the mobile component are reduced in comparison with the template extracted materials. The CP-kinetics of the peak at 140 ppm is typical for quaternary carbon sites. Similarly to the other sites, the $T_{1\rho}^H$ time is reduced in comparison with the template extracted materials.

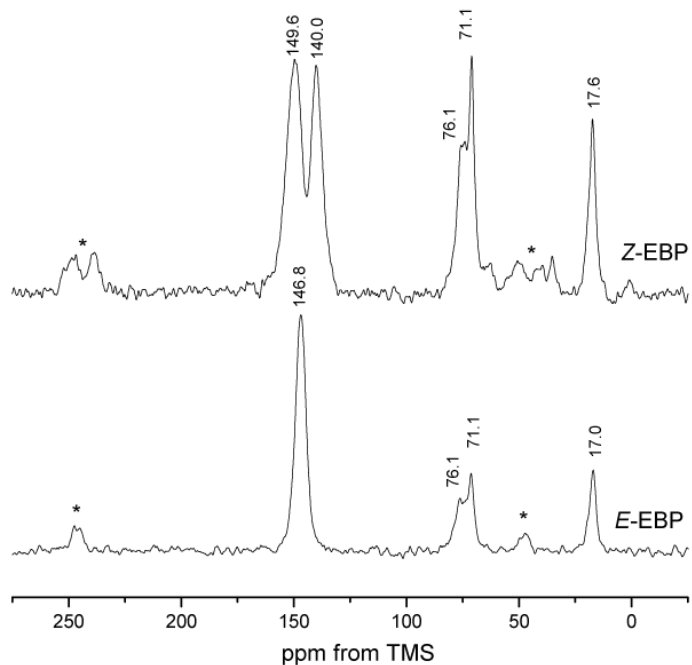


Figure 4.10: ^1H - ^{13}C CP/MAS NMR spectra of as-synthesized *E*-EBP and *Z*-EBP, acquired using a 1.5ms contact time at a MAS rate of 8.0 kHz. Asterisks denote spinning sidebands.

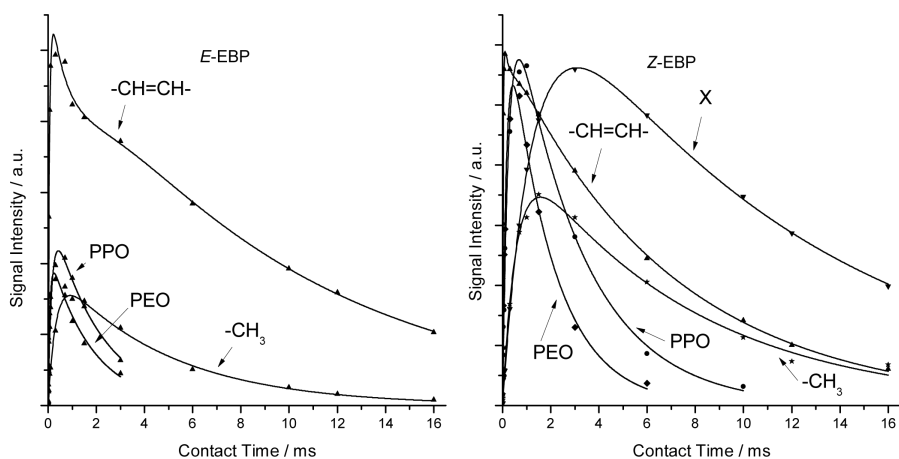


Figure 4.11: ^1H - ^{13}C CP/MAS kinetic curves for as-synthesized *E*-EBP and *Z*-EBP.

By means of ^1H - ^{13}C CP/MAS dynamics the strength of the template-framework interactions could be assessed. The ^{13}C resonance at *ca.* 71 ppm attributable to the PEO block of the template shows faster CP-kinetics in comparison with the peaks of the PPO blocks ($-\text{OCH}_2\text{CH}(\text{CH}_3)-$ at *ca.* 76 ppm, $-\text{OCH}_2\text{CH}(\text{CH}_3)-$ at 74 ppm and $-\text{OCH}_2\text{CH}(\text{CH}_3)-$ at *ca.* 17 ppm). This is indicative of its restricted mobility due to location at the pore interface. The slower CP-kinetics of the peaks corresponding to the PPO blocks is due to their location in the middle of the pores. Such distribution of different blocks of the template is confirmed by the 2D Wideline Separation (WISE) spectra of the as-synthesized ethene-PMO 80(*E,Z*)-EBP (see Figure 4.12). The ^1H - ^{13}C WISE spectrum correlates the ^{13}C spectrum (structure) in the direct dimension with the ^1H spectrum (mobility) in the indirect dimension. That is the ^1H line width is dependent upon the mobility with narrower lines observed for increasingly mobile ^1H environments. The ^{13}C dimension shows the same template resonances as described in the CP/MAS spectra (Figure 4.7) correlating to the broad lines in the ^1H dimension.

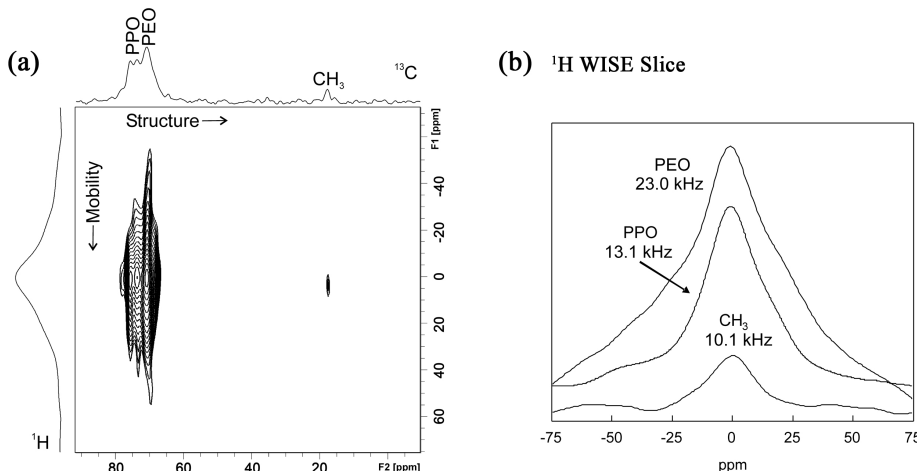


Figure 4.12: ^1H - ^{13}C WISE NMR spectrum of as-synthesized 80(*E,Z*)-EBP (a) and corresponding ^1H projections (b).

The ^1H wideline corresponding to the PEO block confirms the rigidity of its protons as a line width of 23.0 kHz is observed. However, the ^1H lines correlating to the ^1H PPO environments are significantly narrower than that of the PEO species providing further confirmation that the PPO block is highly mobile within the pores of the mesoporous framework. It is also worth noting that the ^1H projection of the $\text{CH}=\text{CH}$ groups display a broad resonance superimposed on a narrow peak, confirming two different ^1H mobility's depending on the location of the functionalities within the framework consistent with ^1H - ^{13}C CP kinetics studies.

The ^1H - ^{13}C CP/MAS kinetics curves and 2D WISE NMR spectra have both provided complementary information on the environments of the template components in as-synthesized ethene-PMOs. The similarity in the CP-kinetics parameters between the as-synthesized well-ordered *Z*- and *E*-configured ethenylene-bridged

PMOs is indicative of comparable strength of template-framework interactions leading to materials with similar degree of mesoscopic ordering. The PEO component is strongly interacting with the hybrid pore walls whereas, the PPO block is mobile in the pores (Figure 4.13). The interactions between the hybrid walls and the PEO block are H-bonding through terminal PEO-OH groups and the Si-O-Si environments as well as ion-pairing through the halide anion of the protonated ether functionality in the PEO blocks and the protonated silanol functionalities in the PMO framework, as shown in Figure 4.13.

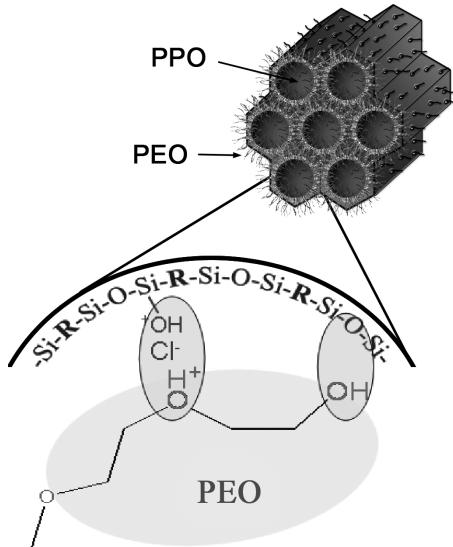


Figure 4.13: Template-framework interactions inferred from the ^1H - ^{13}C CP/MAS kinetics and WISE experiments.

4.4 Hydrothermal stability of ethenylene-bridged PMOs

To investigate the influence of the isomeric configuration of the ethenylene bridges in the PMO pore walls on the stability of these materials, the surfactant-free PMOs *E*-EBP and 80(*E,Z*)-EBP were steamed for 24 h in an autoclave at 105 °C, the results of which are illustrated in Figure 4.14. 80(*E,Z*)-EBP was chosen as a reference as this sample comes closest (in terms of isomeric configuration) to the ethenylene-bridged PMOs which have been reported upon so far. Clearly, the hydrothermal treatment has a significantly larger negative effect on the properties of 80(*E,Z*)-EBP in comparison to *E*-EBP, indicating that the stability of ethenylene-bridged PMOs can be enhanced by employing *E*-BTSE instead of the commonly applied precursor 80(*E,Z*)-BTSE. Most interesting is the contraction of the pore walls of 80(*E,Z*)-EBP, while these of *E*-EBP remain unaffected. This may be explained by the poorer packing of the ethenylene groups in 80(*E,Z*)-EBP when compared to

E-EBP. The contraction of the pore walls after hydrothermal treatment, confirms the hypothesis that the increase of the pore wall thickness with increasing amount of *Z*-isomer, can be related to the poorer stacking of the *Z*-configured ethenylene bridges when compared to that of the *E*-configured ethenylene bridges.

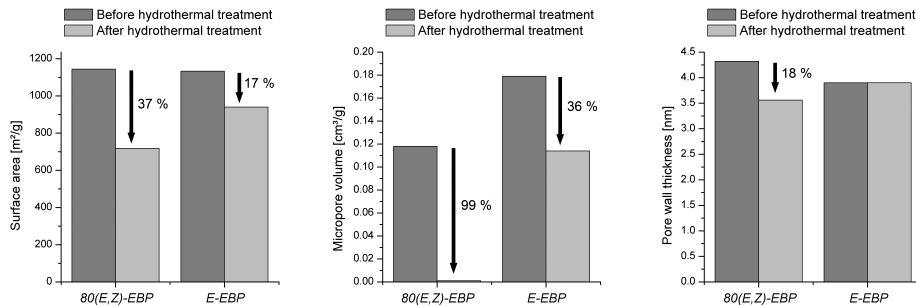


Figure 4.14: Influence of the isomeric configuration on the hydrothermal stability.

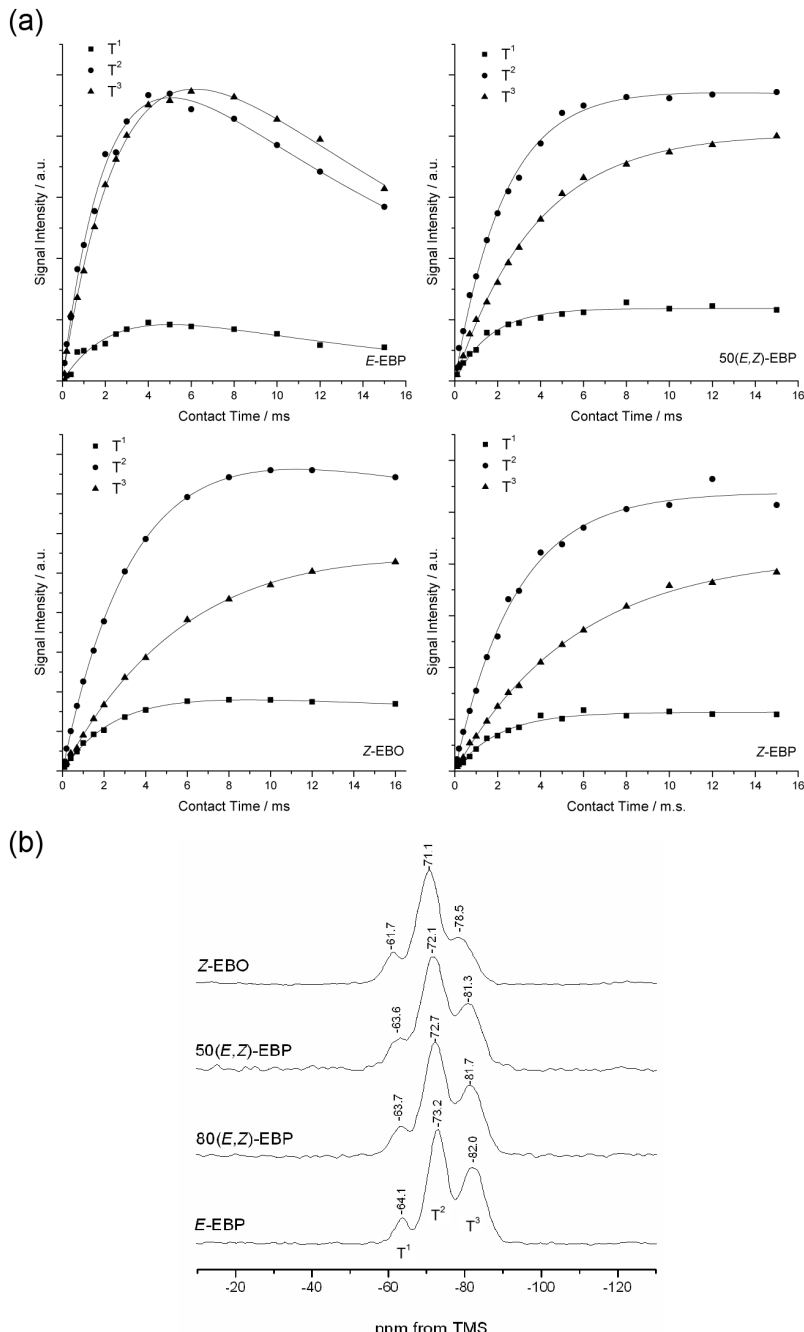
The lower hydrothermal stability of the ethenylene-bridged PMOs containing the *Z*-isomer can also be assigned to the lower condensation degree in the PMO pore walls. The degree of condensation of pore walls was assessed using the ^1H - ^{29}Si CP/MAS kinetics, represented in Figure 4.15 (a).

All ethenylene-bridged PMOs reveal an increase of the T_{1S} times with Si condensation from R-Si(OH)₂(OSi) (T^1) to R-Si(OSi)₃ (T^3) environments. This is to be expected due to protons in the Si-OH moieties facilitating CP “build up”. The PMOs containing *Z*-configured CH=CH bridges show no evidence of $T_{1\rho}^H$ relaxation suggesting the “proton pool” is sparsely populated and only weak ^1H - ^1H dipolar coupling is present. *E*-EBP shows a significant $T_{1\rho}^H$ relaxation, suggesting a stronger ^1H - ^1H dipolarly coupled network. Therefore, the degree of condensation of the framework was calculated taking into account the differences in ^1H - ^{29}Si CP/MAS kinetics. Thus, the $(T^1+T^2)/T^3$ ratio is the lowest for *E*-EBP and is much higher for the PMOs consisting of *Z*-configured CH=CH bridges, indicating a more condensed framework in the former (see Table 4.2).

Table 4.2: Degree of framework condensation calculated using the areas obtained under Gaussian fitting, acquired using 2ms contact time

Sample	% <i>Z</i> -isomer	$(T^1+T^2)/T^3$
<i>E</i> -EBP	0	1.37
80(<i>E,Z</i>)-EBP	20	1.68
50(<i>E,Z</i>)-EBP	50	1.92
<i>Z</i> -EBP	100	2.53
<i>Z</i> -EBO	100	2.75

The line widths of ^{29}Si resonances are the largest for *Z*-EBO, as illustrated in Figure 4.15 (b).



4.5 Chemical accessibility of the ethene functions: bromination

The chemical accessibility of the PMO ethene functionalities was investigated by means of bromination. Figure 4.16 gives the FT-Raman spectra of *E*-EBP, (a) before and (b) after bromination. An intense peak at 639 cm^{-1} is visible in spectrum (b), which can be assigned to the C–Br stretch vibration. A reduction of the peaks at 1573 and 1300 cm^{-1} , which can be assigned to the C=C stretch vibration and the in-plane C–H deformation, is also visible.

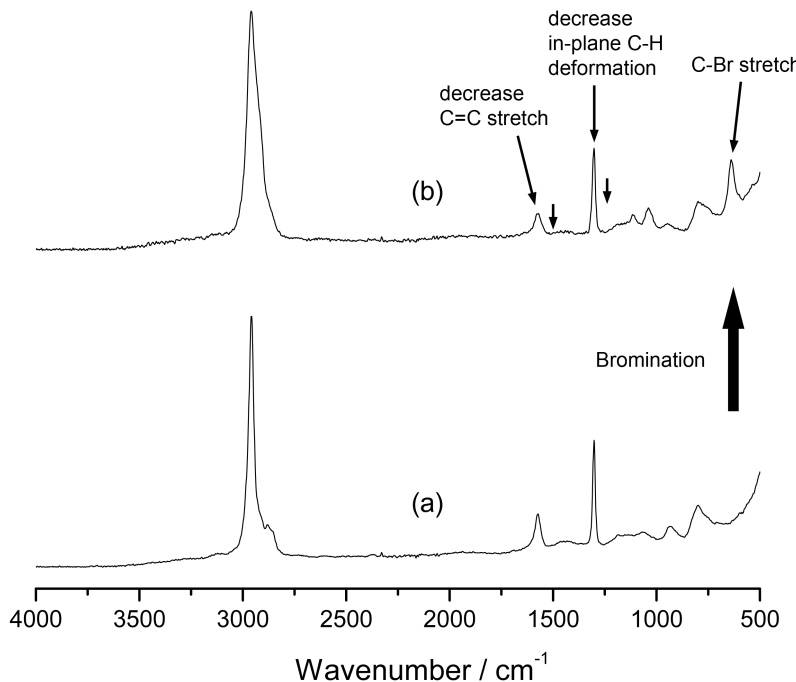


Figure 4.16: FT-Raman spectra of *E*-EBP, (a) before and (b) after bromination.

In Figure 4.17 the ^{13}C CP/MAS NMR spectra are given of *E*-EBP, (a) before and (b) after bromination. In spectrum (b), an additional resonance at 34.4 ppm is apparent, which can be assigned to the C–Br organic groups. These results confirm the FT-Raman data, indicating that the surface CH=CH functionalities react readily with bromine.

By means of gravimetric analysis the bromine accessibility of the surface ethene functionalities was also investigated, as a function of reaction time. The bromine vapor reacts rapidly with the PMO ethene groups. After 30 minutes the amount of brominated ethene functions is estimated at *ca.* 1.7 per nm^2 . After 60 and 120 minutes, *ca.* 1.8 and 1.9 ethene functions per nm^2 are brominated, respectively. By further prolonging the reaction time, no significant increase in bromination is established, indicating that all accessible C=C double bonds have reacted with

bromine. Via FT-Raman spectroscopy, the percentage of accessible C=C double bonds is estimated at approximately 30 %. This is in good agreement with the elementary analysis which suggested that ca. 25 % of the C=C double bonds are accessible to bromine.

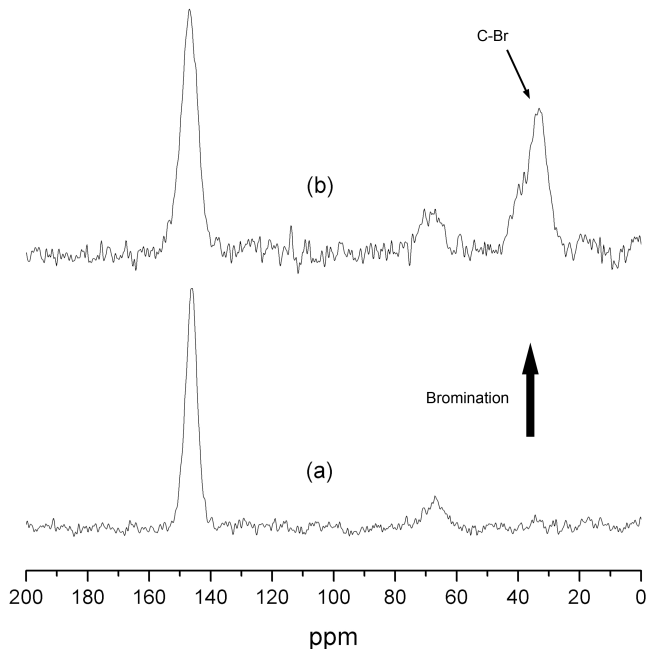


Figure 4.17: ^{13}C CP/MAS NMR spectra of *E*-EBP, (a) before and (b) after bromination.

4.6 Conclusions on the synthesis of diastereoisomeric PMOs

By employing home-made isomeric PMO precursors, diastereoisomeric pure *E*- and *Z*-configured ethenylene-bridged PMOs were synthesized for the very first time. We have shown that both diastereoisomers of 1,2-bis(triethoxysilyl)ethene have totally different reactivities, and that this has to be taken into account when using diastereoisomeric mixtures for the synthesis of ethenylene-bridged PMOs. The use of the pure *E*-isomer of 1,2-bis(triethoxysilyl)ethene, as alternative to the diastereoisomeric mixture, as a precursor for the synthesis of ethenylene-bridged PMOs, enhances the structural ordering, the pore size uniformity and the hydrothermal stability.

In order to develop *Z*-configured ethenylene-bridged PMOs, the pH of the reaction mixture has to be lowered considerably. Otherwise, disordered microporous materials are attained.

With the aim of understanding the local structure of the described ethenylene-bridged PMOs, a solid-state NMR investigation was performed. In particular, an unexpected resonance in the ^1H - ^{13}C CP/MAS NMR spectra of ethene-PMOs consisting of *Z*-configured CH=CH functionalities lead us to conduct a more detailed examination of these hybrid materials.

Variable contact time experiments revealed that the concerned unexpected resonance has much slower CP-kinetics, which is indicative of ^{13}C sites with no directly attached protons. On the other hand, the heteronuclear correlation spectrum of a *Z*-configured ethene-PMO revealed the same cross-peak pattern for the resonances of both isomers. This is indicative for two types of ^{13}C species, represented by the respective lines in the ^{13}C spectra, that are in close proximity to the same ^1H source, i.e. sp² hydrogen atoms, and belong to the same porous network.

To elucidate template-framework interactions, variable contact time and 2D wide-line separation experiments of as-synthesized PMOs were performed. Both techniques have provided complementary information on the environments of the template components in as-synthesized ethene-PMOs. The PEO blocks of the surfactant template strongly interact with the hybrid pore walls whereas, the PPO block is mobile in the pores. The interactions between the hybrid walls and the PEO blocks are H-bonding through terminal PEO-OH groups and Si-O-Si environments as well as ion-pairing through the halide anion of the protonated ether functionality in the PEO blocks and the protonated silanol functionalities in the PMO framework.

We have also demonstrated that ethene-PMOs can be further modified through olefin chemistry. Ethene-PMOs react readily with bromine, allowing about 25 % bromination of the CH=CH organic groups. The fast reactivity of these PMOs with bromine indicates that the surface functionallities are easily accessible through the uniform and open pore structures, even though bromine is quite a bulky molecule. The highly accessible surface groups of ethene-PMOs make these porous architectures very appealing and potentially interesting for various applications, such as catalysis and environmental technology.

The research described in this chapter has been accepted to be published in the literature as a peer review article.⁴⁵⁴

Chapter 5

Understanding Mesostructure Formation

The mechanisms involved in mesostructure formation are very complex and difficult to grasp. Many research efforts have therefore been made to explain the formation process of mesostructured materials in order to be able to control the synthesis parameters and guide the self-assembly toward desired porous architectures. Moreover, with the complexity of mesostructure design, the interpretation of results is not always straightforward. Extensive characterization is often required in order to fully elucidate developed mesostructures.

During research projects, unexpected and ambiguous results are often obtained. Sometimes these are discarded or even overlooked. In any case, such puzzling data often lead to the most interesting, yet challenging discoveries. The results described in this chapter belong to this category. When examining the influence of pH on mesostructure formation, ethene-PMOs were attained which exhibited peculiar nitrogen sorption isotherms with unexpected hysteresis loops. Further investigation revealed a very interesting relation between the reaction mixture pH and the shape of the hysteresis loops in the nitrogen sorption isotherms of the obtained PMO materials. Aiming to explain this phenomenon, a more profound investigation was conducted, which kind of started a snow ball effect. With the aim of gathering expertise from different research groups to fully elucidate the ambiguous physisorption results, a collaboration with the University of Utrecht, the Catholic University of Leuven, and Rutgers (State University of New Jersey) was made. The true nature of these periodic mesoporous organosilicas was ultimately disclosed by means of nitrogen gas physisorption, non-local density functional theory (NLDFT), SAXS, TEM and electron-tomography (ET).

5.1 Influence of pH on N₂-physisorption properties of ethene-PMOs

A set of diastereoisomerically pure *E*-configured ethylene-bridged PMOs with various pore systems was developed by fine-tuning the acidity of the reaction mix-

ture during the synthesis. In Table 5.1 the different PMO samples and their synthesis details are given.

Table 5.1: Synthesis details of *E*-configured ethenylene-bridged PMOs (EBPs)

Sample	P123 / mmol	<i>E</i> -BTSE / mmol	n-butanol / mmol	-log[HCl]
EBP-1	1	30	0	-0.200
EBP-2	1	30	0	0
EBP-3	1	30	0	0.125
EBP-4	1	30	0	0.308
EBP-5	1	30	0	0.606
EBP-6	1	30	0	0.801
EBP-7	1	30	0	0.903
EBP-8	1	30	0	1.203
EBP-9	1	30	155	0.10

Typical nitrogen isotherms of these PMOs are illustrated in Figure 5.1. The described PMOs are characterized by type IV adsorption isotherms with sharp one-step capillary condensations, indicating uniform mesopores. The desorption isotherms are distinctive for each of these mesoporous systems. Herein, the occurrence of open cylindrical, blocked or confined interconnected pores of different sizes and shapes determine the desorption behavior. The capillary evaporation is related to the equilibrium gas-liquid phase transition in the pores. In the case of EBP-9, a one-step desorption isotherm and a narrow H1 type hysteresis loop is apparent. These characteristics of equilibrium desorption are typical for materials with cylindrical mesopores which are open at both ends. EBP-1 on the other hand, reveals a delayed one-step desorption isotherm and a H2 type hysteresis loop which is typical for materials with confined mesopores or mesopores with ink-bottle necks. When large mesopores are connected and confined by smaller passages, the capillary evaporation of the condensed nitrogen in the pore center is delayed until the vapor pressure is reduced below the equilibrium desorption pressure of these passages. This phenomenon is often referred to as pore blocking. The relative pressure at which the hysteresis loop closes is related to the size of the interconnecting passages, or pore entrances in the case of ink-bottle pores, and on the number of interconnecting passages versus mesopore cavities. However, in the case of nitrogen physisorption at 77 K, the closing point of the hysteresis loop can never occur at relative pressures smaller than ≈ 0.42 . Below this relative pressure value, the capillary condensate is unstable, and spontaneous cavitation of nitrogen occurs at $p/p_0 > 0.42$, resulting in a sharp capillary evaporation step in the desorption isotherm.⁴⁵⁷ This is clearly illustrated by EBP-1 in Figure 5.1.

EBP-6 and EBP-2, exhibit remarkable two-step desorption isotherms (see Figure 5.1), indicating the presence of both open cylindrical and confined or blocked mesopores. Herein, the high relative pressure desorption step corresponds to the equilibrium desorption in open mesopores, as schematically illustrated by Figure 5.2. At these relatively high pressures, the blocked pores remain filled until the vapor relative pressure is reduced to ≈ 0.48 , at which the cavitation of the condensed nitrogen in the blocked pores takes place. In other words, the fraction of blocked pores in EBP-2 is substantially larger than in EBP-6.

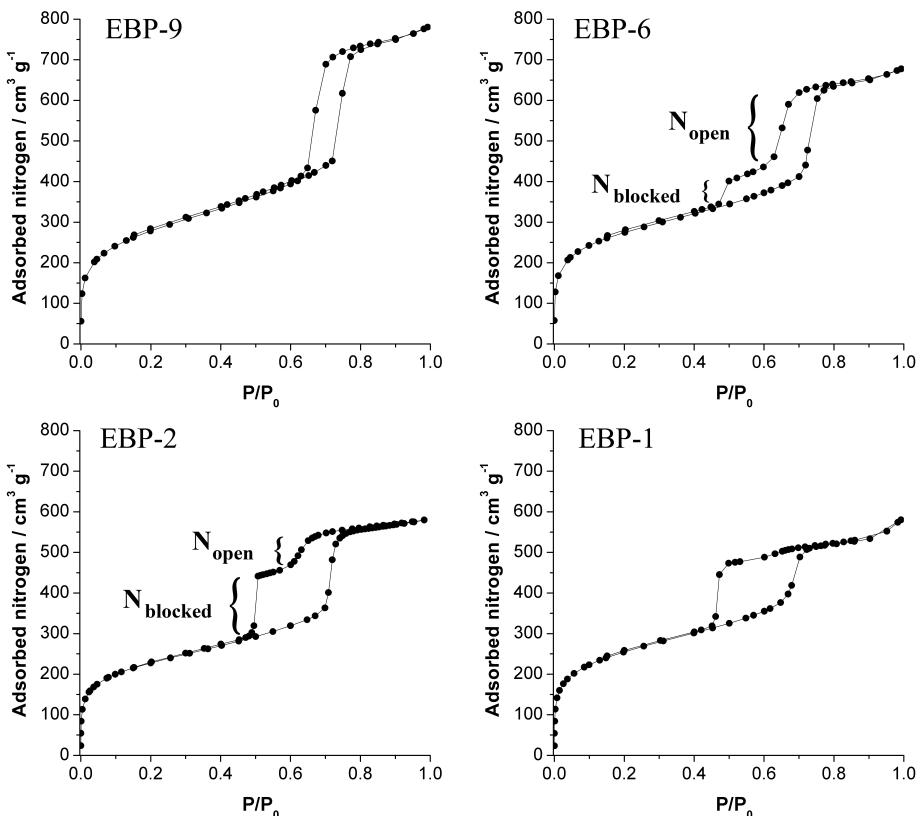


Figure 5.1: N₂-isotherms of ethene-PMOs with different fractions of blocked mesopores. EBP-9 consists exclusively of open mesopores, EBP-6 has a relatively small fraction of blocked mesopores, EBP-2 has a relatively large fraction of blocked mesopores and EBP-1 consists mainly of blocked mesopores.

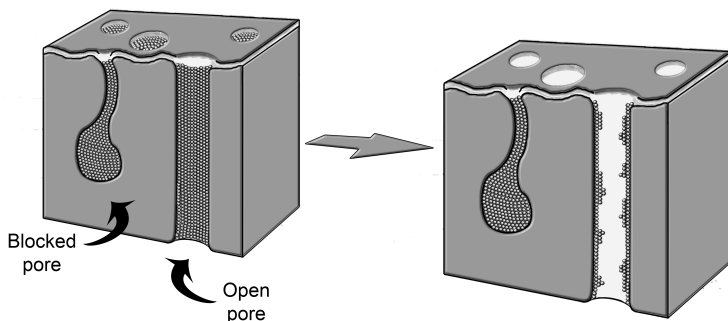


Figure 5.2: Capillary evaporation of nitrogen in open cylindrical mesopores, while the blocked mesopores remain filled.

These unusual two-step desorption isotherms are very similar to those previously reported upon by Van Der Voort et al.⁴⁵⁸ Herein, the mesopores of the described silica materials (PHTS or Plugged Hexagonal Templated Silicas) are blocked by microporous nanocapsules, referred to as plugs. However, the PMOs described in this study reveal a different morphology, as will be elucidated.

A remarkable feature of the described ethene-PMOs is the dependence of the pore-blocking on the acidity of the reaction mixture. By adjusting the acidity, the fraction of open and blocked mesopores can be accurately fine-tuned, as illustrated by Figure 5.3. To the best of our knowledge such a correlation has never been reported before. A detailed study of the isotherms was performed by means of an NLDFT analysis, which allows for the calculation of the mesopores size distributions and determination of volumes of open and blocked pores.⁴⁵⁹ The NLDFT data are given in Table 5.2.

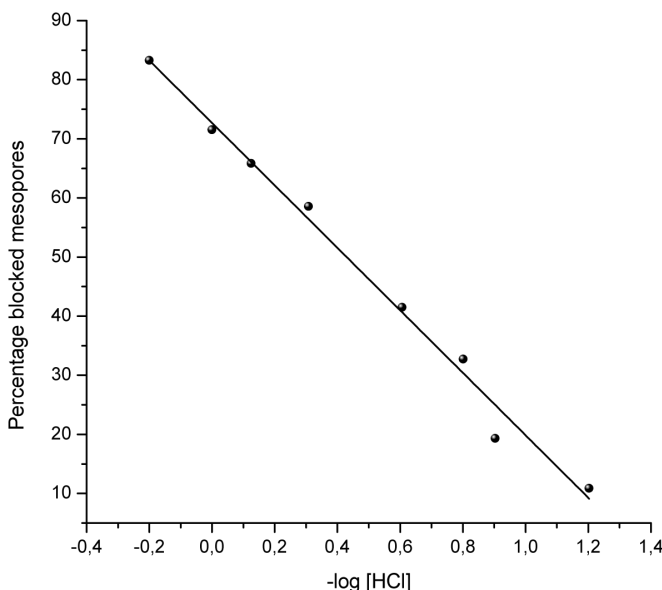


Figure 5.3: Percentage of blocked mesopores, calculated from the nitrogen desorption isotherms using NLDFT, as a function of $-\log [\text{HCl}]$.

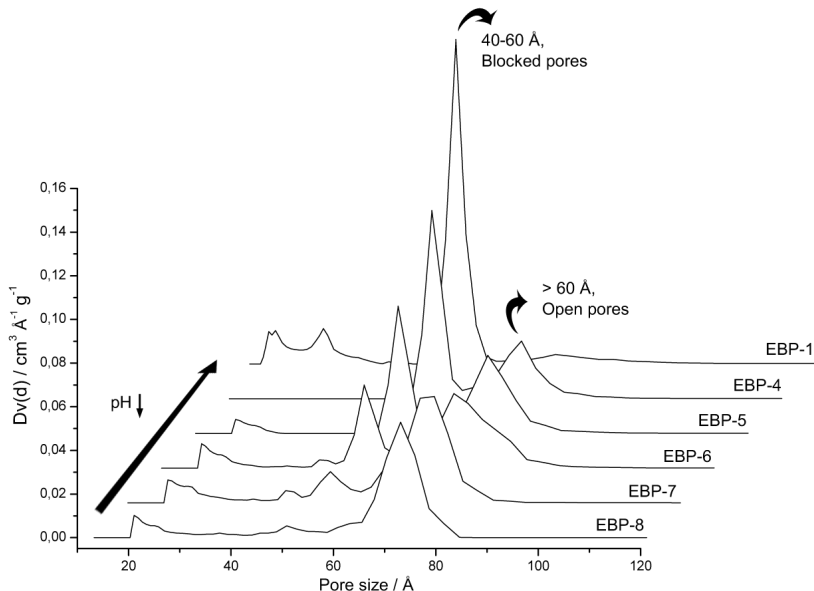
When comparing EBP-1 to EBP-8, it is clear from the pore diameter distributions in Table 5.2 that the described PMOs exhibit both blocked and open mesopores. Herein, the contribution of blocked and open pores is calculated from the pore size distribution (PSD) function between 40 - 60 Å, and above 60 Å, respectively. The corresponding PSD graphs are represented in Figure 5.4. The desorption of nitrogen from the blocked pores occurs through the cavitation mechanism, thus the pore size distribution corresponding with the second step in the desorption branch is not related to the sizes of the blocked pores. The pore size distributions between 20 - 40 Å, reflect the roughness of the pore walls.⁴⁶⁰ The micropores are calculated from the pore size distributions below 20 Å.

The absence of a correlation between the micropore volume and the relative fraction

Table 5.2: NLDFT data of ethenylene-bridged PMOs synthesized at different acid concentrations

Sample	-log [HCl]	BP ^[a] / %	V _μ ^[b] / m ³ g ⁻¹	D _p ^[c] / nm	Pore diameter distribution ^[d] / %			
					<20 Å	20-40 Å	40-60 Å	>60 Å
EBP-1	-0.200	83.3	0.15		8.3	10.8	67.4	13.5
EBP-2	0	71.5	0.08	6.8	8.3	1.0	64.9	25.8
EBP-3	0.125	65.8	0.05	6.8	3.6	0	63.4	33.0
EBP-4	0.308	58.6	0.06	7.0	4.3	0	56.0	39.7
EBP-5	0.606	41.5	0.10	7.0	9.9	3.3	36.0	50.8
EBP-6	0.801	32.7	0.16	7.0	14.3	6.2	26.0	53.5
EBP-7	0.903	19.3	0.15	7.2	12.6	8.1	15.3	64.0
EBP-8	1.203	10.9	0.13	7.3	15.4	8.3	8.3	68.0
EBP-9 ^[e]	0.100	5.4	0.14	8.1	7.6	13.1	4.3	75.0

^[a] Blocked pores (calculated using NLDFT), ^[b] Micropore volume (calculated using t-plot), ^[c] Pore diameter, calculated from the desorption isotherm using NLDFT, ^[d] Calculated from the desorption isotherm using NLDFT, ^[e] Synthesized with *n*-butanol.

**Figure 5.4:** NLDFT pore size distributions calculated from the desorption isotherms of ethene-PMOs synthesized at different pH values.

of blocked mesopores (see Figure 5.5) is a first indication that these PMO materials have different pore structures than PHTS. That is, the nanoparticles which block the pores of PHTS are microporous, and thus there should be a relationship between the amount of plugs in the mesopores and the micropore volume if the PMOs consist of plugs.

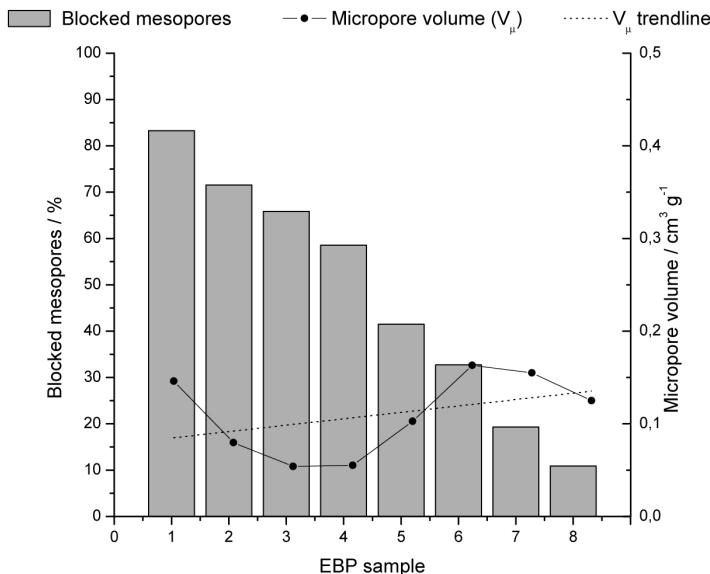


Figure 5.5: Relation between percentage of blocked mesopores and micropore volume.

As the pore-blocking effect is related to the acidity of the reaction mixture, it seems to be a kinetic phenomenon. However, in the previous chapter we described the synthesis of well-ordered diastereoisomerically pure ethenylene-bridged PMOs with open cylindrical mesopores under highly acidic conditions, with the aid of butanol as a cosolvent. By adapting this synthesis procedure, no pore-blocking occurs at a pH of 0.1 (EBP-9) and nitrogen isotherms with a type H1 hysteresis are obtained (see Figure 5.1), whereas without butanol, about 66 % of the mesopores are blocked. This suggests that the occurrence of pore-blocking, while being dependent on the pH of the reaction mixture, is not a purely kinetic happening.

To explain these findings and elucidate the structure of these PMO materials, a detailed study was carried out using SAXS, TEM and ET. Herein, three samples were investigated: 1) a PMO which consists of open cylindrical mesopores (EBP-9), 2) a PMO which consists of both open and blocked mesopores (EBP-6) and 3) a PMO which consists of blocked mesopores (EBP-1).

5.2 Investigation of PMO structures with SAXS, TEM and ET

5.2.1 Ethenylene-bridged PMO with open cylindrical mesopores

Figure 5.6 gives both the SAXS pattern and the most probable underlying form factor curve of EBP-9. The SAXS pattern is typical for a well-ordered 2D hexagonal structure, revealing three well-resolved peaks which can be assigned to the (100), (110) and (200) reflections. The observed intensity can miss some expected reflections at s -values where the form factor - in the present case due to the cylindrical lattice motif - goes through zero. After all, the observed scattered intensity is proportional to the product of the lattice interference function (producing the main reflections) with the form factor. This is helpful in determining the diameter of the cylinders. The missing (120) reflection and the equally intense (110) and (200) reflections lead to a cylinder with a diameter of 8.2 nm, which is in very good agreement with the pore size determined from the desorption isotherm using NLDFT, namely 8.1 nm. With a d_{100} spacing of 9.7 nm, EBP-9 has a unit cell of 11.2 nm.

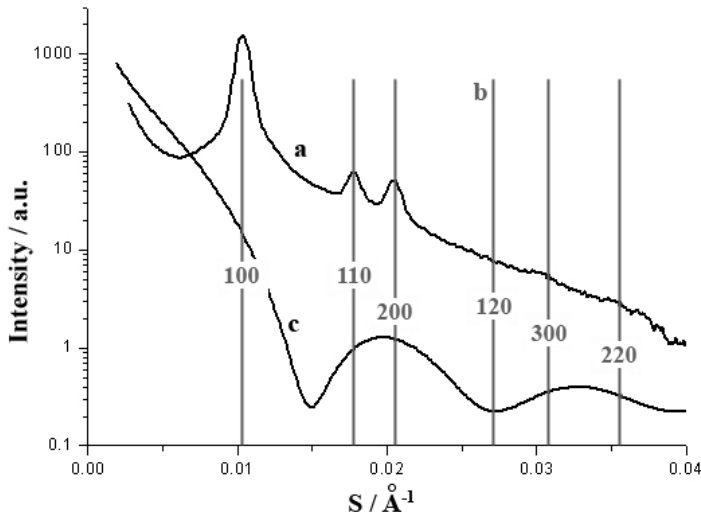


Figure 5.6: SAXS pattern of EBP-9 (a), expected reflections for a 2D hexagonal ordering of cylinders (b), and the theoretical form factor curve for cylinders with a diameter of 8.2 nm (c).⁴⁶¹ Both the SAXS pattern and the form factor curve are normalized against a constant background.

The ordered structure of EBP-9 was confirmed by TEM, as illustrated in Figure 5.7. Both hexagonal and parallel patterns commonly associated with 2D hexagonal ordering are observed. TEM images reveal large ordered domains, up to hundreds of nanometers in size.

To study the local three-dimensional pore structure of EBP-9, ET was employed.

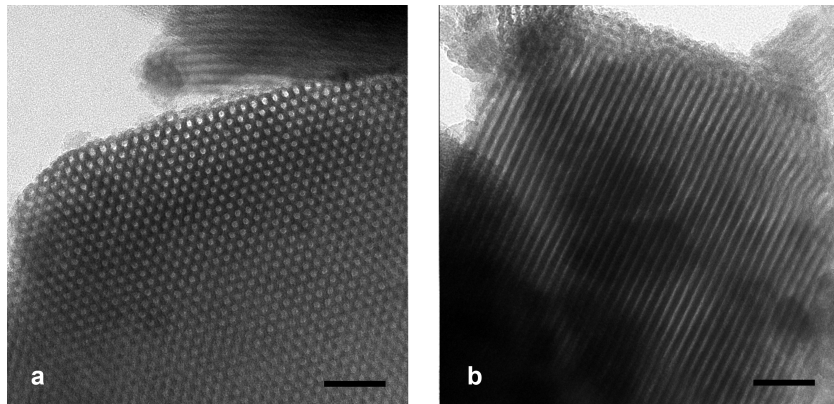


Figure 5.7: TEM images of EBP-9, showing hexagonal (a) and parallel (b) patterns, indicating 2D hexagonal ($P6/mm$) ordering. Scale bars are 50 nm.

Figure 5.8 displays numerical cross-sections through reconstruction perpendicular and parallel to the pore direction.¹ ET results show 2D hexagonally packed cylindrical pores with no significant pore blocking. The observed open pore channels are in good agreement with the N_2 -physisorption measurements, although by ET, very locally pores that terminated inside the particle, which would lead to pore blocking, were observed too. In addition it was found that a single particle can consist of multiple $P6/mm$ domains with different pore directions.

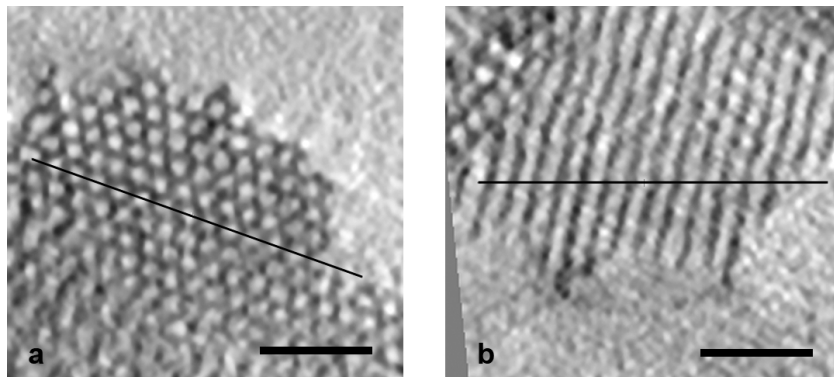


Figure 5.8: Numerical cross-sections through reconstruction of EBP-9, perpendicular to pore direction (a), and parallel to pore direction (b). The black lines indicate the position of the other cutting plane. Scale bars are 50 nm.

The unit cell size was estimated to about 10 nm, both by ET and TEM, which is smaller than the SAXS result. Similar observations were made previously on KIT-6 material.⁴⁶² The difference in lattice spacing most likely arises from shrinking of the material upon exposure to the electron beam.

¹Reconstruction was performed with the computer software packet IMOD by the group of prof. K. de Jong at the university of Utrecht

5.2.2 Ethenylene-bridged PMOs with open and confined mesopores

The experimental SAXS pattern and a suited, calculated cylinder form factor curve of EBP-6 are shown in 5.9. Distinct reflections which can be assigned to a 2D hexagonal structure with a $P6/m\bar{m}$ space group are, (100), (200) and (120). The low intensity of the (110) reflection combined with the comparable intensities of the (200) and (120) reflections, lead to a cylinder with a diameter of 7.0 nm, which is identical to the pore size calculated from the desorption isotherm using NLDFT. With a d_{100} spacing of 9.45 nm, EBP-6 has a unit cell of 10.9 nm. The overall diffraction pattern of EBP-6 is very similar to EBP-9, which can be associated with a well-ordered 2D hexagonal lattice of cylindrical pores. This is also in agreement with TEM results shown in 5.10.

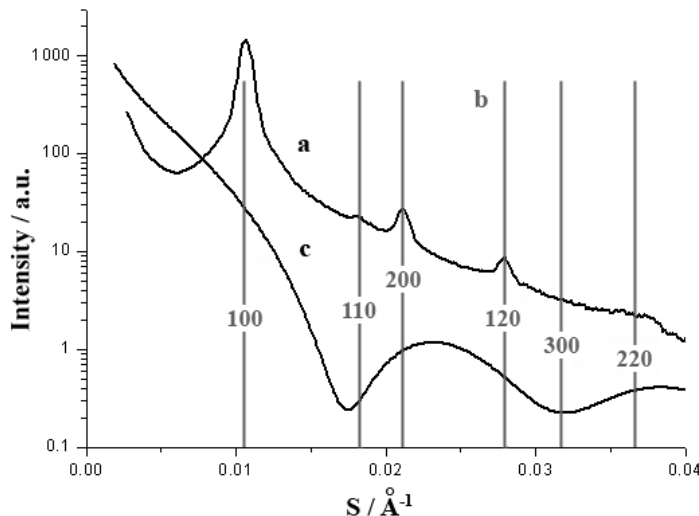


Figure 5.9: SAXS pattern of EBP-6 (a), expected reflections for a 2D hexagonal ordering (b), and the theoretical form factor curve for cylinders with a diameter of 7 nm (c). Both the SAXS pattern and the form factor curve are normalized against a constant background.

To resolve the local 3D pore structure of EBP-6, and to elucidate the nature of the pore-blocking, electron tomography was used. In the numerical cross-section of EBP-6 in Figure 5.11a, the 2D hexagonal ordering is clearly apparent. However, some pores are filled with solid material; i.e. no pores are visible where they are supposed to be based on the 2D hexagonal lattice (see Figure 5.11b). EBP-6 consists of short pores that terminate inside the mesostructure and pores curved on a very local scale. These structural features rationalize the pore-blocking effect that is apparent from nitrogen physisorption. This leads us to the hypothesis that shorter pores are formed with increasing acidity. This is also accompanied by the confinement of mesopores, which causes entrapment of adsorbed nitrogen during the physisorption measurements, yielding a delayed nitrogen desorption step in the nitrogen desorption isotherm.

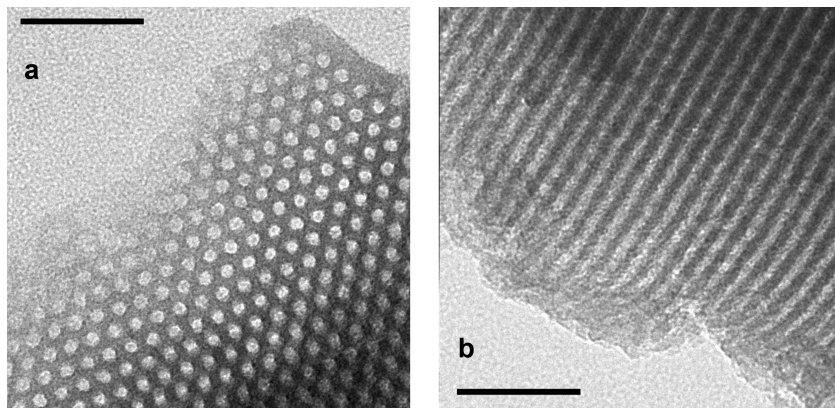


Figure 5.10: TEM images of EBP-6, showing hexagonal (a), and parallel (b) patterns indicating 2D hexagonal ($P6/m\bar{m}$) ordering. Scale bars are 50 nm.

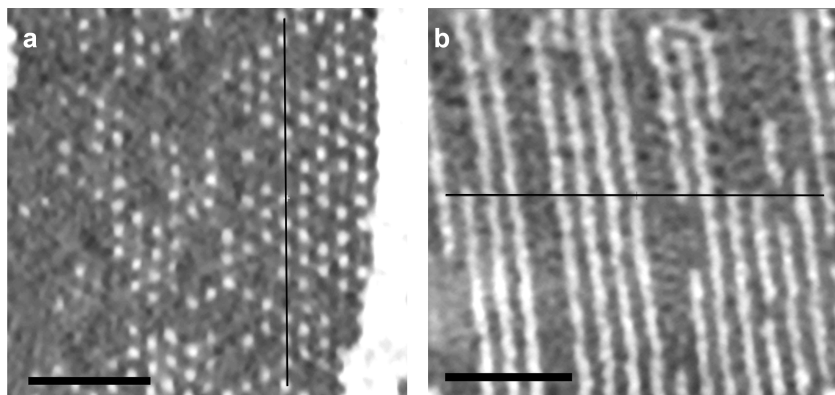


Figure 5.11: Numerical cross-sections through reconstruction of EBP-6, perpendicular to pore direction (a) showing pores filled with solid material, and parallel to pore direction (b) showing short pores terminating inside the mesostructure and a pore curved on a very local scale. The black lines indicate the position of the other cutting plane. Scale bars are 50 nm.

5.2.3 Ethenylene-bridged PMO with globular and blocked mesopores

The SAXS pattern and an appropriate theoretical form factor curve of EBP-1 are shown in Figure 5.12. The SAXS pattern is not characteristic for a 2D hexagonally ordered material, but rather indicates - when considered in conjunction with the TEM data discussed below - a 3D hexagonal structure with a *P*6/*mmm* space group. When comparing the obtained reflections with the expected theoretical reflections for a simple hexagonal packing of spheres, the two well-resolved peaks ($s = 0.0104$ and 0.0189 \AA^{-1}) and the less-resolved peak ($s = 0.0173 \text{ \AA}^{-1}$) can be assigned to the (100), (001) and (110) reflections of a 3D hexagonal lattice, respectively. Higher order reflections in the pattern are absent because of considerable lattice distortions (due to the presence of pores filled with material) and form factor effects. With a d_{100} spacing of 9.7 nm, EBP-1 has a unit cell $a_0 = 11.2 \text{ nm}$. In the *c* direction, $d_{001} = 5.25 \text{ nm}$.

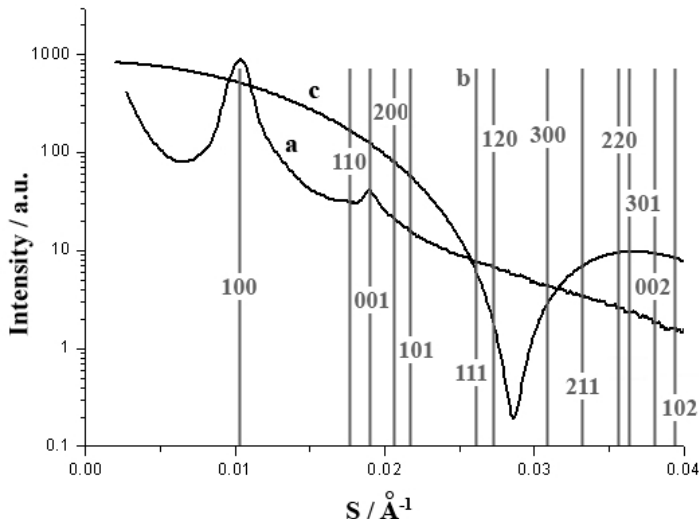


Figure 5.12: SAXS pattern of EBP-1 (a), expected reflections for a 3D simple hexagonal lattice (b), and the theoretical form factor curve for spheres with a diameter of 5 nm (c). The sphere diameter was deducted from the corresponding N_2 -physisorption measurements. Both the SAXS pattern and the form factor curve are normalized against a constant background.

The ordered structure of EBP-1 was confirmed by TEM, as illustrated in Figure 5.13. Herein, parallel, hexagonal, and square patterns are clearly visible, suggesting that the structure has a symmetry more complex than *P*6/*mm*. In context of the SAXS results, the TEM images taken from three different parts of the sample, are considered to reflect three different perspectives of a simple hexagonal lattice with *P*6/*mmm* symmetry, as illustrated in 5.13.

A more detailed insight into the ordering of EBP-1 was obtained by electron tomography. ET results in Figure 5.14 indicate a 3D ordered structure consisting of globular pores. As illustrated in Figure 5.14a, it was often observed that voids were

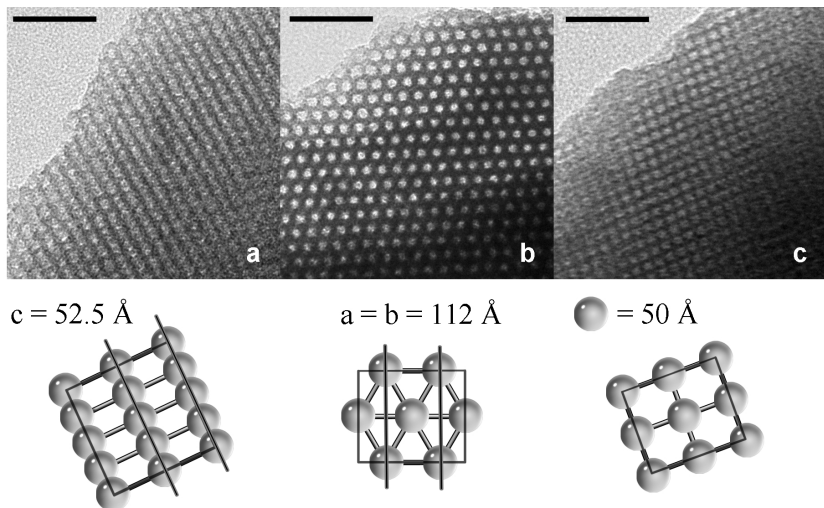


Figure 5.13: TEM images of three different EBP-1 particles, showing parallel (a), hexagonal (b) and square (c) patterns with corresponding perspectives of a simple hexagonal lattice. The scale bars are 50 nm.

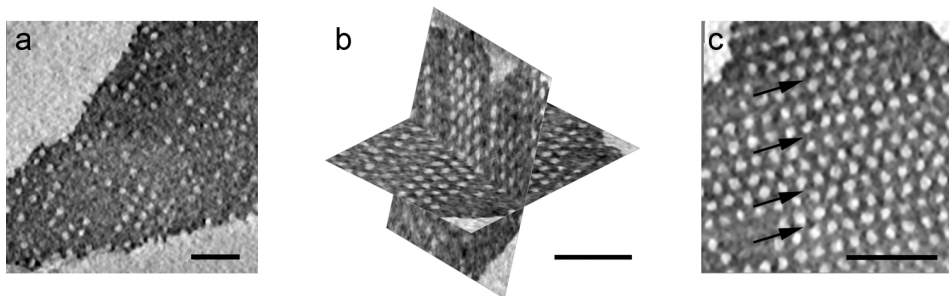


Figure 5.14: Numerical cross-sections through reconstruction of EBP-1. While the material consists of spherical voids, many are filled with solid material (a). Two sections illustrating the stacking of voids in 3D (b). Section showing changes in stacking indicated by arrows (c). Scale bars are 50 nm.

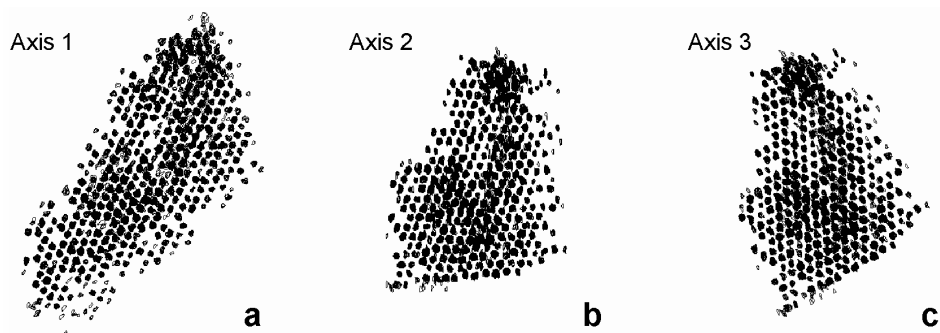


Figure 5.15: Model of the long range 3D stacking of voids in EBP-1, displayed for three axes (a-c), which all expose close to hexagonal symmetry.

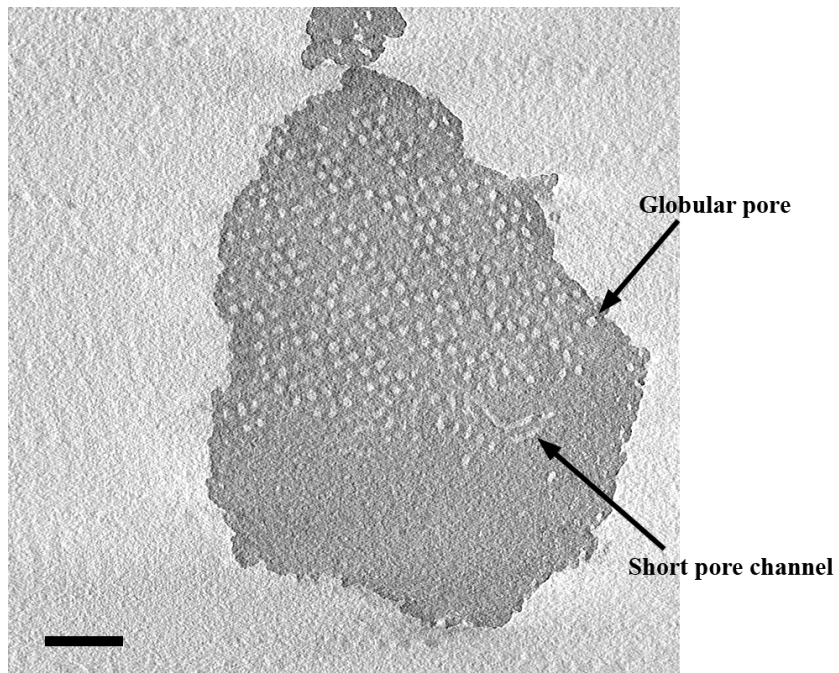


Figure 5.16: Numerical cross-section through reconstruction of EBP-1 showing transition of globular pores into short pore channels. The scale bar is 50 nm.

filled with solid material, similar as for EBP-6. However, a long-range order of the remaining voids is preserved (see Figure 5.15). Moreover, in one instance globular pores and short pore channels were observed (see Figure 5.16). The local disorder, i.e. voids filled with solid material and changes in stacking (5.14c), complicates deriving a unit cell from neighboring voids. As to how the globular pores are stacked in 3D, the SAXS data suggests a predominant $P6/mmm$ symmetry with an AAA stacking of spheres. However, on the local scale, ET found a close-packed structure with an ABC stacking.

5.2.4 The pore-blocking effect: Hypothesis

When comparing the results obtained by SAXS, TEM and ET with those obtained by nitrogen physisorption, the pore-blocking effect can be ascribed to the filling of the mesopores with solid material and to the shortening of the pore channels (pore confinement). For the PMOs with both open and blocked mesopores (EBP-2 to EBP-8), a fraction of the hexagonally packed cylinders terminate inside the mesostructure, thus forming short pore channels, as evidenced by ET. This phenomenon causes confinement of the adsorbed nitrogen. As only a fraction of the pores are blocked, the confinement of nitrogen is only partial and hence a two-step desorption isotherm is obtained. Consequently, the hysteresis of such a PMO is a combination of a H1 and a H2 type hysteresis. As the fraction of blocked pores versus open pores gradually increases with decreasing pH, the amount of confined nitrogen which desorbs at relatively low pressures increases, and the hysteresis gradually converts into a H2 type hysteresis. At very low pH values a 3D hexagonally ordered mesostructure consisting mainly of globular pores is found (EBP-1). These globular pores can be considered as confined cavities which are interconnected with each other by smaller passages (< 4 nm). The H2 type hysteresis of EBP-1 is related to the absence of open cylindrical pores, to the confinement of the globular mesopores and to the filling of some of the mesopores with solid material, as evidenced by ET.

The effect of the synthesis pH on the pore structures of these PMOs is related to an alteration in the hydrophobic/hydrophilic volume ratio of the surfactant template. With increasing acidity of the reaction mixture, the ionization of the ethylene oxide chains of the triblock copolymer enhances the fraction of the hydrophilic block relative to the hydrophobic block, which causes an increase in the interfacial curvature of the mesophase.⁴⁶³ This can rationalize the formation of globular pores at very low pH values. By increasing the pH of the reaction mixture, the globular micelles coalesce into a 2D hexagonally ordered structure, leading to the formation of cylindrical pores. This phase transformation is illustrated in Figure 5.17. This hypothesis is further supported by the ET-image of EBP-1 in Figure 5.16 which displays primarily globular pores and on a very local scale, short pore channels.

When butanol is added to the reaction mixture, the generation of globular pores is circumvented and cylindrical pores are preferentially formed, even at very low pH values. Herein, butanol, which is most probably located mainly at the hydrophilic/hydrophobic interface of the surfactant micelles, stabilizes the cylindrical micellar aggregates and assists the conglomeration of the nano building units into a long-ranged 2D hexagonally packed mesoporous architecture. I.e., butanol induces

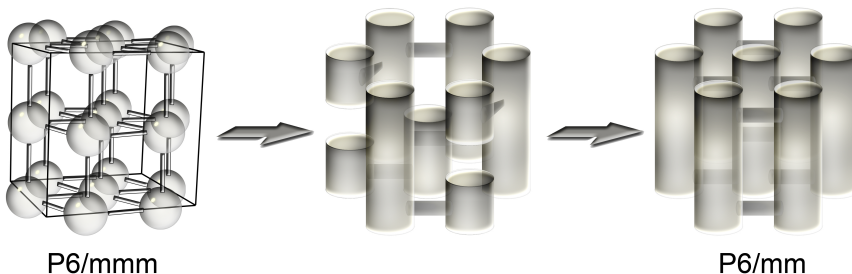


Figure 5.17: Schematic illustration of ideal lattice phase transformation from 3D hexagonally ordered spheres to 2D hexagonally ordered cylinders.

the transformation of the spherical surfactant-organosilica composite micelles into rodlike micelles. This sphere-to-rod transition can be explained by the dehydratation of the ethylene oxide chains in the micelle corona, which is considered to be the driving force for this transition in non-ionic surfactant systems.⁴⁶⁴

5.3 Conclusions on ethene-PMO structure formation

A unique family of periodic mesoporous organosilicas with 100 % *E*-configured ethylene-bridges consisting of various pore structures has been prepared. By means of nitrogen gas physisorption, NLDFT, SAXS, TEM and electron-tomography the detailed structures of these complex PMO materials were determined. Depending on the acidity of the synthesis mixtures, PMOs with open cylindrical, blocked and a mixture of open and blocked mesopores were obtained, as evidenced by nitrogen physisorption.

While two-step nitrogen desorption isotherms are typical for mesoporous materials consisting of microporous nanocapsules, we illustrated that other phenomena can also lead to these type of nitrogen physisorption isotherms, and that these should be taken into account when trying to determine the structural features of porous materials. The second step in the desorption isotherms of these isomeric PMOs were attributed to the generation of confined short pores and interconnected spherical pores. By varying the pH of the reaction mixture, the amount of confined pores could be accurately controlled. At very low pH values, 3D hexagonally ordered mesostructures consisting of globular pores were predominant. By increasing the pH, this mesophase converts to 2D hexagonally ordered structures consisting of cylindrical pores. The effect of the synthesis pH on the pore structures of these PMOs was related to an alteration in the hydrophobic/hydrophilic volume ratio of the surfactant template. That is, the pH influences the interfacial curvature of the mesophase by altering the ionization of the ethylene oxide chains of the triblock copolymer. When butanol is added to the reaction mixture, the generation of globular pores is circumvented and cylindrical pores are preferentially formed. The dehydratation of the ethylene oxide chains in the micelle corona, is probably the driving force for this sphere-to-rod transition.

The research described in this chapter has been published in the literature as a peer review article.⁴⁶⁵

Chapter 6

Ethenylene-bridged PMOs with Controllable Properties

As mentioned earlier (see 1.4.5) the mechanism of mesostructure formation relies strongly on the synthesis conditions, which forms a very complex system in which numerous parameters affect the outcome. The smallest change in one of these parameters such as temperature, molar composition, reaction time, pressure, stirring rate, presence of additives, humidity, ... can have a significant influence on the structure formation. In the previous chapter we have already illustrated the tremendous affect of synthesis pH on the pore structure of ethene PMOs. However, besides influencing the pore structure, the synthesis pH also influences the porosity of the materials. Besides this important relationship, the affect of several reaction parameters on the properties of ethenylene-bridged PMOs was investigated. In addition to influencing the reaction itself, other (post self-assembly) aspects, can play an important role in PMO synthesis. One which is often disregarded, but which has a large influence on the porosity of PMO materials, is template removal. Another approach which was investigated to influence the properties of ethene PMOs, is post thermal treatment. In the course of these investigations, methods have been created to drive the synthesis to desired materials with controllable properties.

6.1 Controlling the porosity of ethenylene-bridged PMOs

6.1.1 Enhancing the efficiency of template removal

An important aspect in PMO synthesis is template removal. Unlike in pure siliceous materials, the surfactant in PMO materials can not be removed by means of calcination as this would result in material degradation and decomposition. PMO materials are commonly extracted with acidified ethanol, regardless of the organic template employed. In this research work, aiming to develop large pore and hydrothermally stable PMOs, P123 was used as a surfactant template. With respect to acidified ethanol, though a very good solvent for the removal of ionic (ammo-

nium) surfactants, its efficiency for the removal of polymeric templates such as the triblock copolymer Pluronic® P123, has not been investigated yet in detail.

By means of FT-Raman spectroscopy, the efficiency of several solvents for the extraction of Pluronic® P123 was studied. To clarify the extraction efficiency of these solvents by avoiding peak convolution in the Raman spectra, the template removal was initially studied for SBA-15. This inorganic ordered mesoporous material, with similar morphological and structural features as our PMOs, has no active Raman vibrations. Therefore, the vibrations resulting in peaks in the FT-Raman spectra can be assigned exclusively to the surfactant template, still present in the pores.

Figure 6.1 gives the FT-Raman spectra (C–H stretch region) of SBA-15: (a) calcined at 400 °C under vacuum, (b) calcined at 380 °C under vacuum (c) acetone-extracted (5 hours), (d) ethanol-extracted (5 hours) and (e) as-synthesized. It is evident that for the extraction of P123, acetone is far more efficient than acidified ethanol. Moreover, to quantitatively remove the surfactant by means of calcination under vacuum, a temperature of 400 °C is required.

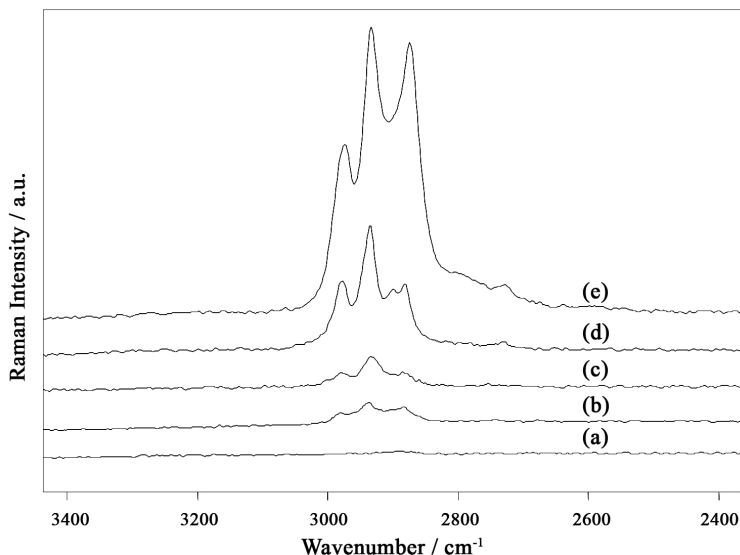


Figure 6.1: FT-Raman spectra of SBA-15: (a) calcined at 400 °C under vacuum, (b) calcined at 380 °C under vacuum (c) acetone-extracted (5 hours), (d) ethanol-extracted (5 hours), (e) as-synthesized.

To assure reliable quantitative measurements a calibration curve was set up for P123, using CDCl_3 as an internal standard. Deuteriochloroform was chosen as an internal standard because, at 2253 cm^{-1} , it does not interfere with the C–H stretch region of Pluronic® P123. In Table 6.1, the efficiency of several solvents for the extraction of P123 is given. Acetone is the most efficient solvent removing over 94 mol% of the template after a single Soxhlet extraction of 5 hours.

This novel extraction procedure was implemented in the removal of P123 out of an ethenylene-bridged PMO, the results of which are given in Table 6.2. Consistent with the FT-Raman data of the SBA-15 materials, the ethenylene-bridged

Table 6.1: Extraction efficiency of several solvents for the removal of P123

Extraction solvent	Mol% extracted ^[a]
Dichloromethane	66.7
Chloroform	69.9
Acidified ethanol	71.8
Ethyl acetate	77.0
Isopropanol	78.6
Acetone	94.2

^[a] Amount of P123 extracted after five hours.

PMO extracted with acetone, reveals an enhanced surface area, total pore volume and pore diameter, indicating a more efficient removal of the template due to the improved extraction procedure. Remarkably, the pore size increases nearly 10 % when compared to the ethanol extracted PMO, while the micropore volume increases nearly 20 %. As can be expected, the removal of P123 by calcination results in a decrease in pore size and micropore volume, due to pore contractions. Although the calcination is performed under vacuum, partial decomposition of the ethenylene-bridged PMO is also inevitable, causing both a decrease in surface area and total pore volume. These results illustrate that for the removal of Pluronic® P123 out of the described mesoporous materials, acetone is a better alternative than acidified ethanol.

Table 6.2: Influence of template removal on structural properties of ethenylene-bridged PMOs

PMO sample ^[a]	S ^[b] / m ² g ⁻¹	V _t ^[c] / m ³ g ⁻¹	V _μ ^[d] / m ³ g ⁻¹	D _p ^[e] / nm
As-synthesized	263	0.45	0	5.0
Ethanol-extracted	970	0.98	0.16	5.4
Acetone-extracted	1018	1.03	0.19	5.9
Calcined ^[f]	700	0.71	0.08	4.8

^[a] EBP-9, ^[b] Surface area, ^[c] Total pore volume, ^[d] Micropore volume, ^[e] Pore diameter (calculated from desorption isotherm with BJH method), ^[f] Calcination under vacuum at 380°C.

6.1.2 Influence of synthesis pH on porosity of ethenylene-bridged PMOs

To investigate the influence of synthesis pH on the porosity properties of ethene-PMOs, a set of diastereoisomerically pure *E*-configured ethenylene-bridged PMOs was prepared at different pH values. In previous chapter we illustrated that *n*-butanol has a large affect on the structural properties of ethene-PMOs. Therefore, a similar series of PMOs was also synthesized in the presence of *n*-butanol. In Table 6.3 the different PMO samples and their synthesis details are given.

To obtain highly ordered ethenylene-bridged PMOs with high surface areas and pore volumes, it is important that the rates of hydrolysis and condensation of the precursor are correctly adjusted to the rate of the template self-assembly. Below

Table 6.3: Synthesis details of *E*-configured ethenylene-bridged PMOs (EBPs)

Sample	P123 / mmol	E-BTSE / mmol	<i>n</i> -butanol / mmol	pH
EBP-10	1	30	0	1.51
EBP-11	1	30	0	1.21
EBP-12	1	30	0	1.00
EBP-13	1	30	0	0.90
EBP-14	1	30	0	0.85
EBP-15	1	30	0	0.80
EBP-16	1	30	0	0.60
EBP-17	1	30	0	0.30
EBP-18	1	30	155	1.00
EBP-19	1	30	155	0.52
EBP-20	1	30	155	0.30
EBP-21	1	30	155	0.10
EBP-22	1	30	155	0.05
EBP-23	1	30	155	0

the isoelectric point of silica ($\text{pH} < 2$), the silicate species are cationic (I^+) and both the template-precursor interfacial energy and the condensation rate of the precursor are proportional to the acid concentration. Figure 6.2 illustrates the strong influence of the reaction mixture pH on the surface area and the total pore volume of ethenylene-bridged PMOs, synthesized in the absence of a cosolvent. Both curves reveal an optimum in surface area and pore volume at a pH of 0.9 (sample EBP-13). The isotherms of sample E-EBP-13, shown in Figure 6.3, contain sharp capillary evaporation and condensation steps, indicating uniform mesopores. When the pH is lowered below this optimum, both the surface area and the pore volume drop significantly. This is most likely caused by the excessive polycondensation rate of the PMO-precursor, relative to the surfactant self-organization, whereby the formation of disordered amorphous material is stimulated. This is corroborated by the results described in the previous chapter, wherein pore blocking is induced by increasing the reaction mixture acidity. When the synthesis mixture has a $\text{pH} < 1$, the excessive polycondensation of the precursor causes filling of the pore channels with solid material, as evidenced by electron tomography (ET).⁴⁶⁵ In Figure 6.4 the numerical cross-section of an ethenylene-bridged PMO synthesized at a pH of 0.8 is presented. While overall a 2D hexagonal ordering of the mesopores is observed, some are filled with material, that is, no pores are visible in some locations of the 2D hexagonal lattice. Due to filling of the mesopores with solid material, the nitrogen physisorption isotherms show a characteristic two-step desorption, as seen in Figure 6.5. Herein, the desorption step at high relative pressure corresponds to the equilibrium desorption in open mesopores, while the desorption step at low relative pressure is related to cavitation of condensed nitrogen in the blocked mesopores. In the later case, the nitrogen desorption can not proceed *via* the primary mesopores, as the mesopore ends are sealed, but rather has to occur *via* the pore walls, which are perforated by secondary unblocked mesopores or micropores.

On the other hand, when the HCl concentration is lowered below the optimum, the surface area and pore volume diminish probably due to the reduced double-

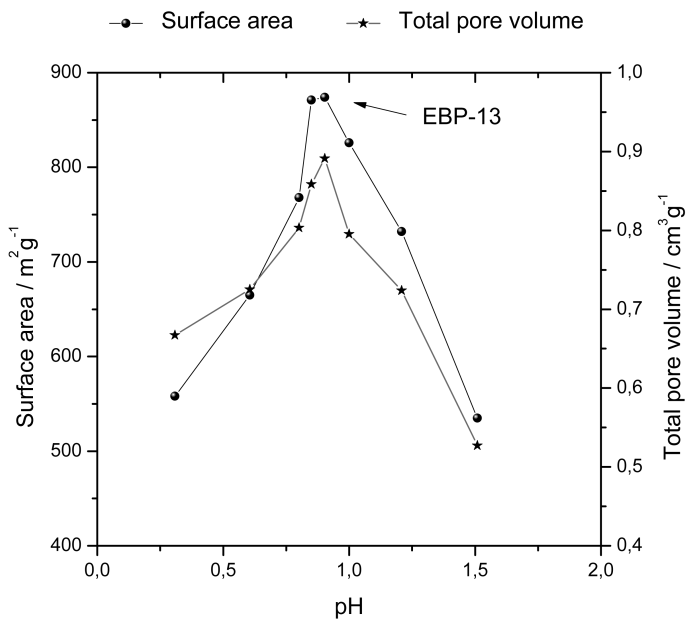


Figure 6.2: Surface area and total pore volume as a function of pH for ethenylene-bridged PMOs synthesized without *n*-butanol (EBP-10 to E-EBP-17).

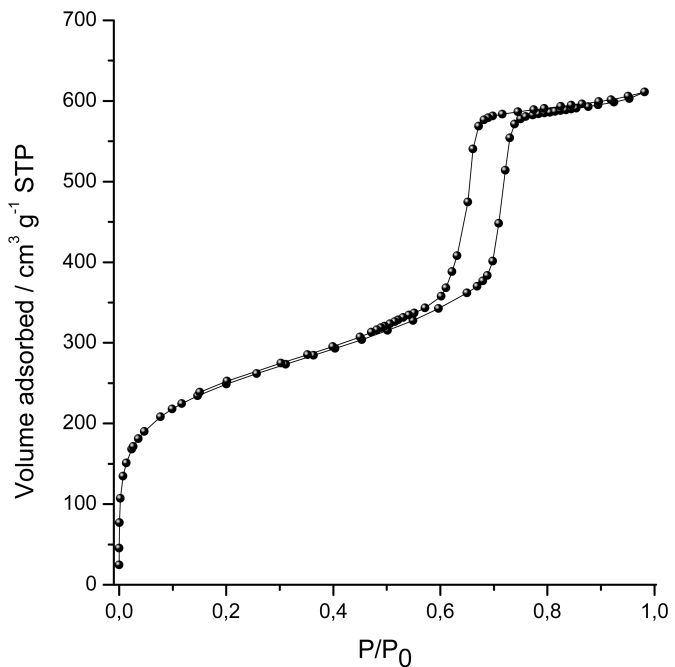


Figure 6.3: Nitrogen physisorption isotherms of the ethenylene-bridged PMO synthesized at the optimum pH value in the absence of a cosolvent (EBP-13).

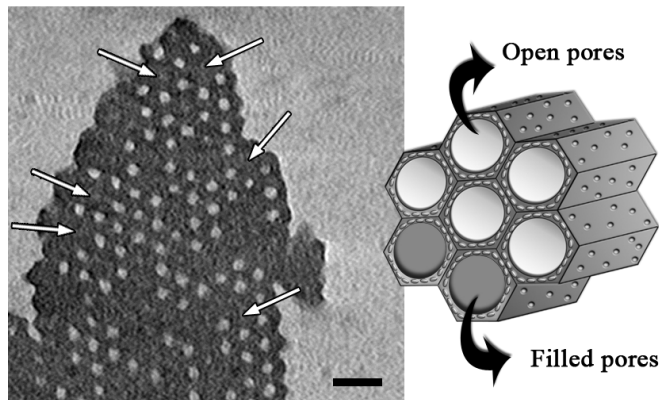


Figure 6.4: Numerical cross-section through reconstruction of EBP-15, perpendicular to the pore direction. The arrows in the ET image indicate some pores which are filled with solid material.

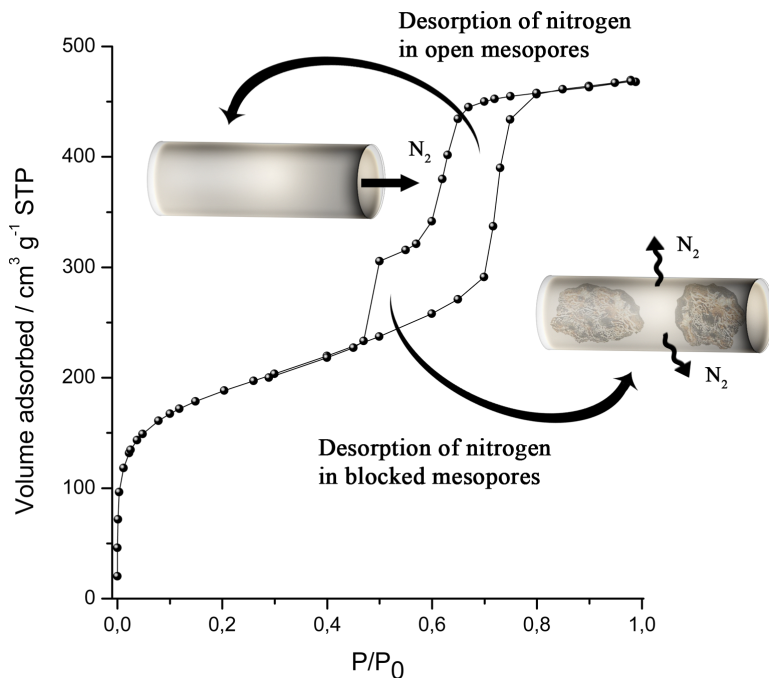


Figure 6.5: Typical nitrogen isotherms of an ethenylene-bridged PMO synthesized in the absence of a cosolvent at a pH < 1 (EBP-16). The two-step desorption isotherm is related to the presence of both open cylindrical and blocked mesopores.

layer hydrogen-bonding interaction ($S^0H^+X^-I^+$) between the nonionic surfactant template (S^0) and the PMO-precursor (I^+), whereby the long-range hexagonal packing decreases.

The influence of the reaction mixture pH on the surface area and the total pore volume of ethylene-bridged PMOs, synthesized in the presence of *n*-butanol as a cosolvent was also investigated. The results, given in Figure 6.6, disclose an optimum in surface area and pore volume at a pH of 0.10. In comparison to the synthesis without *n*-butanol (Figure 6.2), the optimum is shifted to a significantly lower pH, suggesting that *n*-butanol slows down the polymerization of the precursor.

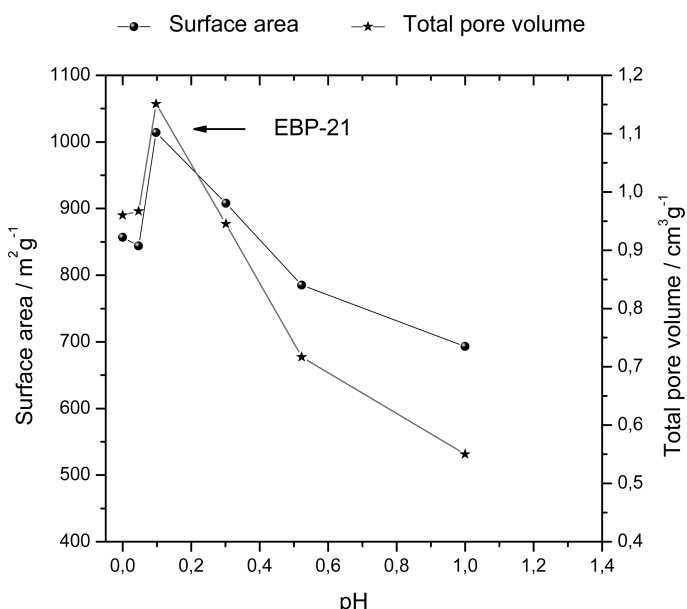


Figure 6.6: Surface area and total pore volume as a function of pH for ethylene-bridged PMOs synthesized with *n*-butanol (EBP-18 to EBP-23).

Under these increased acidic conditions the template-precursor interaction is more profound, leading to an enhanced aggregation of the nano-building blocks into a long-range 2D hexagonally packed architecture. When the pH is further reduced beyond the optimum, both the surface area and pore volume decrease. However, when compared to the synthesis without *n*-butanol, the decrease is far less pronounced. This can be explained by the fact that *n*-butanol prevents the filling of mesopores with solid material, even at low pH values (see previous Chapter).⁴⁶⁵ Due to the absence of blocked mesopores, typical type IV nitrogen isotherms are obtained as illustrated in Figure 6.7.

Taking TEM and XRD results (vide infra) into account, *n*-butanol ensures the formation of 2D hexagonal ordering, which explains the moderate decrease in porosity. The decrease can however be linked to the reduction in micropores, indicating that the high acidity induces the degradation of the surfactant template, whereby the

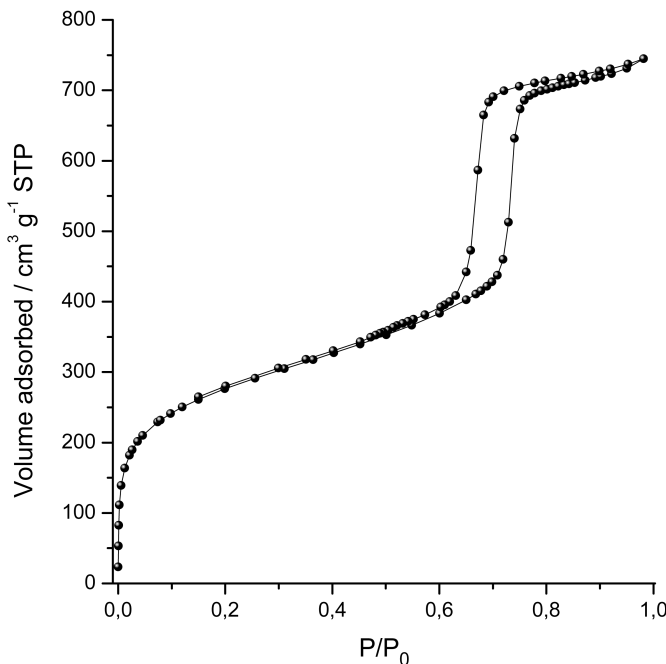


Figure 6.7: Nitrogen isotherms of the ethenylene-bridged PMO synthesized at the optimum pH in the presence of *n*-butanol (EBP-21). The single-step desorption isotherm indicates cylindrical mesopores which are open at both ends.

hydrolysis of the alkoxy bridges is catalyzed by hydrochloric acid, as illustrated in Figure 6.8.

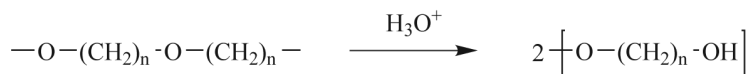


Figure 6.8: Acid catalyzed hydrolysis of the ethylene-oxide chains in the surfactant template.

In Figure 6.9, low-angle XRD-patterns are given of the ethenylene-bridged PMOs synthesized at the optimized pH, without *n*-butanol (EBP-13) and with *n*-butanol (EBP-21) as a cosolvent. The XRD pattern of EBP-13 reveals an intense peak at $2\theta \approx 0.92^\circ$, which is attributed to the (100) diffraction peak from the 2D hexagonal unit cells ($a_0 \approx 11.1$ nm). Two smaller, but well-resolved peaks which can be assigned to the (200) and (120) reflections are also apparent, indicating a well-ordered structure. The XRD pattern of EBP-21 reveals (100), (110) and (200) diffraction peaks also suggesting a well-ordered 2D hexagonal structure. In comparison to EBP-13, EBP-21 has a larger unit cell ($a_0 \approx 11.9$ nm), which explains the difference in both diffraction patterns.

These XRD-results indicate that well-ordered ethenylene-bridged PMOs can be

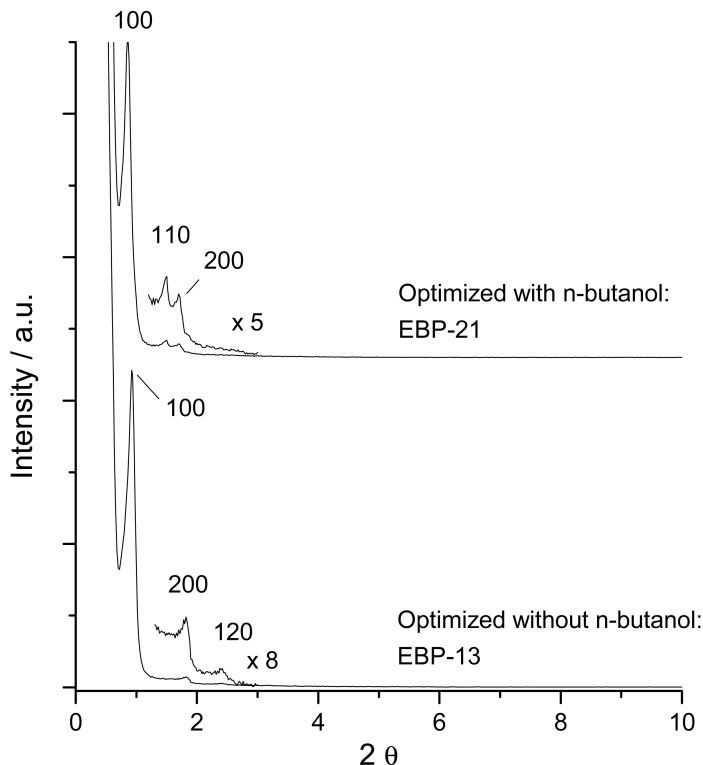


Figure 6.9: XRD-plots of ethenylene-bridged PMOs synthesized at the optimized pH, without *n*-butanol (EBP-13) and with *n*-butanol (EBP-21).

synthesized both with and without *n*-butanol, by optimizing the pH of the synthesis mixture.

6.1.3 Influence of the *n*-butanol concentration on porosity of ethenylene-bridged PMOs

The concentration of *n*-butanol also has an influence on the material properties, as illustrated by the data in Table 6.4. At a pH of 0.3, a *n*-butanol:P123 ratio of 155 gives the best material in terms of surface area and pore volume. The *n*-butanol concentration also influences the microporosity of the PMOs. When the *n*-butanol:P123 ratio is raised to 195, a substantial fraction (64 %) of the total pore volume is micropore volume. This suggests that the ethylene oxide chains of P123 are less likely to withdraw from the solution into the micelle core that consists primarily of hydrophobic propylene oxide chains. This is also supported by the fact that at high *n*-butanol:P123 ratios the pore diameter increases, indicating that the micelle cores swell.

Besides affecting the porosity of the PMOs, the concentration of *n*-butanol also determines the particle morphology (vide infra). This may also influence the porosity of the materials.

Table 6.4: Influence of the *n*-butanol concentration on the properties of ethenylene-bridged PMOs

PMO sample	<i>n</i> -butanol: P123 ^[a]	S ^[b] / m ² g ⁻¹	V _t ^[c] / m ³ g ⁻¹	V _{mes} ^[d] / m ³ g ⁻¹	V _μ ^[e] / m ³ g ⁻¹	V _μ /V _t / %	D _p ^[f] / nm
EBP-24	95	767	0.771	0.655	0.116	15.0	6.2
EBP-25	115	652	0.655	0.570	0.085	13.0	6.2
EBP-26	135	695	0.700	0.604	0.096	13.7	6.2
EBP-20	155	908	0.945	0.799	0.146	15.4	7.0
EBP-27	175	854	0.738	0.558	0.180	24.4	8.1
EBP-28	195	766	0.411	0.148	0.263	64.0	-

^[a] Only the *n*-butanol:P123 was varied while keeping all other reaction parameters constant. For molar composition see EBP-20 in Table 6.3. ^[b] Surface area, ^[c] Total pore volume, ^[d] Mesopore volume, ^[e] Micropore volume, ^[f] Pore diameter.

6.1.4 Role of synthesis temperature in controlling the pore size, structure, connectivity and volume

In Table 6.5 the pore and surface properties, as a function of the aging temperature, of some ethenylene-bridged PMOs, are given. An increase in aging temperature from 50 °C to 90 °C, results in a pore enlargement of about 69 %. It is commonly known that the hydrophylicity of the EO blocks in poly(alkylene oxide) triblock copolymers, such as Pluronic® P123, is temperature dependent. By raising the aging temperature of the reaction mixture, the hydrophobicity of the EO blocks increase, upon which they withdraw into the hydrophobic micelle cores. This results in a swelling of the micelle cores, causing the pores to enlarge. However, no additional increase in pore size is observed when the aging temperature is further elevated from 90 °C to 150 °C. This indicates that some of the EO blocks, instead of withdrawing into the micelle cores, decompose. Furthermore, it is feasible that the PMO mesostructure does not permit further swelling of the micelles in the pores as it is only flexible to a certain extent.

Table 6.5: Influence of aging temperature on the properties of ethenylene-bridged PMOs

PMO sample	T _{aging} / °C	S ^[a] / m ² g ⁻¹	V _t ^[b] / m ³ g ⁻¹	V _{mes} ^[c] / m ³ g ⁻¹	V _μ ^[d] / m ³ g ⁻¹	V _μ /V _t / %	D _p ^[e] / nm
EBP-29 ^[f]	50	535	0.542	0.529	0.013	2.4	4.8
EBP-30 ^[f]	60	736	0.693	0.601	0.092	13.3	5.4
EBP-31 ^[f]	70	996	1.004	0.828	0.176	17.5	7.0
EBP-21	90	1014	1.151	0.995	0.156	13.6	8.1
EBP-32 ^[f]	110	971	1.133	0.998	0.135	11.9	8.1
EBP-33 ^[f]	150	783	1.181	1.140	0.041	3.5	8.1

^[a] Surface area, ^[b] Total pore volume, ^[c] Mesopore volume, ^[d] Micropore volume, ^[e] Pore diameter, ^[f] Same molar composition as EBP-21, see Table 6.3.

The temperature dependent behavior of Pluronic® P123 can also explain the microporosity of ethenylene-bridged PMOs. Non-ionic micelles of P123 in water are surrounded by a corona of hydrated PEO chains, protruding by about 1 nm from the average micelle surface.¹³² When an isotropic micellar solution is formed, the

repulsion between hydrated PEO chains drives the micelles to a distance of at least 3 to 4 nm. With other words, at low temperatures, adjacent micelles do not share their hydration shells (see Figure 6.10). This rationalizes the low micropore volume of EBP-29 and EBP-30, synthesized at temperatures below 70 °C.

Coinciding with an increase in pore size, the micropore volume decreases with elevated aging temperatures (above 70 °C). When raising the temperature from 70 °C to 150 °C, the micropore volume decreases with about 77 %. This can be attributed to the collapse or sealing of the micropores in the PMO pore walls upon withdrawal of the PEO blocks. However, with increasing aging temperature the total pore volume does not decrease. On the contrary, an increase in total pore volume is apparent, which can be related to an increase in mesopore volume. These findings suggest that with increasing temperature, at least some of the PEO-blocks of the surfactant template gather together instead of withdrawing in the micelle core. Doing so, the micropore connections which would normally be generated in the pore walls between adjacent mesopores upon template removal, are transformed into secondary mesopores (see Figure 6.10). This hypothesis may also explain why the mesopores do not enlarge when the aging temperature is raised beyond 90 °C. These results confirm similar findings made by Galarneau *et al.*¹³¹ and Jaroniec *et al.*¹¹⁸

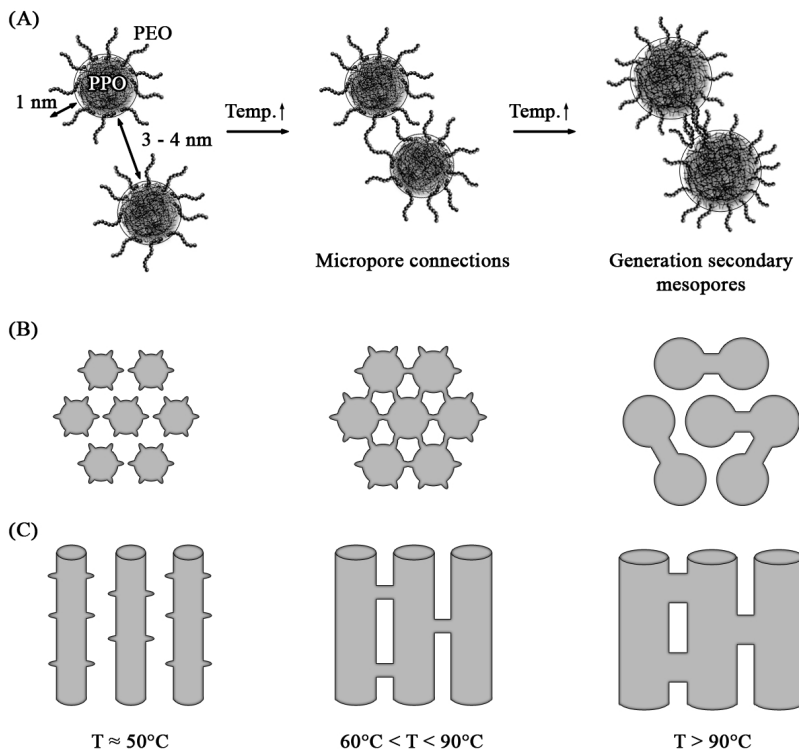


Figure 6.10: Influence of synthesis temperature on micellar behavior (A) and PMO pore size, structure and connectivity (B, top view) and (C, side view).

6.2 The role of cosolvent in controlling the morphology of ethene-PMOs

The manner in which organic-inorganic species self-assemble into mesostructured architectures determines the particle morphology. Many factors such as micelle structure, hydrolysis and condensation rates of the silica precursors and the interactions between surfactant micelles and condensating silicate species affect the final morphology of the particles. As illustrated by the SEM images in Figure 6.11, for ethenylene-bridged PMOs, the presence of cosolvents and the variation of cosolvent concentration has a tremendous affect on the particle morphology.

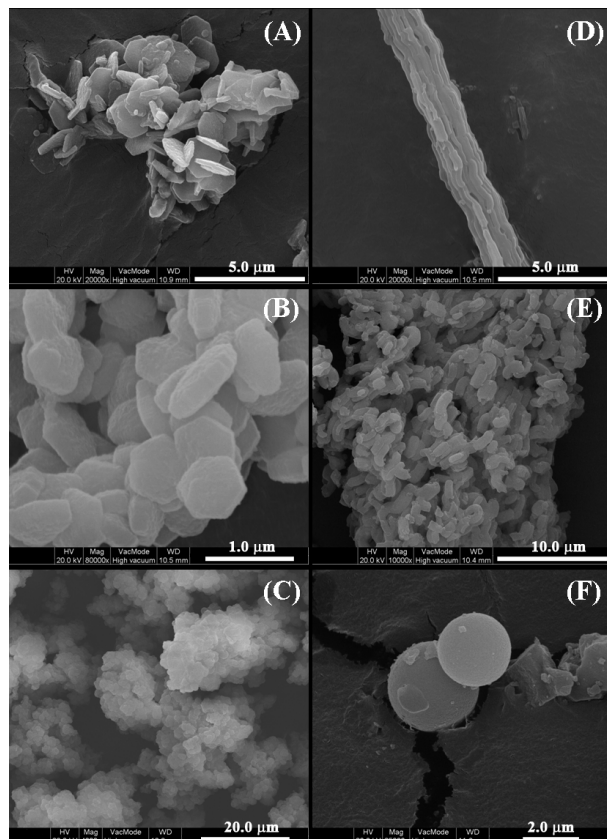


Figure 6.11: FE-SEM images of ethenylene-bridged PMOs prepared with various cosolvents or with different cosolvent concentrations: (A) *n*-ethanol, (B) *n*-propanol, (C) *n*-pentanol, (D) *n*-butanol:P123 = 95:1, (E) *n*-butanol:P123 = 115:1 and (F) *n*-butanol:P123 = 175:1. Other reaction parameters are the same as EBP-24 (see Table 6.4).

For the PMOs synthesized in the presence of *n*-ethanol (A) and *n*-propanol (B), hexagonal crystal-like disks are predominant. The discs of (A) have a diameter of approximately 1.6 μm and are about 0.2 μm thick, while the hexagonal shaped discs

of (B) are about $0.8 \mu\text{m}$ in diameter and $0.2 \mu\text{m}$ thick. The angles between adjacent edges of the disks are 120° . When taking a closer look at the mesostructure of these crystal-like disks with TEM, the channels are perpendicular to the disk plane (Figure 6.12B). These findings suggest that *n*-ethanol and *n*-propanol facilitate the assembly of surfactant-organosilica composite micellar rods into hexagonal crystal nuclei *via* the cooperative self-assembly mechanism. As previously reported for MCM-41 with similar morphologies,¹⁰⁰ such hexagonal crystal-like structures can arise when all faces of the nucleus grow at the same rate (Figure 6.12C). When this is not the case distorted hexagonal disks or disks with irregular shapes are obtained.

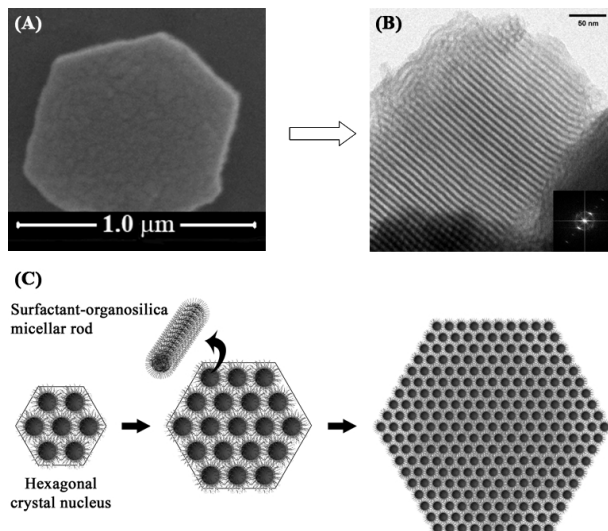


Figure 6.12: (A) FE-SEM (disk viewed from top) and (B) TEM image (disk viewed edge on) of a hexagonal disk with $P6mm$ pore ordering (synthesized with *n*-ethanol). (C) Crystal growth of ethylene-bridged PMOs with crystal-like disk morphologies.

By applying *n*-butanol as a cosolvent (Figure 6.11D), the morphology completely shifts from crystal-like hexagonal discs to ropelike macrostructures with lengths of over $150 \mu\text{m}$ and diameters ranging from 2 to $10 \mu\text{m}$ (Figure 6.11D). Moreover, the difference in morphology between (D) and the other samples, is visible to the eye. While other PMOs discussed in this work are fine powders, (D) is fibrous.

The alteration in morphology caused by changing the cosolvent suggests that the cosolvent affects the micelle curvature and growth of the micellar aggregates. If the cosolvent is located at the surfactant-organosilica interface, it influences the interactions between these species and affects the particle growth and morphology. In the presence of *n*-butanol, the surfactant-organosilica composite micellar rods seems to grow faster along the fiber-axis than along the axis perpendicular to the pore channels, as sketched in Figure 6.13.

By increasing the butanol:P123 molar ratio from 95 (D) to (E), the morphology changes from isolated fibers to clusters of short curved rods, ranging from 2 to $3.5 \mu\text{m}$

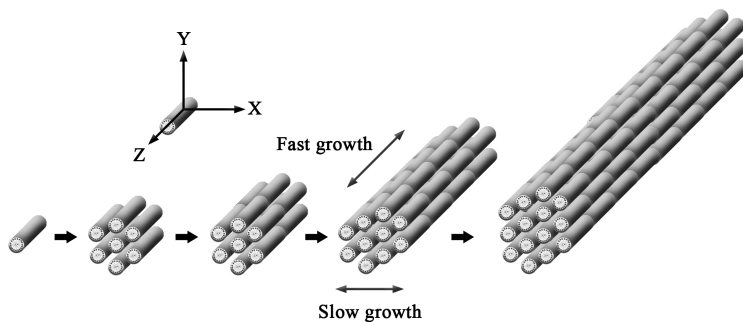


Figure 6.13: Schematic illustration of ethenylene-bridged PMO growth in the presence of *n*-butanol at low concentrations. The surfactant-organosilica composite micellar rods grow faster along the Z-axis than along the X- and Y-axis's.

μm in length and about $0.9 \mu\text{m}$ in width (see Figure 6.11). By further increasing the *n*-butanol:P123 ratio to 175 (F) the morphology changes to primarily spherical particles of approximately 1.9 to $3.8 \mu\text{m}$ (Figure 6.11). The concentration of *n*-butanol is found to affect the dispersion of the organosilica particles, with the formation of spheres at high alcohol concentrations similar to the modified Stöber method.⁴⁶⁶ Due to the high acidity of the reaction mixture in which (F) is formed, most of the spheres are aggregated and are accompanied by irregular shapes. When *n*-pentanol is used as a cosolvent (C), large clusters of irregular shapes are formed (Figure 6.11). The non-uniform morphology is probably caused by the low miscibility of *n*-pentanol in water.

6.3 Thermally induced metamorphosis in ethene-PMOs

6.3.1 Thermal properties of ethene-PMOs

Post-thermal treatment is an easy and straightforward method to control the hydrophobicity of siliceous materials. This process, which is referred to as self-hydrophobization, proceeds as illustrated in Figure 6.14.

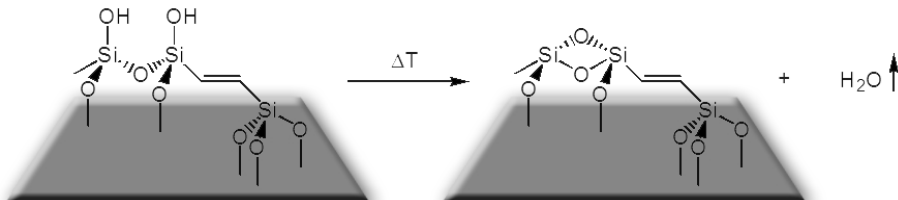


Figure 6.14: Schematic illustration of self-hydrophobization of ethenylene-bridged PMOs through post-thermal treatment.

To investigate the thermal properties, an ethenylene-bridged PMO was thermally

treated under vacuum and monitored *via* in-situ DRIFT (see Figure 6.15). After vacuum drying at 50 °C, the PMO clearly still consists of physisorbed water, which is apparent from the broad band between 3000 and 3650 cm⁻¹. The sharp peak at 3733 cm⁻¹, which can be assigned to the PMO silanol functions, indicates though that the PMO is no longer saturated with water. By prolonging the vacuum treatment, and steadily elevating the temperature, the amount of physisorbed water decreases which reflects in an increase in intensity of the peak at 3733 cm⁻¹ and a decrease of the broad band between 3000 and 3650 cm⁻¹. However, once a temperature of 250 °C is reached, the silanol peak also decreases in intensity, which can be assigned to the self-hydrophobization process. Even at these high temperatures the ethene-PMO still consists of a considerable amount of physisorbed water, illustrating the hygroscopic nature of these materials. Above 250 °C the peak at 2967 cm⁻¹, which can be assigned to the C–H stretch vibration of the ethene groups, decreases, indicating that at these high temperatures the organic groups start to decompose. To fully remove all physisorbed water, a temperature of 500 °C is required. However, at these temperatures a significant amount of the organic groups are decomposed.

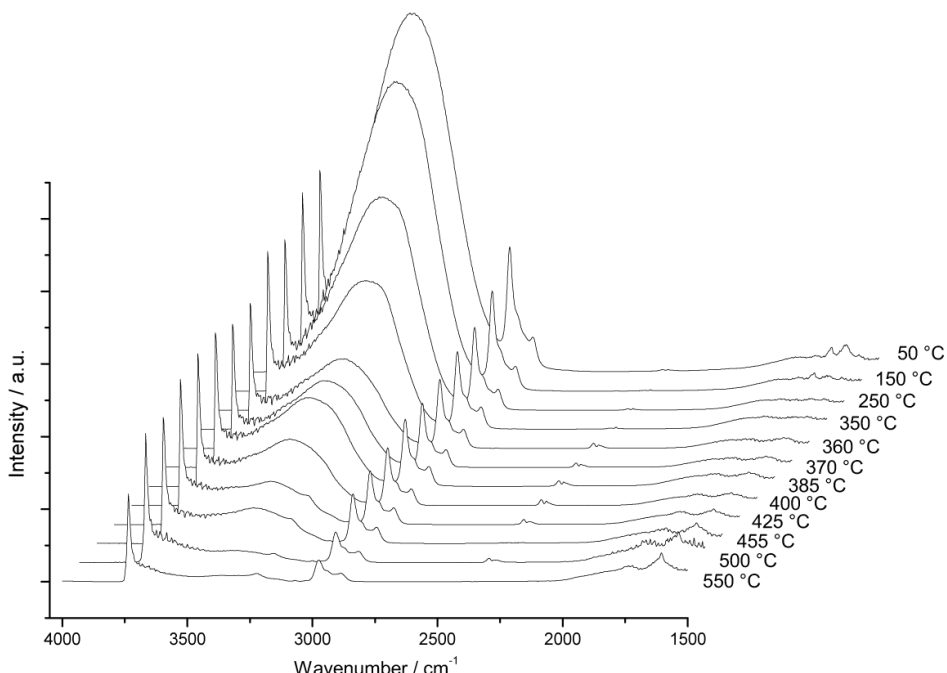


Figure 6.15: In-situ DRIFT spectra of ethenylene-bridged PMOs, as a function of temperature.

In Figure 6.16 the TGA curves are given of an *E*-configured ethenylene-bridged PMO (*E*-EBP)). The PMO displays a high thermal stability up to 435 °C, which is in accordance to the data obtained from the DRIFT analysis.

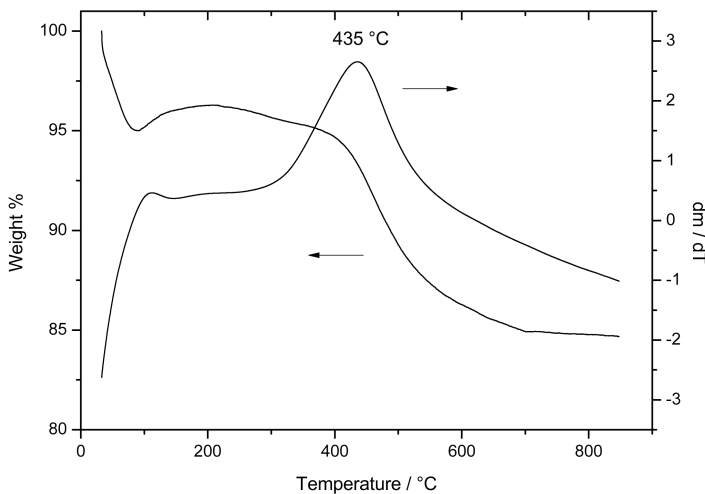


Figure 6.16: TGA-curves of *E*-EBP.

6.3.2 PMO metamorphism: Ethene-bridge, where art thou?

Detailed spectroscopic investigation of the self-hydrophobization process of ethenylene-bridged PMOs revealed a remarkable side reaction, as will be elaborated further on in this section. In Figure 6.17 the XRD-patterns of the diastereoisomerically pure ethenylene-bridged PMOs, ante- (EBP-AT) and post- (EBP-PT) thermal treatment (vacuum dried at 380 °C), are given. The XRD-patterns of EBP-AT and EBP-PT reveal intense peaks with d_{100} spacings of 9.10 and 7.95 nm, respectively. The two smaller, but well-resolved peaks, can be ascribed to the (110) and (200) reflections. These assignments are consistent with hexagonally well-ordered PMO materials with *P6mm* space groups. The slight decrease in intensity of the reflections upon thermal treatment suggests some material deterioration. However, the pore ordering of the remaining material is not affected.

In Figure 6.18(A) the N_2 -physisorption isotherms of EBP-AT and EBP-PT are given. All isotherms are of type IV and display sharp capillary condensation and evaporation steps, indicating very uniform mesopores. The BJH pore size distributions of these samples are illustrated in Figure 6.18(B). Both pore size distributions are very narrow, and confirm the uniformity of the mesopores. Moreover, the thermal treatment seems to have a positive affect on the pore size distribution, though, some contraction of the mesopores is apparent. From Table 6.6 it is evident that the thermal treatment results in a decrease in surface area and overall porosity of the PMO material. Furthermore, as expected, some shrinkage of the unit cell is visible, which confirms the results obtained from the BJH pore size distributions. The thermal treatment only has little affect on the pore wall thickness, indicating that these stay intact. The slight decrease of the wall thickness can be attributed to the self-hydrophobization process which can affect the roughness of the pore walls.

After thermally treating the ethene-PMO EBP-AT at 380 °C under vacuum, DRIFT,

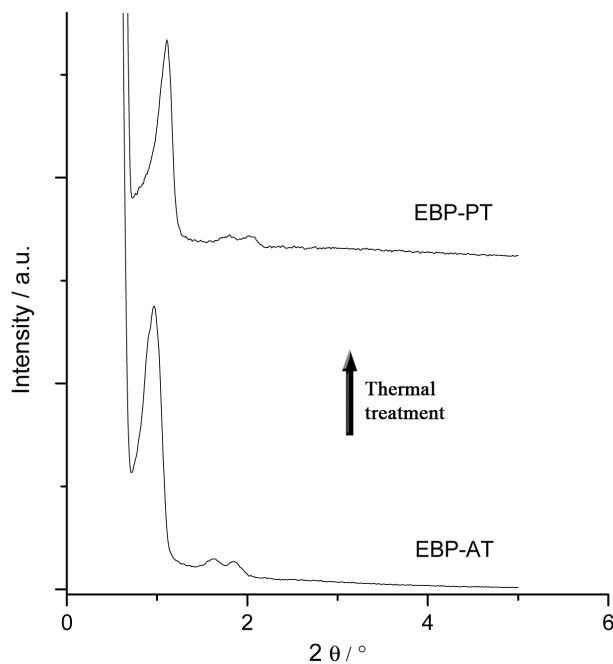


Figure 6.17: XRD-patterns of an ethenylene-bridged PMO, before (EBP-AT) and after (EBP-PT) thermal treatment.

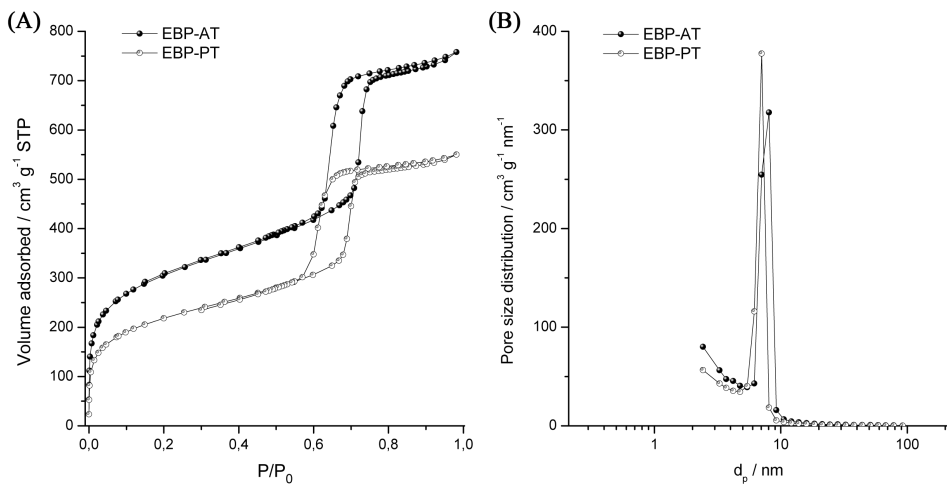


Figure 6.18: (A) N₂-physisorption and (B) BJH pore size distributions of EBP-AT and EBP-PT.

Table 6.6: Properties of an ethenylene-bridged PMO, before (EBP-AT) and after (EBP-PT) thermal treatment

PMO sample	$S^{[a]}$ / $m^2 g^{-1}$	$V_t^{[b]}$ / $m^3 g^{-1}$	$V_\mu^{[c]}$ / $m^3 g^{-1}$	$D_p^{[d]}$ / nm	$a_0^{[e]}$ / nm	$t_w^{[f]}$ / nm
EBP-AT	1112	1.17	0.19	8.1	10.5	2.4
EBP-PT	795	0.85	0.11	7.0	9.2	2.2

[a] Surface area, [b] Total pore volume, [c] Micropore volume, [d] Pore diameter, [e] Unit cell, [f] Pore wall thickness.

FT-Raman and 1H - ^{13}C CP/MAS NMR spectroscopy indicated the occurrence of an intramolecular side reaction. In Figure 6.19 the DRIFT-spectra are given of EBP-AT and EBP-PT. As a reference, the DRIFT-spectrum of pure vinylsilica is also illustrated. The thermally treated PMO exhibits four additional peaks at 3067, 3026, 1602 and 1411 cm^{-1} . When compared to the DRIFT-spectrum of vinylsilica, these peaks can be assigned to the anti-symmetric and symmetric C–H stretch, the C=C stretch and the =CH₂ deformation of thermally generated vinyl groups, respectively. The thermally treated PMO also exhibits a band at 2890 cm^{-1} . The presence of this band is unexpected, as it cannot be assigned to thermally generated vinyl groups. Moreover, the frequency of the band is typical for a C–H stretch vibration of an alkane, implying the formation of an aliphatic group.

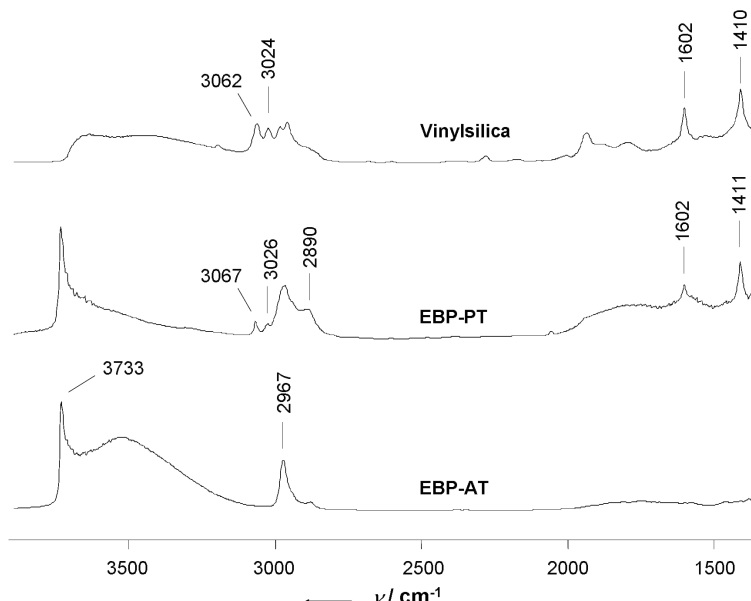


Figure 6.19: DRIFT-spectra of EBP-AT, EBP-PT and pure vinylsilica.

In Figure 6.20 the FT-Raman spectra of EBP-AT and EBP-PT are presented. Here also, the spectrum of pure vinylsilica is given for reference purposes. The

FT-Raman spectrum of EBP-AT reveals three intense peaks at 2961, 1572 and 1302 cm⁻¹. These peaks can be assigned to the C—H stretch, C=C stretch and in-plane C—H deformation vibrations of the ethenylene bridges, respectively. Besides the typical Raman frequencies of the ethenylene bridges, the FT-Raman spectrum of the thermally treated PMO EBP-PT, exhibits additional well-resolved peaks at 3068, 1603 and 1412 cm⁻¹. These peaks, when compared to the spectrum of pure vinylsilica, can be assigned to the anti-symmetric C—H stretch, the C=C stretch and the symmetric =CH₂ deformation of thermally generated vinyl groups. The FT-Raman spectrum of EBP-PT also reveals two shoulder peaks at 2986 and 1279 cm⁻¹ which can be assigned to the C—H stretch and the in-plane C—H deformation of the vinyl groups, respectively. These Raman results confirm the thermally induced generation of vinyl groups. The spectrum of EBP-PT in Figure 6.20 reveals an additional intense peak at 2908 cm⁻¹. This peak, which is typical for the C—H stretch of an aliphatic group, further suggests that the thermal treatment also induces the formation of a saturated C—C bond.

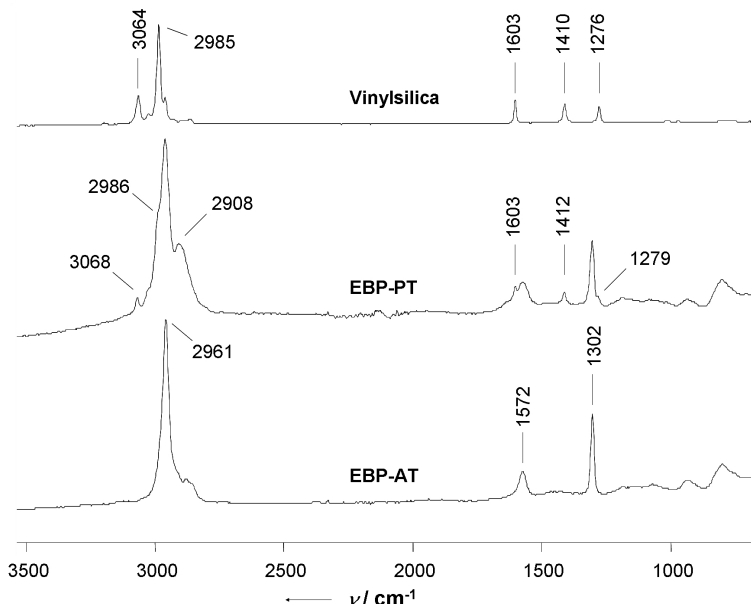


Figure 6.20: FT-Raman spectra of EBP-AT, EBP-PT and pure vinylsilica.

Figure 6.21 illustrates the ¹H-¹³C CP/MAS NMR spectra of EBP-AT, EBP-PT and pure vinylsilica. The ¹H-¹³C CP/MAS NMR spectrum of the template extracted ethene-PMO EBP-AT shows a single resonance at *ca.* 146.4 ppm corresponding to the CH=CH bridging organic groups. The thermal treatment resulted in appearance of additional resonances at 6.1, 18.9, 129.6, and 136.4 ppm. The resonances at 129.6 and 136.4 ppm can be assigned to terminal vinyl groups, as confirmed by the ¹H-¹³C CP/MAS NMR spectrum of pure vinylsilica. This is consistent with the results obtained with DRIFT and FT-Raman spectroscopy (Figure 6.19 and 6.20 respectively). The resonances at 6.1 and 18.9 ppm are somewhat unexpected. The

line at 6.1 ppm is typical of an aliphatic $\text{O}_3\text{Si}-\text{CH}_2\text{CH}_2-\text{SiO}_3$ bridging group, in agreement with the observation of an aliphatic C–H stretch vibration in the DRIFT and FT-Raman spectra. The broad resonance at 18.9 ppm suggests the formation of terminal $\equiv\text{Si}-\text{CH}_2\text{CH}_3$ functionalities with a broad line at *ca.* 19 ppm resulting from the CH_2 groups and the resonance at 6.1 ppm resulting from the terminal CH_3 .

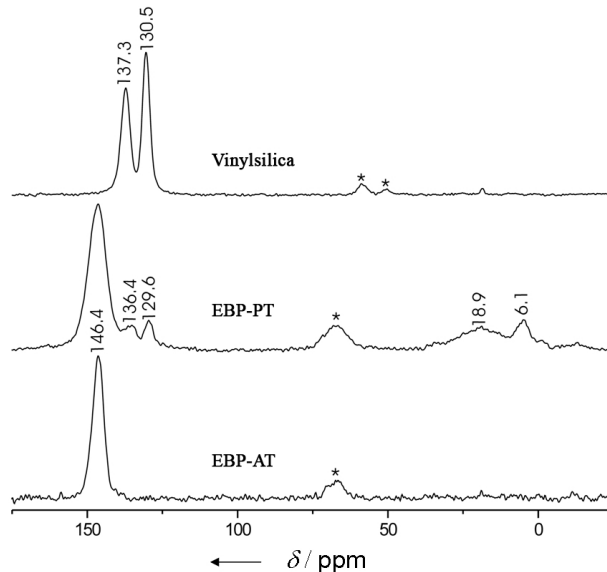


Figure 6.21: ^1H - ^{13}C CP/MAS NMR spectra of EBP-AT, EBP-PT and pure vinylsilica. Asterisks denote spinning sidebands.

^1H - ^{29}Si CP/MAS NMR is indicative of the degree of condensation of pore walls and integrity of the framework upon synthesis, template extraction and thermal treatment. The three resonances in the ^1H - ^{29}Si CP/MAS NMR spectrum of EBP-AT, illustrated in Figure 6.22, can be assigned as follows: T¹ ($\text{R}-\text{Si}(\text{OSi})(\text{OH})_2$) sites at -64.2 ppm; T² ($\text{R}-\text{Si}(\text{OSi})_2(\text{OH})$) sites at -73.6 ppm and fully condensed T³ ($\text{R}-\text{Si}(\text{OSi})_3$) sites at -82.9 ppm. The absence of Qⁿ silicon species in the region of -90 to -120 ppm confirms that no Si–C bond cleavage occurred during synthesis or template extraction.

The ^1H - ^{29}Si CP/MAS NMR spectrum of the thermally treated PMO EBP-PT, shows the same three major resonances although broadening of the peaks is observed. An increased intensity of the resonance at -65.7 ppm suggests the presence of $-\text{CH}_2\text{CH}_2-$ and $-\text{CH}_2\text{CH}_3$ T³ sites along with $-\text{CH}=\text{CH}-$ T¹ sites. A shoulder line at -58.6 ppm is a result of T² resonance representing silicon sites bound to the aliphatic carbon, also consistent with the DRIFT, FT-Raman and ^1H - ^{13}C CP/MAS NMR data. The low intensity line at *ca.* -100 ppm is a silicon Qⁿ site, a direct result of some Si–C bond cleavage during thermal treatment.

Consistent with the DRIFT, FT-Raman and NMR data, revealing both a decrease in $\equiv\text{Si}-\text{OH}$ and $-\text{CH}=\text{CH}-$ species and an increase in $\equiv\text{Si}-\text{O}-\text{Si}\equiv$ and $-\text{CH}=\text{CH}_2$ species, we propose a mechanism, as depicted in Figure 6.23. Herein, by means of

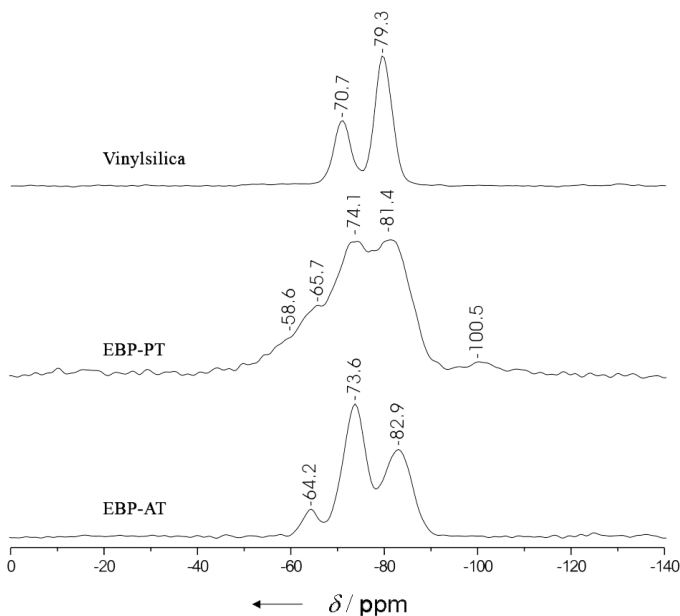


Figure 6.22: ^{1}H - ^{29}Si CP/MAS NMR spectra of EBP-AT, EBP-PT and pure vinylsilica.

elevating the temperature, terminal vinyl groups and siloxane bridges are generated *via* proton transfer from silanol groups to ethylene bridging groups. The absence of any surfactant in the pores excludes the possibility that the proton transfer arises from the surfactant template.

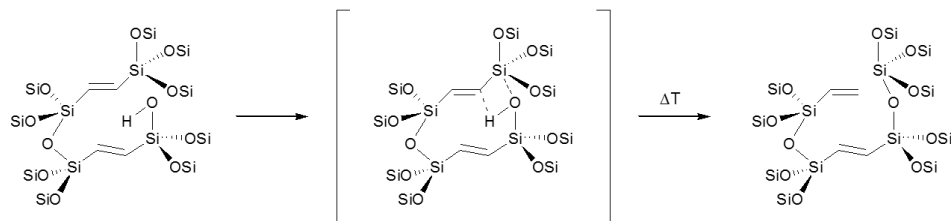


Figure 6.23: Schematic representation of the silanol-ethene interaction and the cleavage of the Si–C bond of the ethenylene-bridge upon thermal treatment, leading to the formation of a pendant vinyl group and a siloxane bridge.

While the spectral data give conclusive evidence of the thermally induced generation of vinylic functions in ethene-PMOs, the proposed mechanism has yet to be proven. Obtaining direct proof of this remarkable intramolecular reaction is however not straightforward. Therefore, with the aim of proving this hypothesis, an indirect method was developed in which the proton transfer from silanol groups to the ethenylene bridging groups can be deduced. Herein, the PMO silanol groups are first reacted with hexamethyldisilazane ($(\text{Me})_3\text{SiNHSi}(\text{Me})_3$), leading to hy-

drophobic ethene-PMOs, before performing the thermal treatment at 380 °C under vacuum. This way the hydrogen transfer reaction from the silanol to the ethene groups is prevented, and thus no vinylic groups should be generated upon thermal treatment (see Figure 6.24).

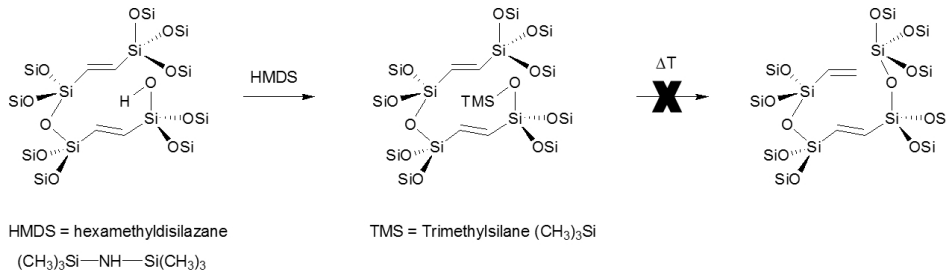


Figure 6.24: Schematic representation of how the thermally induced formation of pendant vinyl groups can be prevented by treating the ethene-PMO with hexamethyldisilazane prior to the thermal treatment.

In Figure 6.25 the DRIFT-spectra of the HMDS hydrophobized ethene-PMO, before (HMDS-EBP-AT) and after thermal treatment (HMDS-EBP-PT) are given. The absence of a sharp peak at 3733 cm⁻¹ in the spectrum of HMDS-EBP-AT, confirms the successful removal of the ethene-PMO silanol groups. The absence of peaks at 3067, 3026, and 1602 cm⁻¹ in the spectrum of HMDS-EBP-PT indicates that no vinylic groups are generated during the thermal treatment, which confirms the stated hypothesis and proves that the PMO silanol functions take part in the thermally induced generation of vinylic functions.

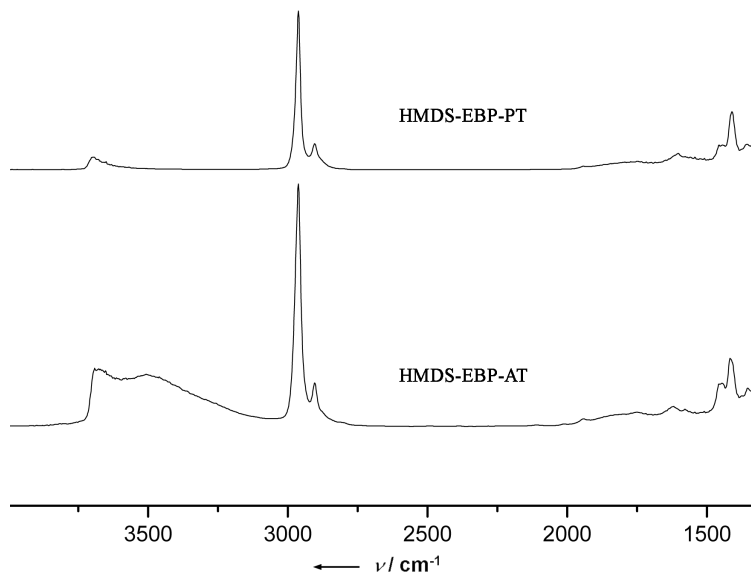


Figure 6.25: DRIFT-spectra of HMDS-EBP-AT and HMDS-EBP-PT.

6.4 Conclusions on ethenylene-bridged PMOs with controllable properties

By using acetone as an extracting solvent, the more efficient removal of the surfactant template enhances the porosity properties of the investigated materials. The porosity of ethenylene-bridged PMOs can further be controlled by fine-tuning the reaction conditions. Herein, the pH and the presence and concentration of *n*-butanol as a co-solvent play a key role. Without *n*-butanol, the optimum pH is 0.9. By further lowering the pH the excessive polycondensation of the precursor relative to the self-assembly process, causes filling of the mesopores, yielding materials with lower surface areas and pore volumes. On the other hand, increasing the pH beyond the optimum reduces the double-layer hydrogen-bonding interaction between the nonionic surfactant and the PMO-precursor, whereby the long-range hexagonal packing decreases. When *n*-butanol is used as a cosolvent, the filling of mesopores with solid material is prevented, even at very low pH values. As a result the optimum pH (0.1) is much lower than the synthesis without *n*-butanol. Overall, by fine-tuning the reaction conditions, both with and without *n*-butanol, well-ordered PMO materials with high surface areas and pore volumes can be attained.

Furthermore, the PMO synthesis temperature gives a means to control the pore size, structure, connectivity and volume. By increasing the synthesis temperature larger mesopores can be attained through withdrawal of the PEO blocks of the surfactant template in the micelle core. However, the pore diameter is only flexible to a certain extent, after which further temperature increasement has no affect on the pore size. This can also be attributed to the gathering of PEO blocks which protrude from micelle surface and generate secondary mesopores that form connections between the primary mesopores. Thus, fine-tuning the synthesis temperature gives perfect control of the meso- and micropore volume and the connectivity of the mesopores.

Other than controlling the porosity properties of ethenylene-bridged PMOs, by utilizing various cosolvents and tuning their concentration, the morphology of the PMOs can be accurately controlled to consist of crystal-like disk shaped, fibrous or spherical particles. Control of the particle morphology is a powerful tool in designing materials for particular applications. For instance for chromatographic applications, spherical particles are required for efficient column packing and good separation properties, while for catalysis applications, hexagonal crystal-like disks with short pore channels may be of interest by limiting diffusion problems.

In addition, clear spectroscopic evidence is given of a thermally induced transformation in pure *E*-configured ethenylene-bridged PMOs, whereby bridging ethene groups are converted to dangling vinyl groups. On the basis of spectroscopic data (DRIFT, FT-Raman and solid-state NMR), we propose a mechanism wherein terminal vinyl groups and siloxane bridges are generated *via* proton transfer from silanol groups to ethenylene bridging groups. This mechanism has been indirectly confirmed by hydrophobizing the PMO surface with hexamethyldisilazane prior to the thermal treatment. Once the silanol groups in ethene-PMOs are removed, no thermally induced generation of vinylic groups occurs, which proves that the silanol groups participate in the intramolecular reaction leading to PMO metamorphosis. This easy and straightforward approach allows the formation of multifunctional

hybrid materials consisting of direct anchoring points for catalysts. These solid supports can be of significant importance in catalysis applications, requiring materials with stereochemical configurations.

The results described in this chapter have been published in the literature as several peer review articles.^{453,467,468}

Chapter 7

Isomeric Ethenylene-bridged PMOs with Ultra-Large Mesopores

Due to their structural rigidity and controllable hydrophobic character, PMOs are highly interesting for applications in catalysis,³¹⁶ environmental technology,³⁵⁰ and chromatography³⁴⁷. Still, the applicability of PMOs is often limited by their pore sizes, which typically range between 2 and 8 nm. In some applications, such as in biocatalysis or controlled drug release, larger mesopores are required to allow the diffusion, adsorption or immobilization of large biomolecules such as enzymes, proteins or drugs.^{469–471} To date, the synthesis of ethenylene-bridged PMOs with mesopores larger than 10 nm has not been reported, so with this goal in mind, we probed the possibility of adapting Pluronic P123 as a template, in combination with 1,3,5-trimethylbenzene (TMB) as a sweller.

7.1 Principal of pore expansion

Addition of organic additives such as alcohols, aromatics or alkanes during the PMO self-assembly process, can have a significant impact on mesostructure formation. In chapter 5 and 6 we have demonstrated that alcohols can change the surface energy of surfactant micelles and affect both the pore structure and the morphology of the final products. By adding hydrophobic molecules such as TMB, the pore size of PMOs can also be enlarged. Herein, TMB migrates into the hydrophobic micelle core which consists of propylene oxide chains, causing the micelles to swell, and subsequently leading to hybrid materials with enlarged pores (see Figure 7.1). With the aid of hydrophobic additives such as TMB in combination with nonionic surfactants, the pore sizes of mesoporous silicates can be enlarged to 40 nm.⁴⁷² However, when TMB is added to a P123 templated system, the hexagonally packed pore structure is maintained only when employing low concentrations of TMB. Upon increasing the TMB-P123 ratio, a phase transition takes place and disordered mesocellular foams are obtained.^{472,473} So far, in the case of SBA-15, the addition

of hydrophobic additives can only lead to an increase in pore size to *ca.* 15 nm, without loosing the pore ordering.⁴⁷⁴ In the latter case, a low temperature approach in combination with NH₄F is adopted to control the self-assembly process and avoid phase transition. Besides SBA-15, the use of swellers has also assisted in the synthesis of other large pore silica materials. For instance, assisted by TMB and KCl, face-centered cubic mesoporous silicas (FDU-12) with exceptionally large pore sizes in the range of 27 nm have been obtained by lowering the synthesis temperature to 15 °C.⁴⁷⁵

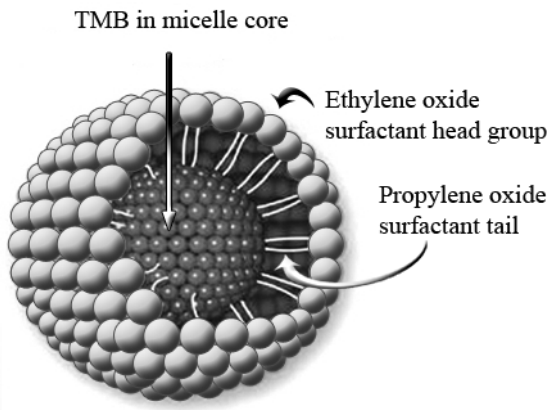


Figure 7.1: Schematic illustration of micelle expansion through addition of TMB during the self-assembly process.

7.2 Ethene-PMOs with ultra-large mesopores

7.2.1 Influence of TMB on mesostructure formation

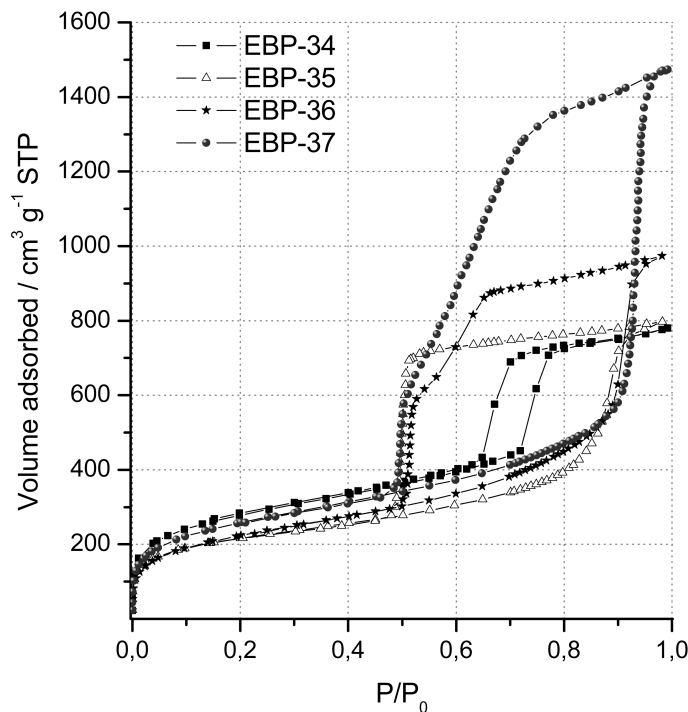
By varying the amount of TMB the pore size of ethenylene-bridged PMOs can be engineered from approximately 8.1 to 28.3 nm (see Table 7.1). Moreover, by increasing the amount of TMB, PMOs with extremely high pore volumes can be obtained. When employing 7.76 mmol of TMB (TMB/P123 = 45), a PMO with a pore diameter of 28.3 nm and a total pore volume of 2.25 cm³/g was acquired, which is the largest pore size and volume ever reported for a PMO material. These hybrid materials also have relatively high micropore volumes (up to 0.22 cm³/g), which can be attained by adapting a mild extraction procedure.

Figures 7.2 and 7.3 show the nitrogen adsorption-desorption isotherms and the BJH pore size distributions of EBP-34, EBP-35, EBP-36 and EBP-37, respectively, illustrating the impact of the swelling agent on the physisorption properties of the PMOs. The capillary condensation steps in the isotherms of these PMOs are very sharp and occur at very high relative pressures, indicating very uniform and ultra-large mesopores, as is confirmed by the pore size distributions given in Figure 7.3. The delayed nitrogen desorption of the PMOs synthesized with TMB suggests that the pores are confined.

Table 7.1: Influence of TMB on the properties of ethenylene-bridged PMOs

PMO sample	TMB/P123	$S^{[a]}$ / $\text{m}^2 \text{ g}^{-1}$	$V_t^{[b]}$ / $\text{m}^3 \text{ g}^{-1}$	$V_\mu^{[c]}$ / $\text{m}^3 \text{ g}^{-1}$	$D_p^{[d]}$ / nm
EBP-34	0	1018	1.03	0.14	8.1
EBP-35	10	783	1.23	0.15	18.5
EBP-36	15	819	1.50	0.10	21.3
EBP-37	45	944	2.25	0.22	28.3

[a] Surface area, [b] Total pore volume, [c] Micropore volume, [d] Pore diameter (calculated from adsorption isotherm with BJH method).

**Figure 7.2:** Nitrogen adsorption-desorption isotherms of EBP-34, EBP-35, EBP-36 and EBP-37.

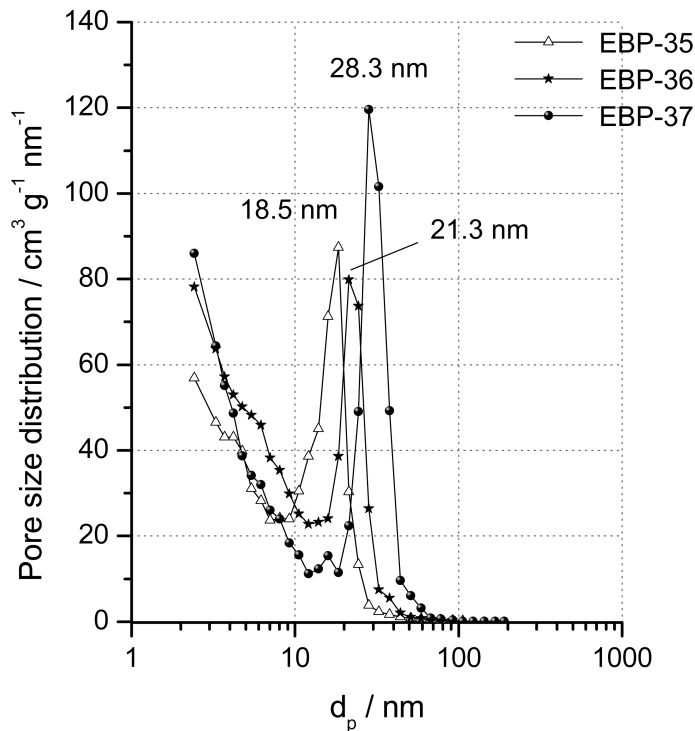


Figure 7.3: BJH pore size distributions of EBP-35, EBP-36 and EBP-37, calculated from the adsorption isotherms.

Commonly the use of swelling agents, such as TMB, results in materials with very poor to no structural ordering, especially when materials with very large pores are obtained. In fact, only a few reports on ultra-large pore PMOs exist.^{476,477} These reports however deal with ethane-PMOs.

By using *E*-1,2-bis(triethoxysilyl)ethene according to an optimized synthesis procedure, ordered ultra-large pore ethylene-bridged PMOs were obtained, as illustrated by the SAXS-plots in Figure 7.4. However, the addition of TMB clearly has an affect on the long-range ordering of the materials. EBP-34 reveals three well-resolved peaks which can be assigned to the (100), (110) and (200) reflections of a 2D hexagonally well-ordered structure. Due to lattice distortions and the presence of different mesophases, the assignment of the reflections in the SAXS-patterns of EBP-35, EBP-36 and EBP-37 is not straightforward. Assuming that the maxima are caused by next neighbor correlations, a predominant hexagonal arrangement can be derived when relying on the position of the first two peaks. Relating the first peak with the (100) reflection and assuming a close packed arrangement of spheres, one can calculate sphere diameters of 20.0, 22.2 and 30.4 nm, respectively.

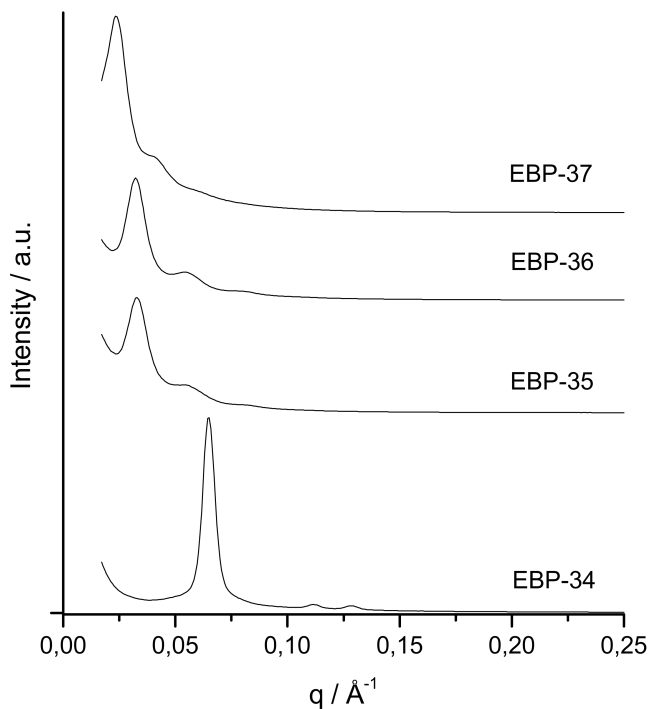


Figure 7.4: SAXS-plots of EBP-34, EBP-35, EBP-36 and EBP-37.

Looking at the local ordering with TEM, the ultra-large pore PMOs reveal different mesophases, as illustrated in Figure 7.5. Locally, mesostructures which consist of linearly connected spherical pores (nodular strings), are present (see Figure 7.5A and Figure 7.6). In addition, very large domains of foam-like, uniformly sized mesopores are found (see Figure 7.7) with, as illustrated in Figure 7.5B, a

local hexagonal packing. A third type of mesophase consists of 3D highly ordered spherical pores (Figure 7.5C), as illustrated in detail by the TEM-graphs in the tilt-series in Figure 7.8. Herein the spheres seem to have a face-centered cubic structure.

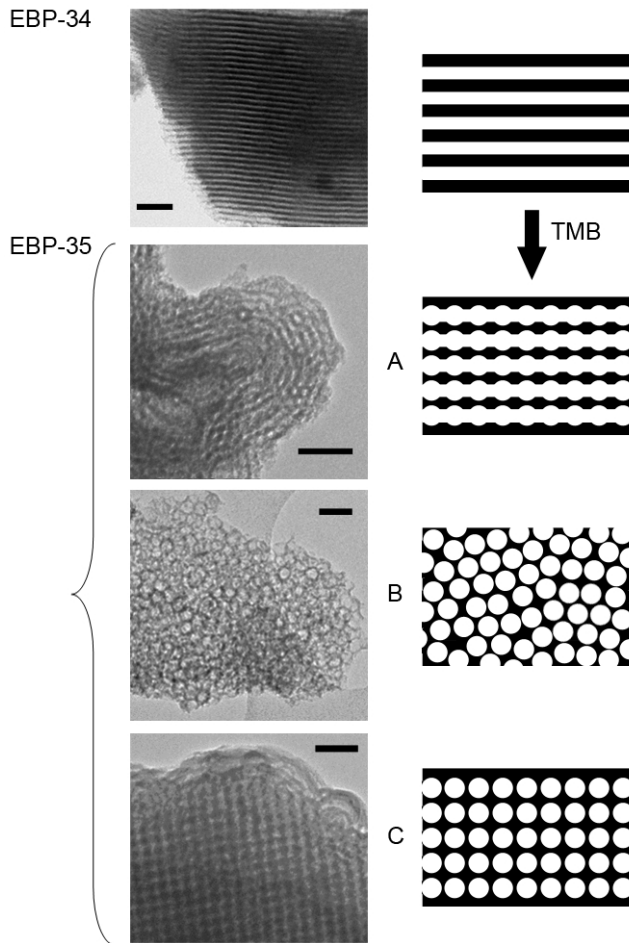


Figure 7.5: TEM images of EBP-34 and EBP-35 (scale bars are 50 nm), illustrating the phase transformation induced by TMB and a schematic representation of (A) nodular strings, (B) foam-like material and (C) ordered spherical pores.

The phase transition induced by TMB is caused by an alteration in the interfacial curvature of the surfactant micelles. Hereby TMB influences the hydrophilic-hydrophobic volume ratio of the surfactant. By adding TMB, the rod-like surfactant-organosilica composite micelles transform into spherical micelles, which leads to the formation of spherical pores. This rod-to-sphere transition accounts for the different mesostructures observed by TEM and explains the change in the nitrogen desorption behavior of the ultra-large pore PMOs when compared to EBP-1

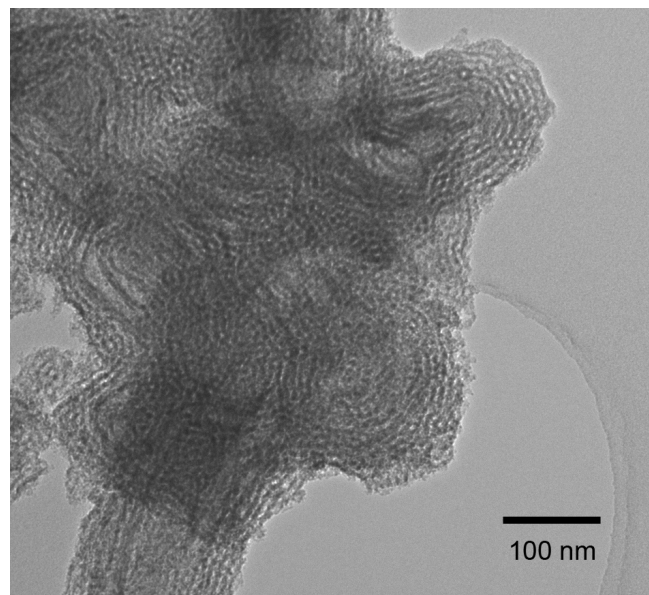


Figure 7.6: TEM-image of EBP-35, illustrating the presence of linearly connected spherical pores (nodular strings).

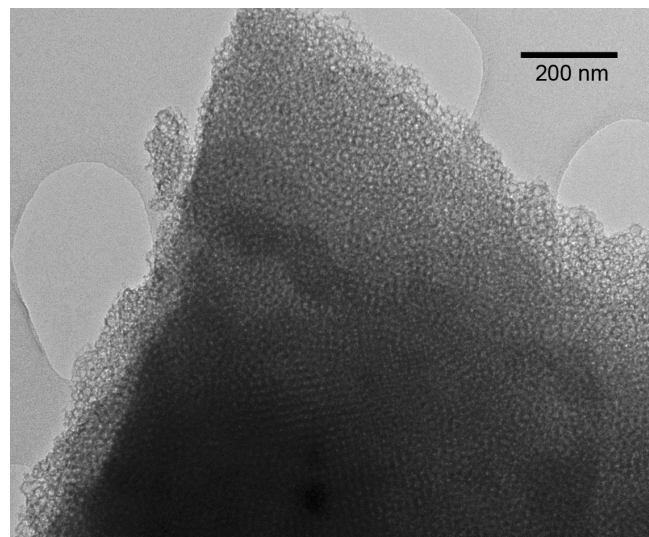


Figure 7.7: TEM-image of EBP-35, illustrating large domains of foam-like, uniformly sized mesopores.

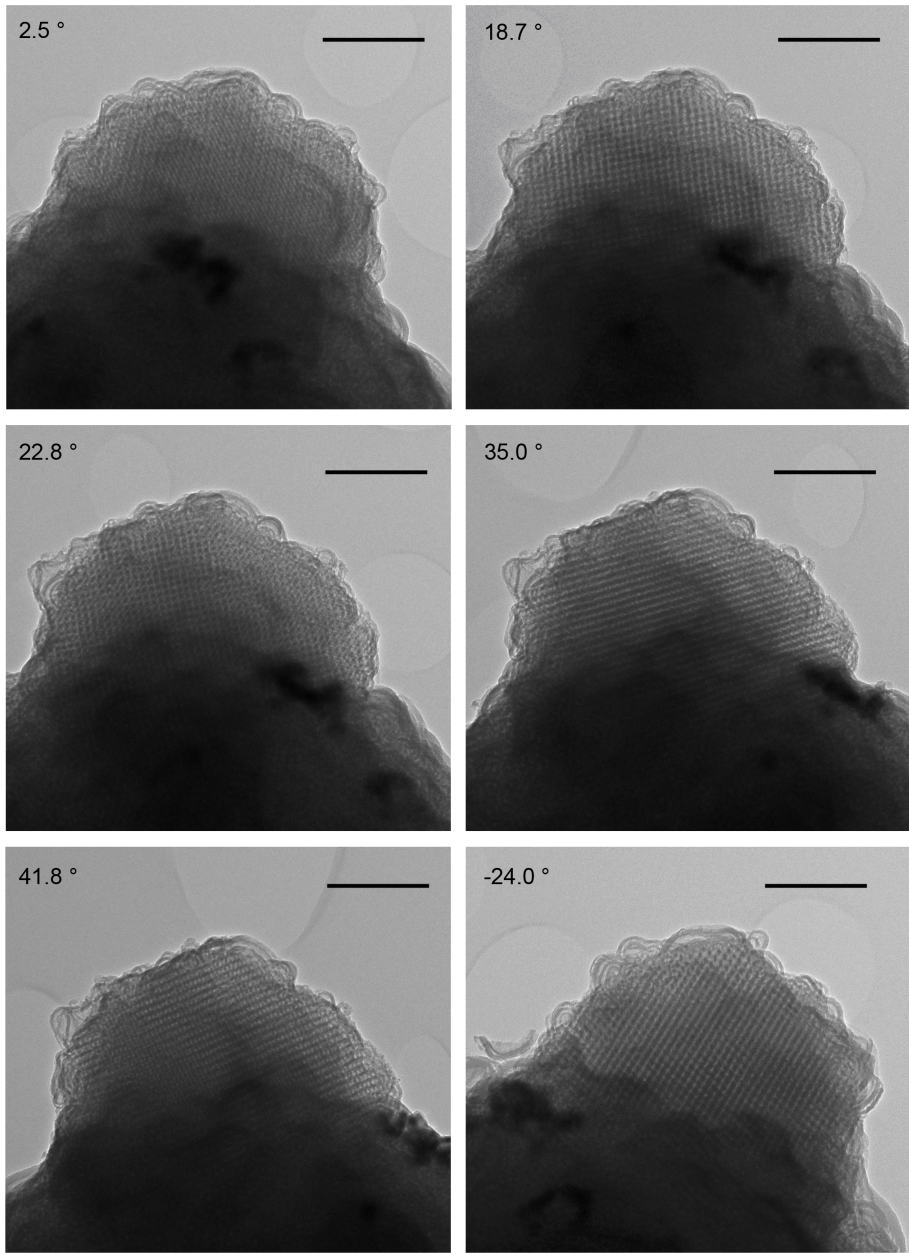


Figure 7.8: TEM-images of EBP-35, illustrating well-ordered spherical pores (presumably with a face-centered cubic structure). The specimen was tilted 2.5, 18.7, 22.8, 35, 41.8 and -24°. The scale bars are 200 nm.

(Figure 7.2). Herein, the delayed nitrogen desorption in the desorption isotherms of EBP-35, EBP-36 and EBP-37 is caused by the confinement of nitrogen in the mesopores.

7.2.2 Role of TMB in the self-assembly process

To investigate the role of TMB in the self-assembly process, different PMOs were synthesized under identical conditions, while varying the time at which TMB was added to the mixture. In Table 7.2, the properties of these PMOs are given, while the nitrogen adsorption-desorption isotherms are represented in Figure 7.9

Table 7.2: Influence of TMB on the properties of ethenylene-bridged PMOs

PMO sample	Time ^[a] / min	S ^[b] / m ² g ⁻¹	V _t ^[c] / m ³ g ⁻¹	V _μ ^[d] / m ³ g ⁻¹	D _p ^[e] / nm
EBP-38	0	857	1.43	0.16	28.3
EBP-39	10	903	1.56	0.15	18.5 and 28.3
EBP-40	16	800	0.90	0.20	-
EBP-41	180	981	1.03	0.15	7.1

^[a] Time after which TMB was added to the synthesis mixture, ^[b] Surface area, ^[c] Total pore volume, ^[d] Micropore volume, ^[e] Pore diameter (calculated from adsorption isotherm with BJH method).

When TMB is added together with the surfactant, typical ethenylene-bridged PMOs with ultra-large mesopores are attained, similar as described above (7.2.1). When TMB is added to the synthesis mixture after 10 minutes of reaction, a slight change in the nitrogen isotherms of the resulting PMO (EBP-39) is apparent. Analysis of the pore size distribution of EBP-39 *via* the BJH method, reveals two pore systems, as illustrated in Figure 7.10. Such a pore size distribution is referred to as a bimodal pore size distribution. While EBP-38 has uniform pores of *ca.* 28.3 nm, EBP-39 both has pores of 18.5 and 28.3 nm. The change in pore size distribution is probably related to the inhomogeneous dispersion of TMB throughout the micellar aggregates.

By prolonging the time after which TMB is added to the synthesis mixture to 16 minutes (time at which the mixture is a viscous gel, just before precipitation occurs), a material is obtained of which the nitrogen adsorption isotherm displays a capillary condensation step with a gradual slope, indicating an irregular pore system. These results suggest that after 16 minutes of reaction the self-assembly process is well on its way and is disturbed by the addition of TMB.

When TMB is added to the synthesis mixture after 3 hours, the mesostructure formation has already taken place and the PMO is fully precipitated. In this case TMB does not take part in the self-assembly process and the resulting material displays typical type IV nitrogen isotherms which can be associated with a mesoporous material with open cylindrical pores of *ca.* 7.1 nm. In other words, if TMB does not take part in the self-assembly process, no pore expansion can be realized. This can be explained by the structural rigidity of the materials, which, once formed, prohibits pore expansion.

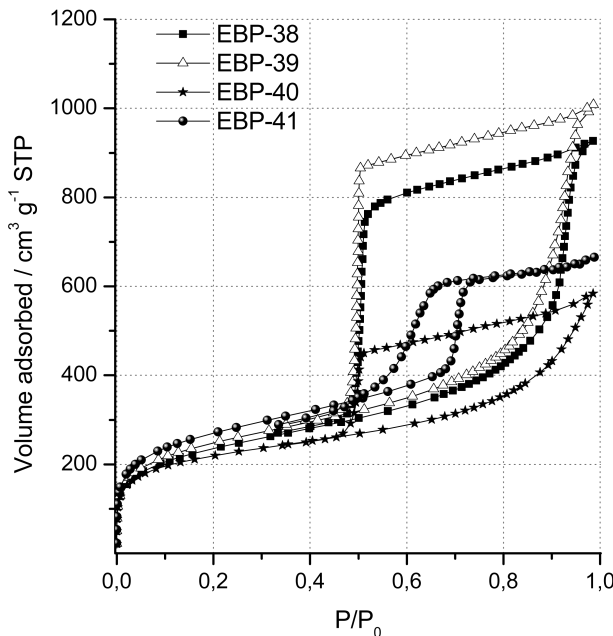


Figure 7.9: Nitrogen physisorption isotherms of EBP-38, EBP-39, EBP-40 and EBP-41.

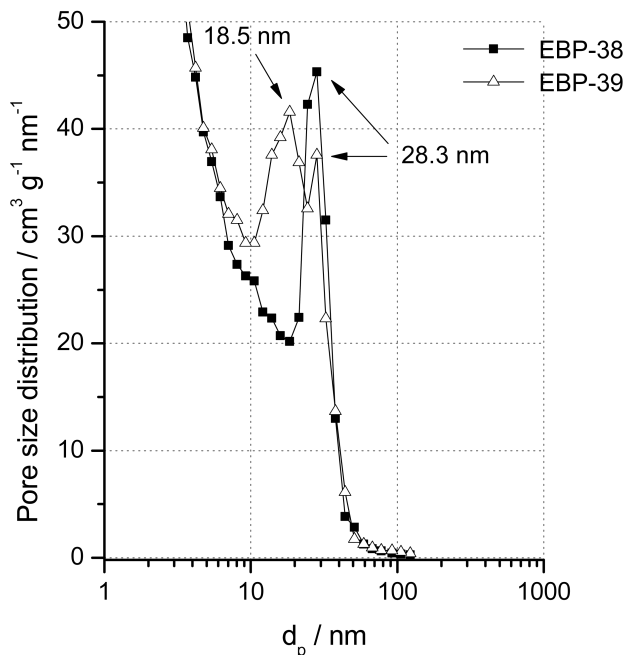


Figure 7.10: BJH pore size distributions of EBP-38 and EBP-39, calculated from the adsorption isotherms.

The use of TMB is a good means to enlarge the mesopores of ethylene-bridged PMOs. However, it has proven to be a difficult task to avoid phase transition. With the aim of obtaining ultra-large cylindrical mesopores, as supposed to spherical pores, the influence of synthesis temperature was also investigated. Though a low-temperature synthesis approach in combination with NH_4F has been implemented with success for the preparation of SBA-15 with large cylindrical mesopores,⁴⁷⁴ this method was ineffective for ethylene-bridged PMOs.

With respect to developing ethene-PMOs with ultra-large open cylindrical mesopores, another approach was investigated in which the type of swelling agent is altered. In Table 7.3 the influence of the swelling agent on the properties of these PMOs is given. For comparison reasons, the properties of the PMO prepared with TMB under identical conditions is also given (EBP-37). TMB results in the largest pore expansion and produces the PMO with the largest pore volume. The other aromatic swelling agents also produced PMOs with ultra-large mesopores, though these are somewhat smaller than when TMB is used. When hexadecane is used, no pore expansion is observed and a PMO with open cylindrical mesopores is attained. This indicates that hexadecane does not migrate in the micelle cores and does not take part in the self-assembly process. Possibly this is caused through phase separation between the surfactant mixture and hexadecane. When smaller aliphatic additives are used (hexane and pentane), pore expansion is observed, though the impact is smaller than when bulky aromatic swelling agents are employed.

Table 7.3: Influence type of swelling agent on the properties of ethylene-bridged PMOs

PMO sample	Swelling agent ^[a]	$S^{[b]}$ / $\text{m}^2 \text{ g}^{-1}$	$V_t^{[c]}$ / $\text{m}^3 \text{ g}^{-1}$	$V_\mu^{[d]}$ / $\text{m}^3 \text{ g}^{-1}$	$D_p^{[e]}$ / nm
EBP-37	TMB	944	2.25	0.22	28.3
EBP-42	<i>p</i> -cymene	993	2.03	0.20	21.3
EBP-43	<i>p</i> -xylene	938	1.84	0.18	21.3
EBP-44	<i>tert</i> -butylbenzene	911	1.92	0.16	21.3
EBP-45	hexadecane	912	1.10	0.13	8.1
EBP-46	hexane	899	1.35	0.16	13.9
EBP-47	pentane	802	1.00	0.15	9.2

^[a] Sweller/P123 = 45, ^[b] Surface area, ^[c] Total pore volume, ^[d] Micropore volume, ^[e] Pore diameter (calculated from adsorption isotherm with BJH method).

The impact of various swelling agents on the physisorption properties of ethylene-bridged PMOs is illustrated in Figure 7.11. Clearly no H1 type hysteresis is apparent in the isotherms of the ultra-large pore PMOs. The PMO synthesized with hexadecane (EBP-45) reveals a typical type IV isotherm with a H1 type hysteresis, indicating uniform cylindrical mesopores.

Though the development of ethylene-bridged PMOs with ultra-large open cylindrical mesopores is yet to be achieved, the above described synthesis strategies are very appealing. They can be employed to tune the pore diameter of ethene-PMOs in a broad range from *ca.* 7 to 30 nm. Besides having potentially large mesopores, these PMOs reveal narrow pore size distributions, extremely high pore volumes, high surface areas and relatively high micropore volumes.

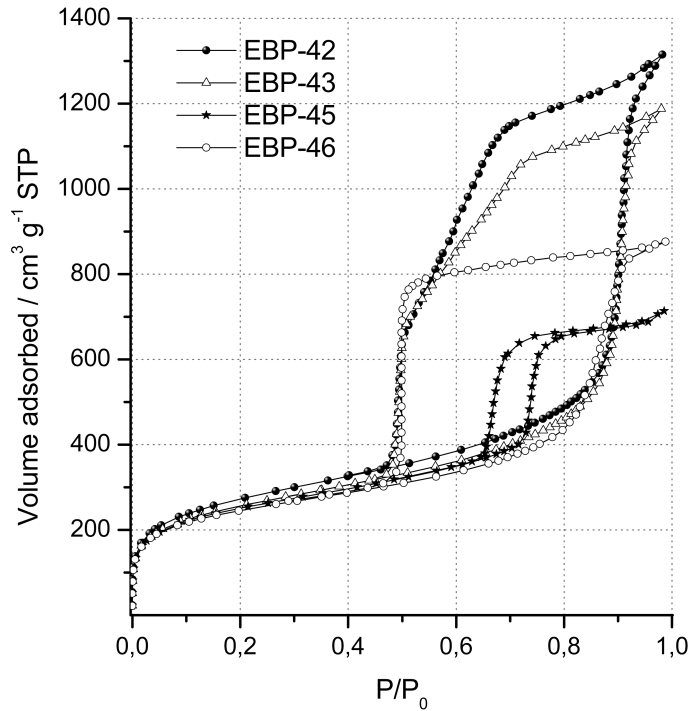


Figure 7.11: Nitrogen adsorption-desorption isotherms of PMOs synthesized with different swelling agents: *p*-cymene (EBP-42), *p*-xylene (EBP-43), hexadecane (EBP-45) and hexane (EBP-46).

7.2.3 Bimodal ethene-PMOs with ultra-large mesopores

Besides PMOs with monomodal pore size distributions, PMOs with bimodal pore size distributions can be developed by slightly changing the reaction conditions. When using the same molar composition as for EBP-36 (see Table 7.1, page 147), but by performing the aging step at atmospheric pressure at 90 °C instead of autoclaving at 100 °C, a PMO with a bimodal pore size distribution is obtained, as illustrated by Figure 7.12. Herein the bimodal PMO, abbreviated as EBP-48, both has pores of 21.3 nm like EBP-36 and pores of 8.1 nm like EBP-34 (see Table 7.1, page 147). The two-step adsorption isotherm, related to the bimodal pore size distribution, is clearly visible (see Figure 7.13). To disclose the morphological composition, the sample was studied with TEM. TEM clearly shows that both pore systems are present within a single particle, excluding the presence of two separate mesophases with two different pore size distributions (see Figure 7.14).

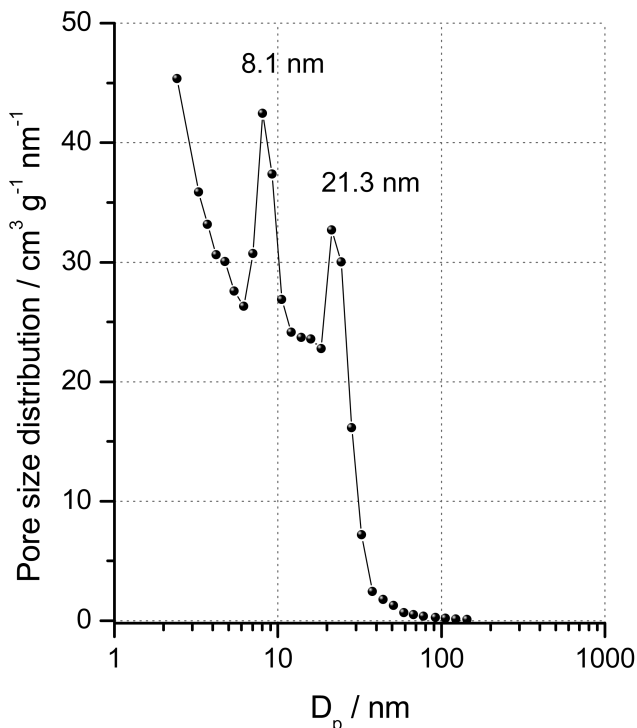


Figure 7.12: BJH pore size distribution of EBP-48, calculated from the adsorption isotherm, revealing two separate pore systems.

7.2.4 There is nothing so stable as change

An important parameter when considering materials with large mesopores is stability. Intuition might lead us to presume that larger pores are more susceptible to collapse. In this context, the shelf life of some ultra-large pore PMOs was in-

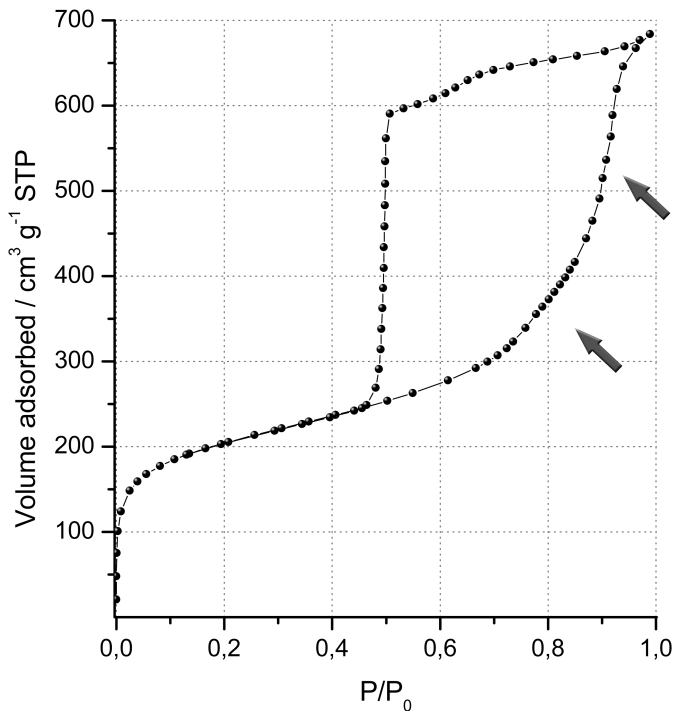


Figure 7.13: Nitrogen physisorption isotherms of EBP-48, revealing a small, but well-resolved second step in the adsorption isotherm.

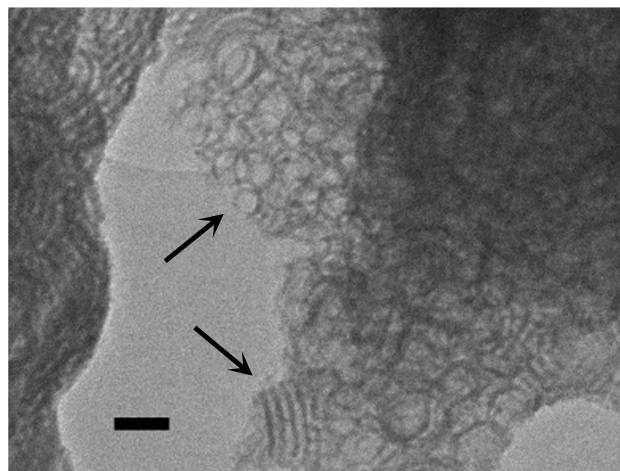


Figure 7.14: TEM-image of EBP-48, illustrating the presence of two interconnected mesopore systems. Scale bar is 50 nm.

vestigated by storing the materials under ambient conditions during one year, the results of which are given in Table 7.4. Both SAXS and nitrogen physisorption (see Figure 7.15) results, show that the framework structure is maintained, indicating that the pore size does not affect the stability of the materials. However some pore shrinkage was observed. The high stability of these materials is a result of the thickness of the pore walls, which can be as high as 8.2 nm. Furthermore, the change in mesostructure induced by TMB may have a positive influence on its stability.

Table 7.4: Properties of ethylene-bridged PMOs after storing for one year under ambient conditions

PMO sample	$S^{[a]}$ / $\text{m}^2 \text{ g}^{-1}$	$V_t^{[b]}$ / $\text{m}^3 \text{ g}^{-1}$	$V_\mu^{[c]}$ / $\text{m}^3 \text{ g}^{-1}$	$D_p^{[d]}$ / nm	$a_0^{[e]}$ / nm	$t_w^{[f]}$ / nm
EBP-35	695	1.13	0.10	13.9	22.1	8.2
EBP-36	729	1.39	0.03	16.0	22.5	6.5
EBP-37	934	2.36	0.18	24.5	31.1	6.6

[a] Surface area, [b] Total pore volume, [c] Micropore volume, [d] Pore diameter (calculated from adsorption isotherm with BJH method), [e] Unit cell, [f] Pore wall thickness.

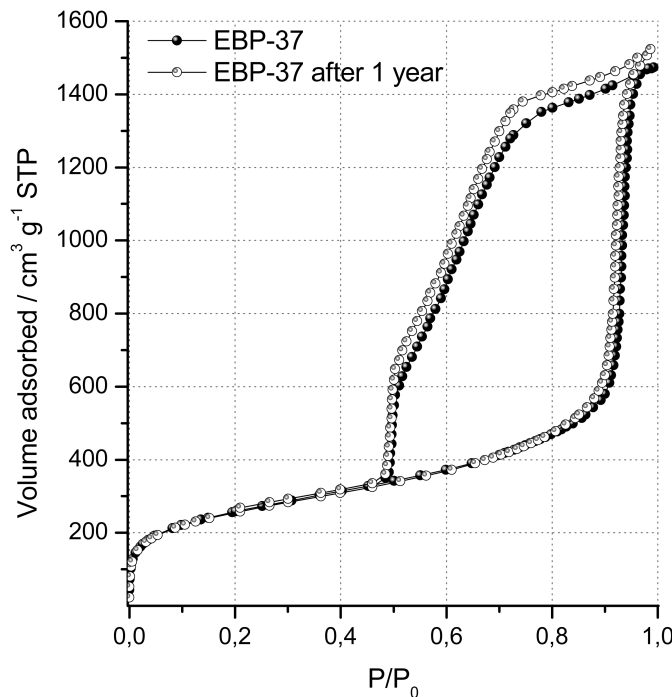


Figure 7.15: Nitrogen physisorption isotherms of EBP-37, before and after storing under ambient conditions for one year.

7.3 Conclusions on ethene-PMOs with ultra-large mesopores

Synthesis strategies were successfully developed to fine-tune the pore size and volume of ethenylene-bridged PMOs. By using swelling agents, such as TMB, *p*-cymene, *p*-xylene, *tert*-butylbenzene and hexane, in combination with Pluronic P123 as a surfactant template, PMOs with ultra-large mesopores (up to 28.3 nm) and astonishing pore volumes (up to 2.25 cm³/g) were synthesized for the first time. Moreover, these PMOs reveal surprisingly narrow pore size distributions, high surface areas and relatively high micropore volumes. Despite having such large mesopores, these ethenylene-bridged PMOs are also very stable. With a shelf-life exceeding one year, these ultra-large pore PMOs can be stored under ambient conditions without suffering from deterioration.

Besides having an impact on the pore size and volume, the addition of swelling agents also affects the mesostructure, as was deducted from SAXS and TEM. The ultra-large pore PMOs reveal various pore systems, including foam-like pore structures with uniformly sized mesopores, 3D stacked spherical pores and nodular strings, i.e. cylinders built from linearly connected spheres. The phase transition induced by the swelling agents is caused by an alteration in the interfacial curvature of the surfactant micelles. By influencing the hydrophilic-hydrophobic volume ratio of the surfactant, the hydrophobic swellers cause the rod-like surfactant-organosilica composite micelles to transform into spherical micelles, leading to the formation of spherical pores.

Investigation of the role of swelling agents in the self-assembly process, showed that TMB immediately takes part in the mesostructure formation. Addition of swelling agent after PMO precipitation has no impact on the pore size and volume. The synthesis of ethenylene-bridged PMOs with ultra-large open cylindrical mesopores is yet to be achieved. Possibly this can be realized through careful fine-tuning of the reaction conditions and the molar composition of the synthesis mixture. Especially, lowering the reaction temperature should assist in avoiding phase transition. Though, the synthesis mixture has to be adequately adjusted to allow mesostructure formation and precipitation.

A novel and straightforward method to obtain ethenylene-bridged PMOs with bimodal pore size distributions has also been developed. By carefully adjusting the synthesis conditions, PMOs consisting of interconnected pore systems with different diameters can be synthesized, which opens up the road to novel hierarchically ordered hybrid materials. That is, materials with several different degrees of porosity incorporated into one composite material.

These types of hybrid materials with unprecedented pore sizes may be interesting in applications requiring large pore volumes such as in catalysis, environmental technology and nanoelectronics. The easily modifiable ethenylene-bridges give a means to immobilize catalysts or heavy metal scavengers *via* the organic carbon bond as supposed to the commonly used and less stable siloxane bond, while the large pore cavities when sealed can be potentially interesting in designing low-*k* materials by air-trapping. Ultra-large pore PMOs are especially interesting for applications involving large biomolecules, such as in biocatalysis or controlled drug release. Herein, larger mesopores are required to allow the diffusion, adsorption or

immobilization of enzymes, proteins or drugs. Hierarchically ordered PMOs, such as the described bimodal systems which comprise of micropores, medium sized and ultra-large mesopores, are also very appealing for bulk-chemistry applications in which reactant molecules need to readily access the interior pore structure while the internal surface area is maximized. For such applications, a ramified pore structure with large pores leading to smaller and smaller pores is desired (similar to the structure of our lungs).

Part of the research described in this chapter has been published in the literature as a peer review article.⁴⁷⁸

Chapter 8

Expanding the Scope of Olefinic PMOs

8.1 Perspective

The previous four chapters have dealt with extensive research in the development and characterization of diastereoisomeric ethylene-bridged PMOs with diverse properties. This chapter is somewhat different as it describes some interesting research topics in the field of olefinic PMOs without going into much detail. Its intent is to stimulate further investigation in a field of which the surface of its potential has only been scratched.

A first topic is expanding the family of olefinic PMOs. To date, ethylene-bridged PMOs are the only olefinic PMOs which have been reported upon. Being one of the most interesting hybrid materials in terms of modifiability and applicability, there is need to further explore the possibility of developing novel olefinic hybrid materials. In chapter 3, the first synthesis of a diastereoisomeric pure butenylene-bridged PMO precursor was described, opening the way to novel isomeric butene-PMOs.

A second topic is attempting to develop ethylene-bridged PMOs with the aid of gemini surfactants. In the process, synthesis of PMOs with crystalline pore walls is desired. Using novel synthesis strategies, such as changing the surfactant or pH, can lead to materials with novel structures and properties and can be potentially interesting for various applications.

A third topic is expanding the potential of ethylene-bridged PMOs, by using their backbones as a means to convert these olefinic PMOs into materials which can be employed in acid catalyzed reactions. Herein, the intention is to transform isomeric ethene-PMOs *via* a single-step reaction into sulfonic acid PMOs.

A last topic is the synthesis of PMOs which can be used in olefin metathesis. Here, a synthesis strategy is introduced to develop a boomerang-type metathesis catalyst through co-condensation of 1,2-bis(triethoxysilyl)ethene with a linker molecule. The latter reacts with homogeneous olefin metathesis catalysts in a single step, producing hybrid heterogeneous catalytic systems.

8.2 One builds too many walls and not enough bridges

Sir Isaac Newton

8.2.1 The challenges

To extend the family of olefinic PMOs is not an easy task. First of all there is the question of how to prepare a pure and adequate precursor. Second, how can this precursor be implemented in the synthesis of a mesoporous hybrid architecture. Chapter 3 dealt with the first question. Herein the synthesis of a novel pure PMO precursor with butenylene bridges is described. The next step is to successfully use this precursor for the synthesis of butenylene-bridged PMOs. However, the size of this organic bridge will introduce an extra challenge and will contribute in the complexity of the PMO synthesis. As the bridge consists of four carbon atoms, the flexibility of the chain and the distance between two hydrolyzable silicon species may cause the material to be instable and collapse. Furthermore, there is the possibility of phase separation and gelation. Therefore, the synthesis conditions have to be optimized from scratch. Herein, pH, molar composition, presence of additives, temperature, reaction time, ... will play a significant role in designing PMO materials with desirable properties.

8.2.2 Butenylene-bridged hybrid materials: a first step

By adapting a synthesis procedure similar as described for the isomeric ethenylene-bridged PMO EBP-24, a hybrid material consisting of diastereoisomeric butenylene bridges was synthesized. In Figure 8.1 the nitrogen adsorption-desorption isotherms are given of this novel hybrid nanocomposite.

The isotherms are quite special with a peculiar hysteresis loop. Furthermore, the capillary condensation and evaporation steps in the isotherms of this PMO are relatively sharp and occur at extremely high relative pressures, indicating uniform and ultra-large mesopores, as is confirmed by the pore size distribution given in Figure 8.2.

The occurrence of ultra-large mesopores without using swelling agents is very unique and somewhat unexpected. Moreover, in contrast to the ultra-large pore PMOs discussed in chapter 7 the nitrogen desorption is not delayed and proceeds at a high relative pressure, indicating pores which are open at both ends and that do not consist of ink-bottle necks. Calculated from the desorption isotherm, using the BJH method, this butenylene-bridged hybrid material consists of mesopores of *ca.* 21.3 nm. However, when calculated from the adsorption isotherm, the material has mesopores in the range of 50 nm. With a surface area of about 573 m²/g and a total pore volume of *ca.* 1.14 cm³/g, the successful synthesis of this hybrid composite is a promising first step in the development of novel olefinic PMOs. However, SAXS-data (see Figure 8.3) indicate that the mesopores are not ordered. This is also confirmed by TEM (see Figure 8.4). Though the ultra-large mesopores and thick pore walls are clearly apparent, they reveal no pattern which accounts for the absent reflections in the SAXS-plot.

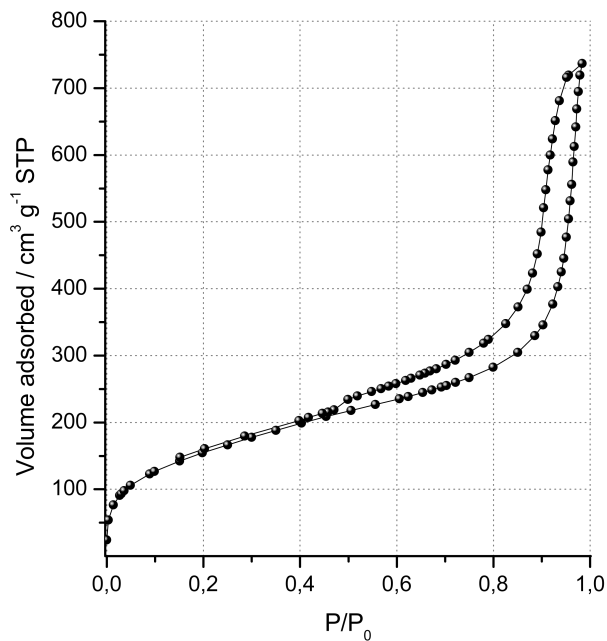


Figure 8.1: Nitrogen adsorption-desorption isotherms of a diastereoisomeric butenylene-bridged PMO.

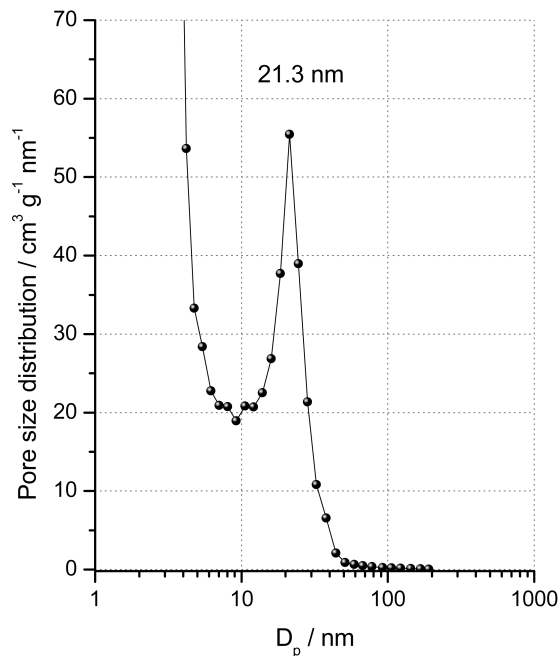


Figure 8.2: BJH pore size distribution of a diastereoisomeric butenylene-bridged PMO, calculated from the desorption isotherm.

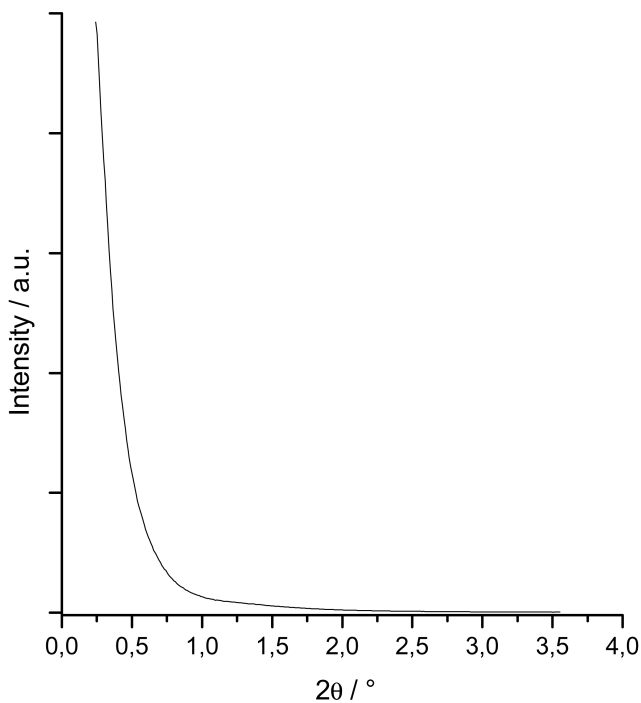


Figure 8.3: SAXS-plot of a butenylene-bridged hybrid nanocomposite.

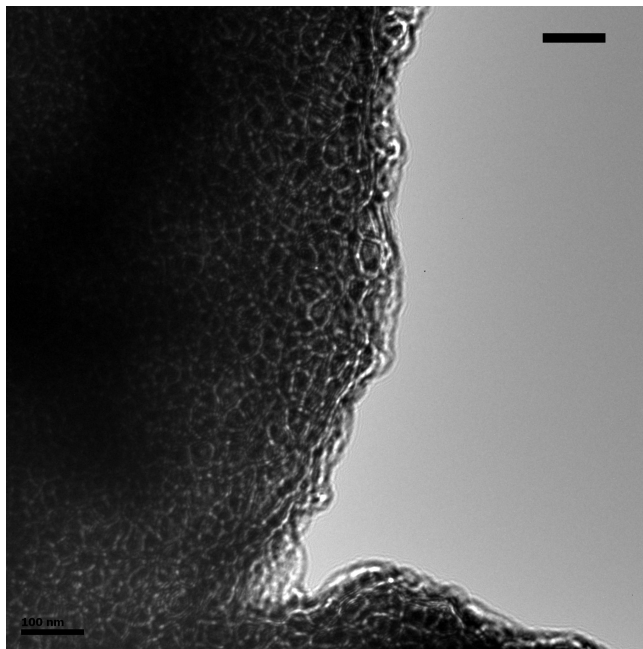


Figure 8.4: TEM-image of a butenylene-bridged hybrid material. Scale bar is 100 nm.

In Figure 8.5, SEM-images are given of the described butenylene-bridged hybrid material. Interestingly, spherical particles of *ca.* 1.3 to 2.5 μm are apparent.

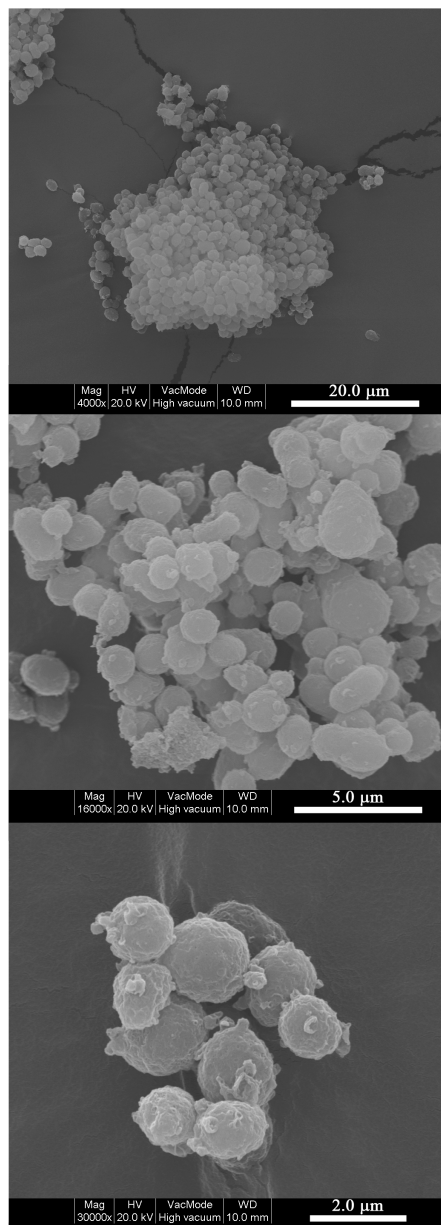


Figure 8.5: SEM-images of a butenylene-bridged hybrid nanocomposite.

On the one hand, the synthesis of butenylene-bridged PMO materials needs to be further optimized. Herein, reaction parameters as ascribed above need to be carefully tuned to allow mesostructure formation with highly ordered mesopores. On

the other hand, the described butenylene-bridged hybrid material can be potentially interesting in various applications such as catalysis and chromatography. For chromatographic applications, spherical particles are highly desirable. Mesoporous materials with spherical particle morphologies offer new opportunities in separation due to their high surface areas and narrow pore size distributions. Usually, pure silica materials are functionalized *via* a post-synthetic treatment to produce reversed phases. However, hybrid mesoporous materials can be potentially more appealing due to their intrinsic hydrophobic organic functionalities and relatively (in comparison to pure silica materials) high stabilities at low and high pH values.

8.3 A place for everything, everything in its place

Benjamin Franklin

So far, all the discussed PMO materials have been synthesized under acidic conditions using Pluronic P123 as a surfactant template. This method has the advantage of producing ordered materials with relatively large mesopores and thick pore walls. Though, under some circumstances, synthesis under basic conditions is preferred. That is, the synthesis can be performed under milder reaction conditions (less corrosive) and in some cases materials can be obtained which, under acidic conditions, would be difficult to develop (for instance co-condensation of Si- and Al-species). Moreover, changing the pH of a synthesis mixture, or using other surfactants as templates can lead to PMOs with various (novel) pore structures.

8.3.1 Gemini surfactants

Gemini surfactants represent a relatively new class of detergents consisting of two amphiphilic moieties. These moieties have the same structure as conventional surfactants, but they are connected by a spacer group, as illustrated in Figure 8.6. A gemini surfactant with two tails (with m carbon atoms) and one spacer (with s carbon atoms) is represented as $m\text{-}s\text{-}m$.

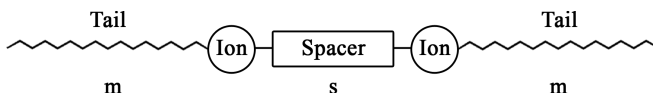


Figure 8.6: Schematic representation of ionic gemini surfactant.

When compared to conventional surfactants, gemini surfactants usually have better surface-active properties and are therefore promising as industrial detergents. But more importantly, they offer new opportunities in the field of materials chemistry. By influencing the packing parameter g (see section 1.4.1, p13) they enable the synthesis of mesoporous materials with various pore structures. The cubic mesophase ($\text{Ia}\bar{3}d$) is preferentially formed for g -values between 0.5 and 0.65, while the hexagonal mesophase ($\text{P}6/m\text{m}$) forms when the g -value is < 0.5 .

Alami *et al.* showed that the headgroup area a_0 changes significantly with the length of the spacer (s) of a gemini surfactant.⁴⁷⁹ In a surfactant-water system, at s -values < 10 , the spacer is in contact with the surrounding water, lying more or less stretched at the air-water interface. At s -values > 10 , the spacer becomes too hydrophobic to remain in contact with the water and folds to the air side of the interface. As a consequence, the formation of a cubic MCM-48 ($Ia\bar{3}d$) phase is favored for gemini surfactants with the formula represented below and a spacer of 12 carbons: $[C_nH_{2n+1}(CH_3)_2N^+-(CH_2)_{12}-N^+(CH_3)_2C_mH_{2m+1}]_2Br^-$.

8.3.2 Using gemini surfactants in PMO synthesis

For this preliminary investigation the gemini surfactant 16-12-16 was employed, which was synthesized by refluxing stoichiometric amounts of 1,12-dibromoalkane and N,N-dimethylhexadecylamine in acetone, followed by several recrystallization steps (see Figure 8.7).



Figure 8.7: Synthesis of 16-12-16 gemini surfactant.

Optimizing the synthesis conditions

As there has been no previous report on the synthesis of ethylene-bridged PMOs using gemini surfactants as templates, it is difficult to predict which reaction conditions are required to prepare well-ordered hybrid materials with decent surface areas and pore volumes. Therefore, the influence of several reaction parameters on the porosity properties was examined. Hereby, one reaction parameter at a time was varied while keeping other parameters constant. In Table 8.1 the surface area and pore volume of PMO samples prepared under different reaction conditions are given.

A first reaction parameter which proved to play a very important role in obtaining materials with high surface areas and pore volumes, is surfactant/precursor ratio. This is clearly illustrated in Figure 8.8. Good materials, in terms of surface area and pore volume, can only be attained in a narrow surfactant/precursor ratio range between 0.12 and 0.15. Of course, this is only valid under the specified reaction conditions. Changing the pH, *n*-butanol concentration, temperature, reaction time, ... will effect this optimum.

Tuning the *n*-butanol/precursor ratio is also important to produce hybrid composites with high surface areas and pore volumes, though its effect is less extreme. The highest surface areas and pore volumes are attained when the *n*-butanol/precursor ratio ranges between 2.0 and 5.0. The presence of *n*-butanol does seem to be essential though, as without it both the surface area and pore volume drop drastically (see EBP-53 in Table 8.1).

Table 8.1: Influence of several reaction parameters on the surface area and pore volume of ethenylene-bridged PMOs

Sample	<i>E</i> -BTSE / mmol	16-12-16 / mmol	<i>n</i> -butanol / mmol	NaOH / mmol	$S^{[a]}$ / $\text{m}^2 \text{g}^{-1}$	$V_t^{[b]}$ / $\text{m}^3 \text{g}^{-1}$
EBP-49	1	0.07	2.3	1.2	522	0.33
EBP-50	1	0.12	2.3	1.2	957	0.58
EBP-51	1	0.15	2.3	1.2	1010	0.57
EBP-52	1	0.19	2.3	1.2	115	0.11
EBP-53	1	0.12	0	1.2	387	0.21
EBP-54	1	0.12	3.0	1.2	1094	0.62
EBP-55	1	0.12	4.0	1.2	989	0.52
EBP-56	1	0.12	5.0	1.2	924	0.55
EBP-57	1	0.12	6.0	1.2	694	0.42
EBP-58	1	0.12	2.3	1.0	1005	0.66
EBP-59	1	0.12	2.3	0.8	774	0.52
EBP-60	1	0.12	2.3	0.6	867	0.55
EBP-61	1	0.12	2.3	0.4	682	0.49
EBP-62	1	0.12	2.3	0.1	480	0.31

[a] Surface area, [b] Total pore volume.

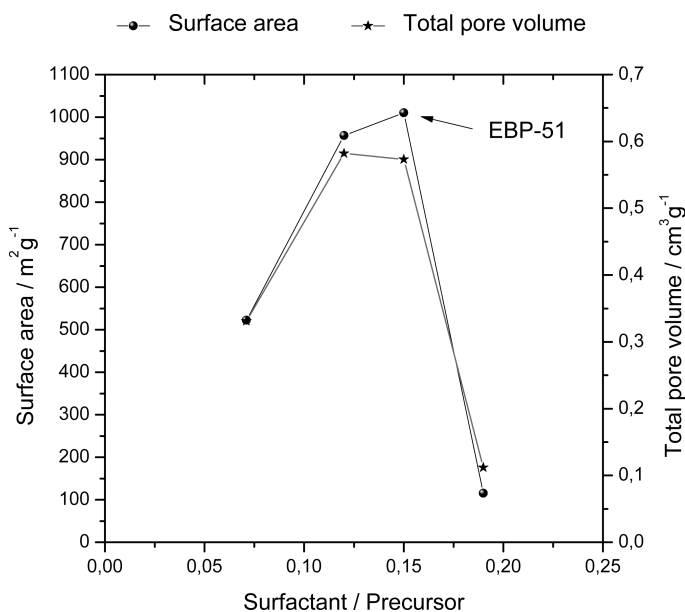


Figure 8.8: Surface area and total pore volume of ethenylene-bridged PMOs as a function of surfactant/precursor ratio (EBP-49 to EBP-52).

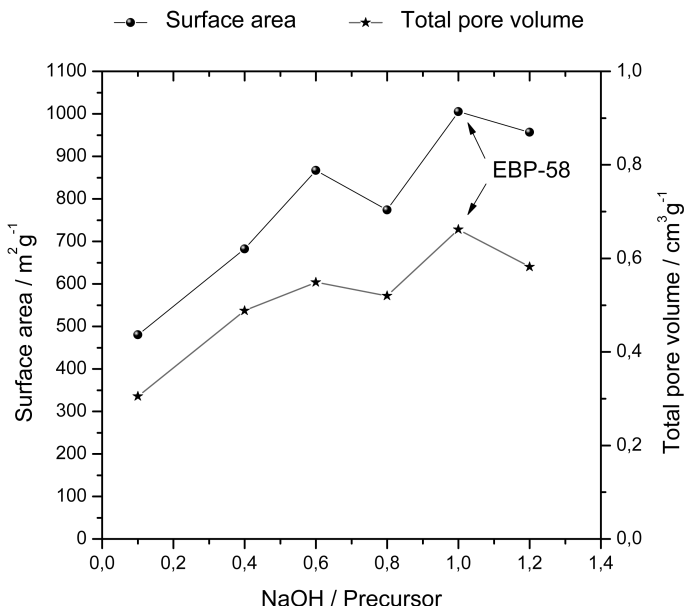


Figure 8.9: Surface area and total pore volume of ethenylene-bridged PMOs as a function of NaOH/precursor ratio (EBP-50 and EBP-58 to EBP-62).

A third and last reaction parameter which was investigated is the NaOH/precursor ratio. As illustrated in Figure 8.9 this parameter can also drastically affect the surface area and pore volume of ethenylene-bridged hybrid materials prepared with the 16-12-16 gemini surfactant. The highest surface area and pore volume is attained when the NaOH/precursor ratio is ≈ 1 . Below this optimum, both the surface area and pore volume steadily decrease. Once more, this optimum is highly dependable on the other reaction parameters.

In Figure 8.10 some nitrogen adsorption isotherms are given of PMOs with high surface areas and pore volumes. Clearly these samples do not exhibit typical type IV isotherms with sharp capillary condensation steps, though the materials can not be considered as pure microporous. This indicates that these materials have pores on the border-line of micro-meso size. The largest mesopore size in this PMO series is 3.5 nm (EBP-61).

Although the above described synthesis strategy enables the preparation of ethenylene-bridged hybrid materials with relatively high surface areas and pore volumes, it should be considered as preliminary. Much more research is required to further optimize the material properties, especially in terms of pore structure and size.

Solid-state NMR spectroscopy

To investigate the molecular composition of the ethenylene-bridged PMOs, synthesized with the gemini surfactant 16-12-16, solid state NMR was performed. The ^1H - ^{13}C CP/MAS NMR spectrum of EBP-51, represented in Figure 8.11A, clearly exhibits an intense and narrow single resonance at 146.4 ppm corresponding to

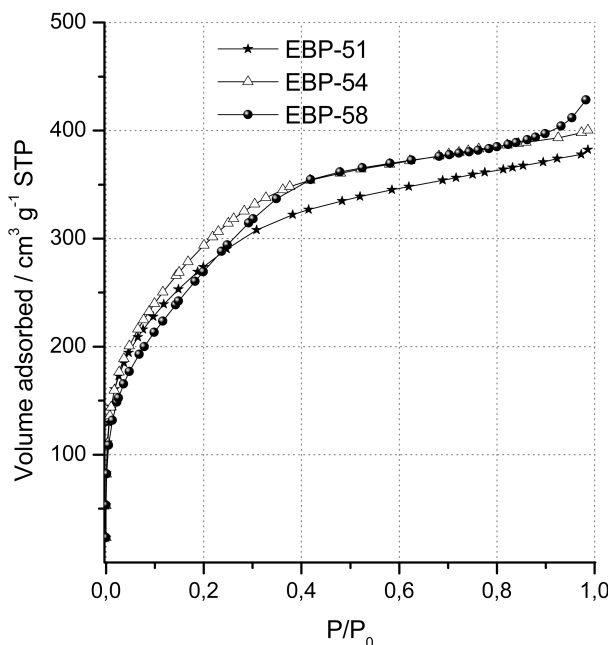


Figure 8.10: Nitrogen isotherms of ethenylene-bridged PMOs synthesized with the gemini surfactant 16-12-16.

the *E*-configured CH=CH bridging organic groups. The two small resonances at 48.2 and 30.1 ppm can be assigned to residual gemini surfactant still present in the pores, indicating that the surfactant is not fully removed. This can be explained by the nature of template-precursor interaction. When gemini surfactants are employed under basic conditions an ionic S^+I^- interaction takes place, which is stronger than the $N^0H^+X^-I^+$ interaction that takes place when Pluronic P123 is used as surfactant under acidic conditions.

In Figure 8.11B the ^1H - ^{29}Si CP/MAS NMR spectrum of EBP-51 is given, which is indicative of the degree of condensation of the pore walls. The three resonances at -64.5, -71.4 and -83.6 ppm can be assigned to R-Si(OSi)(OH)₂ (T¹ sites), R-Si(OSi)₂(OH) (T² sites) and R-Si(OSi)₃ (T³ sites). The absence of Qⁿ silicon species in the region of -90 to -120 ppm confirms that no Si-C bond cleavage occurred during synthesis or template extraction.

The $(T^1+T^2)/T^3$ ratio of EBP-51 is *ca.* 0.74, which is much lower than that obtained under acidic conditions using Pluronic P123 as surfactant (1.37, see Table 4.2, p100). This indicates that a much higher degree of framework condensation is obtained when the hybrid materials are synthesized under basic conditions. Moreover, the relatively narrow line widths in the ^1H - ^{29}Si CP/MAS NMR spectrum of EBP-51, suggest a very well-ordered system.

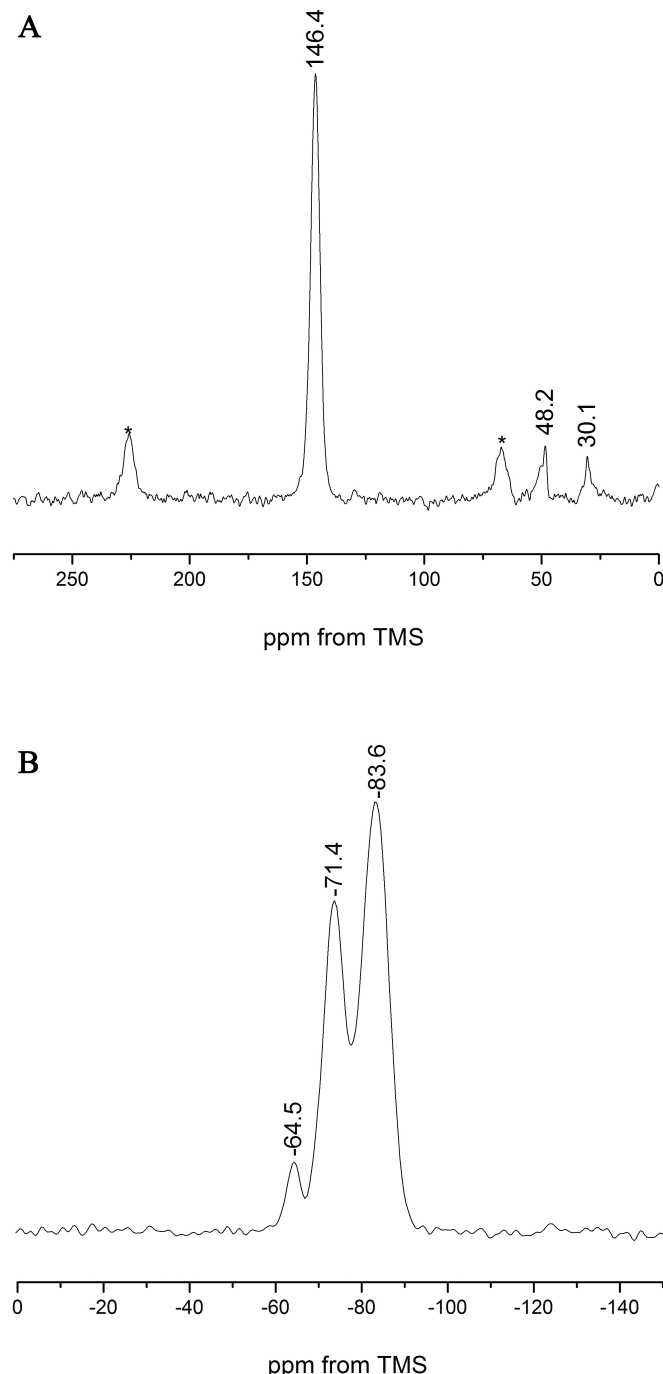


Figure 8.11: (A) ^1H - ^{13}C CP/MAS and (B) ^1H - ^{29}Si CP/MAS NMR spectra of EBP-51. Asterisks denote spinning sidebands.

8.3.3 A well-ordered system: Organizing bridges at a molecular level

One of the most challenging things in the field of ordered mesoporous siliceous materials, is introducing molecular ordering in the pore walls. This is exemplified by the very few reports on these type of materials (see section 2.1.2, p45). Moreover, so far it has only been realized under basic conditions. Therefore, the possibility of introducing molecular scale ordering in the pore walls of diastereoisomeric ethenylene-bridged PMOs, prepared under basic conditions with the gemini surfactant 16-12-16, was examined.

The structural ordering of the hybrid materials was evaluated by powder X-ray diffraction. In Figure 8.12 the XRD-pattern is given of EBP-51. Clearly reflections in the wide-angle range are apparent at $2\theta \approx 16.5^\circ$ and 33° , indicating molecular scale ordering in the pore walls of this PMO sample (as illustrated schematically in Figure 8.12), with basal spacings of *ca.* 5.3 and 2.7 Å, respectively. The reflection at 16.5° has also been reported by Mokaya *et al.*³⁰⁴ Only one reflection is visible in the low-angle region at $2\theta \approx 2^\circ$, making it difficult to predict the pore structure of EBP-51. Therefore, high-resolution TEM was performed.

In Figure 8.13 some TEM images are illustrated, showing (A) long pore channels with a diameter of *ca.* 1 nm (Due to exposure to the electron beam this value is underestimated) and (B) pore spacings of *ca.* 2.5 Å. Very interesting is the fact that the latter corresponds well to the basal spacing calculated from the reflection at $2\theta \approx 33^\circ$ in the XRD-pattern, indicating that TEM image (B) reveals the molecular scale ordering in the pore walls of EBP-51.

Though the TEM images indicate that EBP-51 is hexagonally ordered, without images revealing hexagonal pore arrangement, nothing conclusive can be said. Further TEM investigation is required to fully elucidate the pore structure of EBP-51.

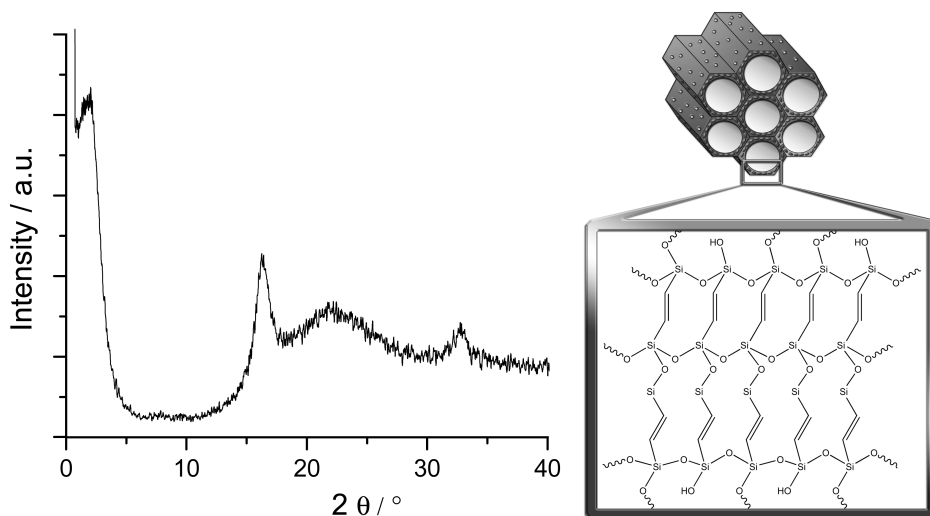


Figure 8.12: XRD-plot of EBP-51, revealing wide-angle reflections. Schematic representation of molecular ordering in the pore walls of ethene-PMOs.

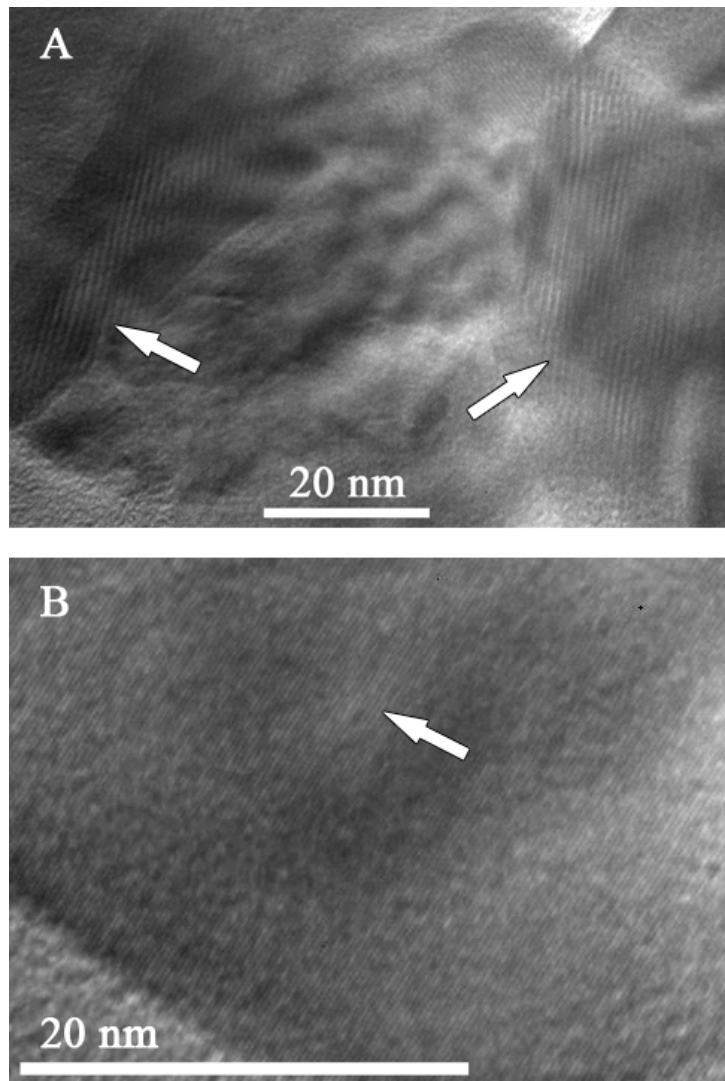


Figure 8.13: High-resolution TEM images of EBP-51, revealing (A) long pore channels with a diameter of *ca.* 1 nm and (B) molecular ordering with spacings of *ca.* 2.5 Å.

8.4 PMOs in practice: novel solid acid catalysts

Developing novel materials is satisfying and rewarding, though their true potential is only recognized when they are put into practice. As previously mentioned, ethenylene-bridged PMOs are potentially interesting for various applications such as catalysis, chromatography, environmental technology, sensing, controlled drug release, and nanoelectronics.

A large part of this Ph.D. research work has been designing hybrid materials with controllable properties. However, when considering applications, often materials with certain functionalities are required which, depending on the application, can act as catalytic sites, metal scavengers, sensors, Incorporation of such functionalities during mesostructure formation, implies that reaction conditions have to be reevaluated in order to design materials in a controllable fashion.

Therefore, our first intention was to develop catalytic systems through single step modification of homemade isomeric ethenylene-bridged PMO materials. This method has the advantage that catalyst design is feasible without having to worry about catalyst incorporation effecting mesostructure formation. If ethenylene-bridged PMOs with controllable properties can be prepared and transformed into desirable materials through easy post-synthetic modification procedures, these versatile materials may be potentially interesting in various applications.

8.4.1 Sulfonic acid ethene-PMOs

So far, there has been no report on the direct sulfonation of ethenylene-bridged PMO materials. The only report on ethenylene-bridged PMOs consisting of sulfonic acid groups is that of Kondo *et al.*, in which the ethenylene-bridges are converted *via* a two-step chemical modification, involving a Diels-Alder and a sulfonation reaction (see Figure 2.2, p43).³⁰⁶ Usually, sulfonic acid PMOs are synthesized either through a co-condensation or a post-synthetic grafting procedure with 3-mercaptopropyltrimethoxysilane followed by an oxidation reaction with H_2O_2 or HNO_3 .^{326,338,480,481} The only report on sulfonic acid PMOs synthesized through a single step modification step is that of sulfonic acid phenylene-bridged PMOs.⁴⁸² In a similar way we probed the sulfonation of ethene-PMOs.

In Figure 8.14 the direct sulfonation of ethenylene-bridged PMOs is illustrated. Herein, previously prepared ethene-PMOs are treated with chlorosulfonic acid at 0 °C.

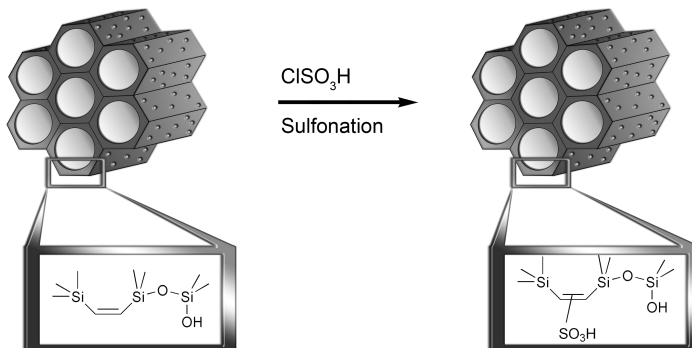


Figure 8.14: Direct sulfonation of ethenylene-bridged PMOs with chlorosulfonic acid.

Quantification of the sulfonic acid groups incorporated in the ethenylene-bridged PMOs was estimated by means of titration with NaOH. Prior to the titration, the sulfonated PMOs were sufficiently washed with water (until filtrate had a neutral

pH), methanol and acetone to remove any physisorbed chlorosulfonic acid and successfully vacuum dried to remove any physisorbed solvents.

To establish the required reaction time for sufficient sulfonation of the ethene groups, the sulfonation of ethenylene-bridged PMOs was monitored as a function of synthesis time. After 6 hours of reaction, 0.69 mmol H⁺/g PMO was found. By prolonging the reaction to 24 hours, 1.08 mmol H⁺/g PMO could be incorporated. Further prolonging the reaction time resulted in no significant increase in the amount of incorporated sulfonic acid groups. Moreover, when the reaction is carried out too long, carbonization of the PMO organic groups is established. Although this carbonization process, which probably occurs through generation of sulfuric acid, can be inhibited by performing the reaction under inert atmosphere, some carbonization takes place after long reaction times (3 days).

To investigate whether the sulfonation reaction influences the pore structure, two types of ethenylene-bridged PMOs (with different pore sizes and structure) were analyzed, before and after sulfonation, by means of nitrogen physisorption. In Figure 8.15 the isotherms of these samples are given, illustrating that the sulfonation reaction has no significant impact. Herein, EBP-63 and EBP-42 are diastereoisomeric ethene-PMOs with cylindrical and spherical mesopores, respectively. The sulfonated ethenylene-bridged PMOs are abbreviated as SEBP. In Table 8.2 the properties of the concerned PMOs are given.

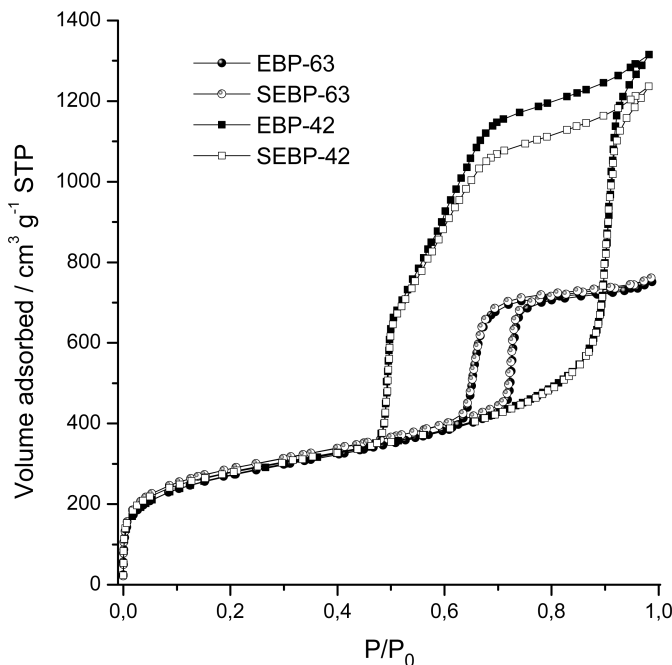


Figure 8.15: Nitrogen isotherms of ethenylene-bridged PMOs, before (EBP-63 and EBP-42) and after (SEBP-63 and SEBP-42) sulfonation.

The sulfonation reaction clearly has no negative effect on the porosity properties of ethenylene-bridged PMOs. On the contrary, a slight increase in surface area

Table 8.2: Porosity properties of ethenylene-bridged PMOs before and after sulfonation

PMO sample	Sulfonation	$S^{[a]}$ / $\text{m}^2 \text{ g}^{-1}$	$V_t^{[b]}$ / $\text{m}^3 \text{ g}^{-1}$	$V_\mu^{[c]}$ / $\text{m}^3 \text{ g}^{-1}$	$D_p^{[d]}$ / nm
EBP-63	no	987	1.16	0.15	8.1
SEBP-63	yes	1047	1.18	0.18	8.1
EBP-42	no	993	2.03	0.20	21.3
SEBP-42	yes	1015	1.91	0.21	21.3

[a] Surface area, [b] Total pore volume, [c] Micropore volume, [d] Pore diameter (calculated from adsorption isotherm with BJH method).

is observed. This method of modification is therefore superior to traditional post-synthetic modification procedures which produce materials with lower surface areas and pore volumes as a consequence of incorporating larger organic entities.

8.4.2 PMOs put to the test: A model esterification reaction

As a model reaction to test the activity of the sulfonic acid ethene-PMOs, the esterification of acetic acid with *n*-propanol was chosen (see Figure 8.16). All reactions were monitored as a function of time by means of GC-analysis. To help drive the reaction to completion, generated water was removed from the reaction mixture *via* a Dean-Stark apparatus. Therefore, toluene was used as a solvent and a relatively high reaction temperature of 135 °C was adapted.

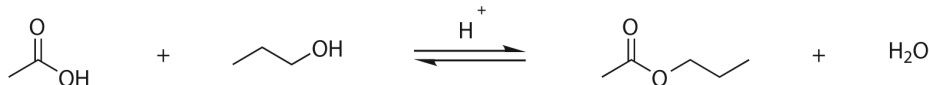


Figure 8.16: Esterification of acetic acid with *n*-propanol using sulfonic acid PMOs.

Homogeneous *vs.* heterogeneous

To evaluate the activity of sulfonic acid ethene-PMOs for the esterification of acetic acid with *n*-propanol, it was compared to that of an active homogeneous catalyst, *p*-toluenesulfonic acid. In Figure 8.17, the conversion plots are given.

Remarkably, the sulfonic acid PMO SEBP-63 has a comparable activity to *p*-toluenesulfonic acid. With a catalyst loading of 0.49 and 0.45 %, a maximum conversion of 100 % was observed after 80 and 40 minutes for SEBP-63 and *p*-toluenesulfonic acid, respectively. With other words, SEBP-63 has a TON of 204, which is very close to that of the homogeneous catalyst (TON = 222). When the catalyst loading is lowered to 0.15 %, a maximum conversion of 70 % is observed after 3.5 hours, giving a TON of 467. The high catalytic activity of SEBP-63 can be a result of the high surface area and readily accessible mesopores, which limits diffusion problems. These first results indicate that sulfonic acid ethenylene-bridged PMOs are potentially interesting for acid catalyzed reactions. However, besides activity, a high stability of the catalyst is also desirable.

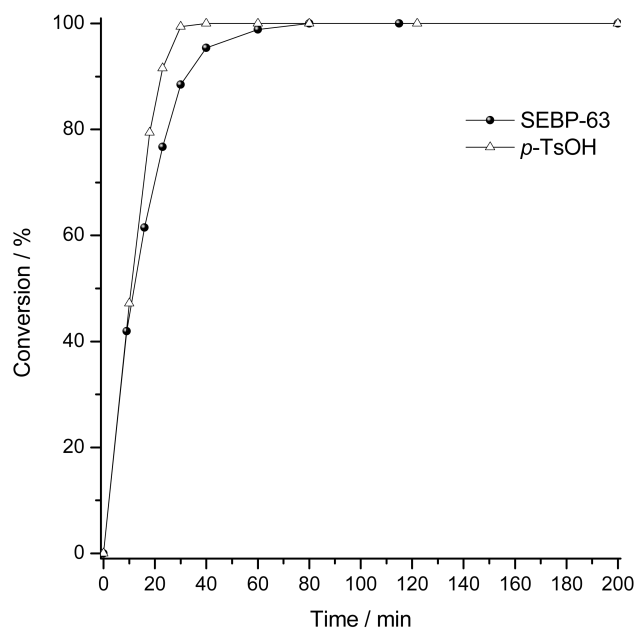


Figure 8.17: Conversions of *n*-propanol with SEBP-63 and *p*-toluenesulfonic acid.

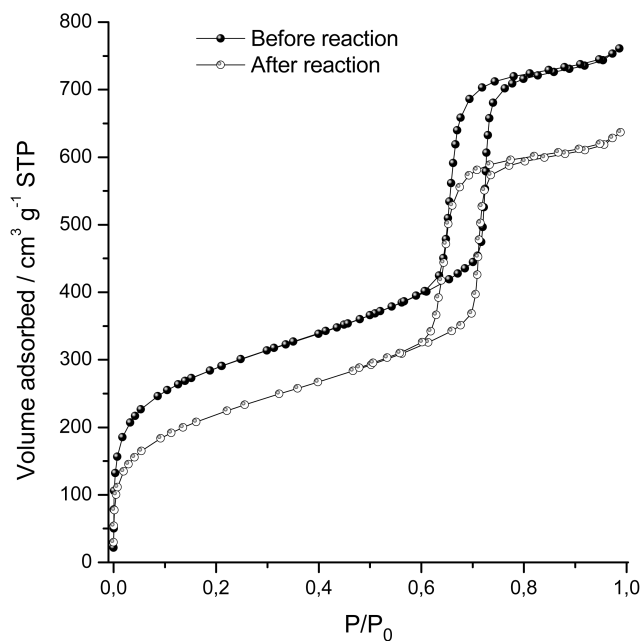


Figure 8.18: Nitrogen isotherms of SEBP-63, before and after the esterification of *n*-propanol with acetic acid at 137 °C.

PMO stability toward esterification reaction

To investigate the impact of the reaction conditions on SEBP-63, the sample was analyzed *via* nitrogen physisorption after completion of the esterification reaction. In Figure 8.18 the isotherms are given of SEBP-63, before and after the esterification reaction. Unfortunately, SEBP-63 shows some deterioration as a consequence of the adapted reaction conditions. The surface area decreases from 1047 to 800 m²/g, while the total pore volume diminishes from 1.18 to 0.98 m³/g. The pore size also reveals a slight decrease from 8.1 to 7.1 nm. Therefore, a different reaction procedure, in which the Dean-Stark apparatus is left out and the reaction temperature is lowered to 90 °C, was probed.

In Figure 8.19, the conversion plots are given of SEBP-63, using both reaction procedures. As would be expected, a decrease in conversion is observed when the Dean-Stark apparatus is left out and the reaction temperature is lowered. However, with a TON of 182 after 80 minutes, SEBP-63 gives satisfactory results under these less harsh conditions. Moreover, as illustrated by the nitrogen isotherms in Figure 8.20, the pore structure is not affected during the esterification reaction, in contrast to the procedure with the Dean-Stark apparatus at 137 °C. Thus, with the intention of performing multiple successive esterification reactions with a single batch of PMO catalyst, this less harsh reaction procedure is potentially more appealing.

Ultra-large pore PMOs put to the test

The ultra-large pore sulfonic acid ethylene-bridged PMO SEBP-42 was also tested in the esterification of acetic acid with *n*-propanol. Herein, the procedure at 90 °C was used. In Figure 8.21 the conversion of *n*-propanol with SEBP-42 is given. For reasons of comparison, the conversion plot of SEBP-63 is also illustrated. On first sight SEBP-63 reveals a lower activity than SEBP-42. However, SEBP-63 has a lower catalyst loading (0.42 *vs.* 1.08 mmol H⁺/g). In fact, SEBP-42 has a high TON of 453 (after 260 minutes), which is much higher than SEBP-63. This can probably be explained by the enhanced accessibility of the catalytic sites in the ultra-large mesopores of the acid PMO.

As with SEBP-63, the esterification reaction has little impact on the PMO structure, as illustrated by the isotherms of SEBP-42, before and after the esterification reaction, in Figure 8.22. There is only a slight decrease in pore volume (from 1.91 to 1.85 m³/g) and surface area (from 1015 to 979 m²/g), while the pore size remains constant.

PMO Recyclability

Being powders, sulfonic acid PMOs can easily be separated from the reaction mixture, giving clean reaction products without requiring further purification. After SEBP-63 was tested in the esterification of acetic acid with *n*-propanol (procedure with Dean-Stark), the sample was filtrated, washed, vacuum dried and immediately reused in a second run. Unfortunately, the *n*-propanol conversion dropped from 100 to 70 % (see Figure 8.23). This can be explained by a loss of protons. By means of titration with NaOH, the amount of sulfonic acid groups after the first

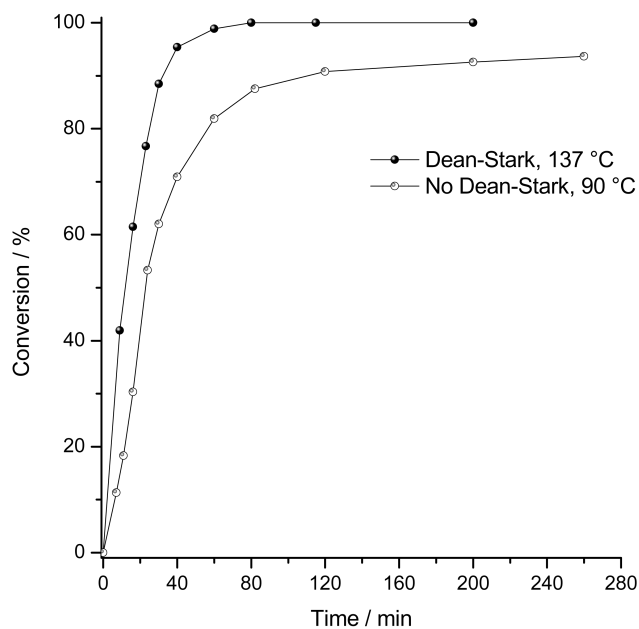


Figure 8.19: Conversions of *n*-propanol with SEBP-63 using different reaction procedures: with Dean-Stark at 137 °C and without Dean-Stark at 90 °C.

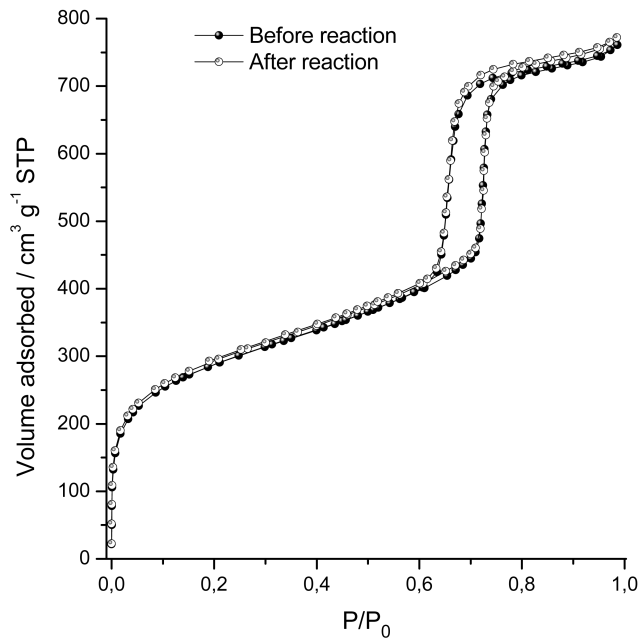


Figure 8.20: Nitrogen isotherms of SEBP-63, before and after the esterification of *n*-propanol with acetic acid at 90 °C.

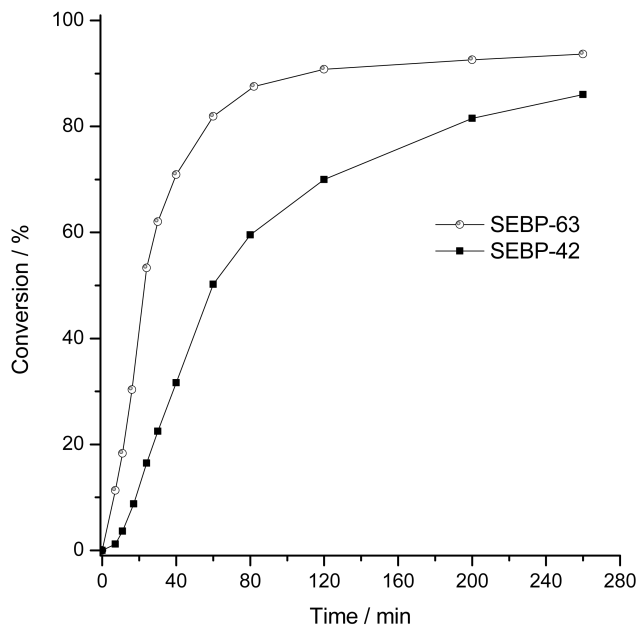


Figure 8.21: Conversions of *n*-propanol with SEBP-63 and SEBP-42, using the reaction procedure without Dean-Stark at 90 °C.

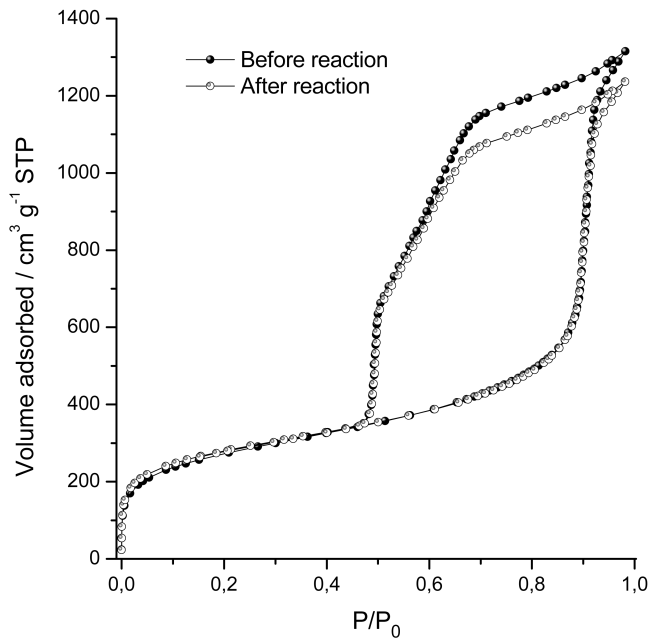


Figure 8.22: Nitrogen isotherms of SEBP-42, before and after the esterification of *n*-propanol with acetic acid at 90 °C.

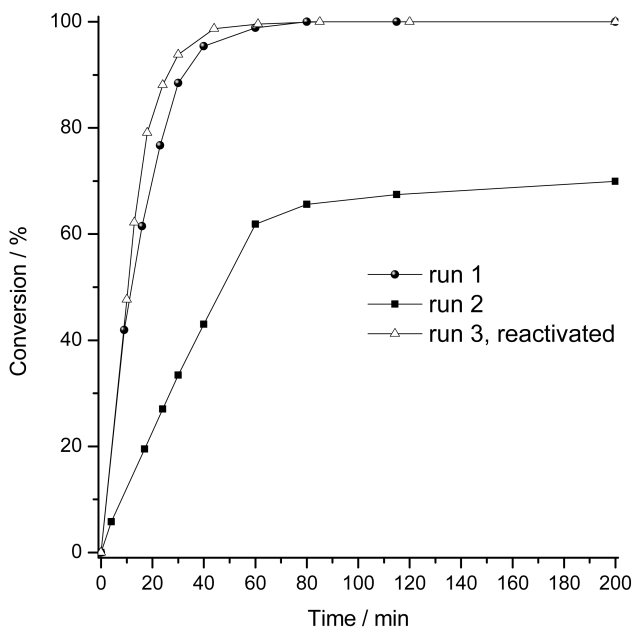


Figure 8.23: Conversions of *n*-propanol with SEBP-63 in 3 successive reaction runs. SEBP-63 was reactivated prior to run 3.

run was estimated at 0.35 mmol/g. After reactivation with chlorosulfonic acid, the acid PMO regained its activity and revealed full conversion. The loss of protons during the reaction is a major drawback, which at the time can not be explained, but which has to be resolved in the future.

8.5 Closing the cycle: PMO catalysts for olefin metathesis

8.5.1 The challenges in olefin metathesis

Olefin metathesis is a powerful transformation tool in modern chemistry. By mediating the exchange of olefin substituents, metathesis catalysts enable reactions as ring-closing metathesis (RCM), cross-metathesis, self-metathesis, and ring-opening metathesis polymerization (ROMP). Because of their stability towards air and moisture, and their tolerance of a broad range of functional groups, ruthenium complexes, such as the Grubbs' type catalysts, are particularly useful for these reactions.

Unfortunately, metathesis transformations usually require relatively large amounts of catalyst, especially in total synthesis. For this reason, modern homogeneous catalysts significantly add to the total cost of a product. Moreover, the most undesirable feature of modern homogeneous metathesis catalysts is that they contaminate the reaction products. The homogeneous nature of these systems implies that the

heavy-metal containing products often require exhaustive chromatographic purification treatments. Therefore, the development of greener metathesis processes is of great importance.

For the above stated reasons, easy separation and recyclability of olefin metathesis catalysts is highly desirable, both from an environmental and economic point of view. Heterogeneous catalysts offer an answer to this need, allowing catalyst reuse and giving access to high-throughput techniques and continuous flow reactors. However, when compared to homogeneous systems, heterogeneous catalysts often display poorer reactivity. Moreover, they often suffer from diffusion limitations, that is, difficult transport of reactants to the active sites, or back-diffusion of the generated products.

An ideal catalyst would be one that combines the advantages of homogeneous and heterogeneous systems, being: high activity, easy separation, recyclability and zero contamination of reaction products. To achieve this goal much research efforts have gone into the immobilization of highly active homogeneous catalysts to various supports, such as organic polymers, monoliths and silica materials.

Although organic polymers are often used as supports for olefin metathesis catalysts, they typically suffer from a number of disadvantages including diffusion-related problems or the requirement for the addition of solvents for precipitation of the soluble carrier. Inorganic materials, such as silica, reveal many advantages when compared to organic polymer support materials, being: high chemical, thermal and mechanical stability, no swelling properties, easy separation and the ability to develop tailor-made particles with high surface areas and large pore systems.

Although to this date PMOs have never been implemented as supports for olefin metathesis catalysts, their easily tailorable chemical, physical and structural properties make them ideal candidates in the development of hybrid catalysts for olefin metathesis.

8.5.2 Ethene-PMOs with anchor points for olefin metathesis catalysts

With the aim of designing a novel class of hybrid olefin metathesis catalysts an ethene-PMO which consists of styrene functionalities was developed by means of a co-condensation reaction between 1,2-bis(triethoxysilyl)ethene (*E*-BTSE) and styrylethyltrimethoxysilane (SETS), using Pluronic P123 as a SDA. Figure 8.24 gives a schematic illustration of the resulting styrene-ethene bifunctional PMO.

To establish whether the styrene functions were successfully incorporated in the PMO structure, a FT-Raman investigation was performed. In Figure 8.25 the FT-Raman spectrum of the bifunctional styrene-ethene-PMO is represented. For reference purpose, the spectra of a typical ethene-PMO and of a pure styrylethylsilica material are also given.

Besides the typical Raman frequencies of the ethenylene bridges (2957, 1574 and 1302 cm⁻¹), the FT-Raman spectrum of the bifunctional styrene-ethene-PMO, exhibits additional well-resolved peaks at 3059, 2880, 1632, 1605, 1406 and 1000 cm⁻¹. These peaks, when compared to the spectrum of pure styrylethylsilica, clearly can be assigned to the styrene functionalities, indicating the successful incorporation of these groups in the PMO matrix. The peaks at 3059 and 2880 cm⁻¹ can be as-

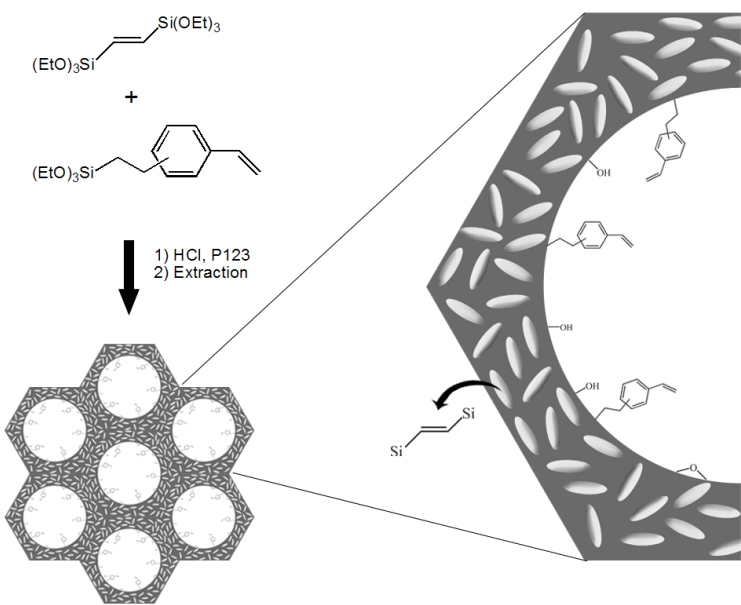


Figure 8.24: Schematic illustration of a styrene-ethene bifunctional PMO.

cribed to the C–H stretch vibration of the aromatic and ethyl groups, respectively. The peaks at 1632 and 1605 cm^{−1} can be attributed to the C=C stretch and the aromatic ring stretch of the styrene groups, respectively. The peak at 1406 cm^{−1} can be assigned to the =CH₂ deformation of the styrene functionalities, while the peak at 1000 cm^{−1} can be ascribed to the aromatic ring “breathing” vibrations of these groups.

Though the incorporation of the styrene functionalities in the ethene-PMO matrix can be confirmed by the represented FT-Raman data, it is important to verify whether this material has decent structural properties, in particular because this often is not the case when co-condensation procedures are employed. In Figure 8.26 the nitrogen isotherms and BJH pore size distribution of the bifunctional styrene-ethene-PMO are given. The isotherms are of type IV and display sharp capillary condensation and evaporation steps, indicating very uniform mesopores. This is confirmed by the narrow pore size distribution represented in Figure 8.26B. Furthermore with a BET surface area of 730 m²/g and total a total pore volume of 0.752 cm³/g, this bifunctional PMO material can be considered as a good support for olefin metathesis catalysts.

8.5.3 Styrene-ethene PMOs as supports for olefin metathesis catalysts: prospect

Having styrene functionalities embedded in the framework, the described bifunctional styrene-ethene-PMO can be easily transformed into a hybrid olefin metathesis

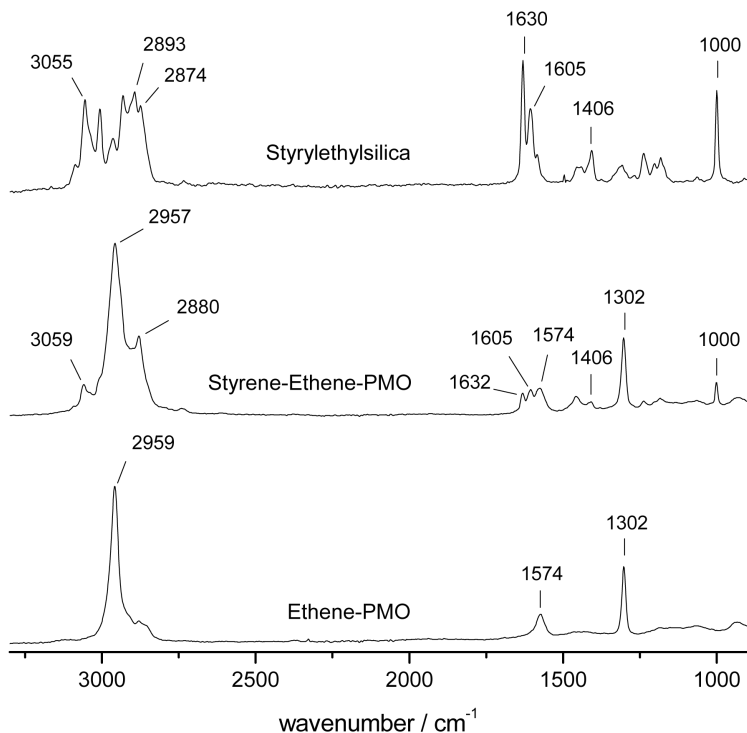


Figure 8.25: FT-Raman spectra of a bifunctional styrene-ethene-PMO, a typical ethene-PMO and of a pure styrylethylsilica material.

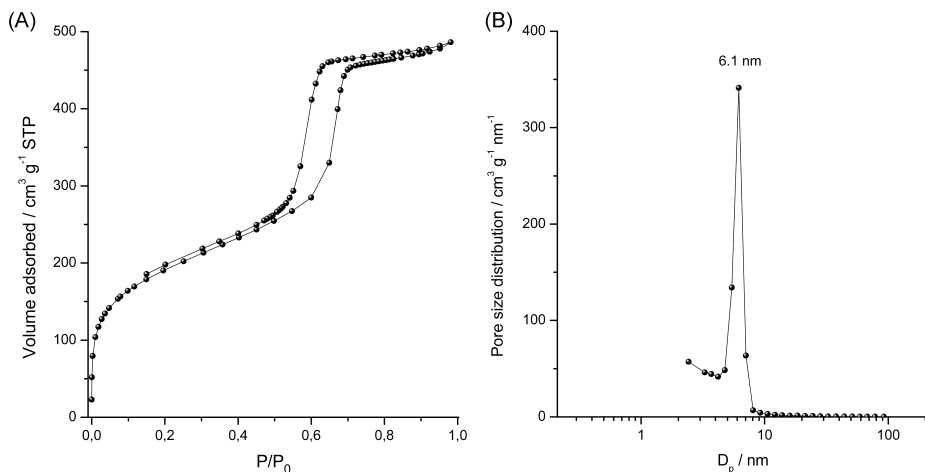


Figure 8.26: (A) N_2 -physisorption and (B) BJH pore size distributions of a bifunctional styrene-ethene-PMO.

sis catalyst *via* a single-step modification procedure. Herein, a small amount of an active homogeneous ruthenium carbene catalyst is mixed with the bifunctional PMO material, preferably under an argon atmosphere. *Via* a olefin metathesis reaction, illustrated in Figure 8.27 the homogeneous catalyst is immobilized onto the PMO surface, rendering a hybrid olefin metathesis catalyst. The main benefit of adapting such a synthesis procedure is that any type of ruthenium carbene catalyst can be linked to the PMO support, giving easy access to a large family of easily recyclable and active olefin metathesis catalysts.

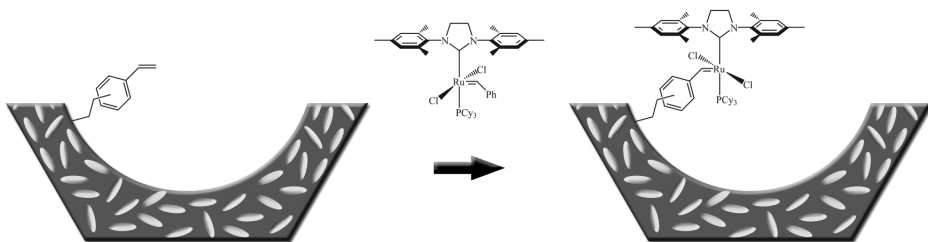


Figure 8.27: Schematic representation, illustrating the immobilization of a ruthenium carbene catalyst to a bifunctional styrene-ethene-PMO.

Important to mention is that these type of olefin metathesis catalysts, that are immobilized *via* the alkylidene moiety, detach from the surface during the olefin metathesis reaction. Thus, during the catalytic cycle the catalysts are in fact homogeneous. When the reaction is finished, ideally the catalyst returns and reattaches to the surface. This catalytic feature has provided these systems with the name “boomerang catalyst”. Clearly the advantage of such a system, being in the homogeneous state during reaction, is its potentially high activity. However, as in most cases, activity goes hand in hand with stability; if the catalyst does not reattach before decomposing, these systems may suffer some leaching.

An alternative approach is to immobilize a metathesis catalyst *via* the NHC ligand to the PMO surface, as illustrated in Figure 8.28. This type of catalyst is permanently immobilized to the surface, and is less likely to leach. A first attempt to synthesize such a system has been made, however, coordination of the NHC ligand to the Grubbs first generation complex was quite problematic and is therefore not discussed in this dissertation.

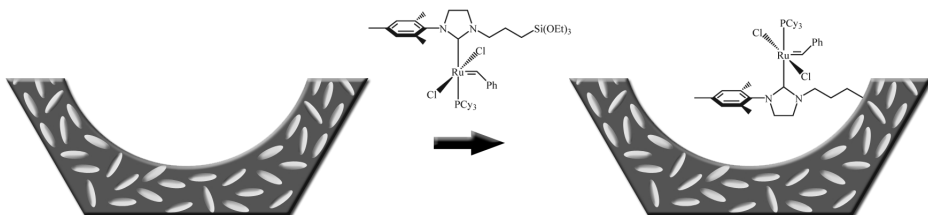


Figure 8.28: Schematic representation, illustrating the immobilization of a ruthenium carbene catalyst to the PMO surface *via* the NHC ligand.

8.6 Conclusions on expanding the scope of olefinic PMOs

The intention of the research work presented in this chapter was to expand the scope of olefinic PMOs by introducing novel synthesis strategies.

A first aim was to develop a completely new olefinic PMO material. We have shown that 1,4-bis(trimethoxysilyl)butene, the synthesis of which is described in chapter 3, can be successfully employed for the synthesis of diastereoisomeric butenylene-bridged hybrid materials. Especially interesting is that the described material reveals ultra-large mesopores without requiring the addition of any swelling agents. Furthermore, the hysteresis loop in the nitrogen physisorption isotherms of the butenylene-bridged hybrid material is different from the ultra-large pore ethenylene-bridged PMOs. The narrow loop indicates cylindrical or slitlike mesopores which are open at both ends. Although these materials are potentially interesting for catalytic or chromatographic applications, particularly having spherical morphologies, more research is required to understand the mesostructure self-assembly process, to optimize the synthesis procedure and control the material properties. Due to the large and flexible organic group, the development of pure butenylene-bridged PMOs with well-ordered mesopores will be a big challenge, but will introduce a new class of olefinic PMOs.

A second challenge was to open the way to the development of ethenylene-bridged PMOs with different pore structures and “crystalline” pore walls, through employing a gemini surfactant as template under basic conditions. Although materials with relatively high surface areas and pore volumes could be attained through optimization of several reaction parameters, the synthesis of ethene-PMOs with well-ordered pore structures and large pores proved to be difficult, and requires more research work.

A nice achievement was the synthesis of an ethenylene-bridged PMO which revealed molecular ordering in the pore walls. Furthermore, ^1H - ^{29}Si CP/MAS NMR disclosed a relatively low $(T^1+T^2)/T^3$ ratio, indicating that the pore walls have a high degree of framework condensation. These two important aspects are related to the basic conditions under which the PMOs were synthesized, which allow both for a controlled framework structure formation and an enhanced cross-linking of the siliceous species.

A third objective was to illustrate the potential of ethenylene-bridged PMOs in catalytic applications. With this intent in mind, sulfonic acid PMOs were successfully synthesized *via* a one-step modification procedure involving homemade diastereoisomeric ethene-PMOs and chlorosulfonic acid. By means of this procedure, PMOs consisting of *ca.* 1 mmol H⁺/g were prepared. *Via* nitrogen physisorption, it was established that the sulfonation reaction has no significant influence on the mesostructure, even a small increase in surface area was observed. This synthesis procedure enables development of acidic PMOs with controllable properties which can be used in acid catalyzed reactions.

The sulfonic acid ethene-PMOs prepared according to this method reveal a high activity in the model esterification reaction of acetic acid with *n*-propanol. Moreover, their activity is comparable to that of the homogeneous acid catalyst *p*-toluenesulfonic acid. We found though that the reaction temperature should not

be too high, in order to avoid deterioration of the PMO framework. When the reaction is performed at 90 °C, the PMO structure remains intact during the esterification reaction and reveals no significant decrease in surface area. A sulfonic acid ultra-large pore ethene-PMO, with mesopores of 21 nm, was also put to the test in the same model reaction. This catalyst displayed a high TON, though the number of catalytic sites was rather low (0.42 mmol H⁺/g). The latter brings us to an important challenge: increasing the amount of acid sites in the PMO framework. More research is required to achieve this goal. A possible synthesis strategy is to sulfonate the PMO precursor 1,2-bis(triethoxysilyl)ethene (preferentially in the gas phase) and use this novel precursor for the synthesis of sulfonic acid PMOs. However, as the sulfonic acid groups will effect the self-assembly process, the synthesis conditions will have to be reevaluated and optimized.

An important drawback of the described acid PMOs is the need to reactivate them when performing multiple successive reactions. This is also a matter which has to be thoroughly investigated.

A last objective was to develop an ethenylene-bridged PMO material which consists of anchor points to immobilize olefin metathesis catalysts. This was achieved through co-condensation of *E*-BTSE with SETS. The successful incorporation of styrene entities in the PMO framework was confirmed by FT-Raman spectroscopy. These novel bifunctional styrene-ethene-PMOs can be easily transformed into hybrid olefin metathesis catalysts *via* a single-step modification procedure, involving a metathesis reaction with a homogeneous ruthenium carbene complex. The synthesis of permanently immobilized metathesis catalysts onto PMO materials is also an interesting, but challenging approach.

Chapter 9

General Conclusions and Outlook

9.1 Conclusions

The work represented in this dissertation addresses the research and development of olefinic periodic mesoporous organosilicas and their application in catalysis. The main goal was to develop a novel class of versatile olefinic PMOs, which consist of diastereoisomerically configured organic bridges in their pore walls. To date, only limited research had been done on these very promising type of organic-inorganic hybrid materials and their potential in various applications had not been explored yet. Moreover, ethenylene-bridged PMOs, synthesized from diastereoisomeric mixtures of 1,2-bis(triethoxysilyl)ethene, were the only olefinic PMOs which had been reported upon so far. Being one of the most interesting hybrid materials in terms of modifiability and applicability, there was a need to investigate both the potential of ethenylene-bridged PMOs and the possibility of developing novel olefinic hybrid materials.

The initial goal of developing diastereoisomeric ethenylene-bridged PMO precursors has been realized *via* the self-metathesis of vinyltriethoxsilane. Use of the commercially available first generation Grubbs catalyst rendered the ($\approx 100\ %$) pure *E*-diastereoisomer of 1,2-bis(triethoxysilyl)ethene (*E*-BTSE) with a TON of 3167, which is a great improvement when compared to the commonly used synthesis procedure, involving the catalyst $(PPh_3)_3RuCl_2$, which produces a diastereoisomeric mixture ($\approx 80\ %$ *E*-isomer) with a TON of 670.

Furthermore, we have established that the catalyzed self-metathesis of vinyltriethoxsilane is thermodynamically controlled, making it difficult to produce precursors with high *Z/E* ratios. Nevertheless, the ($\approx 100\ %$) pure *Z*-isomer of 1,2-bis(triethoxysilyl)ethene (*Z*-BTSE) has been successfully prepared for the first time by carefully performing multiple successive vacuum distillations of a diastereoisomeric mixture containing 20 % of the desired *Z*-isomer.

By employing home-made isomeric PMO precursors, PMOs which display dia-

stereoisomeric pure *E*- and *Z*-configured ethylene-bridges in the pore walls have been synthesized for the very first time. We have shown that both diastereoisomers of 1,2-bis(triethoxysilyl)ethene have totally different reactivities, and that this has to be taken into account when using diastereoisomeric mixtures for the synthesis of ethylene-bridged PMOs. The use of the pure *E*-isomer of 1,2-bis(triethoxysilyl)ethene, as supposed to diastereoisomeric mixtures thereof, for the synthesis of ethylene-bridged PMOs, enhances the structural ordering, the pore size uniformity and the hydrothermal stability. We have also illustrated that in order to develop *Z*-configured ethylene-bridged PMOs, the pH of the reaction mixture has to be lowered considerably when compared to that required for the synthesis of *E*-configured ethylene-bridged PMOs.

Using advanced solid state NMR techniques, the template-framework interactions of these highly ordered PMO materials have been elucidated. The PEO blocks of the surfactant template strongly interact with the hybrid pore walls whereas, the PEO blocks are mobile in the pores. The template-precursor interactions ensure mesostructure formation and enable the synthesis of ethylene-bridged PMOs with remarkable properties. However, to obtain high quality materials, it is important that the rates of hydrolysis and condensation of the precursor are correctly adjusted to the rate of the self-assembly process. Because the described synthesis procedures are optimized for *E*-BTSE, *E*-configured ethylene-bridged PMOs have superior properties to PMOs synthesized from diastereoisomeric mixtures. Herein, the presence of the *Z*-isomer disturbs the self-assembly which results in an inferior structural ordering and pore size uniformity. When *Z*-BTSE is used as a PMO precursor, adjusting the rates of hydrolysis and condensation by lowering the pH of the reaction mixture, enhances the template/*Z*-BTSE interaction and favors the formation of well-ordered materials with uniform pores.

Other than the synthesis of isomeric ethylene-bridged PMOs with good structural properties, another aim of this research work was to develop synthesis strategies which enable control of the PMO properties. Therefore, in an initial stage, an attempt was made to help understand the mesostructure formation process involved in ethene-PMO synthesis. As stated above, the rates of hydrolysis and condensation are important parameters in PMO structure formation. By varying the pH of the synthesis mixture, ethene-PMOs with various pore structures, consisting of open cylindrical, blocked and a mixture of open and blocked mesopores, could be attained. By means of nitrogen gas physisorption, NLDFT, SAXS, TEM and electron-tomography the detailed structures of these complex PMO materials have been determined.

We have shown that interpretation of nitrogen physisorption data is not always easy and can lead to faulty conclusions if not evaluated alongside SAXS, TEM or even ET data. We have found that two-step desorption isotherms do not necessarily imply the presence of microporous nanocapsules in the mesopores or pores with ink-bottle necks. The second step in the desorption isotherms of these isomeric PMOs have been attributed to the filling of the mesopores with solid material and to the shortening of the pore channels (pore confinement). By varying the pH of the reaction mixture, the amount of confined pores can be accurately controlled. For the PMOs with both open and blocked mesopores, a fraction of the hexagonally

packed cylinders terminate inside the mesostructure, thus forming short pore channels, as evidenced by ET. This phenomenon causes confinement of the adsorbed nitrogen. As only a fraction of the pores are blocked, the confinement of nitrogen is only partial and hence a two-step desorption isotherm is obtained. Consequently, the hysteresis of such a PMO is a combination of a H1 and a H2 type hysteresis. As the fraction of blocked pores versus open pores gradually increases with decreasing pH, the amount of confined nitrogen which desorbs at relatively low pressures increases, and the hysteresis gradually converts into a H2 type hysteresis. At very low pH values a 3D hexagonally ordered mesostructure consisting mainly of globular pores is found. These globular pores can be considered as confined cavities which are interconnected with each other by smaller passages (< 4 nm). The H2 type hysteresis of such a material is related to the absence of open cylindrical pores, to the confinement of the globular mesopores and to the filling of some of the mesopores with solid material, as evidenced by ET.

The effect of the synthesis pH on the pore structures of these PMOs has been related to an alteration in the hydrophobic/hydrophilic volume ratio of the surfactant template. That is, the pH influences the interfacial curvature of the mesophase by altering the ionization of the ethylene oxide chains of the triblock copolymer. We have also shown that when *n*-butanol is added to the reaction mixture, the generation of globular pores is circumvented and cylindrical pores are preferentially formed. The dehydratation of the ethylene oxide chains in the micelle corona, is considered as the driving force for this sphere-to-rod transition.

These insights in ethene-PMO synthesis have helped in understanding the processes involved in mesostructure formation and have allowed for the synthesis of materials with controllable properties. When considering porosity properties of ethene-PMOs, knowledge of the relation between synthesis pH and PMO structure is an important tool in establishing the optimum acidity of a synthesis mixture. We have found that at very low pH-values, the excessive polycondensation of the precursor relative to the self-assembly process, produces materials with lower surface areas and pore volumes due to the filling of mesopores with solid material. On the other hand, increasing the pH beyond the optimum, reduces the double-layer hydrogen-bonding interaction between the nonionic surfactant and the PMO-precursor, whereby the long-range hexagonal packing decreases. When *n*-butanol is used as a cosolvent, the filling of mesopores with solid material is prevented, even at very low pH values. As a result the optimum pH is much lower than the synthesis without *n*-butanol.

Besides pH, we have also illustrated that the PMO synthesis temperature gives a means to control the pore size, structure, connectivity and volume. By increasing the synthesis temperature larger mesopores can be attained through withdrawal of the PEO blocks of the surfactant template in the micelle core. However, we found that the pore diameter is only flexible to a certain extent, after which further temperature increasement has no effect on the pore size. This phenomenon can also be attributed to the gathering of PEO blocks which protrude from micelle surface and generate secondary mesopores that form connections between the primary mesopores. Thus, fine-tuning the synthesis temperature gives perfect control of the meso- and micropore volume and the connectivity of the mesopores.

An other important feature of porous materials, of which control is highly desirable,

is morphology. By using different cosolvents and varying their concentration, the morphology of ethene-PMOs has been accurately controlled to consist of crystal-like disk shaped, fibrous or spherical particles. Control of the particle morphology is a powerful tool in designing materials for particular applications. For instance for chromatographic applications, spherical particles are required for efficient column packing and good separation properties, while for catalysis applications, hexagonal crystal-like disks with short pore channels may be of interest by potentially limiting diffusion problems.

During the investigation of the thermal properties of ethenylene-bridged PMOs an additional appealing feature was discovered. When thermally treated under vacuum, a transformation in the pore walls of ethenylene-bridged PMOs occurs, whereby bridging ethene groups are converted to dangling vinyl groups. This peculiar intermolecular reaction was subject of close examination by means of DRIFT, FT-Raman and solid-state NMR spectroscopy. The spectroscopic data clearly reveals the occurrence of thermally induced vinylic groups. A mechanism has been proposed wherein terminal vinyl groups and siloxane bridges are generated *via* proton transfer from silanol groups to ethenylene bridging groups. This mechanism has been indirectly confirmed by hydrophobizing the PMO surface with hexamethyldisilazane prior to the thermal treatment. Once the silanol groups in ethene-PMOs are removed, no thermally induced generation of vinylic groups occurs, which proves that the silanol groups participate in the intramolecular reaction leading to PMO metamorphosis. This easy and straightforward approach allows the formation of multifunctional hybrid materials consisting of direct anchoring points for catalysts.

An other important goal of this research work was to develop materials which can be used in catalysis and environmental technology. The applicability of PMOs, and nanoporous materials in general, is however often limited by their pore sizes, which typically range between 2 and 8 nm. In some applications, such as in biocatalysis, larger mesopores are required to allow the diffusion, adsorption or immobilization of large biomolecules such as enzymes. To date, the synthesis of ethenylene-bridged PMOs with mesopores larger than 10 nm has not been reported, so with this goal in mind, we have probed the possibility of producing ethene-PMOs with ultra-large mesopores.

Synthesis strategies have been successfully developed to fine-tune the pore size and volume of ethenylene-bridged PMOs. By using swelling agents, such as TMB, *p*-cymene, *p*-xylene, *tert*-butylbenzene and hexane, in combination with Pluronic P123 as a surfactant template, PMOs with ultra-large mesopores (up to 28.3 nm) and astonishing pore volumes (up to 2.25 cm³/g) have been synthesized for the first time. Moreover, these PMOs reveal surprisingly narrow pore size distributions, high surface areas and relatively high micropore volumes. Despite having such large mesopores, these ethenylene-bridged PMOs are also very stable. With a shelf-life exceeding one year, these ultra-large pore PMOs can be stored under ambient conditions without suffering from deterioration.

Besides having an impact on the pore size and volume, the addition of swelling agents also effects the mesostructure. The ultra-large pore PMOs reveal various pore systems, including foam-like pore structures with uniformly sized mesopores, 3D stacked spherical pores and nodular strings, i.e. cylinders built from linearly

connected spheres. The phase transition induced by the swelling agents is caused by an alteration in the interfacial curvature of the surfactant micelles. By influencing the hydrophilic-hydrophobic volume ratio of the surfactant, the hydrophobic swellers cause the rod-like surfactant-organosilica composite micelles to transform into spherical micelles, leading to the formation of spherical pores.

A novel and straightforward method to obtain ethylene-bridged PMOs with bimodal pore size distributions has also been developed. By carefully adjusting the synthesis conditions, PMOs consisting of interconnected pore systems with different diameters can be synthesized, which opens up the road to novel hierarchically ordered hybrid materials. That is, materials with several different degrees of porosity incorporated into one composite material.

These types of hybrid materials with unprecedented pore sizes may be interesting in applications requiring large pore volumes such as in catalysis, environmental technology and nanoelectronics. The easily modifiable ethylene-bridges give a means to immobilize catalysts or heavy metal scavengers *via* the organic carbon bond as supposed to the commonly used and less stable siloxane bond. Ultra-large pore PMOs are especially interesting for applications involving large biomolecules, such as in biocatalysis or controlled drug release. Hierarchically ordered PMOs, such as the described bimodal systems which comprise of micropores, medium sized and ultra-large mesopores, are also very appealing for bulk-chemistry applications in which reactant molecules need to readily access the interior pore structure while the internal surface area is maximized. For such applications, a ramified pore structure with large pores leading to smaller and smaller pores is desired.

A last but important goal in this dissertation was to expand the scope of olefinic PMOs by producing novel synthesis strategies. To achieve this goal several topics, related to olefinic PMOs have been investigated.

A first aim was to develop a completely new olefinic PMO material. To realize this, a new precursor had to be prepared. With the intention of extending the scope of olefin metathesis in the development of the novel PMO precursor 1,4-bis(trimethoxysilyl)butene, several catalysts were initially screened for the self-metathesis of allyltrimethoxysilane. However, the synthesis of 1,4-bis(trimethoxysilyl)butene proved to be somewhat more complicated than that of 1,2-bis(triethoxysilyl)ethene. Unlike the self-metathesis reaction of vinyltriethoxysilane, the metathesis of allyltrimethoxysilane can be accompanied by an isomerization reaction, i.e. migration of the double bond along the alkyl chain by 1,3-H shifts. All tested commercial catalysts which revealed good activity in the metathesis of allyltrimethoxysilane also produced isomerization products. Therefore, alternative catalysts were investigated. Latent Schiff base containing catalysts, required from the University of Ghent spin-off ViaCatt, revealed very good activity in the metathesis of allyltrimethoxysilane, when activated with phenyltrichlorosilane. Moreover, no isomerization products were produced with these complexes. However, GC-analysis of the reaction products revealed some impurities which could not be ascribed. More importantly, in all cases, diastereoisomeric mixtures were obtained. Based on a previous synthesis procedure reported by researchers of our group, a second generation Hoveyda type catalyst bearing a chiral ligand was synthesized and successfully implemented in the synthesis of a diastereoisomeric butenylene-bridged

PMO precursor. This chiral catalyst revealed a relatively high TON of 780 and produced no isomerization products. Moreover, the ($\approx 100\%$) pure *E*-isomer of 1,4-bis(trimethoxysilyl)butene could be attained, as evidenced by GC analysis. These results show that olefin metathesis is a powerful tool which can be exploited in the synthesis of novel olefinic PMO precursors.

We have also shown that 1,4-bis(trimethoxysilyl)butene, can be successfully employed for the synthesis of diastereoisomeric butenylene-bridged hybrid materials. Especially interesting is that the described material reveals ultra-large mesopores without requiring the addition of any swelling agents. Furthermore, the hysteresis loop in the nitrogen physisorption isotherms of the butenylene-bridged hybrid material is different from the ultra-large pore ethenylene-bridged PMOs. The narrow loop indicates cylindrical or slitlike mesopores which are open at both ends.

A second challenge was to open the way to the development of ethenylene-bridged PMOs with different pore structures and “crystalline” pore walls. This objective was partially reached through employing a gemini surfactant as template under basic conditions. Although materials with relatively high surface areas and pore volumes have been attained through optimization of several reaction parameters, the synthesis of ethene-PMOs with well-ordered pore structures and large pores has proved to be difficult. A nice achievement is the synthesis of an ethenylene-bridged PMO which reveals molecular ordering in the pore walls. Furthermore, ^1H - ^{29}Si CP/MAS NMR discloses a relatively low $(T^1+T^2)/T^3$ ratio, indicating that the pore walls have a high degree of framework condensation. These two important aspects are related to the basic conditions under which the PMOs have been synthesized, which allow both for a controlled framework structure formation and an enhanced cross-linking of the siliceous species.

A third objective was to illustrate the potential of ethenylene-bridged PMOs in catalytic applications. With this intent in mind, sulfonic acid PMOs have been successfully synthesized *via* a one-step modification procedure involving homemade diastereoisomeric ethene-PMOs and chlorosulfonic acid. By means of this procedure, PMOs consisting of *ca.* 1 mmol H⁺/g could be prepared. *Via* nitrogen physisorption, it has been established that the sulfonation reaction has no significant influence on the mesostructure. This synthesis procedure enables development of acidic PMOs with controllable properties which can be used in acid catalyzed reactions. The sulfonic acid ethene-PMOs prepared according to this method reveal a high activity in the model esterification reaction of acetic acid with *n*-propanol. Moreover, their activity is comparable to that of the homogeneous acid catalyst *p*-toluenesulfonic acid. We found though that the reaction temperature should not be too high, in order to avoid deterioration of the PMO framework. When the reaction is performed at 90 °C, the PMO structure remains intact during the esterification reaction and reveals no significant decrease in surface area. A sulfonic acid ultra-large pore ethene-PMO, with mesopores of 21 nm, has also been put to the test in the same model reaction. This catalyst displayed a high TON, though the number of catalytic sites was rather low (0.42 mmol H⁺/g). An important downfall of the described acid PMOs is the need to reactivate them when performing multiple successive reactions. This is a matter which has to be thoroughly investigated.

A last objective was to develop an ethenylene-bridged PMO material which con-

sists of anchor points to immobilize olefin metathesis catalysts. This was achieved through co-condensation of *E*-BTSE with styrylethyltrimethoxysilane. The successful incorporation of styrene entities in the PMO framework has been confirmed by FT-Raman spectroscopy. These novel bifunctional styrene-ethene-PMOs can be easily transformed into hybrid olefin metathesis catalysts *via* a single-step modification procedure, involving a metathesis reaction with a homogeneous ruthenium carbene complex.

Summarized, the presented synthesis strategies have made it possible to both expand the family and potential of olefinic PMOs by introducing a novel butenylene-bridged PMO, and by illustrating the versatility of olifinic PMOs. They are easily modifiable by means of olefin chemistry and can lead to readily applicable catalysts for various reactions.

In general olefinic PMOs, and especially those with isomerically configured bridges in their pore walls, are an emerging class of versatile hybrid materials which can be implemented in various research fields and applications, going from catalysis to chromatography to environmental technology. Combining knowledge from different research areas such as organometallics and materials chemistry can lead to new insights and help design and create novel materials. Furthermore, a good understanding of the processes involved in mesostructure formation enables control of material properties, opening the road to new developments and applications.

9.2 Outlook

The research and developments described in this dissertation not only illustrate the potential of olifinic PMOs, but also emphasize that there is still much room for future developments. Especially, in terms of application.

The described sulfonic acid PMOs should be further investigated. Herein, increasing the amount of acid sites in the PMO framework is an important issue which should be addressed. A possible synthesis strategy is to sulfonate the PMO precursor 1,2-bis(triethoxysilyl)ethene (preferentially in the gas phase) and use this novel precursor for the synthesis of sulfonic acid PMOs. However, as the sulfonic acid groups will effect the self-assembly process, the synthesis conditions will have to be reevaluated and optimized.

In the context of developing new acid PMOs, an other interesting topic may be the development of super acids consisting both of sulfonic acid sites as aluminum lewis acid sites. Such materials may be potentially applied in various acid catalyzed reactions such as Friedel-Crafts alkylation, esterification, transesterification, Fries rearrangement,...

Other than acid catalyzed reactions, olefinic PMOs can be applied in other reactions such as carbon-carbon coupling reactions. The described styrene-ethene-PMO can be easily transformed into hybrid olefin metathesis catalysts *via* a single-step modification procedure, involving a metathesis reaction with homogeneous ruthenium carbene complexes. A very appealing investigation can be the immobilization of various metathesis catalysts onto these bifunctional PMOs and establish the effect

of both catalyst environment as PMO structural properties on olefin metathesis activity.

An other topic is the utilization of the bridging olefinic groups in PMOs to immobilize both catalysts as heavy metal scavengers. We have already demonstrated that ethene-PMOs can be further modified through olefin chemistry. Ethene-PMOs react readily with bromine, allowing about bromination of the CH=CH organic groups. The fast reactivity of these PMOs with bromine indicates that the surface functionalities are easily accessible through the uniform and open pore structures, even though bromine is quite a bulky molecule. The highly accessible surface groups of ethene-PMOs make these porous architectures very appealing and potentially interesting for various applications, such as catalysis and environmental technology.

Although this dissertation describes the synthesis of the novel butenylene-bridged PMO, much research is still required to understand the mesostructure self-assembly process, to optimize the synthesis procedure and control the material properties. Due to the large and flexible organic group, the development of pure butenylene-bridged PMOs with well-ordered mesopores will be a big challenge, but will introduce a new class of olefinic PMOs. Furthermore, having spherical morphologies, these materials can be tested in chromatographic applications. The same goes for the ethenylene-bridged PMOs with spherical morphologies. Moreover, the influence of the organic bridging groups in the PMO pore walls on the separation properties of these materials can be investigated.

Most of the described research deals with PMOs synthesized with the surfactant Pluronic P123. Novel PMO structures can be prepared through implementation of different templates. Also the synthesis of olefinic PMOs under basic conditions can be further investigation. In particular the synthesis of PMOs with crystalline pore walls is an appealing subject.

Chapter 10

Experimental

10.1 General information

10.1.1 Chemical compounds and synthesis

Products that were commercially purchased from Aldrich and ABCR, were used as received. All solvents and cosolvents were purchased from Fiers. Vinyltrimethoxysilane, tetraethyl orthosilicate, tetrachlorosilane, trichlorosilane, ethyltrichlorosilane, phenyltrichlorosilane, Grubbs' 1st generation (catalyst **3**) and Hoveyda-Grubbs' 1st and 2nd generation (catalysts **5** and **6**), RuCl₂(PPh₃)₃ (catalyst **1**), Pluronic P123, bromine, ethyl chlorooxoacetate, 2,6-diisopropylaniline, (-)-isopinocampheylamine, borane tetrahydrofuran complex, triethyl orthoformate, triethylamine, 1,3,5-trimethylbenzene, *p*-cymene, *p*-xylene, *tert*-butylbenzene, hexadecane, chlorosulfonic acid, 1,12-dibromododecane, N,N-dimethylhexadecylamine were purchased from Sigma-Aldrich. Allyltrimethoxysilane and styrylethyltrimethoxysilane were obtained from ABCR.

[Ru(*p*-cymene)Cl₂]₂ (Catalyst **2**)⁴⁸³ Grubbs' 2nd and 3rd generation (catalysts **4**⁴⁰⁶ and **7**⁴²⁴) and catalyst **12**⁴²³ were prepared according to known literature procedures. The indenylidene catalysts **8**, **9**, **10** and **11** were generously provided by the university of Ghent spin-off ViaCatt.

All synthetic procedures involving organometallic compounds were performed in oven-dried glassware under argon atmosphere using standard Schlenk techniques. The following solvents were distilled and dried under argon according to standard procedures: tetrahydrofuran (sodium, benzophenone), toluene (sodium) and dichloromethane (calcium hydride). All other solvents were used as received.

10.1.2 Characterization techniques and procedures

Nitrogen gas physisorption

Nitrogen gas physisorption experiments were conducted at 77 K using a Belsorp-mini II gas analyzer. Samples were vacuum dried overnight at 120 °C prior to analysis. The specific surface area (S) was determined from the linear part of the BET plot ($P/P_0 = 0.05\text{--}0.15$). The total pore volume (V_t) was determined from

the amount of nitrogen adsorbed at $P/P_0 = 0.98$. The pore size distribution was calculated using either NLDFT⁴⁸⁴ or the BJH method. The micropore volume (V_μ) was calculated using the *t*-plot method. The pore wall thickness (t_w) was estimated using the equation $t_w = (a_0 - D_p)$, where a_0 and D_p are the unit cell dimension and pore size, respectively. NLDFT calculations were made by prof. Alex Neimark at Rutgers, the state university of New Jersey, department of chemical and biochemical engineering.

TEM, ET and SEM

TEM and ET measurements were performed by Fridrich Heiner, Petra de Jongh and Johannes Meeldijk at the university of Utrecht, department of inorganic chemistry and catalysis (group of prof. dr. Krijn de Jong). TEM measurements of the PMOs synthesized with gemini surfactants were performed by Veerle Cloet at the university of Ghent. TEM and ET samples were prepared by grinding the dry powder in a mortar; subsequently dispersing a portion of the material in ethanol using ultra-sonication for 60 s; after which a few droplets of the suspension were placed on a Quantifoil R2/1 lacey carbon support film; followed by drying under a lamp. Alternatively, ET samples were prepared by applying the dry powder directly to the TEM grid. The carbon support film for ET experiments had 5 or 10 nm gold colloids attached to it, which aid in the alignment of the dataset with respect to a common origin and rotation axis. TEM images and ET image series were acquired in bright-field mode using a Tecnai 20 electron microscope (FEI Company). The microscope, operated at 200 keV, was equipped with a LaB6 electron source, a Twin objective lens, and a 2k × 2k Tietz CCD Camera (TVIPS, Gauting). Acquisition of single-axis tilt-series was performed in Xplore3D (FEI company) over an angular range of *ca.* 70° at 2° increments. Alignment, reconstruction, and denoising were carried out in IMOD.⁴⁸⁵ Reconstructions were denoised by nonlinear anisotropic diffusion.⁴⁸⁶ Segmentation was done in IMOD or Amira 3.1 (Mercury Computer Systems, Inc.).

Scanning electron microscopy (SEM) images were collected on a Quanta 200 FEG instrument from FEI.

SAXS and XRD

Small-angle X-ray scattering (SAXS) experiments were carried out at the Dutch-Belgian Beamline (DUBBLE, BM26-B) of the European Synchrotron Radiation Facility (ESRF, Grenoble) by Bart Goderis from the catholic university of Leuven.⁴⁸⁷ Data were collected during 60 s using an X-ray wavelength, $\lambda = 0.775 \text{ \AA}$, on a two-dimensional position sensitive gas-filled wire chamber detector at 4 m from the sample. The covered scattering vector range $0.0027 < s < 0.04 \text{ \AA}^{-1}$ was calibrated with a Silver Behenate specimen ($s = 2\sin\theta/\lambda$, where 2θ is the scattering angle).⁴⁸⁸ The isotropic data were corrected for the detector response, azimuthally integrated and normalized to the intensity of the primary beam, measured by an ionization chamber placed downstream from the sample. The background scattering due to the experimental setup and the sample holder was subtracted according to standard procedures, taking into account transmission differences. Hermetic aluminum DSC pans (TA instruments) were used as sample holders. X-ray powder

diffraction patterns were collected on a Siemens D5000 Diffractometer with Cu K α radiation with 0.15418 nm wavelength.

FT-Raman and DRIFT

FT-Raman spectra were acquired on an Equinox 55S hybrid FT-IR/FT-Raman spectrometer with a Raman module FRA 106 from Bruker. The spectrometer is fitted with a N₂-cooled germanium high sensitivity detector D418-T and a N₂-cooled MCT-B detector. The Raman laser wavelength is the 1064 nm line of an air cooled diode pumped neodymium yttrium aluminium garnet laser (Nd:YAG). The laser power was manually set to 300 mW. DRIFT spectra were acquired on the same instrument using a sealed and thermally controlled in-situ DRIFT cell.

Solution and solid-state NMR

The ¹H and ¹³C solution NMR spectra were collected on a Varian Unity 300 MHz spectrometer equipped with a 300AutoSW probe (4NUC/30-122 MHz). Standard parameters for ¹H NMR: frequency = 299.87 MHz, number of scans = 64. Standard parameters for ¹³C NMR: frequency = 75.41 MHz, number of scans: 4096. GC analysis was conducted on a Finnigan Trace GC ultra GC equipped with a standard FID detector. A wall coated open tubular column with a length of 10 m, an internal diameter of 0.10 mm and a coating of 0.40 μ m (5 % diphenyl and 95 % dimethyl polysiloxane) was used. Helium was used as carrier gas at a flow rate of 0.5 ml/min. The inlet temperature was 250 °C and the split flow was 150 ml/min. The temperature was kept at 40 °C for one minute after which it was raised at 200 °C/min to 250 °C and kept at this temperature for one minute.

Solid-state NMR measurements were performed at the university of Liverpool, department of chemistry, by the group of prof. Yaroslav Khimyak. All solid-state NMR experiments were conducted at 9.4 T using a Bruker DSX-400 spectrometer operating at 79.49, 100.61, and 400.13 MHz for ²⁹Si, ¹³C and ¹H respectively. All chemical shifts are quoted in ppm from external TMS. ¹H-¹³C CP/MAS NMR spectra were acquired at a MAS rate of 8.0 kHz. A ¹H $\pi/2$ pulse length was 3.0 μ s and a recycle delay of 8.0 s was used during acquisition. The CP contact time was 2.0 ms with the Hartmann-Hahn matching condition set using Hexamethylbenzene (HMB). ¹H-¹³C Variable Contact Time (VCT) CP/MAS NMR spectra were acquired using contact times in the range of 0.01 to 12.0 ms. ¹H-²⁹Si CP/MAS NMR spectra were acquired at a MAS rate of 4.0 kHz. A ¹H $\pi/2$ pulse length of 3.1 μ s and the recycle delay of 10 s was used during acquisition. The CP contact time was 2.0 ms with the Hartmann-Hahn matching condition set using kaolinite. The ¹H-²⁹Si VCT/CP MAS NMR measurements used contact times ranging from 0.05 to 16.0 ms. 2D ¹H-¹³C Wideline SEparation (WISE) MAS NMR spectra were acquired at a MAS rate of 8 kHz. The ¹H $\pi/2$ pulse length was 3.1 μ s TPPM decoupling with a rf field strength of 84.7 kHz was used during the acquisition in t_2 . The Hartmann-Hahn condition was set using HMB. A fixed contact time of 80 μ s was used to limit the effect of spin diffusion. Longer contact times would lead to an equilibration of the proton magnetization due to spin diffusion, and consequently to the same proton lineshape for all carbon sites.⁴⁸⁹ States for phase-sensitive detection in the indirect dimension was implemented to recover pure absorption lineshape. The

recycle time was 2 s. 256 increments were recorded in t_1 corresponding to a dwell time of 16.7 μ s at a spectral width of 59880.238 Hz. 496 transients were acquired per t_1 increment in the direct dimension.

Thermographic analysis

TGA analysis was performed on a SDT 2960 van TA instruments.

10.2 Synthesis of ethene-PMO precursors

10.2.1 Classic synthesis of 1,2-bis(triethoxysilyl)ethene (80(*E,Z*)-BTSE)

1,2-bis(triethoxysilyl)ethene (80(*E,Z*)-BTSE) was prepared *via* metathesis of VTES with RuCl₂(PPh₃)₃, according to a method described by Marciniec *et al.*⁴³⁶ In a typical synthesis, RuCl₂(PPh₃)₃ (0.051g, 0.053 mmol) and VTES (10.086 g, 0.053 mol) were added to a Schlenk flask under argon. After stirring and refluxing for 24 h, unreacted VTES was distilled off. Subsequently, 80(*E,Z*)-BTSE was vacuum distilled to give a clear colorless liquid. Yield: 6.25 g (67 %). 80(*E,Z*)-BTSE was identified by ¹H and ¹³C NMR and GC-analysis as a diastereoisomeric mixture (\approx 80 % *E*). ¹H NMR (CDCl₃): δ = 6.77 (s, 2 H; *Z*-isomer), δ = 6.66 (s, 2 H; *E*-isomer), δ = 3.84 (m, 12 H; *Z*-and *E*-isomer), δ = 1.23 ppm (t, 18 H; *Z*-and *E*-isomer); ¹³C NMR (CDCl₃): δ = 151.42 (*Z*-isomer), δ = 145.92 (*E*-isomer), δ = 58.82 (*E*-isomer), δ = 58.71 (*Z*-isomer), δ = 18.45 (*E*-isomer), δ = 18.40 ppm (*Z*-isomer).

10.2.2 Direct synthesis of the diastereoisomerically pure *E*-isomer of 1,2-bis(triethoxysilyl)ethene (*E*-BTSE)

For the synthesis of the diastereoisomerically pure *E*-isomer of 1,2-bis(triethoxysilyl)ethene (*E*-BTSE), the Grubbs' first-generation catalyst was used. In a typical synthesis of *E*-BTSE, (PCy₃)₂Cl₂Ru=CHPh (0.0535 g, 0.065 mmol) and VTES (42.95 ml, 0.2038 mol) were added to a Schlenk flask under argon. The mixture was left to stir for one hour and subsequently refluxed for an additional three hours. Unreacted VTES was distilled off, after which *E*-BTSE was vacuum distilled to give a clear colorless liquid. Yield: 33.8 g (94 %). *E*-BTSE was identified by ¹H and ¹³C NMR and GC-analysis as a diastereoisomerically pure product (\approx 100 % *E*). ¹H NMR (CDCl₃): δ = 6.66 (s, 2 H), δ = 3.84 (q, 12 H), δ = 1.23 ppm (t, 18 H); ¹³C NMR (CDCl₃): δ = 145.92, 58.82, 18.45 ppm.

10.2.3 Synthesis of 1,2-bis(triethoxysilyl)ethene with catalysts 2, 4, 5, and 6

Synthesis of 1,2-bis(triethoxysilyl)ethene with the ruthenium dimer [Ru(*p*-cymene)Cl₂]₂, **2**, was performed according to the above described procedure for the synthesis of 80(*E,Z*)-BTSE. Yield: 66 %.

Synthesis of the ethene-PMO precursor with the Grubbs' second-generation catalyst **4**, and the Hoveyda-Grubbs' first- and second generation, **5** and **6** respectively, proceeded according to the above described procedure for the synthesis of *E*-BTSE. Yield: 92, 91, 93 % respectively.

10.2.4 Indirect synthesis of the diastereoisomerically pure *Z*-isomer of 1,2-bis(trimethoxysilyl)ethene (*Z*-BTSE)

The pure *Z*-isomer of 1,2-bis(trimethoxysilyl)ethene (*Z*-BTSE) was prepared via successive fractionated vacuum distillations of 80(*E,Z*)-BTSE. The distillation was monitored with ^1H NMR and GC to obtain a clear colorless liquid with the desired isomeric purity (≈ 100 % *Z*-isomer). ^1H NMR of *Z*-BTSE (CDCl_3): $\delta = 6.77$ (s, 2 H), $\delta = 3.86$ (q, 12 H), $\delta = 1.23$ ppm (t, 18 H); ^{13}C NMR of *Z*-BTSE (CDCl_3): $\delta = 151.37$, 58.70, 18.39 ppm.

10.2.5 Indirect synthesis of 1,2-bis(trimethoxysilyl)ethene with 50 % *E*- and *Z*-isomers (50(*E,Z*)-BTSE)

The synthesis of 50(*E,Z*)-BTSE proceeded according to the above described procedure for the synthesis of *Z*-BTSE. The distillation was monitored with ^1H NMR and GC to obtain a clear colorless liquid with the desired isomeric purity (≈ 50 % *E*- and *Z*-isomer).

10.3 Synthesis of butene-PMO precursor

10.3.1 Monitoring the self-metathesis of allyltrimethoxysilane with ^1H NMR

The catalyzed self-metathesis reactions of allyltrimethoxysilane (ATMS) were monitored by means of ^1H NMR, as a function of time. The reaction conditions depend on the employed catalysts, and are given below. To determine the conversion, the $-\text{CH}=\text{CH}_2$ - and $-\text{CH}=\text{CH}-$ protons of allyltrimethoxysilane and 1,4-bis(trimethoxysilyl)butene, respectively, were integrated in the ^1H NMR spectra. ^1H NMR (CDCl_3 , δ in ppm): ATMS: 4.94 - 5.06 (2H); BTSB: 5.36 - 5.46 (2H). To determine the conversion to isomerization products, the $-\text{CH}=\text{CH}-$ protons of the isomer in the ^1H NMR spectra were integrated: ^1H NMR (CDCl_3) $\delta = 6.4$ - 6.5 ppm.

Reactions with catalysts **3**, **4**, **6**, **7** and **12**

In a typical reaction, the catalyst (0.036 mmol) and allyltrimethoxysilane (36.0 mmol) were added to a oven-dried Schlenk flask under argon. No solvents were added to the reaction mixtures. The reaction was carried out at 50 °C. At different time intervals a sample was taken from the reaction mixture and analyzed with ^1H NMR. The same procedure was also followed wherein either the reaction temperature was lowered to 40 °C or the ATMS/Catalyst ratio was lowered to 800.

Reactions with indenylidene catalysts **8**, **9**, **10** and **11**

In a typical reaction, the catalyst (0.036 mmol) and allyltrimethoxysilane (36.0 mmol) were added to a oven-dried Schlenk flask under argon. The temperature of the reaction mixture was thermostated at 50 °C, after which the co-catalyst (1.08 mmol) was added. At different time intervals a sample was taken from the reaction mixture and analyzed with ^1H NMR.

10.3.2 Direct synthesis of the diastereoisomerically pure *E*-isomer of 1,4-bis(trimethoxysilyl)butene

For the synthesis of the diastereoisomerically pure *E*-isomer of 1,4-bis(trimethoxysilyl)ethene, catalyst **12** was used. In a typical synthesis, catalyst **12** (0.10 mmol) and ATMS (0.1 mol) were added to a Schlenk flask under argon. The mixture was left to stir overnight at 50 °C. Unreacted ATMS was distilled off, after which BTSEB was vacuum distilled to give a clear colorless liquid. Yield: 87 %. BTSEB was identified by ^1H and ^{13}C NMR. ^1H NMR (CDCl_3): $\delta = 1.60$ (q, 4 H), $\delta = 3.55$ (s, 18 H), $\delta = 5.38$ ppm (m, 2 H); ^{13}C NMR (CDCl_3): $\delta = 10.71$, 15.36, 50.67, 122.23, 123.74 ppm. The isomeric purity of the sample was established by means of GC-analysis, which revealed a single peak in the chromatogram.

10.4 Synthesis of ethenylene-bridged PMOs

10.4.1 Synthesis of *E*-EBP, 80(*E,Z*)-EBP, 50(*E,Z*)-EBP, and *Z*-EBO

A series of PMOs was synthesized by varying the precursor and keeping all other reaction parameters constant. In a typical synthesis procedure, 1.00 g of Pluronic P123 was diluted in an acidified solution containing 47.80 ml of H_2O , 3.42 ml of concentrated HCl and 2.45 ml of *n*-butanol. The solution was stirred at room temperature for 1.5 hours upon which 1.86 ml of *E*-BTSE, *Z*-BTSE, 50(*E,Z*)-BTSE or 80(*E,Z*)-BTSE was added. The final reactant molar composition was: P123 : BTSE : HCl : H_2O : *n*-butanol = 1 : 29 : 238 : 16097 : 155. This solution was stirred for 4 hours at 35 °C upon which 18.0 ml of *n*-butanol was added. The PMO material was successively aged for an additional 23 hours at 90 °C under static conditions. The mixture was left to cool down to room temperature after which the precipitated PMO was filtrated and washed with distilled water. The surfactant was removed by means of Soxhlet extraction using acetone over a period of 5 hours. This procedure led to ethenylene-bridged hybrid materials with different isomeric configurations.

10.4.2 Synthesis of *Z*-EBP

For the synthesis of *Z*-EBP, a procedure similar to that of *E*-EBP was followed. Herein all reaction parameters were kept the same, except for the acid concentration. Instead of adding 3.42 ml of concentrated HCl to the reaction mixture, 8.9

ml was added. The higher acid concentration is required to enhance template-precursor interaction and produce ordered mesopores.

10.4.3 Synthesis of EBP-1 to EBP-9

In a typical synthesis procedure of an *E*-configured ethenylene-bridged PMO, 1.00 g P123 was diluted in an acidified solution containing 34.10 ml of distilled H₂O and 0.456 ml of concentrated HCl. The solution was stirred for 1.5 hours at room temperature, upon which 1.90 ml of *E*-BTSE was added. This solution was stirred for 4 hours at 35 °C and successively aged for an additional 17 hours at 90 °C. The surfactant template was removed by Soxhlet extraction using acetone over a period of 5 hours. A series of PMOs synthesized with different acid concentrations was prepared: 1.58, 1.00, 0.75, 0.492, 0.248, 0.158, 0.125 and 0.063 mol/l. All other reactions parameters were kept constant. These samples are denoted as EBP-1 to EBP-8. An additional PMO sample was prepared using *n*-butanol as a co-solvent. This sample was prepared using the procedure described above in a HCl solution of 0.8 mol/l, in the presence of 2.4 ml of *n*-butanol. This PMO is abbreviated as EBP-9.

10.4.4 Synthesis of EBP-10 to EBP-33

In a typical synthesis procedure, 1.00 g of Pluronic P123 was diluted in an acidified solution containing 47.8 ml of H₂O, 3.42 ml of concentrated HCl and 2.45 ml of *n*-butanol. The solution was stirred at room temperature for 1.5 hours upon which 1.86 ml of the homemade *E*-BTSE was added. The final reactant molar composition was: P123 : *E*-BTSE : HCl : H₂O : *n*-butanol = 1 : 29 : 238 : 16097 : 155. This solution was stirred for 4 hours at 35 °C and successively aged for an additional 16 hours at 90 °C under static conditions. The mixture was left to cool down to room temperature after which the precipitated PMO was filtrated and washed with distilled water. The surfactant was removed by means of Soxhlet extraction using acetone over a period of 5 hours. To investigate the influence of cosolvent, reactant molar ratio, acidity and temperature, a series of different cosolvents (*n*-ethanol, *n*-propanol, *n*-butanol and *n*-pentanol), different concentrations of HCl (0.031, 0.062, 0.10, 0.125, 0.141, 0.158, 0.25, 0.30, 0.50, 0.80, 0.90 and 1.0 M), or different molar ratios of *n*-butanol:P123 (95, 115, 135, 155, 175, 195), were used in the synthesis process described above, at various aging temperatures (50, 70, 90, 110 and 150 °C). Only one reaction parameter was changed in each experiment while keeping the other parameters constant.

10.4.5 Synthesis of EBP-AT and EBP-PT

Pluronic P123 (1.0 g) was diluted in an acidified solution containing 47.8 ml of distilled H₂O, 3.42 ml of concentrated HCl and 2.45 ml of *n*-butanol. The solution was stirred at room temperature for 1.5 hours upon which 1.86 ml of *E*-BTSE was added. The final reactant molar composition was: P123 : *E*-BTSE : HCl : H₂O : *n*-butanol = 1 : 29.3 : 238 : 16097 : 155. This solution was stirred for 4 hours at 35 °C, after which 18 ml of *n*-butanol was added. The precipitated PMO was successively aged for an additional 16 hours at 90 °C under static conditions. The

template was removed by means of Soxhlet extraction using acetone over a period of 5 hours. Prior to the thermal treatment the PMO, abbreviated as EBP-AT, was dried under vacuum at 120 °C. EBP-AT was then thermally treated at 380 °C for 10 hours under vacuum, producing EBP-PT.

10.4.6 Hydrophobization of ethene-PMOs with HMDS

To investigate whether PMO silanol groups participate in the thermally induced generation of vinylic functions in ethene PMOs, according to the mechanism proposed in chapter 6 (section 6.3.2, p141), the ethene-PMO (EBP-AT) was hydrophobized with HMDS. During the hydrophobization reaction all silanol groups are transformed to $\equiv\text{Si}-\text{O}-\text{Si}(\text{CH}_3)$. To a portion of dried EBP-AT (0.2 g), 10 ml of HMDS was added under an argon atmosphere, using standard Schlenk techniques. The mixture was refluxed under argon during 8 hours. The sample was filtrated, washed with acetone and hexane, and vacuum dried at 90 °C. This sample was thermally treated using the same procedure as described in 10.4.5.

10.4.7 Synthesis of ultra-large pore ethene-PMOs: EBP-34 to EBP-47

In a typical synthesis of an ultra-large pore ethene-PMO, 1.0 g of P123 was diluted in a solution containing 48.7 ml of H₂O, 1.2 ml of *n*-butanol and 2.1 ml of concentrated HCl. The mixture was stirred at room temperature until P123 fully dissolved, after which a varying amount of swelling agent was added. This solution was stirred for 0.5 hours, after which 1.86 ml of *E*-BTSE was added. Finally, the mixture was stirred for 3 hours at 35 °C and successively aged for 24 hours in an autoclave at 100 °C. The PMO was filtrated and washed with distilled H₂O. The template was removed by means of Soxhlet extraction with acetone.

The different swelling agents which were investigated are: TMB, *p*-cymene, *p*-xylene, *tert*-butylbenzene, hexadecane, hexane, and pentane. The impact of TMB on the pore expansion was examined by varying the TMB/P123 ratio: 0, 10, 15, and 45. To investigate the role of TMB in the self-assembly process, the time at which the swelling agent TMB was added to the mixture was varied. Herein, TMB was added 0, 10, 16 or 180 minutes after the addition of *E*-BTSE to the reaction mixture.

10.4.8 Synthesis of bimodal ethene-PMO EBP-48

For the synthesis of bimodal ethene-PMO EBP-48, the same molar compositon as for EBP-36 was employed (TMB/P123 = 15). However, the aging step was performed at atmospheric pressure at 90 °C. Other reaction parameters were kept the same as those described above for EBP-36.

10.4.9 Synthesis of ethene-PMOs with gemini surfactant 16-12-16: EBP-49 to EBP-62

In a typical synthesis, 0.313 g of gemini surfactant 16-12-16 was diluted in a solution containing 13.0 ml of H₂O, 0.51 ml of *n*-butanol and 0.115 g of NaOH. The mixture

was stirred at room temperature for one hour, after which 0.885 ml of *E*-BTSE was added. This solution was stirred for 4 hours at 35 °C and successively aged for 16 hours at 90 °C. The PMO was filtrated and washed with distilled H₂O. The template was removed by means of Soxhlet extraction with acidified methanol (MeOH/HCl = 9/1 vol%).

To investigate the influence of reactant molar ratio on the PMO properties, a series of different molar ratios of surfactant/precursor (0.07, 0.12, 0.15, and 0.19), *n*-butanol/precursor (0, 2.3, 3.0, 4.0, 5.0, and 6.0), NaOH/precursor (0.1, 0.4, 0.6, 0.8, 1.0, and 1.2) were used in the synthesis process described above. Only one reaction parameter was changed in each experiment while keeping the other parameters constant.

10.5 Synthesis of a butenylene-bridged PMO

The butenylene-bridged PMO was synthesized according to a similar procedure as described for the ethene-PMO EBP-24. Herein, 1.00 g of Pluronic P123 was diluted in an acidified solution containing 48.7 ml of H₂O, 2.12 ml of concentrated HCl and 1.17 ml of *n*-butanol. The solution was stirred at room temperature for 1.5 hours upon which 1.59 ml of BTSE was added. The final reactant molar composition was: P123 : BTSE : HCl : H₂O : *n*-butanol = 1 : 30 : 147 : 16098 : 74. This solution was stirred for 4 hours at 35 °C and successively aged for 7 days at 90 °C under static conditions. The mixture was left to cool down to room temperature after which the precipitated PMO was filtrated and washed with distilled water. The surfactant was removed by means of Soxhlet extraction using acetone over a period of 5 hours.

10.6 Synthesis of sulfonic acid ethene-PMOs: SEBP-42 and SEBP-63

In a typical synthesis of a sulfonic acid ethene PMO, a previously synthesized ethene PMO is vacuum dried at 120 °C in a Schlenk flask. Under an argon atmosphere, 20 ml of dry CH₂Cl₂ is added, upon which the flask is cooled in an ice bath. Additionally, 4.5 ml of chlorosulfonic acid is added. The reaction mixture is stirred for 24 hours under an argon atmosphere (the flask is equipped with an argon-filled balloon). The mixture is carefully pored out in a beaker of H₂O. The PMO is filtered and washed with H₂O until the pH of the filtrate is neutral. The PMO is washed with methanol and acetone, and successively vacuum dried.

EBP-63 was synthesized as followed: 2.82 g of P123 was diluted in an acidified solution containing 95.75 ml of H₂O, 4.43 ml of concentrated HCl and 3.15 ml of *n*-butanol. The solution was stirred at room temperature for 1.5 hours upon which 5.0 ml of BTSE was added. This solution was stirred for 24 hours at 35 °C and successively aged for 24 hours in an autoclave at 100 °C under static conditions. The mixture was left to cool down to room temperature after which the precipitated PMO was filtrated and washed with distilled water. The surfactant was removed by means of Soxhlet extraction using acetone over a period of 5 hours. Both the

sulfonation of EBP-63 and of the ultra-large pore PMO, EBP-42, was performed according to the above described procedure.

10.7 Synthesis of styrylethyl-modified ethene-PMO: Styrene-Ethene-PMO

The bifunctional styrene-ethene-PMO was synthesized *via* a co-condensation reaction between *E*-BTSE and styrylethyltrimethoxysilane (SETs). Herein, 1.00 g of Pluronic P123 was diluted in an acidified solution containing 47.8 ml of H₂O, 3.42 ml of concentrated HCl and 2.45 ml of *n*-butanol. The solution was stirred at room temperature for 1.5 hours upon which 1.86 ml of *E*-BTSE. This solution was stirred for 2 hours after which 0.16 ml of SETs was added. The final reactant molar composition was: P123 : *E*-BTSE : SETs : HCl : H₂O : *n*-butanol = 1 : 29.3 : 3.25 : 238 : 16098 : 155. This solution was successively stirred for an additional 2 hours at 35 °C and successively aged for 16 hours at 90 °C under static conditions. The mixture was left to cool down to room temperature after which the precipitated PMO was filtrated and washed with distilled water. The surfactant was removed by means of Soxhlet extraction using acetone over a period of 6 hours.

10.8 Syntheses without surfactants: disordered amorphous materials

10.8.1 Synthesis of vinylsilica

To establish whether the thermally generated peaks in the FT-Raman, DRIFT and ¹³C CP MAS NMR spectra of EBP-PT can be attributed to vinylic groups, a pure vinylsilica material was prepared. Herein, 2.0 ml of VTES was diluted in an acidified solution containing 15.0 ml of H₂O and 2.5 ml of concentrated HCl. The mixture was stirred at 35 °C during 4 hours after which a sticky polymer was obtained. This material was vacuum dried.

10.8.2 Synthesis of styrylethylsilica

For reference purposes, a pure styrylethylsilica material was synthesized without adding any surfactant. Herein, 0.4 ml of SETs was diluted in an acidified solution containing 4 ml of H₂O and 0.6 ml of concentrated HCl. The mixture was sonificated during 2 hours after which it was stirred for an additional 2 hours at 35 °C. The obtained material was vacuum dried.

10.9 Synthesis of SBA-15 and extraction investigation

SBA-15 was synthesized according to the following procedure: a mixture of 12.0 g of P123, 381.0 g of distilled H₂O and 69.6 g of concentrated HCl were mixed

for 1.5 hours at 45 °C after which, 25.5 g of TEOS was added and left to stir for an additional 6 hours. The final reactant molar composition was: P123 : TEOS : HCl : H₂O = 1 : 59 : 341 : 11389. This solution was subsequently aged at 80 °C for 15 hours under static conditions. The mixture was left to cool down to room temperature after which the precipitated silica material was filtrated and washed with distilled water. To investigate the efficiency of several organic solvents (dichloromethane, chloroform, acidified ethanol, ethyl acetate, isopropanol and acetone) for the extraction of the polymeric template, the surfactant containing SBA-15 material was divided in portions. The surfactant was removed by means of Soxhlet extraction using the respective solvents over a period of 5 hours. Two portions of the surfactant containing SBA-15 material were calcined under vacuum at 380 and 400 °C.

10.10 Bromination of ethylene-bridged PMOs

The accessibility of the C=C double bonds in the ethene-PMOs was investigated by means of a bromine addition reaction. The PMOs, which were vacuum dried in advance in a Schlenk flask, were treated with bromine vapor under vacuum at 35 °C, by using a Schlenk set-up as illustrated in Figure 10.1. The reaction time was varied (0.5, 1, 2 and 6 hours). Physisorbed bromine was removed under vacuum at 90 °C.

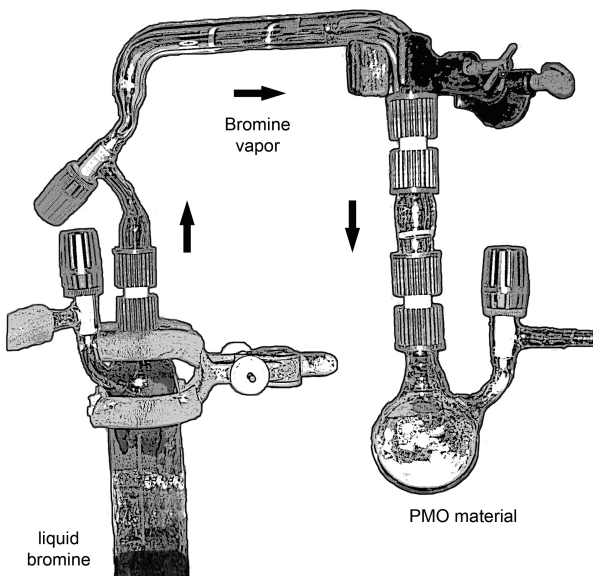


Figure 10.1: Schlenk set-up used for the bromination of ethene-PMOs under vacuum.

10.11 Synthesis gemini surfactant 16-12-16

The gemini surfactant 16-12-16 was prepared by refluxing a stoichiometric amount of 1,12-dibromododecane (1.2 g, 3.66 mmol) and *N,N*-dimethylhexadecylamine (2.5 ml, 7.43 mmol) in acetone during 24 hours, followed by several recrystallizations from acetone. The surfactant is filtrated and vacuum dried.

10.12 Esterification of *n*-propanol with acetic acid

Prior to the reaction, the sulfonic acid ethene-PMO was brought into an oven-dried Schlenk flask and dried under vacuum at 110 °C (dried weight: 0.207 g). Toluene (4.9 ml, 46 mmol), *n*-propanol (3.4 ml, 45.5 mmol), acetic acid (3.86 ml, 67.4 mmol) and butyl acetate (1.0 ml, 7.6 mmol) were added successively to the acid PMO. The flask was equipped with a Dean-Stark apparatus to remove the generated H₂O during the reaction. The reaction mixture was heated to 135 °C, and stirred well. Samples were taken during the reaction after different time intervals, and analyzed by means of GC.

A similar reaction procedure was also followed without the Dean-Stark apparatus. In this case the reaction temperature was 90 °C. In order to compare the activity of the different catalysts in each esterification reaction, the molar ratio of acid sites/*n*-propanol was kept constant (except for sample SEBP-42, which revealed less acid sites).

Chapter 11

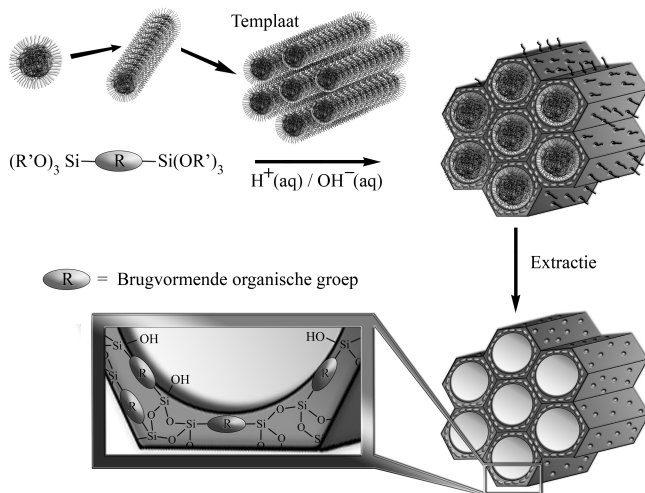
Nederlandse samenvatting

11.1 Inleiding

Deze doctoraatsthesis gaat over de ontwikkeling, karakterisatie en toepassing van periodische mesoporeuze organosilica's (PMOs). Dergelijke materialen behoren tot de klasse van organische-anorganische hybride materialen met geordende mesoporiën (mesoporiteit: 2 tot 50 nm). Ze worden gesynthetiseerd door directe condensatie van gebruikte organosilanen, vaak $(R'O)_3Si-R-Si(OR')_3$ met R een brugvormende organische groep, in aanwezigheid van een surfactant. Onder de juiste reactiecondities vormt het surfactant micellen die aggregeren tot een vloeibaar kristallijne fase. Deze fase fungeert als een templaats waarrond het organosilaan polycondenseert, zoals schematisch voorgesteld in Figuur 11.1. Na verwijdering van het surfactant uit de poriën wordt een PMO materiaal met open geordende mesoporiën bekomen. Afhankelijk van het aangewende surfactant zijn deze mesoporiën met elkaar verbonden door microporiën (< 2 nm). Dit is het geval wanneer het triblok copolymer P123 ($EO_{20}PO_{70}EO_{20}$, EO: ethyleen oxide en PO: propyleen oxide) wordt gebruikt. Hierbij worden de microporiën gegenereerd door de hydrofiele PEO (polyethyleen oxide) ketens die uitsteken aan het oppervlakte van de hydrofobe micelkernen, die worden gevormd door hydrofobe PPO (polypropyleen oxide) ketens.

PMOs hebben een heel unieke structurele samenstelling. De organische groepen zijn covalent gebonden in het silica netwerk en zijn bijgevolg intrinsieke bouwstenen van de mesoporeuze PMO matrix. Het hoge gehalte aan organische groepen en de uniforme verdeling ervan in de poriewanden is een kenmerkende eigenschap van deze poreuze hybride materialen, en het laat toe om zowel de chemische als fysische eigenschappen ervan gemakkelijk te regelen terwijl de structurele stabiliteit kan worden behouden.

Verder, kunnen PMOs een heel nauwe poriegrootte distributie, hoog specifiek oppervlakte, grote mesoporiën, dikke poriewanden en grote porievolumes vertonen. Bovendien, zijn de organische groepen geïntegreerd in de poriewanden waardoor de poriën volledig open blijven en bijgevolg gemakkelijk toegankelijk zijn voor eventuele verdere modificaties van de oppervlakte functies. Deze eigenschappen zorgen ervoor dat PMOs van potentieel belang kunnen zijn voor toepassingen in



Figuur 11.1: Synthese van periodische mesoporeuze organosilica's in aanwezigheid van een niet-ionisch poly(alkleen oxide) block copolymer als templaat.

de katalyse, milieutechnologie, chromatografie en micro-electronica.

Het overgrote deel van de internationale publicaties over PMOs gaan over de synthese van geordende mesoporeuze ethaansilica's. Dit is waarschijnlijk het gevolg van de wijde commerciële beschikbaarheid van de precursor 1,2-bis(triethoxysilyl)-ethaan. De verzadigde organische groep van deze PMOs levert echter weinig mogelijkheden voor verdere modificaties en zijn bijgevolg moeilijk toepasbaar. In deze context zijn PMOs waarvan de organische groepen bestaan uit olefinische functies veel interessanter. Deze kunnen namelijk eenvoudig worden gemodificeerd *via* olefine chemie.

Dit doctoraatsonderzoek speelt in op de vraag naar veelzijdige nanoporeuze materialen die potentieel kunnen worden toegepast in de katalyse, chromatografie en milieutechnologie. Hierbij werd geopteerd voor olefinische PMOs. De gemakkelijk modificeerbare alkeen-bruggen kunnen worden gebruikt om katalysatoren of verbindingen die kunnen complexeren met zware metalen, te immobiliseren *via* de C–C binding in plaats van de frequent gebruikte, maar minder stabiele siloxaan binding. In het bijzonder gaat dit onderzoek over de ontwikkeling van diastereoiso-mere olefinische PMOs met controleerbare eigenschappen.

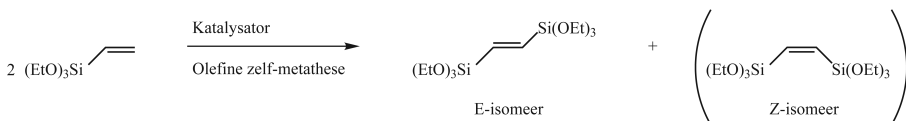
11.2 Ontwikkeling van diastereo-isomere olefinsche PMO precursoren

11.2.1 Etheen-PMO precursoren

Tot heden werden etheen-PMOs gesynthetiseerd door gebruik te maken van een diastereoismeer mengsel (*E*- en *Z*-isomeren) van 1,2-bis(triethoxysilyl)etheen, dat oftewel commercieel werd bekomen oftewel werd gesynthetiseerd *via* een methode

dat werd beschreven door de groep van Marciniec.⁴³⁶

De precursor 1,2-bis(triethoxysilyl)etheen wordt gesynthetiseerd *via* een olefine zelf-metathese reactie van vinyltriethoxysilaan in aanwezigheid van een katalysator, zoals voorgesteld in Figuur 11.2.



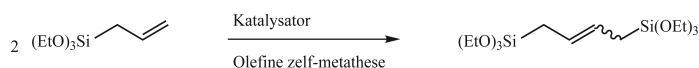
Figuur 11.2: Olefine zelf-metathese van vinyltriethoxysilaan.

In de methode van Marciniec werd gebruik gemaakt van $\text{CeRuCl}_2(\text{PPh}_3)_3$ als katalysator. Met deze katalysator werd een diastereoisomeer mengsel met een *E/Z*-ratio van ongeveer 80/20 bekomen. Met het oog op het ontwikkelen van een zuiver isomeer van 1,2-bis(triethoxysilyl)etheen, werden verschillende katalysatoren getest in de metathese reactie van vinyltriethoxysilaan. Uit dit onderzoek bleek dat de Grubbs eerste generatie katalysator $(\text{PCy}_3)_2\text{Cl}_2\text{Ru}=\text{CHPh}$ de meest efficiënte en selectieve katalysator is. Hiermee kon het zuiver *E*-isomeer van 1,2-bis(triethoxysilyl)etheen worden bekomen met een opbrengst van 94 %.

De hoge selectiviteit voor het *E*-isomeer suggerert dat deze reactie thermodynamisch is gecontroleerd. Een mogelijke verklaring hiervoor is dat de vorming van *E*-geconfigureerde species met relatief sterisch ongehinderde triethoxy groepen wordt bevoordeeld ten opzichte van *Z*-geconfigureerde species met sterisch meer gehinderde triethoxy groepen. Hierdoor kan het *Z*-isomeer niet *via* een directe katalytische methode worden bekomen. M.a.w., om 1,2-bis(triethoxysilyl)etheen met een lage *E/Z*-ratio te bekomen, moet een andere synthese procedure worden gevuld. In deze context werd beoogd om de twee isomeren te scheiden door het uitvoeren van meerdere gefractioneerde vacuumdestillaties. Hoewel het scheiden van deze isomeren heel intensief bleek te zijn (als gevolg van het geringe kookpuntsverschil), kon het zuiver *Z*-isomeer van 1,2-bis(triethoxysilyl)etheen worden gesynthetiseerd.

11.2.2 Buteen-PMO precursoren

Met het oog op het ontwikkelen van een nieuwe olefinische PMO werd beoogd om een nieuwe precursor te synthetiseren, namelijk 1,4-bis(trimethoxysilyl)butene. Hiervoor werden een reeks katalysatoren getest in de zelf-metathese reactie van allyltrimethoxysilaan (zie Figuur 11.3).

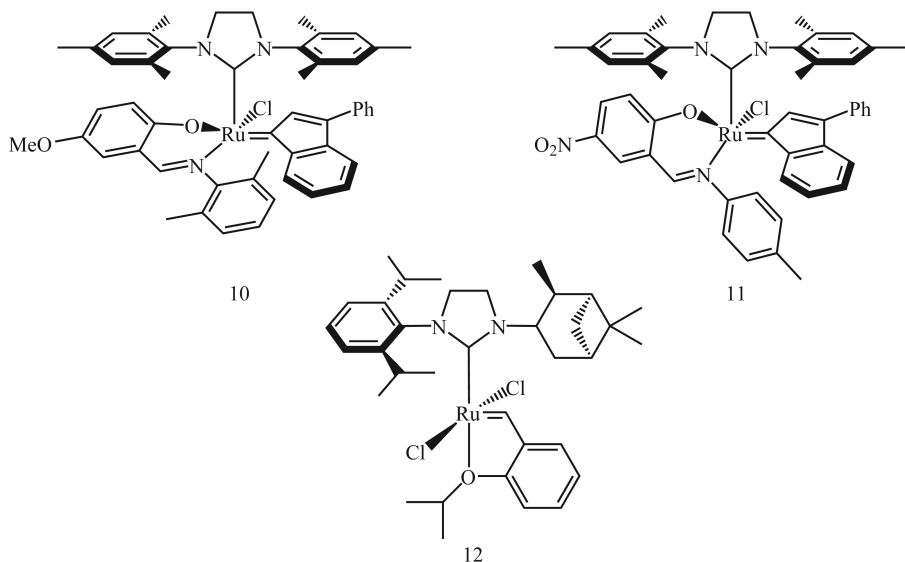


Figuur 11.3: Olefine zelf-metathese van allyltrimethoxysilaan.

Preliminair onderzoek heeft aangetoond dat de metathese van allyltrimethoxysilane bij een veel lagere reactietemperatuur (50 °C) kan verlopen dan vinyltriethoxysilane

(160 °C). Dit kan een gevolg zijn van de sterisch minder gehinderde alkeenfunctie. Van de benzylideen type katalysatoren (Grubbs eerste, tweede en derde generatie en de Hoveyda-Grubbs tweede generatie), vertoont de Grubbs tweede generatie de hoogste activiteit. De metathese reactie met behulp van deze type katalysatoren gaat echter gepaard met een isomerisatie reactie (migratie van de dubbele binding *via* 1,3-H shifts), die in competitie treedt met de metathese reactie. Hoewel het verlagen van de reactietemperatuur deze nevenreactie kan onderdrukken, is dit geen efficiënte oplossing gezien ook de metathese activiteit wordt verlaagd. Een goed alternatief voor de benzylideen type katalysatoren zijn de indenylideen type katalysatoren, en in het bijzonder deze met Schiffse base liganden. Deze katalysatoren, die werden gesynthetiseerd door de spin-off ViaCatt, noemt men latente katalysatoren omdat ze inactief zijn bij kamertemperatuur of in afwezigheid van een activator.

In aanwezigheid van een activator zoals phenyltrichlorosilaan, zijn deze katalysatoren heel actief in de metathese reactie van allyltrimethoxysilaan. Bovendien produceren ze geen isomerisatieproducten. Met de katalysatoren **10** en **11** (zie Figuur 11.4) kon allyltrimethoxysilaan zelfs kwantitatief worden omgezet. Hoewel deze katalysatoren heel goed bleken te zijn voor de synthese van de buteen-PMO precursor, kon aan de hand van GC analyse worden vastgesteld dat de reactieproducten onvoldoende zuiver zijn om geïmplementeerd te worden in PMO synthese. Daarom werd verder onderzoek verricht om de synthese van een zuiver buteen-PMO precursor te verwezenlijken en te optimaliseren.



Figuur 11.4: Actieve katalysatoren in de metathese van allyltrimethoxysilaan.

De beste katalysator voor de metathese van allyltrimethoxysilaan, is een Hoveyda type katalysator met een chiraal NHC ligand (katalysator **12**, zie Figuur 11.4). Deze katalysator, die voor het eerst werd ontwikkeld door Ledoux,⁴²³ vertoont zowel een hoge activiteit (83 % conversie) en een hoge selectiviteit. *Via* GC kon

achterhaald worden dat er geen isomerisatieproducten worden gevormd tijdens de metathese reactie. Bovendien vertoont het reactieproduct maar één piek in het chromatogram, wat erop wijst dat katalysator **12** het zuivere *E*-isomeer van 1,4-bis(trimethoxysilyl)buteen produceert.

11.3 Etheen-PMOs: Van *E* tot *Z*

Aan de hand van FT-Raman en ^1H - ^{13}C CP MAS NMR kon worden aangetoond dat de isomere configuratie van de etheen-PMO precursor wordt behouden in de uiteindelijke PMO matrix. De samenstelling van de precursor heeft echter een grote invloed op de eigenschappen van de etheen-PMOs.

11.3.1 Invloed diastereoisomere configuratie op structurele PMO eigenschappen

De invloed van de isomere configuratie van de precursor 1,2-bis(trimethoxysilyl)etheen (BTSE) op de eigenschappen van de resulterende etheen-PMO materialen werd onderzocht aan de hand van X-stralen diffractie en stikstof fysisorptie. Hieruit blijkt dat de isomere configuratie van de etheen-PMO precursor een drastische impact heeft op de materiaaleigenschappen. Wanneer het zuivere *E*-isomeer van 1,2-bis(trimethoxysilyl)etheen (*E*-BTSE) wordt aangewend, vertonen de resulterende PMOs een hogere graad van structurele ordening en een nauwere poriegrootte distributie dan in het geval deze precursor bestaat uit zowel *E*- als *Z*-isomeren.

Wanneer onder dezelfde reactiecondities het zuivere *Z*-isomeer van 1,2-bis(trimethoxysilyl)etheen (*Z*-BTSE) wordt gebruikt als precursor, wordt zelfs geen geordend mesoporeus materiaal meer bekomen, maar een microporeus materiaal met ongeordende poriën. Deze resultaten suggereren dat *Z*-BTSE een compleet andere reactiviteit heeft dan *E*-BTSE. Dit moet dus in rekening worden gebracht wanneer diastereoisomere mengsels van de precursor worden aangewend voor de synthese van etheen-PMOs.

De hogere graad van porieordering en de nauwere poriegrootte distributie van de etheen-PMO met *E*-geconfigureerde etheen-bruggen in de poriewanden, is wellicht het gevolg van de homogene polycondensatie van de precursor en de regelmatige cross-linking en stapeling van de *E*-geconfigureerde etheen-bruggen. Wanneer de precursor bestaat uit zowel *E*- en *Z*-isomeren, zal de cross-linking en stapeling ervan willekeurig gebeuren. Omdat de syntheseprocedure werd geoptimaliseerd voor *E*-BTSE, zal de aanwezigheid van het *Z*-isomeer de structuurvorming van de PMO belemmeren, wat resulteert in een materiaal met inferieure eigenschappen.

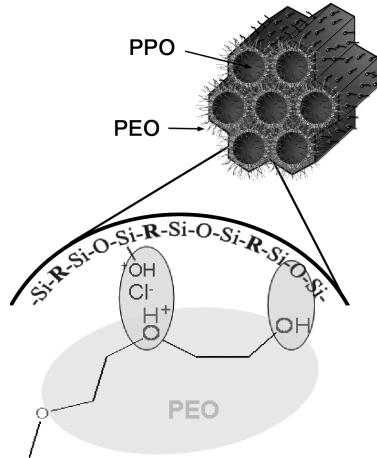
Deze hypothese wordt bevestigd door het totale verlies aan porieordering wanneer *Z*-BTSE wordt gebruikt voor de PMO synthese. Zowel de structurele ordening als de uniformiteit van de poriën van PMOs met *Z*-geconfigureerde etheen-bruggen in de poriewanden, kan drastisch worden verhoogd door het verlagen van de pH van het reactiemengsel. Dit is waarschijnlijk het gevolg van een verhoogde templaatt-prefragment interactie bij lagere pH-waarden. De vereiste lagere pH van het reactiemengsel wanneer *Z*-BTSE wordt gebruikt als precursor, verifieert het verschil in reactiviteit tussen beide isomeren en verklaart de lagere porieordering en uni-

formiteit van materialen die werden bekomen uit diastereoisomere mengsels van 1,2-bis(triethoxysilyl)etheen.

Naast de ordening en de uniformiteit van de poriën, heeft de samenstelling van de precursor tevens een invloed op de grootte van de mesoporiën en op de dikte van de poriewanden, terwijl de eenheidscel niet significant verandert. Bijgevolg kan de systematische daling van de poriegrootte bij toenemende concentratie van *Z*-geconfigureerde etheen-bruggen in de poriewanden, worden toegeschreven aan de toenemende dikte van de poriewanden. De dichtere pakking van *E*-isomeren in vergelijking met *Z*-isomeren is een algemeen gekend fenomeen, dat gerelateerd is aan hun meer lineaire structuur, en verklaart de toenemende wanddikte van etheen-PMOs met toenemende concentratie aan *Z*-geconfigureerde etheen-bruggen.

11.3.2 Templaat-PMO interacties

Om de templaat-PMO interacties te achterhalen, werden complexe NMR studies uitgevoerd aan de universiteit van Liverpool. Hierbij werden PMOs geanalyseerd waarvan het surfactant, Pluronic P123 nog aanwezig was in de mesoporiën. De PEO blokken van het surfactant interageren sterk met de poriewanden van de PMOs, terwijl de PPO blok mobiel is in de poriën. De interacties tussen de hybride PMO wanden en de PEO blokken worden gevormd door H-bindingen tussen eindstandige PEO-hydroxyl en Si—O—Si groepen, alsook door ionenpaar interacties tussen halide anionen van geprotoneerde etherfuncties in PEO blokken en geprotoneerde silanolgroepen in de PMO matrix (zie Figuur 11.5).



Figuur 11.5: Templaat-PMO interacties, afgeleid uit ^1H - ^{13}C CP/MAS kinetiek and WISE (Wideline Separation) experimenten.

11.3.3 Hydrothermale stabiliteit

Om de invloed van de diastereoisomere configuratie van de poriewanden van etheen-PMOs op de stabiliteit van de materialen te achterhalen, werden een reeks PMOs

met verschillende isomere samenstelling gestoomd in een autoclaaf. Uit de resultaten bleek dat de PMOs die gesynthetiseerd werden met *E*-BTSE het meest stabiel zijn. In het bijzonder werd vastgesteld dat er na de hydrothermale behandeling contractie optreedt van de poriewanden van etheen-PMOs die *Z*-geconfigureerde etheen-bruggen bevatten, terwijl dit niet het geval is voor etheen-PMOs met enkel *E*-geconfigureerde etheenfuncties in de wanden.

De contractie van poriewanden als gevolg van de hydrothermale behandeling, bevestigt de hypothese dat de toenemende wanddikte met toenemende concentratie van *Z*-isomeren in de PMO matrix, gerelateerd kan zijn aan de slechtere stapeling van de *Z*-geconfigureerde etheenfuncties in vergelijking met de *E*-geconfigureerde etheenfuncties.

Bovendien kon aan de hand van ^1H - ^{29}Si CP/MAS NMR worden vastgesteld dat de stabiliteit van PMO materialen gelinkt kan worden aan de graad van condensatie in de poriewanden. Naarmate de concentratie aan *Z*-isomeren in de PMO matrix toeneemt, hoe lager de graad van condensatie. Dit wil zeggen dat er minder cross-linking in de wanden optreedt, en bijgevolg dat deze minder stabiel zijn.

11.3.4 Chemische toegankelijkheid van de etheenfuncties

Door middel van een bromeringsreactie kon de bereikbaarheid en reactiviteit van de etheenfuncties aan het oppervlak van de PMOs worden bepaald. Etheen-PMOs reageren snel met broom, waarbij 25 % van de totale aantal etheenfuncties kunnen worden gemodificeerd. De snelle reactiviteit van deze etheen-PMOs suggerert dat de oppervlaktegroepen gemakkelijk bereikbaar zijn, zelfs door grote broom moleculen, als gevolg van de uniforme en open poriestructuren. Deze eigenschap maakt van etheen-PMOs ideale kandidaten om toegepast te worden in de katalyse en milieutechnologie, waar gunstige diffusie eigenschappen van de katalysator of adsorbens een belangrijke rol spelen.

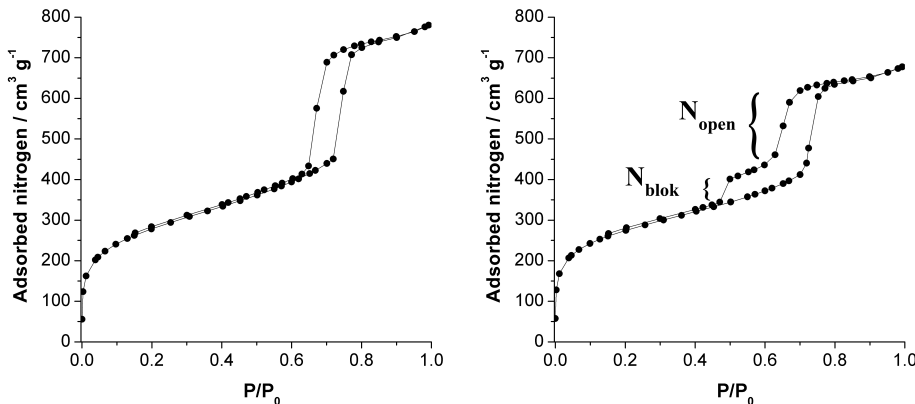
11.4 Doorgroden van mesostructuur vorming

Bij het onderzoeken van de invloed van pH op mesostructuur vorming, werden etheen-PMOs bekomen die eigenaardige hysteresisen vertoonden in hun stikstof fysisorptie isothermen. Uit bijkomend onderzoek bleek een verband te bestaan tussen de pH van het synthesemengsel en de vorm van deze hysteresislussen. Om dit verband te verklaren en de structuur van deze materialen te achterhalen, werd een uitvoerige karakterisatie uitgevoerd.

11.4.1 Stikstof fysisorptie analyse

Typische stikstof isothermen van etheen-PMOs met open cilindrische poriën worden weergegeven in Figuur 11.6A. De porievorm kan afgeleid worden uit de type hysteresislus ($\text{H}1$ type). De vorm van de hysteresislus in de stikstof isothermen weergegeven in Figuur 11.6B, is wat complexer. De tweestaps desorptie isotherm suggerert de aanwezigheid van zowel open cilindrische als geblokkeerde poriën. Hierbij kan de desorptiestap bij relatieve hoge drukken worden toegeschreven aan de

desorptie van stikstof uit open cilindrische poriën, terwijl de uitgestelde desorptiestap gerelateerd kan worden aan poriën waaruit het stikstof moeilijker desorbeert. Dit fenomeen kan worden veroorzaakt als de poriën ingesloten zijn door smallere poriën of als de poriën kleine poriemonden bevatten (bottle necks). Hierdoor wordt de capillaire evaporatie van het gecondenseerde stikstof in de ingesloten poriekeren uitgesteld tot de dampdruk verlaagd wordt onder de evenwichtsdesorptie druk van de poriemonden.

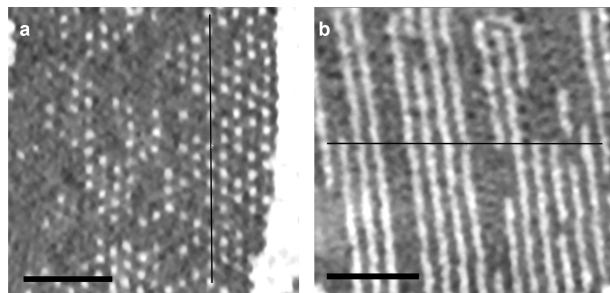


Figuur 11.6: N_2 -isothermen van etheen-PMOs met verschillende poriestructuren. A) PMO met open cilindrische poriën en B) PMO met zowel open en geblokkeerde mesoporiën.

Heel merkwaardig, maar terzelfdertijd interessant, is de lineaire correlatie tussen de zuurtegraad van een synthetemengsel en de graad van porieblokkering in het gevormde PMO materiaal. Hoewel dit op het eerste zicht een kinetisch fenomeen lijkt te zijn, kunnen PMOs worden gesynthetiseerd bij zeer lage pH zonder het voorkomen van porieblokkering, door het toevoegen van kleine hoeveelheden *n*-butanol. Deze gegevens suggereren dat het voorkomen van porieblokkering geen zuiver kinetisch gebeuren is. Om deze bevindingen verder te verklaren en de mesostructuur vorming te doorgronden werd een gedetailleerde studie gedaan, gebruik makende van SAXS (small-angle X-ray scattering), TEM (transmission electron microscopy) en ET (electron tomography).

11.4.2 Opheldering van PMO structuren met SAXS, TEM en ET

Bij het vergelijken van de SAXS, TEM en ET data met de stikstof fysisorptie data, kan de porieblokkering worden toegeschreven aan het opvullen van de mesoporiën met vast materiaal en aan het inkorten van de poriekanalen. Dit fenomeen wordt geïllustreerd door de ET-opnames in Figuur 11.7. Hierop zijn de hexagonaal geordende mesoporiën duidelijk te zien. Sommige van de poriën zijn echter gevuld met materiaal, m.a.w. er ontbreken poriën daar waar ze normaal worden verwacht, rekening houdend met het 2D hexagonale rooster (zie Figuur 11.7b).

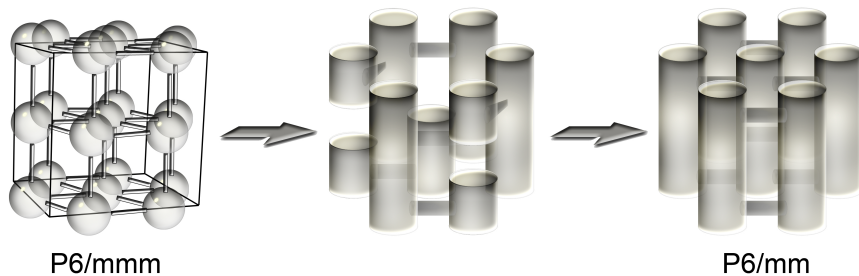


Figuur 11.7: ET-opnames van een etheen PMO met zowel open als geblokkeerde poriën.
 (a) Gevulde poriën zichtbaar, parallel aan de porierichting; (b) Ingekorte poriën zichtbaar, loodrecht op de porierichting. De zwarte lijnen geven de positie van het andere snijvlak. Schaalbalken zijn 50 nm.

Hoe lager de pH van het reactiemengsel, hoe meer mesoporiën worden opgevuld met vast materiaal. Dit fenomeen verklaart de uitgestelde desorptiestap in de stikstof fysisorptie isothermen en rationaliseert tevens de correlatie tussen pH en porieblokkering. Indien niet alle poriën opgevuld zijn met materiaal zal niet al het stikstof worden ingesloten in de poriën en wordt een tweestaps desorptie isotherm bekomen. Bijgevolg is de hysteresis van dergelijk materiaal een combinatie van een H1 en H2 type hysteresis. Met toenemende fractie aan geblokkeerde poriën ten opzichte van open poriën, bij dalende pH, zal de hoeveelheid stikstof dat desorbeert bij een relatieve lage druk toenemen, en zal de hysteresis geleidelijk overgaan naar het type H2.

Bij zeer lage pH ($-\log \text{HCl} = -0.2$) treedt er tevens een verandering in mesostructuur op van 2D hexagonaal geordende cilindrische poriën naar een 3D hexagonaal geordende sferische poriën. Deze sferische poriën kunnen beschouwd worden als ingesloten holtes die onderling verbonden zijn met elkaar door smalle kanalen. In dit geval vertoont het PMO materiaal een type H2 hysteresis in de stikstof isothermen, die gerelateerd kan worden aan de afwezigheid van open cilindrische poriën, de insluiting van de mesoporiën en de opvulling van de poriën met vast materiaal. De invloed van de pH op de poriestructuur van deze PMOs is geassocieerd met een verandering in de hydrofobe/hydrofiele volume ratio van het surfactant. Bij een toenemende zuurtegraad van het synthesemengsel, zal de ionisatie van de ethyleen oxide ketens van het surfactant de hydrofiliciteit van deze ketens relatief verhogen ten opzichte van de hydrofobe ketens. Dit zorgt voor een toename van de oppervlaktekromming van de mesofase en induceert een fasetransformatie van cilindrische naar sferische micellen. Anderzijds zullen deze sferische micellen bij een toenemende pH coaguleren tot een 2D hexagonaal geordende structuur, met de vorming van cilindrische poriën tot gevolg. Deze fasetransformatie wordt schematisch weergegeven in Figuur 11.8.

Wanneer *n*-butanol wordt toegevoegd aan het reactiemengsel, wordt de generatie van sferische poriën omzeilt en worden cilindrische poriën preferentieel gevormd, zelfs bij hele lage pH-waarden. Hierbij zorgt *n*-butanol voor de dehydratatie van de ethyleen oxide ketens in de micel corona, welke de transitie van sferische naar cilindrische micellen induceert.



Figuur 11.8: Schematische illustratie van de fasetransformatie van 3D hexagonaal geordende sferen naar 2D hexagonaal geordende cilinders.

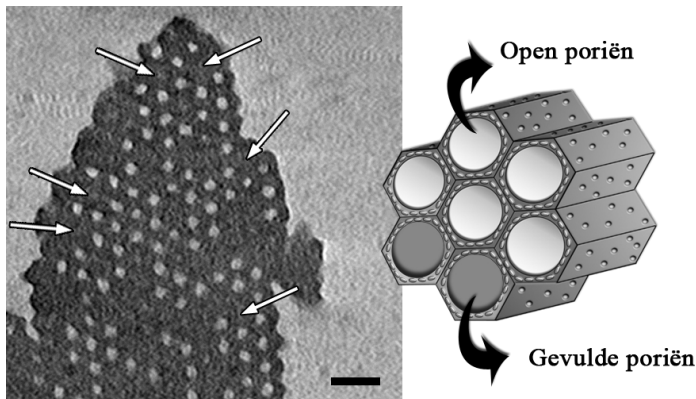
11.5 PMOs met controleerbare eigenschappen

De mechanismen die betrokken zijn bij de vorming van geordende mesostructuren hangen nauw samen met de synthesecondities, en vormen een complex systeem waarin talrijke parameters de uitkomst beïnvloeden. De kleinste verandering van één van deze parameters, zoals temperatuur, pH, molaire samenstelling, reactietijd, druk, aanwezigheid van additieven,... kan een grote impact uitoefenen op de structuur vorming. In deze context werden een aantal reactieparameters onderzocht, met het oog op het controleren van de mesostructuur vorming en het sturen van de synthese naar materialen met gewenste eigenschappen.

11.5.1 Controle van de porositeit

In eerste instantie werd de porositeit van etheen-PMOs verhoogd door het optimaliseren van de surfactant extractie. Tot heden werden PMOs geëxtraheerd met aangezuurd ethanol, ongeacht het aangewende surfactant. Hoewel ethanol een heel efficiënt solvent is voor het verwijderen van ionische surfactanten, werd de efficiëntie ervan nog niet in detail onderzocht voor het verwijderen van polymerische surfactanten zoals het triblok copolymer P123. Uit dit onderzoek bleek aceton een superieur solvent te zijn, waarbij reeds na 5 uur extractie 94 % van het surfactant kon worden verwijderd. Als gevolg vertonen PMOs die geëxtraheerd worden met aceton een verhoogd specifiek oppervlak, grotere porievolumes en grotere mesoporiën.

De porositeit van etheen-PMOs kan tevens worden gecontroleerd door het optimaliseren van de reactiecondities. Hierbij speelt o.a. de pH van het reactiemengsel, de aanwezigheid van cosolventen en de concentratie aan cosolvent een belangrijke rol. Als er geen cosolvent wordt gebruikt tijdens de PMO synthese, is de optimum pH = 0.9. Bij deze pH wordt het hoogste specifiek oppervlakte en porievolume bekomen. Wanneer de pH wordt verlaagd, zorgt de excessieve polycondensatie van de precursor ervoor dat een fractie van de mesoporiën wordt gevuld met vast materiaal (zie Figuur 11.9) waardoor het porievolume en specifiek oppervlakte dalen. Anderzijds, wanneer de pH wordt verhoogd boven het optimum, neemt de templaat-precursor interactie af waardoor tevens de kwaliteit van het materiaal reduceert. Wanneer tijdens de PMO synthese *n*-butanol wordt gebruikt als cosolvent, wordt



Figuur 11.9: ET-opname van etheen-PMO waarvan sommige poriën gevuld zijn. Hierdoor daalt het specifiek oppervlakte en porievolume van het materiaal. Schaalstaaf is 20 nm.

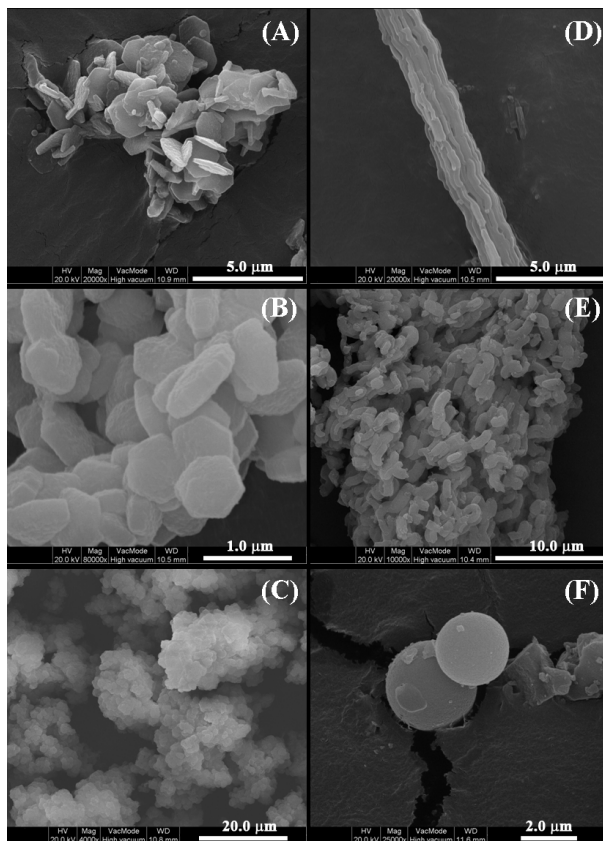
het opvullen van de mesoporiën met vast materiaal voorkomen (zoals besproken in 11.4.2). Omwille van de verhoogde templaat-precursor interactie, is de optimale pH (0.1) bijgevolg veel lager dan in het geval er geen *n*-butanol wordt aangewend. Door het regelen van de reactietemperatuur kan tevens de poriegrootte, -structuur, -connectiviteit, en -volume van etheen-PMOs worden gecontroleerd. Hierbij heeft de temperatuur een impact op de hydrofobicitet van de PEO ketens in het surfactant. Door het verhogen van de reactietemperatuur worden grotere mesoporiën bekomen als gevolg van het terugtrekken van de PEO ketens in de hydrofobe micelkernen. Tevens brengt de temperatuursverhoging een groepering van PEO ketens met zich mee, waardoor de microporeuze connecties tussen de primaire mesoporiën worden vergroot. Hierbij kunnen secundaire mesoporiën worden gegenereerd.

11.5.2 Controle van de externe morfologie

Naast het controleren van de porositeit van etheen-PMOs, kan door het toepassen van verschillende cosolventen, en het “tunen” van de concentratie ervan, de morfologie van etheen-PMOs accuraat worden gecontroleerd. Hierbij kunnen kristalachtige hexagonale plaatjes, vezelachtige structuren of sferische partikels worden bekomen, zoals voorgesteld in Figuur 11.10. Controle van de partikel morfologie is een krachtig middel in de ontwikkeling van materialen voor welbepaalde toepassingen. Voor chromatografische applicaties zijn bijvoorbeeld sferische partikels vereist voor efficiënte kolomspacking en bevredigende scheidingseigenschappen, terwijl voor katalytische toepassingen kristalachtige hexagonale plaatjes met korte poriekanalen interessant kunnen zijn doordat deze diffusieproblemen kunnen limiteren.

11.5.3 Thermische geïnduceerde vorming van multifunctionele PMOs

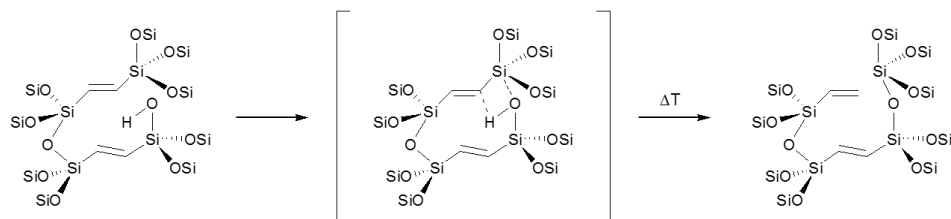
Bij spectroscopisch onderzoek van het zelf-hydrofobisatieproces, waarbij etheen-PMOs hydrofober worden door een thermische behandeling, werd een bijzondere



Figuur 11.10: FE-SEM beelden van etheen-PMOs gesynthetiseerd met verschillende co-solventen of cosolvent concentraties: (A) *n*-ethanol, (B) *n*-propanol, (C) *n*-pentanol, (D) *n*-butanol:P123 = 95:1, (E) *n*-butanol:P123 = 115:1 and (F) *n*-butanol:P123 = 175:1.

nevenreactie vastgesteld. Hierbij worden etheen-bruggen in de poriewanden van etheen-PMOs omgezet tot terminale vinylische functies. Aan de hand van FT-Raman, DRIFT, en ^1H - ^{13}C CP MAS NMR stellen we een mechanisme voor waarin etheen-bruggen vinylische groepen en siloxaan-bruggen thermisch worden gegeneerd *via* proton transfer van PMO silanolen naar etheen-bruggen, zoals voorgesteld in Figuur 11.11.

Deze hypothese werd indirect bevestigd door het hydrofobiseren van het PMO oppervlakte met hexamethyldisilazaan, vooraleer de thermische behandeling werd uitgevoerd. Wanneer de silanolen volgens deze methode worden verwijderd, worden geen vinylische functies meer gegenereerd *via* de thermische behandeling. Dit toont aan dat de silanolen van het PMO oppervlakte effectief betrokken zijn in deze thermisch geïnduceerde metamorfose. Deze eenvoudige techniek laat toe om multifunctionele hybride materialen te synthetiseren die directe ankerpunten bevatten voor katalysatoren. Dergelijke materialen kunnen bijgevolg van significant belang zijn in katalytische toepassingen.



Figuur 11.11: Schematische voorstelling van de silanol-ethene interactie en de thermisch geïnduceerde splitsing van een Si–C binding van een etheen-brug, waarbij een terminale vinylische groep en een siloxaan-brug wordt gevormd.

11.6 Etheen-PMOs met ultra-large mesoporiën

Door hun structurele rigiditeit en controleerbare fysische en chemische eigenschappen, zijn PMOs heel interessant voor toepassingen in de katalyse, milieutechnologie en chromatografie. De toepasbaarheid van PMOs, en mesoporeuze materialen in het algemeen, wordt echter vaak gelimiteerd door de grootte van hun mesoporiën, welke typisch variëren tussen 2 en 8 nm. In sommige toepassingen zoals biokatalyse of “controlled drug release”, zijn grotere poriën vereist om de diffusie, adsorptie of immobilisatie van grote biomoleculen (zoals enzymen, proteïnen of drugs) toe te laten. Tot heden was de ontwikkeling van etheen-PMOs met mesoporiën groter dan 10 nm nog niet verwezenlijkt. Met dit doel voor ogen, werd de mogelijkheid onderzocht om etheen-PMOs met “ultra-large” mesoporiën te ontwikkelen door gebruik te maken van P123 als surfactant in combinatie met verschillende zwellings agentia, zoals 1,3,5-trimethylbenzeen (TMB).

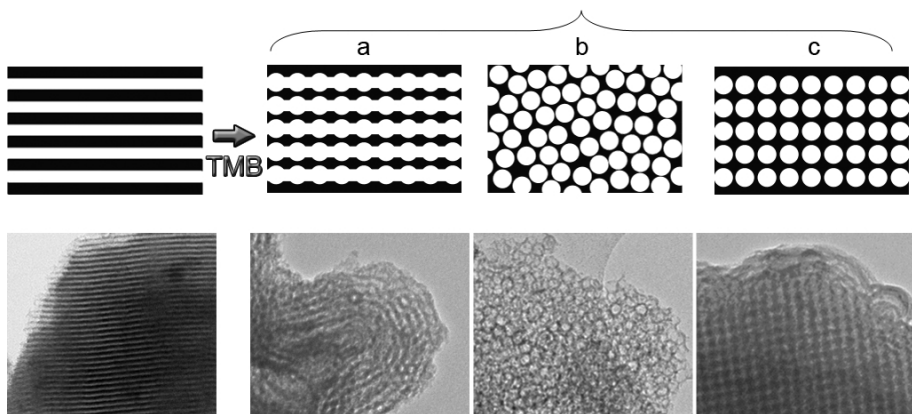
Deze methode van porie-expansie rust op het principe dat hydrofobe additieven migreren naar de hydrofobe micelkernen van P123, waardoor deze opzwollen en bijgevolg leiden tot mesostructuren met grotere mesoporiën.

Via deze techniek worden etheen-PMOs ontwikkeld met mesoporiën tot 28.3 nm en porievolumes tot 2.25 cm³/g. Bovendien vertonen deze materialen relatief nauwe poriegrootte distributies, hoge specifieke oppervlaktes en aanzienlijke microporievolumes. Ondanks hun grote mesoporiën zijn deze PMOs tevens heel stabiel. Met een houdbaarheidsperiode van meer dan een jaar, kunnen deze ultra-large pore PMOs aan de lucht worden opgeslagen zonder te degraderen.

Naast het beïnvloeden van de poriegrootte en -volume, hebben zwelings agentia ook een invloed op de mesostructuur vorming. Deze etheen-PMOs met “ultra-large” mesoporiën vertonen verscheidene poriesystemen, waaronder schuimachtige poriestructuren met uniforme mesoporiën, 3D geordende sferische poriën en “nodular strings” (cilinders opgebouwd uit lineair verbonden sferische poriën). Deze fasevergelijking met bijhorende TEM-beelden wordt weergegeven in Figuur 11.12.

Deze fasetransformatie, geïnduceerd door het zwelings reagens, wordt veroorzaakt door een alteratie in de oppervlaktekromming van de surfactantmicellen. Door een invloed uit te oefenen op de hydrofobe/hydrofiele volume ratio van het surfactant, induceren hydrofobe zwelers een transformatie van cilindrische naar sferische micellen, welke leidt tot de vorming van sferische poriën.

Naast het ontwikkelen van PMOs met monomodale ultra-large mesoporiën, kunnen



Figuur 11.12: TEM-beelden met bijhorende schematische illustraties die de fasetransformatie, geïnduceerd door TMB, weergeven. (A) nodular strings, (B) schuimachtige poriestructuur, and (C) geordende sferische poriën.

tevens etheen-PMOs met bimodale poriestructuren worden ontwikkeld. Dergelijke materialen vertonen twee poriegrootte distributies. Door de reactiecondities te “tunen” kunnen PMOs worden gevormd die bestaan uit onderling verbonden poriesystemen met verschillende poriediameters. Deze techniek laat dus toe om hiëarchische poriestructuren te ontwikkelen, welke interessante toepassingen kunnen hebben in de bulkchemie, waar reagentia gemakkelijk moeten kunnen diffunderen in de poriën terwijl de het interne oppervlak maximaal wordt benut.

11.7 Olefinische PMOs: het uibreiden van hun draagwijdte

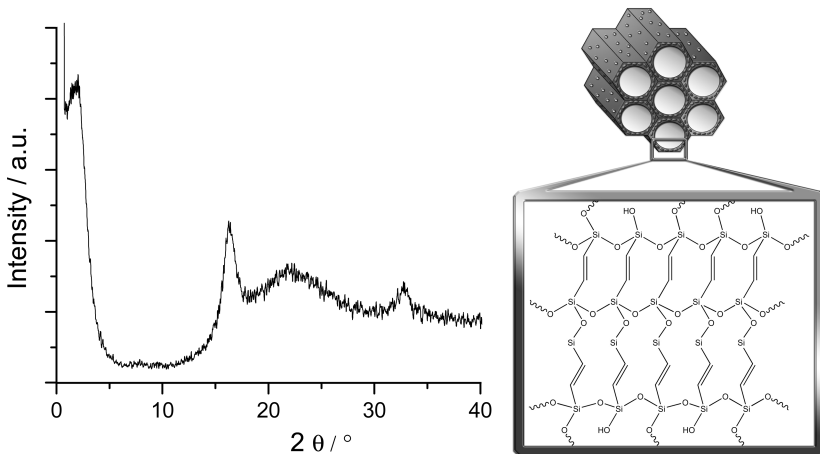
11.7.1 Buteen-PMOs

Tot heden bestond de familie van olefinische PMOs enkel uit deze met etheengebrugde organische functies. Gezien deze PMOs behoren tot de meest veelbelovende hybride materialen, in termen van functionaliteit en toepasbaarheid, is er nood aan verder onderzoek om deze klasse van materialen verder uit te breiden. In deze context werd de nieuwe organosilaanverbinding 1,4-bis(trimethoxysilyl)buteen, die tijdens dit doctoraatsonderzoek werd ontwikkeld (zie 11.2.2), toegepast als precursor voor de synthese van een nieuwe olefinische PMO, de buteen-PMO.

Hoewel tijdens dit onderzoek de resulterende hybride materialen nog geen geordende mesoporiën vertoonden, zijn de eerste resultaten veelbelovend. In eerste plaats omdat deze materialen ultra-large mesoporiën van 21 nm kunnen bevatten, zonder het toepassen van zwellers. Dit fenomeen is heel uniek, en zet aan tot verder onderzoek. Bovendien vertonen deze materialen een sferische morfologie waardoor ze potentieel interessant kunnen zijn voor chromatografische toepassingen.

11.7.2 Etheen-PMOs met semi-kristallijne wanden

Door het aanwenden van gemini surfactanten onder basische omstandigheden kunnen PMOs worden ontwikkeld waarvan de etheen-bruggen in de poriewanden ordening vertonen. Dit werd afgeleid uit zowel hoge resolutie TEM-beelden, waarop moleculaire ordening waarneembaar is, en X-stralen diffractie, welke pieken in het wide-angle gebied vertonen (zie Figuur 11.13).



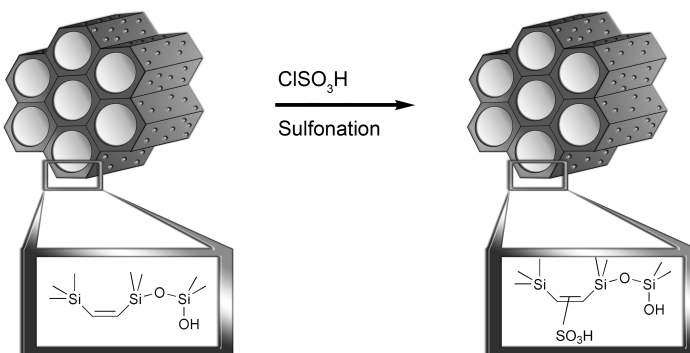
Figuur 11.13: XRD-plot van een etheen-PMO met moleculaire ordening van etheen-bruggen in de poriewanden, zoals schematisch voorgesteld.

Hoewel materialen met hoge specifieke oppervlaktes en porievolumes werden ontwikkeld door het optimaliseren van de synthesecondities (pH, surfactant concentratie, en *n*-butanol concentratie), moet de synthese nog verder worden geoptimaliseerd om semi-kristallijne etheen-PMOs met grotere mesoporiën te bekomen.

11.7.3 Sulfonzure etheen-PMOs

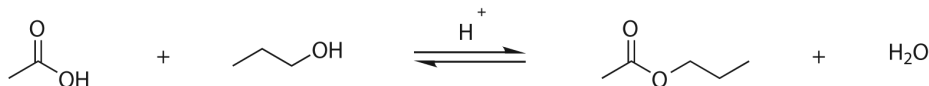
Met het oog op het ontwikkelen van PMOs die kunnen toegepast worden in de katalyse, werd een methode onderzocht waarbij PMOs *via* een éénstaps modificatieprocedure worden omgezet tot zure katalysatoren. Deze methode heeft als voordeel dat het incorporeren van katalytische sites geen impact heeft op de mesostructuur vorming. M.a.w. PMOs met controleerbare eigenschappen kunnen vooraf worden ontwikkeld en door middel van een eenvoudige modificatie worden gebruikt als katalysator.

In deze context werden sulfonzure PMOs ontwikkeld door het sulfoneren van de PMO etheenfuncties met chlorosulfonzuur, zoals voorgesteld in Figuur 11.14). *Via* deze procedure kunnen PMOs met ongeveer 1 mmol H⁺/g worden bereid. Aan de hand van stikstof fysisorptie, kon aangetoond worden dat de sulfoneringsreactie geen negatieve impact heeft op de PMO structuur. Deze syntheseprocedure laat de ontwikkeling toe van zure PMOs met controleerbare eigenschappen, die kunnen gebruikt worden in zuur gekatalyseerde reacties.



Figuur 11.14: Direct sulfonation of ethylene-bridged PMOs with chlorosulfonic acid.

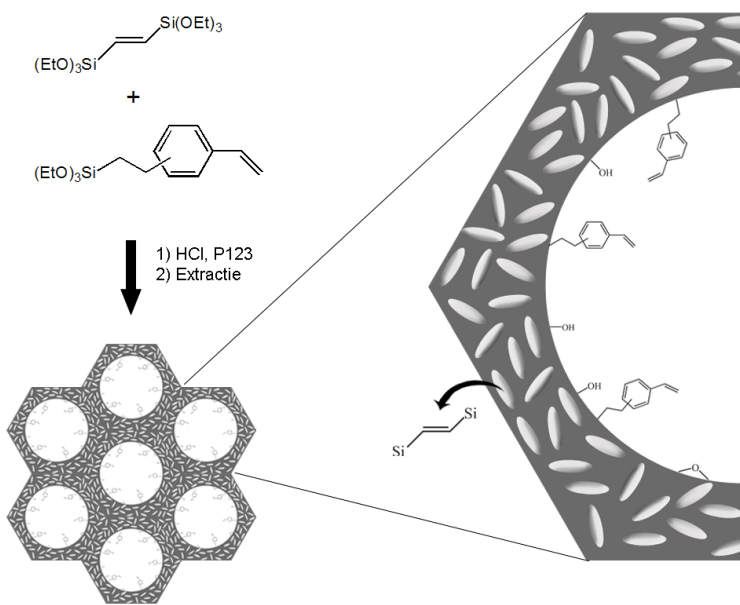
Als modelreactie om de activiteit van de betreffende sulfonzure PMOs te testen, werd de esterificatie van *n*-propanol met azijnzuur gekozen (zie Figuur 11.15). De reacties werden gevolgd in functie van de tijd door middel van GC. De sulfonzure PMOs vertonen een indrukwekkend hoge activiteit in deze esterificatiereactie. Bovendien hebben ze een activiteit die vergelijkbaar is aan deze van de homogene katalysator *p*-tolueensulfonzuur. De hoge activiteit van de sulfonzure PMOs kan het gevolg zijn van hun hoog specifiek oppervlak en grote open mesoporïën. Deze factoren hebben een gunstige invloed op de diffusie eigenschappen van de materialen, en zorgen voor een goede en snelle toegang tot de katalytische sites. Hiertegenover staat wel dat de reactietemperatuur niet te hoog mag zijn, om degeneratie van de PMO te voorkomen. Wanneer de reactie wordt uitgevoerd bij 90 °C blijft de PMO structuur intact tijdens de esterificatiereactie en vertoont geen significante daling in specifiek oppervlak. Deze PMOs vertonen echter één groot nadeel, namelijk dat ze na reactie moeten worden gereactiveerd om het uitvoeren van meerdere reacties na elkaar toe te laten. Dit fenomeen moet nog verder worden onderzocht en opgelost.



Figuur 11.15: Zuurgekatalyseerde esterificatie van *n*-propanol met azijnzuur.

11.7.4 Styreen-Etheen-PMOs: dragermaterialen voor olefine metathese katalysatoren

Tegenwoordig is olefine metathese niet meer weg te denken uit de chemie. Door het faciliteren in de uitwisseling van olefine substituenten maken metathese katalysatoren tal van reacties mogelijk in de organische, polymeer en farmaceutische chemie. Hierbij spelen ruthenium complexen een heel belangrijke rol als gevolg van hun hoge stabiliteit ten opzichte van lucht en water en door hun tolerantie tegenover



Figuur 11.16: Schematische illustratie van een styreen-etheen-PMO synthese.

vele functionele groepen.

Helaas vereisen metathese reacties vaak relatief grote hoeveelheden katalysatoren, vooral in totaalsynthesen. Bovendien is de meest ongewenste eigenschap van moderne homogene metathese katalysatoren de contaminatie van de reactieproducten die ze met zich meebrengen. De homogene aard van deze complexen impliceert dat vaak ingewikkelde en tijdrovende chromatografische technieken vereist zijn om de met zware metalen gecontamineerde reactieproducten op te zuiveren. Daarom is het ontwikkelen van groenere metathese katalysatoren van groot belang.

Omwillen van deze argumenten wordt de ontwikkeling van olefine metathese katalysatoren die gemakkelijk af te zonderen zijn van de reactieproducten en die herbruikbaar zijn in meerdere opeenvolgende reacties, gestimuleerd. Heterogene katalysatoren hebben echter vaak het grote nadeel dat ze minder actief zijn dan hun homogene analogen en dat ze diffusieproblemen met zich meebrengen. Een ideale katalysator is er één die de voordelen van homogene en heterogene systemen combineert, zijnde: hoge activiteit, gemakkelijk af te zonderen, recycleerbaar en zero contaminatie. In het kader van de ontwikkeling van dergelijke katalysatoren, wordt veel onderzoek verricht in het immobiliseren van actieve homogene katalysatoren op verscheidene dragermaterialen. Hierbij spelen silica materialen een belangrijke rol omwillen van hun hoge chemische, thermische en mechanische stabiliteit. Tevens kunnen silicas gemakkelijk worden afgescheiden *via* een eenvoudige filtratietechnieken. Door hun controleerbare chemische, fysische en structurele eigenschappen zijn PMO materialen ideaal voor het ontwikkelen van hybride katalysatoren voor olefine metathese. Tot heden zijn ze echter nog nooit geïmplementeerd als dragerma-

terialen voor olefine metathese complexen. In deze context werd een PMO materiaal ontwikkeld dat voorzien is van functionele groepen die het immobiliseren van actieve homogene olefine metathese katalysatoren mogelijk maakt. Hierbij werd een bifunctionele PMO gesynthetiseerd *via* een co-condensatie reactie tussen 1,2-bis(triethoxysilyl)ethene en styrylethyltrimethoxysilaan, in aanwezigheid van het surfactant Pluronic P123. In Figuur 11.16 wordt de synthese van deze PMO schematisch weergegeven.

De incorporatie van styreen groepen in de PMO matrix werd bevestigd door FT-Raman spectroscopie. Bovendien werd aan de hand van stikstof fysisorptie vastgesteld dat de betreffende bifunctionele PMO een open mesoporiestructuur heeft met poriën van 6.1 nm, een specifiek oppervlak van $730 \text{ m}^2/\text{g}$ en een porievolume van $0.752 \text{ cm}^3/\text{g}$.

Deze nieuwe bifunctionele styreen-etheen-PMOs kunnen gemakkelijk worden omgezet in actieve hybride olefine metathese katalysatoren *via* een éénstaps modificatie procedure. Hierbij kunnen verscheidene ruthenium carbeen complexen worden verankerd aan het PMO oppervlak via een olefine metathese reactie.

References

- [1] Ebbell, B.; Banov, L. *The Papyrus Ebers : the greatest Egyptian medical document*; Levin and Munksgaard, 1937.
- [2] Scheele, C. W.; Bergman, T. *Chemische Abhandlung von der Luft und dem Feuer*; 1777.
- [3] Fontana, F. *Memorie di matematica e di fisica della Societ'a italiana delle Scienze* **1782**, 1, 648.
- [4] de Morveau, L. B. G. *Observations et Mémoires sur la Physique, sur l'Histoire Naturelle et sur les Arts et Métiers* **1783**, 22, 447.
- [5] de Morveau, L. B. G. *Observations et Mémoires sur la Physique, sur l'Histoire Naturelle et sur les Arts et Métiers* **1783**, 23, 116.
- [6] de Morveau, L. B. G. *Observations et Mémoires sur la Physique, sur l'Histoire Naturelle et sur les Arts et Métiers* **1783**, 23, 184.
- [7] Priestley, J. *Observations et Mémoires sur la Physique, sur l'Histoire Naturelle et sur les Arts et Métiers* **1779**, 13, 128.
- [8] Priestley, J. *Expériences et observations sur différentes branches de la physique, avec une continuation des observations sur l'air, ouvrage traduit de l'anglois de M. J. Priestley, par M. Gibelin*; Paris, Nyon l'ainé, 1782; Vol. 1.
- [9] Lavoisier, A. L. *Mémoire dans lequel on a pour objet de prouver que l'eau n'est point une substance simple, un élément proprement dit, mais qu'elle est susceptible de décomposition et de recomposition*; Académie des sciences, 1781; Vol. 2.
- [10] Lowitz, J. T. *Crell's Chemische Annalen* **1786**, 1, 211.
- [11] Lowitz, J. T. *Crell's Chemische Annalen* **1788**, 2, 36.
- [12] Anderson, A. H. *Acta Pharmacol* **1946**, 2, 69.
- [13] Orfila, M. J. B.; Waller, J. A. *A general system of toxicology : or, A treatise on poisons, drawn from the mineral, vegetable, and animal kingdoms, considered as to their relations with physiology, pathology, and medical jurisprudence*; E. Cox, 1821.

- [14] Kayser, H. *Annalen der Physik (Wiedemann's Annalen)* **1881**, 250, 450.
- [15] de Saussure, N. H. *Annalen der Physik (Gilbert's Annalen)* **1814**, 47, 113.
- [16] Mitscherlich, E. A. *Poggendorff's Annalen* **1843**, 59, 94.
- [17] Cronstedt, A. F. *Kongliga Vetenskaps Academiens Handlingar Stockholm* **1756**, 17, 120.
- [18] Baerlocher, C.; McCusker, L. B.; Olson, D.; Meier, W. M.; International Zeolite Association. Structure, C. *Atlas of zeolite framework types*, Sixth Revised Edition ed.; Published on behalf of the Structure Commission of the International Zeolite Association by Elsevier, 2007.
- [19] Deer, W. A.; Howie, R. A.; Wise, W. S.; Zussman, J. *Framework silicates : silica minerals, feldspathoids and the zeolites*; Rock forming minerals, v. 4B; Geological Society, 2004; p 516.
- [20] de St. Claire Deville, H. *Comptes rendus des séances de l'Académie des sciences* **1862**, 54, 324.
- [21] McBain, J. W. *The sorption of gases and vapours by solids*; London, G. Routledge, 1932.
- [22] Barrer, R. M. *Journal of the Chemical Society* **1948**, 127.
- [23] Milton, R. M. *Society of Chemical Industry* **1968**, 199.
- [24] Milton, R. M. *Molecular Sieve Adsorbents*, U.S. Patent 2,882,243, 1959.
- [25] Milton, R. M. *Molecular Sieve Adsorbents*, U.S. patent 2,882,244, 1959.
- [26] Rabo, J. A.; Schoonover, M. W. *Applied Catalysis a-General* **2001**, 222, 261.
- [27] Barrer, R. M.; Denny, P. J. *Journal of the Chemical Society* **1961**, 971.
- [28] Wadlinger, R. L. *Catalytic composition of a crystalline zeolite*, U.S. Patent 3,308,069, 1967.
- [29] Argauer, R. J.; Kensington, M.; Landolt, G. R.; Audubon, N. *Crystalline zeolite ZSM-5 and method of preparing the same*, U.S. Patent 3,702,886, 1972.
- [30] Bhatia, S. *Zeolite catalysis : principles and applications*; CRC Press, 1990.
- [31] Pauling, L. *Proceedings of the National Academy of Sciences* **1930**, 16, 453.
- [32] Bergerhoff, G.; Baur, W.; Nowacki, W. *Neues Jahrbuch fuer Mineralogie-Monatshefte* **1958**, 193.
- [33] Breck, D. W.; Tonawanda, N. *Crystalline zeolite Y*, U.S. Patent 3,130,007, 1961.
- [34] Daniels, R. H.; Kerr, G. T.; Rollmann, L. D. *Journal of the American Chemical Society* **1978**, 100, 3097.

- [35] Barrer, R. M.; Villiger, H. *Zeitschrift Fur Kristallographie Kristallgeometrie Kristallphysik Kristallchemie* **1969**, *128*, 352.
- [36] Meier, W. M. *Zeitschrift Fur Kristallographie Kristallgeometrie Kristallphysik Kristallchemie* **1961**, *115*, 439.
- [37] Lapierre, R. B.; Rohrman, A. C.; Schlenker, J. L.; Wood, J. D.; Rubin, M. K.; Rohrbaugh, W. J. *Zeolites* **1985**, *5*, 346.
- [38] Bennett, J. M.; Gard, J. A. *Nature* **1967**, *214*, 1005.
- [39] Wilson, S. T.; Lok, B. M.; Messina, C. A.; Cannan, T. R.; Flanigen, E. M. *Journal of the American Chemical Society* **1982**, *104*, 1146.
- [40] Wilson, S. T.; Lok, B.; Flanigen, E. *Crystalline metallophosphate compositions*, U.S. Patent 4,310,440, 1982.
- [41] Lok, B. M.; Messina, C. A.; Patton, R. L.; Gajek, R. T.; Cannan, T. R.; Flanigen, E. M. *Journal of the American Chemical Society* **1984**, *106*, 6092.
- [42] Messina, C. A.; Lok, B.; Flanigen, E. *Crystalline Ferroaluminophosphates*, U.S. Patent 4,554,143, 1985.
- [43] Wilson, S. T.; Flanigen, E. *Crystalline Metal Aluminophosphates*, U.S. Patent 4,567,029, 1986.
- [44] Flanigen, E. M.; Lok, B. M.; Patton, R. L.; Wilson, S. T. *Pure and Applied Chemistry* **1986**, *58*, 1351.
- [45] Davis, M. E.; Saldarriaga, C.; Montes, C.; Garces, J.; Crowder, C. *Nature* **1988**, *331*, 698.
- [46] Davis, M. E.; Saldarriaga, C.; Montes, C.; Garces, J.; Crowder, C. *Zeolites* **1988**, *8*, 362.
- [47] Davis, M. E. *Chemistry-a European Journal* **1997**, *3*, 1745.
- [48] Li, H. X.; Davis, M. E. *Catalysis Today* **1994**, *19*, 61.
- [49] Freyhardt, C. C.; Tsapatsis, M.; Lobo, R. F.; Balkus, K. J.; Davis, M. E. *Nature* **1996**, *381*, 295.
- [50] Lobo, R. F.; Tsapatsis, M.; Freyhardt, C. C.; Khodabandeh, S.; Wagner, P.; Chen, C. Y.; Balkus, K. J.; Zones, S. I.; Davis, M. E. *Journal of the American Chemical Society* **1997**, *119*, 8474.
- [51] Wessels, T.; Baerlocher, C.; McCusker, L. B.; Creyghton, E. J. *Journal of the American Chemical Society* **1999**, *121*, 6242.
- [52] Wagner, P.; Yoshikawa, M.; Lovallo, M.; Tsuji, K.; Tsapatsis, M.; Davis, M. E. *Chemical Communications* **1997**, 2179.

- [53] Yoshikawa, M.; Wagner, P.; Lovallo, M.; Tsuji, K.; Takewaki, T.; Chen, C. Y.; Beck, L. W.; Jones, C.; Tsapatsis, M.; Zones, S. I.; Davis, M. E. *Journal of Physical Chemistry B* **1998**, *102*, 7139.
- [54] Richerson, D. W. *Modern ceramic engineering : properties, processing, and use in design*, 3rd ed.; Materials engineering, 29; CRC Press, 2006.
- [55] Ray, S. S.; Okamoto, M. *Progress in Polymer Science* **2003**, *28*, 1539.
- [56] Wang, M. S.; Pinnavaia, T. J. *Chemistry of Materials* **1994**, *6*, 468.
- [57] Lan, T.; Kaviratna, P. D.; Pinnavaia, T. J. *Abstracts of Papers of the American Chemical Society* **1994**, *208*, 284.
- [58] Liu, L. M.; Qi, Z. N.; Zhu, X. G. *Journal of Applied Polymer Science* **1999**, *71*, 1133.
- [59] Hasegawa, N.; Okamoto, H.; Kato, M.; Usuki, A. *Journal of Applied Polymer Science* **2000**, *78*, 1918.
- [60] Jaynes, W. F.; Boyd, S. A. *Soil Science Society of America Journal* **1991**, *55*, 43.
- [61] Haderlein, S. B.; Weissmahr, K. W.; Schwarzenbach, R. P. *Environmental Science and Technology* **1996**, *30*, 612.
- [62] Manning, B. A.; Goldberg, S. *Environmental Science and Technology* **1997**, *31*, 2005.
- [63] Lin, S. H.; Juang, R. S. *Journal of Hazardous Materials* **2002**, *92*, 315.
- [64] Lagaly, G.; Beneke, K. *Colloid and Polymer Science* **1991**, *269*, 1198.
- [65] Khan, S. A.; Riazurrehman,; Khan, M. A. *Waste Management* **1995**, *15*, 271.
- [66] Barbier, F.; Duc, G.; Petit-Ramel, M. *Colloids and Surfaces a-Physicochemical and Engineering Aspects* **2000**, *166*, 153.
- [67] Komarneni, S.; Kozai, N.; Paulus, W. J. *Nature* **2001**, *410*, 771.
- [68] Villemin, D.; Martin, B. *Journal of Chemical Research-S* **1994**, 146.
- [69] Fraile, J. M.; Garcia, J. I.; Massam, J.; Mayoral, J. A. *Journal of Molecular Catalysis a-Chemical* **1998**, *136*, 47.
- [70] Kloprogge, J. T. *Journal of Porous Materials* **1998**, *5*, 5.
- [71] Vaccari, A. *Applied Clay Science* **1999**, *14*, 161.
- [72] Varma, R. S. *Tetrahedron* **2002**, *58*, 1235.
- [73] Speight, J. G. *Petroleum chemistry and refining*; Applied energy technology series; Taylor and Francis, 1997.

- [74] Auerbach, S. M.; Carrado, K. A.; Dutta, P. K. *Handbook of layered materials*; M. Dekker, 2004.
- [75] Hettinger, W. P. *Catalysis Today* **1999**, *53*, 367.
- [76] Somasundaran, P. *Encyclopedia of surface and colloid science*; Taylor and Francis, 2006.
- [77] Barrer, R. M.; Macleod, D. M. *Transactions of the Faraday Society* **1955**, *51*, 1290.
- [78] Zhu, L. Z.; Ren, X. G.; Yu, S. B. *Environmental Science and Technology* **1998**, *32*, 3374.
- [79] Meier, L. P.; Nueesch, R.; Madsen, F. T. *Journal of Colloid and Interface Science* **2001**, *238*, 24.
- [80] Brindley, G. W.; Sempels, R. E. *Clay Minerals* **1977**, *12*, 229.
- [81] Lahav, N.; Shani, U.; Shabtai, J. *Clays and Clay Minerals* **1978**, *26*, 107.
- [82] Vaughan, D.; Lussier, R.; Magee, J. *Pillared interlayered clay materials useful as catalysts and sorbents*, U.S. Patent 4,176,090, 1979.
- [83] Vaughan, D.; Lussier, R.; Magee, J. *Stabilized pillared interlayered clays*, U.S. Patent 4,248,739, 1981.
- [84] Vaughan, D.; Lussier, R.; Magee, J. *Pillared interlayered clay products*, U.S. Patent 4,271,043, 1981.
- [85] Magee, J. S.; Mitchell, M. M. *Fluid catalytic cracking : science and technology*; Studies in surface science and catalysis, 76; Elsevier, 1993.
- [86] Ding, Z.; Kloprogge, J. T.; Frost, R. L.; Lu, G. Q.; Zhu, H. Y. *Journal of Porous Materials* **2001**, *8*, 273.
- [87] Beck, J. S.; Vartuli, J. C.; Roth, W. J.; Leonowicz, M. E.; Kresge, C. T.; Schmitt, K. D.; Chu, C. T. W.; Olson, D. H.; Sheppard, E. W.; McCullen, S. B.; Higgins, J. B.; Schlenker, J. L. *Journal of the American Chemical Society* **1992**, *114*, 10834.
- [88] Yanagisawa, T.; Shimizu, T.; Kuroda, K.; Kato, C. *Bulletin of the Chemical Society of Japan* **1990**, *63*, 988.
- [89] Inagaki, S.; Fukushima, Y.; Kuroda, K. *Journal of the Chemical Society- Chemical Communications* **1993**, 680.
- [90] Beck, J. S. *Method for synthesizing mesoporous crystalline material*, U.S. Patent 5,057,296, 1991.
- [91] Kresge, C. T.; Leonowicz, M.; Roth, W.; Vartuli, J. *Synthetic mesoporous crystalline material*, U.S. Patent 5,098,684, 1992.

- [92] Beck, J. S.; Chu, C.-W.; Johnson, I.; Kresge, C.; Leonowicz, M.; Roth, W.; Vartuli, J. *Synthesis of mesoporous crystalline material*, U.S. Patent 5,108,725, 1992.
- [93] Kresge, C. T.; Leonowicz, M. E.; Roth, W. J.; Vartuli, J. C.; Beck, J. S. *Nature* **1992**, *359*, 710.
- [94] Israelachvili, J. N.; Mitchell, D. J.; Ninham, B. W. *Journal of the Chemical Society-Faraday Transactions* **1976**, *72*, 1525.
- [95] Osterholtz, F. D.; Pohl, E. R. *Journal of Adhesion Science and Technology* **1992**, *6*, 127.
- [96] Schubert, U.; Hüsing, N. *Synthesis of inorganic materials*; Wiley-VCH, 2005.
- [97] Iler, R. K. *The chemistry of silica : solubility, polymerization, colloid and surface properties, and biochemistry*; Wiley, 1979.
- [98] Chen, C.-Y.; Li, H.-X.; Davis, M. E. *Microporous Materials* **1993**, *2*, 17.
- [99] Chen, C.-Y.; Burkett, S. L.; Li, H.-X.; Davis, M. E. *Microporous Materials* **1993**, *2*, 27.
- [100] Cheng, C. F.; He, H. Y.; Zhou, W. Z.; Klinowski, J. *Chemical Physics Letters* **1995**, *244*, 117.
- [101] Huo, Q. S.; Margolese, D. I.; Ciesla, U.; Feng, P. Y.; Gier, T. E.; Sieger, P.; Leon, R.; Petroff, P. M.; Schuth, F.; Stucky, G. D. *Nature* **1994**, *368*, 317.
- [102] Huo, Q. S.; Margolese, D. I.; Ciesla, U.; Demuth, D. G.; Feng, P. Y.; Gier, T. E.; Sieger, P.; Firouzi, A.; Chmelka, B. F.; Schuth, F.; Stucky, G. D. *Chemistry of Materials* **1994**, *6*, 1176.
- [103] Tanev, P. T.; Pinnavaia, T. J. *Science* **1995**, *267*, 865.
- [104] Bagshaw, S. A.; Prouzet, E.; Pinnavaia, T. J. *Science* **1995**, *269*, 1242.
- [105] Zhao, D. Y.; Feng, J. L.; Huo, Q. S.; Melosh, N.; Fredrickson, G. H.; Chmelka, B. F.; Stucky, G. D. *Science* **1998**, *279*, 548.
- [106] Zhao, D. Y.; Huo, Q. S.; Feng, J. L.; Chmelka, B. F.; Stucky, G. D. *Journal of the American Chemical Society* **1998**, *120*, 6024.
- [107] Yang, P. D.; Zhao, D. Y.; Chmelka, B. F.; Stucky, G. D. *Chemistry of Materials* **1998**, *10*, 2033.
- [108] Kipkemboi, P.; Fogden, A.; Alfredsson, V.; Flodstrom, K. *Langmuir* **2001**, *17*, 5398.
- [109] Tian, B. Z.; Liu, X. Y.; Zhang, Z. D.; Tu, B.; Zhao, D. Y. *Journal of Solid State Chemistry* **2002**, *167*, 324.
- [110] Kim, J. M.; Han, Y. J.; Chmelka, B. F.; Stucky, G. D. *Chemical Communications* **2000**, 2437.

- [111] Prouzet, E.; Pinnavaia, T. J. *Angewandte Chemie-International Edition* **1997**, *36*, 516.
- [112] Brinker, C. J.; Scherer, G. W. *Sol-gel science : the physics and chemistry of sol-gel processing*; Academic Press, 1990.
- [113] Zhang, W. Z.; Glomski, B.; Pauly, T. R.; Pinnavaia, T. J. *Chemical Communications* **1999**, 1803.
- [114] Bagshaw, S. A. *Journal of Materials Chemistry* **2001**, *11*, 831.
- [115] Bagshaw, S. A. *Chemical Communications* **1999**, 1785.
- [116] Ishizaki, K.; Komarneni, S.; Nanko, M. *Porous materials : process technology and applications*; Kluwer Academic Publishers, 1998.
- [117] Lukens, W. W.; Schmidt-Winkel, P.; Zhao, D. Y.; Feng, J. L.; Stucky, G. D. *Langmuir* **1999**, *15*, 5403.
- [118] Kruk, M.; Jaroniec, M.; Ko, C. H.; Ryoo, R. *Chemistry of Materials* **2000**, *12*, 1961.
- [119] Miyazawa, K.; Inagaki, S. *Chemical Communications* **2000**, 2121.
- [120] Imperor-Clerc, M.; Davidson, P.; Davidson, A. *Journal of the American Chemical Society* **2000**, *122*, 11925.
- [121] Galarneau, A.; Cambon, H.; Di Renzo, F.; Fajula, F. *Langmuir* **2001**, *17*, 8328.
- [122] Ravikovitch, P. I.; Neimark, A. V. *Journal of Physical Chemistry B* **2001**, *105*, 6817.
- [123] Ryoo, R.; Joo, S. H.; Jun, S. *Journal of Physical Chemistry B* **1999**, *103*, 7743.
- [124] Shin, H. J.; Ryoo, R.; Kruk, M.; Jaroniec, M. *Chemical Communications* **2001**, 349.
- [125] Jun, S.; Joo, S. H.; Ryoo, R.; Kruk, M.; Jaroniec, M.; Liu, Z.; Ohsuna, T.; Terasaki, O. *Journal of the American Chemical Society* **2000**, *122*, 10712.
- [126] Yang, H. F.; Zhao, D. Y. *Journal of Materials Chemistry* **2005**, *15*, 1217.
- [127] Kruk, M.; Jaroniec, M.; Ryoo, R.; Joo, S. H. *Journal of Physical Chemistry B* **2000**, *104*, 7960.
- [128] Ryoo, R.; Joo, S. H.; Kruk, M.; Jaroniec, M. *Advanced Materials* **2001**, *13*, 677.
- [129] Ryoo, R.; Ko, C. H.; Kruk, M.; Antochshuk, V.; Jaroniec, M. *Journal of Physical Chemistry B* **2000**, *104*, 11465.

- [130] Liu, Z.; Terasaki, O.; Ohsuna, T.; Hiraga, K.; Shin, H. J.; Ryoo, R. *ChemPhysChem* **2001**, *2*, 229.
- [131] Galarneau, A.; Cambon, N.; Di Renzo, F.; Ryoo, R.; Choi, M.; Fajula, F. *New Journal of Chemistry* **2003**, *27*, 73.
- [132] Israelachvili, J. N.; Wennerstrom, H. *Journal of Physical Chemistry* **1992**, *96*, 520.
- [133] Mortensen, K.; Pedersen, J. S. *Macromolecules* **1993**, *26*, 805.
- [134] Alexandridis, P.; Hatton, T. A. *Colloids and Surfaces a-Physicochemical and Engineering Aspects* **1995**, *96*, 1.
- [135] Maschmeyer, T.; Rey, F.; Sankar, G.; Thomas, J. M. *Nature* **1995**, *378*, 159.
- [136] Clark, J. H.; Macquarrie, D. J. *Chemical Communications* **1998**, 853.
- [137] Mehnert, C. P.; Weaver, D. W.; Ying, J. Y. *Journal of the American Chemical Society* **1998**, *120*, 12289.
- [138] Jones, C. W.; Tsuji, K.; Davis, M. E. *Nature* **1998**, *393*, 52.
- [139] Brunel, D. *Microporous and Mesoporous Materials* **1999**, *27*, 329.
- [140] Sorokin, A. B.; Tuel, A. *Catalysis Today* **2000**, *57*, 45.
- [141] On, D. T.; Desplantier-Giscard, D.; Danumah, C.; Kaliaguine, S. *Applied Catalysis a-General* **2001**, *222*, 299.
- [142] Bianchini, C.; Barbaro, P. *Topics in Catalysis* **2002**, *19*, 17.
- [143] Mbaraka, I. K.; Radu, D. R.; Lin, V. S. Y.; Shanks, B. H. *Journal of Catalysis* **2003**, *219*, 329.
- [144] Taguchi, A.; Schuth, F. *Microporous and Mesoporous Materials* **2005**, *77*, 1.
- [145] Huh, S.; Chen, H. T.; Wiench, J. W.; Pruski, M.; Lin, V. S. Y. *Angewandte Chemie-International Edition* **2005**, *44*, 1826.
- [146] Corma, A.; Garcia, H. *Advanced Synthesis & Catalysis* **2006**, *348*, 1391.
- [147] Zeidan, R. K.; Hwang, S. J.; Davis, M. E. *Angewandte Chemie-International Edition* **2006**, *45*, 6332.
- [148] Kureshy, R. I.; Ahmad, I.; Khan, N. H.; Abdi, S. H. R.; Pathak, K.; Jasra, R. V. *Journal of Catalysis* **2006**, *238*, 134.
- [149] Mihalcik, D. J.; Lin, W. B. *Angewandte Chemie-International Edition* **2008**, *47*, 6229.
- [150] Han, P.; Zhang, H. M.; Qiu, X. P.; Ji, X. L.; Gao, L. X. *Journal of Molecular Catalysis a-Chemical* **2008**, *295*, 57.

- [151] Liu, G. H.; Yao, M.; Zhang, F.; Gao, Y.; Li, H. X. *Chemical Communications* **2008**, 347.
- [152] Pathak, K.; Ahmad, I.; Abdi, S. H. R.; Kureshy, R. I.; Khan, N. U. H.; Jasra, R. V. *Journal of Molecular Catalysis a-Chemical* **2008**, 280, 106.
- [153] Margelefsky, E. L.; Bendjeriou, A.; Zeidan, R. K.; Dufaud, V.; Davis, M. E. *Journal of the American Chemical Society* **2008**, 130, 13442.
- [154] Maishal, T. K.; Alauzun, J.; Basset, J. M.; Coperet, C.; Corriu, R. J. P.; Jeanneau, E.; Mehdi, A.; Reye, C.; Veyre, L.; Thieuleux, C. *Angewandte Chemie-International Edition* **2008**, 47, 8654.
- [155] Hruby, S. L.; Shanks, B. H. *Journal of Catalysis* **2009**, 263, 181.
- [156] Dai, S.; Burleigh, M. C.; Shin, Y.; Morrow, C. C.; Barnes, C. E.; Xue, Z. L. *Angewandte Chemie-International Edition* **1999**, 38, 1235.
- [157] Ho, K. Y.; McKay, G.; Yeung, K. L. *Langmuir* **2003**, 19, 3019.
- [158] Walcarius, A.; Etienne, M.; Lebeau, B. *Chemistry of Materials* **2003**, 15, 2161.
- [159] Kang, T.; Park, Y.; Choi, K.; Lee, J. S.; Yi, J. *Journal of Materials Chemistry* **2004**, 14, 1043.
- [160] Yokoi, T.; Yoshitake, H.; Tatsumi, T. *Journal of Materials Chemistry* **2004**, 14, 951.
- [161] Kang, T.; Park, Y.; Yi, J. *Industrial & Engineering Chemistry Research* **2004**, 43, 1478.
- [162] Hiyoshi, N.; Yogo, K.; Yashima, T. *Microporous and Mesoporous Materials* **2005**, 84, 357.
- [163] Johnson, B. J.; Melde, B. J.; Charles, P. T.; Cardona, D. C.; Dinderman, M. A.; Malanoski, A. P.; Qadri, S. B. *Langmuir* **2008**, 24, 9024.
- [164] Zelenak, V.; Halamova, D.; Gaberova, L.; Bloch, E.; Llewellyn, P. *Microporous and Mesoporous Materials* **2008**, 116, 358.
- [165] Carter, T. G.; Yantasee, W.; Sangvanich, T.; Fryxell, G. E.; Johnson, D. W.; Addleman, R. S. *Chemical Communications* **2008**, 5583.
- [166] Feng, X.; Fryxell, G. E.; Wang, L. Q.; Kim, A. Y.; Liu, J.; Kemner, K. M. *Science* **1997**, 276, 923.
- [167] Liu, J.; Feng, X. D.; Fryxell, G. E.; Wang, L. Q.; Kim, A. Y.; Gong, M. L. *Advanced Materials* **1998**, 10, 161.
- [168] Mercier, L.; Pinnavaia, T. J. *Environmental Science & Technology* **1998**, 32, 2749.

- [169] Fryxell, G. E.; Liu, J.; Hauser, T. A.; Nie, Z. M.; Ferris, K. F.; Mattigod, S.; Gong, M. L.; Hallen, R. T. *Chemistry of Materials* **1999**, *11*, 2148.
- [170] Brown, J.; Mercier, L.; Pinnavaia, T. J. *Chemical Communications* **1999**, *69*.
- [171] Liu, A. M.; Hidajat, K.; Kawi, S.; Zhao, D. Y. *Chemical Communications* **2000**, *1145*.
- [172] Inumaru, K.; Kiyoto, J.; Yamanaka, S. *Chemical Communications* **2000**, *903*.
- [173] Hanzel, R.; Rajec, P. *Journal of Radioanalytical and Nuclear Chemistry* **2000**, *246*, 607.
- [174] Brown, J.; Richer, R.; Mercier, L. *Microporous and Mesoporous Materials* **2000**, *37*, 41.
- [175] Nooney, R. I.; Kalyanaraman, M.; Kennedy, G.; Maginn, E. J. *Langmuir* **2001**, *17*, 528.
- [176] Lee, B.; Kim, Y.; Lee, H.; Yi, J. *Microporous and Mesoporous Materials* **2001**, *50*, 77.
- [177] Yoshitake, H.; Yokoi, T.; Tatsumi, T. *Chemistry of Materials* **2002**, *14*, 4603.
- [178] Antochshuk, V.; Jaroniec, M. *Chemical Communications* **2002**, *258*.
- [179] Yoshitake, H.; Yokoi, T.; Tatsumi, T. *Chemistry of Materials* **2003**, *15*, 1713.
- [180] Billinge, S. J. L.; McKimmy, E. J.; Shatnawi, M.; Kim, H. J.; Petkov, V.; Wermeille, D.; Pinnavaia, T. J. *Journal of the American Chemical Society* **2005**, *127*, 8492.
- [181] Sayari, A.; Hamoudi, S.; Yang, Y. *Chemistry of Materials* **2005**, *17*, 212.
- [182] Yoshitake, H. *New Journal of Chemistry* **2005**, *29*, 1107.
- [183] Perez-Quintanilla, D.; del Hierro, I.; Fajardo, M.; Sierra, I. *Journal of Materials Chemistry* **2006**, *16*, 1757.
- [184] Sepehrian, H.; Ghannadi-Maragheh, M.; Waqif-Husain, S.; Yavari, R.; Khanchi, A. R. *Journal of Radioanalytical and Nuclear Chemistry* **2008**, *275*, 145.
- [185] Chang, C. Y.; Chau, L. K.; Hu, W. P.; Wang, C. Y.; Liao, J. H. *Microporous and Mesoporous Materials* **2008**, *109*, 505.
- [186] Buchmeiser, M. R.; Seeber, G.; Mupa, M.; Bonn, G. K. *Chemistry of Materials* **1999**, *11*, 1533.
- [187] Gallis, K. W.; Araujo, J. T.; Duff, K. J.; Moore, J. G.; Landry, C. C. *Advanced Materials* **1999**, *11*, 1452.

- [188] Zhao, J. W.; Gao, F.; Fu, Y. L.; Jin, W.; Yang, P. Y.; Zhao, D. Y. *Chemical Communications* **2002**, 752.
- [189] Salesch, T.; Bachmann, S.; Brugger, S.; Rabelo-Schaefer, R.; Albert, K.; Steinbrecher, S.; Plies, E.; Mehdi, A.; Reye, C.; Corriu, R. J. P.; Lindner, E. *Advanced Functional Materials* **2002**, 12, 134.
- [190] Ma, Y. R.; Qi, L. M.; Ma, J. M.; Wu, Y. Q.; Liu, O.; Cheng, H. M. *Colloids and Surfaces a-Physicochemical and Engineering Aspects* **2003**, 229, 1.
- [191] Martin, T.; Galarneau, A.; Di Renzo, F.; Brunel, D.; Fajula, F.; Heinisch, S.; Cretier, G.; Rocca, J.-L. *Chemistry of Materials* **2004**, 16, 1725.
- [192] Guan, L. X.; Li, J. P.; Cao, H.; Zhao, N.; Wang, X. Z.; Wei, W.; Sun, Y. H. *Chemistry Letters* **2006**, 35, 516.
- [193] C. M. Yang, A. T. C. F. M. P. T. G. T. K. J. C. *Advanced Materials* **2001**, 13, 1099.
- [194] Wirnsberger, G.; Yang, P. D.; Scott, B. J.; Chmelka, B. F.; Stucky, G. D. *Spectrochimica Acta Part a-Molecular and Biomolecular Spectroscopy* **2001**, 57, 2049.
- [195] Yu, S. Z.; Wong, T. K. S.; Pita, K.; Hu, X.; Ligatchev, V. *Journal of Applied Physics* **2002**, 92, 3338.
- [196] de Theije, F. K.; Balkenende, A. R.; Verheijen, M. A.; Baklanov, M. R.; Mogilnikov, K. P.; Furukawa, Y. *The Journal of Physical Chemistry B* **2003**, 107, 4280.
- [197] A.R. Balkenende, F. K. d. T. J. C. K. K. *Advanced Materials* **2003**, 15, 139.
- [198] Yu, K.; Wu, X.; Brinker, C. J.; Ripmeester, J. *Langmuir* **2003**, 19, 7282.
- [199] Tanaka, S.; Kaihara, J.; Nishiyama, N.; Oku, Y.; Egashira, Y.; Ueyama, K. *Langmuir* **2004**, 20, 3780.
- [200] Soler-Illia, G. J. A. A.; Innocenzi, P. *Chemistry-a European Journal* **2006**, 12, 4478.
- [201] Domansky, K.; Liu, J.; Wang, L. Q.; Engelhard, M. H.; Baskaran, S. *Journal of Materials Research* **2001**, 16, 2810.
- [202] Liu, N. G.; Chen, Z.; Dunphy, D. R.; Jiang, Y. B.; Assink, R. A.; Brinker, C. J. *Angewandte Chemie-International Edition* **2003**, 42, 1731.
- [203] Yantasee, W.; Lin, Y. H.; Li, X. H.; Fryxell, G. E.; Zemanian, T. S.; Viswanathan, V. V. *Analyst* **2003**, 128, 899.
- [204] Radu, D. R.; Lai, C.-Y.; Wiench, J. W.; Pruski, M.; Lin, V. S. Y. *Journal of the American Chemical Society* **2004**, 126, 1640.
- [205] Balaji, T.; Sasidharan, M.; Matsunaga, H. *Analyst* **2005**, 130, 1162.

- [206] Zhang, H. D.; Sun, Y. H.; Ye, K. Q.; Zhang, P.; Wang, Y. *Journal of Materials Chemistry* **2005**, *15*, 3181.
- [207] Metivier, R.; Leray, I.; Lebeau, B.; Valeur, B. *Journal of Materials Chemistry* **2005**, *15*, 2965.
- [208] Yantasee, W.; Fryxell, G. E.; Conner, M. M.; Lin, Y. H. *Journal of Nanoscience and Nanotechnology* **2005**, *5*, 1537.
- [209] El-Safty, S. A.; Ismail, A. A.; Matsunaga, H.; Mizukami, F. *Chemistry-a European Journal* **2007**, *13*, 9245.
- [210] Wada, A.; Tamaru, S.; Ikeda, M.; Hamachi, I. *Journal of the American Chemical Society* **2009**, *131*, 5321.
- [211] Mal, N. K.; Fujiwara, M.; Tanaka, Y. *Nature* **2003**, *421*, 350.
- [212] Mal, N. K.; Fujiwara, M.; Tanaka, Y.; Taguchi, T.; Matsukata, M. *Chemistry of Materials* **2003**, *15*, 3385.
- [213] Munoz, B.; Ramila, A.; Perez-Pariente, J.; Diaz, I.; Vallet-Regi, M. *Chemistry of Materials* **2003**, *15*, 500.
- [214] Lai, C.-Y.; Trewyn, B. G.; Jeftinija, D. M.; Jeftinija, K.; Xu, S.; Jeftinija, S.; Lin, V. S. Y. *Journal of the American Chemical Society* **2003**, *125*, 4451.
- [215] Ramila, A.; Munoz, B.; Perez-Pariente, J.; Vallet-Regi, M. *Journal of Sol-Gel Science and Technology* **2003**, *26*, 1199.
- [216] Radu, D. R.; Lai, C.-Y.; Jeftinija, K.; Rowe, E. W.; Jeftinija, S.; Lin, V. S. Y. *Journal of the American Chemical Society* **2004**, *126*, 13216.
- [217] Babonneau, F.; Yeung, L.; Steunou, N.; Gervais, C.; Ramila, A.; Vallet-Regi, M. *Journal of Sol-Gel Science and Technology* **2004**, *31*, 219.
- [218] Zhu, Y. F.; Shi, J. L.; Li, Y. S.; Chen, H. R.; Shen, W. H.; Dong, X. P. *Microporous and Mesoporous Materials* **2005**, *85*, 75.
- [219] Zeng, W.; Qian, X. F.; Zhang, Y. B.; Yin, J.; Zhu, Z. K. *Materials Research Bulletin* **2005**, *40*, 766.
- [220] Song, S. W.; Hidajat, K.; Kawi, S. *Langmuir* **2005**, *21*, 9568.
- [221] Balas, F.; Manzano, M.; Horcajada, P.; Vallet-Regi, M. *Journal of the American Chemical Society* **2006**, *128*, 8116.
- [222] Doadrio, J. C.; Sousa, E. M. B.; Izquierdo-Barba, I.; Doadrio, A. L.; Perez-Pariente, J.; Vallet-Regi, M. *Journal of Materials Chemistry* **2006**, *16*, 462.
- [223] Fengyu Qu, G. Z. S. H. S. L. S. Q. *ChemPhysChem* **2006**, *7*, 400.
- [224] Tang, Q.; Xu, Y.; Wu, D.; Sun, Y. *Journal of Solid State Chemistry* **2006**, *179*, 1513.

- [225] Tang, Q. L.; Xu, Y.; Wu, D.; Sun, Y. H. *Chemistry Letters* **2006**, *35*, 474.
- [226] Tang, Q. L.; Xu, Y.; Wu, D.; Sun, Y. H.; Wang, J.; Xu, J.; Deng, F. *Journal of Controlled Release* **2006**, *114*, 41.
- [227] Zeng, W.; Qian, X. F.; Yin, J.; Zhu, Z. K. *Materials Chemistry and Physics* **2006**, *97*, 437.
- [228] Vallet-Regi, M.; Balas, F.; Arcos, D. *Angewandte Chemie-International Edition* **2007**, *46*, 7548.
- [229] Hoang, V.-T.; Huang, Q.; Eic, M.; Do, T.-O.; Kaliaguine, S. *Langmuir* **2005**, *21*, 2051.
- [230] McGovern, M. E.; Kallury, K. M. R.; Thompson, M. *Langmuir* **1994**, *10*, 3607.
- [231] Brzoska, J. B.; Shahidzadeh, N.; Rondelez, F. *Nature* **1992**, *360*, 719.
- [232] Le Grange, J. D.; Markham, J. L.; Kurkjian, C. R. *Langmuir* **1993**, *9*, 1749.
- [233] Angst, D. L.; Simmons, G. W. *Langmuir* **1991**, *7*, 2236.
- [234] Blitz, J. P.; Murthy, R. S. S.; Leyden, D. E. *Journal of the American Chemical Society* **1987**, *109*, 7141.
- [235] Blitz, J. P.; Murthy, R. S. S.; Leyden, D. E. *Journal of Colloid and Interface Science* **1988**, *126*, 387.
- [236] Burkett, S. L.; Sims, S. D.; Mann, S. *Chemical Communications* **1996**, 1367.
- [237] Fowler, C. E.; Burkett, S. L.; Mann, S. *Chemical Communications* **1997**, 1769.
- [238] Huh, S.; Wiench, J. W.; Yoo, J. C.; Pruski, M.; Lin, V. S. Y. *Chemistry of Materials* **2003**, *15*, 4247.
- [239] Babonneau, F.; Leite, L.; Fontlupt, S. *Journal of Materials Chemistry* **1999**, *9*, 175.
- [240] Margolese, D.; Melero, J. A.; Christiansen, S. C.; Chmelka, B. F.; Stucky, G. D. *Chemistry of Materials* **2000**, *12*, 2448.
- [241] Melero, J. A.; Stucky, G. D.; van Grieken, R.; Morales, G. *Journal of Materials Chemistry* **2002**, *12*, 1664.
- [242] Macquarrie, D. J. *Chemical Communications* **1996**, 1961.
- [243] Richer, R.; Mercier, L. *Chemical Communications* **1998**, 1775.
- [244] Mercier, L.; Pinnavaia, T. J. *Chemistry of Materials* **2000**, *12*, 188.
- [245] Lim, M. H.; Stein, A. *Chemistry of Materials* **1999**, *11*, 3285.
- [246] A. Stein, B. J. M. R. C. S. *Advanced Materials* **2000**, *12*, 1403.

- [247] Radu, D. R.; Lai, C. Y.; Huang, J. G.; Shu, X.; Lin, V. S. Y. *Chemical Communications* **2005**, 1264.
- [248] Polarz, S.; Kuschel, A. *Chemistry-a European Journal* **2008**, 14, 9816.
- [249] Van der Voort, P.; Vercaemst, C.; Schaubroeck, D.; Verpoort, F. *Physical Chemistry Chemical Physics* **2008**, 10, 347.
- [250] Asefa, T.; MacLachlan, M. J.; Coombs, N.; Ozin, G. A. *Nature* **1999**, 402, 867.
- [251] Yoshina-Ishii, C.; Asefa, T.; Coombs, N.; MacLachlan, M. J.; Ozin, G. A. *Chemical Communications* **1999**, 2539.
- [252] Inagaki, S.; Guan, S.; Fukushima, Y.; Ohsuna, T.; Terasaki, O. *Journal of the American Chemical Society* **1999**, 121, 9611.
- [253] Asefa, T.; MacLachlan, M. J.; Grondy, H.; Coombs, N.; Ozin, G. A. *Angewandte Chemie-International Edition* **2000**, 39, 1808.
- [254] Temtsin, G.; Asefa, T.; Bittner, S.; Ozin, G. A. *Journal of Materials Chemistry* **2001**, 11, 3202.
- [255] Inagaki, S.; Guan, S.; Ohsuna, T.; Terasaki, O. *Nature* **2002**, 416, 304.
- [256] Kapoor, M. P.; Yang, Q. H.; Inagaki, S. *Journal of the American Chemical Society* **2002**, 124, 15176.
- [257] Kuroki, M.; Asefa, T.; Whitnal, W.; Kruk, M.; Yoshina-Ishii, C.; Jaroniec, M.; Ozin, G. A. *Journal of the American Chemical Society* **2002**, 124, 13886.
- [258] Hunks, W. J.; Ozin, G. A. *Chemistry of Materials* **2004**, 16, 5465.
- [259] Kapoor, M. P.; Yang, Q. H.; Inagaki, S. *Chemistry of Materials* **2004**, 16, 1209.
- [260] Hunks, W. J.; Ozin, G. A. *Chemical Communications* **2004**, 2426.
- [261] Sayari, A.; Wang, W. H. *Journal of the American Chemical Society* **2005**, 127, 12194.
- [262] Cornelius, M.; Hoffmann, F.; Froba, M. *Chemistry of Materials* **2005**, 17, 6674.
- [263] Hunks, W. J.; Ozin, G. A. *Advanced Functional Materials* **2005**, 15, 259.
- [264] Landskron, K.; Ozin, G. A. *Science* **2004**, 306, 1529.
- [265] Asefa, T.; Kruk, M.; Coombs, N.; Grondy, H.; MacLachlan, M. J.; Jaroniec, M.; Ozin, G. A. *Journal of the American Chemical Society* **2003**, 125, 11662.

- [266] Asefa, T.; MacLachlan, M. J.; Grondey, H.; Coombs, N.; Ozin, G. A. *Angewandte Chemie-International Edition* **2000**, *39*, 1808.
- [267] Zhang, W. H.; Daly, B.; O'Callaghan, J.; Zhang, L.; Shi, J. L.; Li, C.; Morris, M. A.; Holmes, J. D. *Chemistry of Materials* **2005**, *17*, 6407.
- [268] Guan, S.; Inagaki, S.; Ohsuna, T.; Terasaki, O. *Journal of the American Chemical Society* **2000**, *122*, 5660.
- [269] Sayari, A.; Hamoudi, S.; Yang, Y.; Moudrakovski, I. L.; Ripmeester, J. R. *Chemistry of Materials* **2000**, *12*, 3857.
- [270] Zhu, H. G.; Jones, D. J.; Zajac, J.; Roziere, J.; Dutartre, R. *Chemical Communications* **2001**, 2568.
- [271] Park, S. S.; Lee, C. H.; Cheon, J. H.; Park, D. H. *Journal of Materials Chemistry* **2001**, *11*, 3397.
- [272] Muth, O.; Schellbach, C.; Froba, M. *Chemical Communications* **2001**, 2032.
- [273] Lee, C. H.; Park, S. S.; Choe, S. J.; Park, D. H. *Microporous and Mesoporous Materials* **2001**, *46*, 257.
- [274] Sayari, A.; Yang, Y. *Chemical Communications* **2002**, 2582.
- [275] Hamoudi, S.; Kaliaguine, S. *Chemical Communications* **2002**, 2118.
- [276] Burleigh, M. C.; Markowitz, M. A.; Spector, M. S.; Gaber, B. P. *Journal of Physical Chemistry B* **2002**, *106*, 9712.
- [277] Matos, J. R.; Kruk, M.; Mercuri, L. P.; Jaroniec, M.; Asefa, T.; Coombs, N.; Ozin, G. A.; Kamiyama, T.; Terasaki, O. *Chemistry of Materials* **2002**, *14*, 1903.
- [278] Guo, W. P.; Kim, I.; Ha, C. S. *Chemical Communications* **2003**, 2692.
- [279] Guo, W. P.; Park, J. Y.; Oh, M. O.; Jeong, H. W.; Cho, W. J.; Kim, I.; Ha, C. S. *Chemistry of Materials* **2003**, *15*, 2295.
- [280] Park, S. S.; Ha, C. S. *Chemical Communications* **2004**, 1986.
- [281] Park, S. S.; Ha, C. S. *Chemistry of Materials* **2005**, *17*, 3519.
- [282] Cho, E. B.; Char, K. *Chemistry of Materials* **2004**, *16*, 270.
- [283] Bao, X. Y.; Zhao, X. S.; Qiao, S. Z.; Bhatia, S. K. *Journal of Physical Chemistry B* **2004**, *108*, 16441.
- [284] Bao, X. Y.; Zhao, X. S.; Li, X.; Li, J. *Applied Surface Science* **2004**, *237*, 380.
- [285] Bao, X. Y.; Zhao, X. S.; Li, X.; Chia, P. A.; Li, J. *Journal of Physical Chemistry B* **2004**, *108*, 4684.

- [286] Zhang, Z. D.; Yan, X. X.; Tian, B. Z.; Shen, S. D.; Chen, D. H.; Zhu, G. S.; Qiu, S. L.; Zhao, D. Y. *Chemistry Letters* **2005**, *34*, 182.
- [287] Zhang, L.; Yang, Q. H.; Zhang, W. H.; Li, Y.; Yang, J.; Jiang, D. M.; Zhu, G. R.; Li, C. *Journal of Materials Chemistry* **2005**, *15*, 2562.
- [288] Liang, Y. C.; Hanzlik, M.; Anwander, R. *Journal of Materials Chemistry* **2005**, *15*, 3919.
- [289] Liang, Y. C.; Hanzlik, M.; Anwander, R. *Chemical Communications* **2005**, 525.
- [290] Lee, H. I.; Pak, C.; Yi, S. H.; Shon, J. K.; Kim, S. S.; So, B. G.; Chang, H.; Yie, J. E.; Kwon, Y. U.; Kim, J. M. *Journal of Materials Chemistry* **2005**, *15*, 4711.
- [291] Bao, X. Y.; Zhao, X. S. *Journal of Physical Chemistry B* **2005**, *109*, 10727.
- [292] Zhao, L.; Zhu, G. S.; Zhang, D. L.; Di, Y.; Chen, Y.; Terasaki, O.; Qiu, S. L. *Journal of Physical Chemistry B* **2005**, *109*, 764.
- [293] Qiao, S. Z.; Yu, C. Z.; Hu, Q. H.; Jin, Y. G.; Zhou, X. F.; Zhao, X. S.; Lu, G. Q. *Microporous and Mesoporous Materials* **2006**, *91*, 59.
- [294] Liang, Y. C.; Hanzlik, M.; Anwander, R. *Journal of Materials Chemistry* **2006**, *16*, 1238.
- [295] Diaz-Morales, U.; Bellussi, G.; Carati, A.; Millini, R.; Parker, W. O.; Rizzo, C. *Microporous and Mesoporous Materials* **2006**, *87*, 185.
- [296] Shylesh, S.; Jha, R. K.; Singh, A. P. *Microporous and Mesoporous Materials* **2006**, *94*, 364.
- [297] Grudzien, R. M.; Grabicka, B. E.; Jaroniec, M. *Colloids and Surfaces a-Physicochemical and Engineering Aspects* **2007**, *300*, 235.
- [298] Asefa, T.; Kruk, M.; MacLachlan, M. J.; Coombs, N.; Grondey, H.; Jaroniec, M.; Ozin, G. A. *Journal of the American Chemical Society* **2001**, *123*, 8520.
- [299] Nakajima, K.; Lu, D. L.; Kondo, J. N.; Tomita, I.; Inagaki, S.; Hara, M.; Hayashi, S.; Domen, K. *Chemistry Letters* **2003**, *32*, 950.
- [300] Wang, W. H.; Xie, S. H.; Zhou, W. Z.; Sayari, A. *Chemistry of Materials* **2004**, *16*, 1756.
- [301] Nakajima, K.; Tomita, I.; Hara, M.; Hayashi, S.; Domen, K.; Kondo, J. N. *Journal of Materials Chemistry* **2005**, *15*, 2362.
- [302] Xia, Y. D.; Wang, W. X.; Mokaya, R. *Journal of the American Chemical Society* **2005**, *127*, 790.
- [303] Xia, Y. D.; Yang, Z. X.; Mokaya, R. *Chemistry of Materials* **2006**, *18*, 1141.

- [304] Xia, Y. D.; Mokaya, R. *Journal of Physical Chemistry B* **2006**, *110*, 3889.
- [305] Xia, Y. D.; Mokaya, R. *Journal of Materials Chemistry* **2006**, *16*, 395.
- [306] Nakajima, K.; Tomita, I.; Hara, M.; Hayashi, S.; Domen, K.; Kondo, J. N. *Catalysis Today* **2006**, *116*, 151.
- [307] Nakai, K.; Oumi, Y.; Horie, H.; Sano, T.; Yoshitake, H. *Microporous and Mesoporous Materials* **2007**, *100*, 328.
- [308] Bao, X. Y.; Li, X.; Zhao, X. S. *Journal of Physical Chemistry B* **2006**, *110*, 2656.
- [309] Landskron, K.; Hatton, B. D.; Perovic, D. D.; Ozin, G. A. *Science* **2003**, *302*, 266.
- [310] Bion, N.; Ferreira, P.; Valente, A.; Goncalves, I. S.; Rocha, J. *Journal of Materials Chemistry* **2003**, *13*, 1910.
- [311] Goto, Y.; Inagaki, S. *Microporous and Mesoporous Materials* **2006**, *89*, 103.
- [312] Goto, Y.; Inagaki, S. *Chemical Communications* **2002**, 2410.
- [313] Morell, J.; Wolter, G.; Froba, M. *Chemistry of Materials* **2005**, *17*, 804.
- [314] Morell, J.; Gungerich, M.; Wolter, G.; Jiao, J.; Hunger, M.; Klar, P. J.; Froba, M. *Journal of Materials Chemistry* **2006**, *16*, 2809.
- [315] Cho, E. B.; Kim, D.; Gorka, J.; Jaroniec, M. *Journal of Materials Chemistry* **2009**, *19*, 2076.
- [316] Baleizao, C.; Gigante, B.; Das, D.; Alvaro, M.; Garcia, H.; Corma, A. *Chemical Communications* **2003**, 1860.
- [317] Jiang, D. M.; Yang, Q. H.; Wang, H.; Zhu, G. R.; Yang, J.; Li, C. *Journal of Catalysis* **2006**, *239*, 65.
- [318] Alvaro, M.; Ferrer, B.; Garcia, H.; Rey, F. *Chemical Communications* **2002**, 2012.
- [319] Jones, J. T. A.; Wood, C. D.; Dickinson, C.; Khimyak, Y. Z. *Chemistry of Materials* **2008**, *20*, 3385.
- [320] Zhu, H. G.; Jones, D. J.; Zajac, J.; Dutartre, R.; Rhomari, M.; Roziere, J. *Chemistry of Materials* **2002**, *14*, 4886.
- [321] Burleigh, M. C.; Dai, S.; Hagaman, E. W.; Lin, J. S. *Chemistry of Materials* **2001**, *13*, 2537.
- [322] Burleigh, M. C.; Markowitz, M. A.; Spector, M. S.; Gaber, B. P. *Chemistry of Materials* **2001**, *13*, 4760.
- [323] Burleigh, M. C.; Markowitz, M. A.; Spector, M. S.; Gaber, B. P. *Langmuir* **2001**, *17*, 7923.

- [324] Burleigh, M. C.; Markowitz, M. A.; Spector, M. S.; Gaber, B. P. *Journal of Physical Chemistry B* **2001**, *105*, 9935.
- [325] Yang, Q. H.; Kapoor, M. P.; Inagaki, S. *Journal of the American Chemical Society* **2002**, *124*, 9694.
- [326] Hamoudi, S.; Kaliaguine, S. *Microporous and Mesoporous Materials* **2003**, *59*, 195.
- [327] Wahab, M. A.; Kim, I. I.; Ha, C. S. *Microporous and Mesoporous Materials* **2004**, *69*, 19.
- [328] Wahab, M. A.; Imae, I.; Kawakami, Y.; Ha, C. S. *Chemistry of Materials* **2005**, *17*, 2165.
- [329] Wahab, M. A.; Imae, I.; Kawakami, Y.; Ha, C. S. *Microporous and Mesoporous Materials* **2006**, *92*, 201.
- [330] Wei, Q.; Liu, L.; Nie, Z. R.; Chen, H. Q.; Wang, Y. L.; Li, Q. Y.; Zou, J. X. *Microporous and Mesoporous Materials* **2007**, *101*, 381.
- [331] Wang, Y. J.; Liu, X. H.; Zhao, R.; Wang, Y. Q.; Guo, Y. L.; Guo, Y.; Zhang, Z. G.; Wang, Y. S.; Lu, G. Z. *Microporous and Mesoporous Materials* **2007**, *102*, 325.
- [332] Zhang, L.; Liu, H.; Yang, H.; Yang, Q. H.; Li, C. *Microporous and Mesoporous Materials* **2008**, *109*, 172.
- [333] Corma, A.; Grande, M. S.; GonzalezAlfaro, V.; Orchilles, A. V. *Journal of Catalysis* **1996**, *159*, 375.
- [334] Cassiers, K.; Linssen, T.; Mathieu, M.; Benjelloun, M.; Schrijnemakers, K.; Van Der Voort, P.; Cool, P.; Vansant, E. F. *Chemistry of Materials* **2002**, *14*, 2317.
- [335] Corma, A. *Chemical Reviews* **1997**, *97*, 2373.
- [336] Zhang, F. Q.; Yan, Y.; Yang, H. F.; Meng, Y.; Yu, C. Z.; Tu, B.; Zhao, D. Y. *Journal of Physical Chemistry B* **2005**, *109*, 8723.
- [337] Guo, W. P.; Li, X.; Zhao, X. S. *Microporous and Mesoporous Materials* **2006**, *93*, 285.
- [338] Yang, Q. H.; Liu, J.; Yang, J.; Kapoor, M. P.; Inagaki, S.; Li, C. *Journal of Catalysis* **2004**, *228*, 265.
- [339] Rac, B.; Hegyes, P.; Forgo, P.; Molnar, A. *Applied Catalysis a-General* **2006**, *299*, 193.
- [340] Alauzun, J.; Mehdi, A.; Reye, C.; Corriu, R. J. P. *Journal of the American Chemical Society* **2006**, *128*, 8718.
- [341] Shylesh, S.; Singh, A. P. *Microporous and Mesoporous Materials* **2006**, *94*, 127.

- [342] Shylesh, S.; Srilakshmi, C.; Singh, A. P.; Anderson, B. G. *Microporous and Mesoporous Materials* **2007**, *99*, 334.
- [343] Melero, J. A.; Iglesias, J.; Arsuaga, J. M.; Sainz-Pardo, J.; de Frutos, P.; Blazquez, S. *Journal of Materials Chemistry* **2007**, *17*, 377.
- [344] Stober, W.; Fink, A.; Bohn, E. *Journal of Colloid and Interface Science* **1968**, *26*, 62.
- [345] Kapoor, M. P.; Inagaki, S. *Chemistry Letters* **2004**, *33*, 88.
- [346] Kim, D. J.; Chung, J. S.; Ahn, W. S.; Kam, G. W.; Cheong, W. J. *Chemistry Letters* **2004**, *33*, 422.
- [347] Rebbin, V.; Schmidt, R.; Froba, M. *Angewandte Chemie-International Edition* **2006**, *45*, 5210.
- [348] Zhu, G. R.; Yang, Q. H.; Jiang, D. M.; Yang, J.; Zhang, L.; Li, Y.; Li, C. *Journal of Chromatography A* **2006**, *1103*, 257.
- [349] Zhu, G. R.; Jiang, D. M.; Yang, Q. H.; Yang, J.; Li, C. *Journal of Chromatography A* **2007**, *1149*, 219.
- [350] Zhang, L. X.; Zhang, W. H.; Shi, J. L.; Hua, Z.; Li, Y. S.; Yan, J. *Chemical Communications* **2003**, *210*.
- [351] Olkhovyk, O.; Jaroniec, M. *Journal of the American Chemical Society* **2005**, *127*, 60.
- [352] Olkhovyk, O.; Pikus, S.; Jaroniec, M. *Journal of Materials Chemistry* **2005**, *15*, 1517.
- [353] Yang, Q. H.; Liu, H.; Yang, H.; Zhang, L.; Feng, Z. C.; Zhang, J.; Li, C. *Microporous and Mesoporous Materials* **2005**, *77*, 257.
- [354] Johnson-White, B.; Zeinali, M.; Shaffer, K. M.; Patterson, C. H.; Charles, P. T.; Markowitz, M. A. *Biosensors & Bioelectronics* **2007**, *22*, 1154.
- [355] Lu, Y. F.; Fan, H. Y.; Doke, N.; Loy, D. A.; Assink, R. A.; LaVan, D. A.; Brinker, C. J. *Journal of the American Chemical Society* **2000**, *122*, 5258.
- [356] Hatton, B. D.; Landskron, K.; Whitnall, W.; Perovic, D. D.; Ozin, G. A. *Advanced Functional Materials* **2005**, *15*, 823.
- [357] Hatton, B. D.; Landskron, K.; Hunks, W. J.; Bennett, M. R.; Shukaris, D.; Perovic, D. D.; Ozin, G. A. *Materials Today* **2006**, *9*, 22.
- [358] Eleuterio, H. S. *Polymerization of cyclic olefins*, U.S. Patent 3,074,918, 1963.
- [359] Eleuterio, H. S. *Journal of Molecular Catalysis* **1991**, *65*, 55.
- [360] Natta, G.; Dallasta, G.; Motroni, G. *Journal of Polymer Science Part B-Polymer Letters* **1964**, *2*, 349.

- [361] Natta, G.; Dallasta, G.; Bassi, I. W.; Carella, G. *Makromolekulare Chemie* **1966**, *91*, 87.
- [362] Calderon, N.; Chen, H. Y.; Scott, K. W. *Tetrahedron Letters* **1967**, 3327.
- [363] Calderon, N.; Ofstead, E. A.; Ward, J. P.; Judy, W. A.; Scott, K. W. *Journal of the American Chemical Society* **1968**, *90*, 4133.
- [364] Calderon, N. *Accounts of Chemical Research* **1972**, *5*, 127.
- [365] Mol, J. C.; Moulijn, J. A.; Boelhouw.C, *Chemical Communications* **1968**, 633.
- [366] Mol, J. C.; Moulijn, J. A.; Boelhouw.C, *Journal of Catalysis* **1968**, *11*, 87.
- [367] Lewandos, G. S.; Pettit, R. *Journal of the American Chemical Society* **1971**, *93*, 7087.
- [368] Lewandos, G. S.; Pettit, R. *Tetrahedron Letters* **1971**, 789.
- [369] Grubbs, R. H.; Brunck, T. K. *Journal of the American Chemical Society* **1972**, *94*, 2538.
- [370] Hughes, W. B. *Organometallics in Chemical Synthesis* **1972**, *1*, 341.
- [371] Mol, J. C.; Moulijn, J. A.; D.D. Eley, H. P.; Weisz, P. B. The Metathesis of Unsaturated Hydrocarbons Catalyzed by Transition Metal Compounds. In *Advances in Catalysis*; Academic Press, 1975; Vol. 24, p 131.
- [372] Grubbs, R. H.; Burk, P. L.; Carr, D. D. *Journal of the American Chemical Society* **1975**, *97*, 3265.
- [373] Katz, T. J.; Rothchild, R. *Journal of the American Chemical Society* **1976**, *98*, 2519.
- [374] Grubbs, R. H.; Carr, D. D.; Hoppin, C.; Burk, P. L. *Journal of the American Chemical Society* **1976**, *98*, 3478.
- [375] Herisson, J. L.; Chauvin, Y. *Makromolekulare Chemie* **1971**, *141*, 161.
- [376] <http://nobelprize.org/nobel-prizes/chemistry/laureates/2005/>.
- [377] Tsuji, J.; Hashiguchi, S. *Tetrahedron Letters* **1980**, *21*, 2955.
- [378] Schrock, R. R.; Murdzek, J. S.; Bazan, G. C.; Robbins, J.; Dimare, M.; Oregan, M. *Journal of the American Chemical Society* **1990**, *112*, 3875.
- [379] Grubbs, R. H. *Handbook of metathesis: Catalyst development*; Wiley-VCH, 2003; Vol. 1.
- [380] Brookhart, M.; Studabaker, W. B. *Chemical Reviews* **1987**, *87*, 411.
- [381] Doyle, M. P.; Pieters, R. J.; Martin, S. F.; Austin, R. E.; Oalmann, C. J.; Muller, P. *Journal of the American Chemical Society* **1991**, *113*, 1423.

- [382] Maxwell, J. L.; Omalley, S.; Brown, K. C.; Kodadek, T. *Organometallics* **1992**, *11*, 645.
- [383] Seitz, W. J.; Saha, A. K.; Hossain, M. M. *Organometallics* **1993**, *12*, 2604.
- [384] Wolf, J. R.; Hamaker, C. G.; Djukic, J. P.; Kodadek, T.; Woo, L. K. *Journal of the American Chemical Society* **1995**, *117*, 9194.
- [385] Doyle, M. P.; Austin, R. E.; Bailey, A. S.; Dwyer, M. P.; Dyatkin, A. B.; Kalinin, A. V.; Kwan, M. M. Y.; Liras, S.; Oalmann, C. J.; Pieters, R. J.; Protopopova, M. N.; Raab, C. E.; Roos, G. H. P.; Zhou, Q. L.; Martin, S. F. *Journal of the American Chemical Society* **1995**, *117*, 5763.
- [386] Fukuda, T.; Katsuki, T. *Tetrahedron* **1997**, *53*, 7201.
- [387] Niimi, T.; Uchida, T.; Irie, R.; Katsuki, T. *Advanced Synthesis & Catalysis* **2001**, *343*, 79.
- [388] Chen, Y.; Fields, K. B.; Zhang, X. P. *Journal of the American Chemical Society* **2004**, *126*, 14718.
- [389] Brumaghim, J. L.; Girolami, G. S. *Organometallics* **1999**, *18*, 1923.
- [390] Castarlenas, R.; Esteruelas, M. A.; Onate, E. *Organometallics* **2005**, *24*, 4343.
- [391] Meng, X.; Tang, G. R.; Jin, G. X. *Chemical Communications* **2008**, 3178.
- [392] Nguyen, S. T.; Johnson, L. K.; Grubbs, R. H.; Ziller, J. W. *Journal of the American Chemical Society* **1992**, *114*, 3974.
- [393] Nguyen, S. T.; Grubbs, R. H.; Ziller, J. W. *Journal of the American Chemical Society* **1993**, *115*, 9858.
- [394] Fu, G. C.; Nguyen, S. T.; Grubbs, R. H. *Journal of the American Chemical Society* **1993**, *115*, 9856.
- [395] Schwab, P.; France, M. B.; Ziller, J. W.; Grubbs, R. H. *Angewandte Chemie-International Edition in English* **1995**, *34*, 2039.
- [396] Schwab, P.; Grubbs, R. H.; Ziller, J. W. *Journal of the American Chemical Society* **1996**, *118*, 100.
- [397] Wu, Z.; Nguyen, S. T.; Grubbs, R. H.; Ziller, J. W. *Journal of the American Chemical Society* **1995**, *117*, 5503.
- [398] Dias, E. L.; Nguyen, S. T.; Grubbs, R. H. *Journal of the American Chemical Society* **1997**, *119*, 3887.
- [399] Maughon, B. R.; Grubbs, R. H. *Macromolecules* **1997**, *30*, 3459.
- [400] Tallarico, J. A.; Bonitatebus, P. J.; Snapper, M. L. *Journal of the American Chemical Society* **1997**, *119*, 7157.

- [401] Cucullu, M. E.; Li, C. B.; Nolan, S. P.; Nguyen, S. T.; Grubbs, R. H. *Organometallics* **1998**, *17*, 5565.
- [402] Ulman, M.; Grubbs, R. H. *Organometallics* **1998**, *17*, 2484.
- [403] Aagaard, O. M.; Meier, R. J.; Buda, F. *Journal of the American Chemical Society* **1998**, *120*, 7174.
- [404] Ulman, M.; Grubbs, R. H. *Journal of Organic Chemistry* **1999**, *64*, 7202.
- [405] Adlhart, C.; Hinderling, C.; Baumann, H.; Chen, P. *Journal of the American Chemical Society* **2000**, *122*, 8204.
- [406] Scholl, M.; Ding, S.; Lee, C. W.; Grubbs, R. H. *Organic Letters* **1999**, *1*, 953.
- [407] Scholl, M.; Trnka, T. M.; Morgan, J. P.; Grubbs, R. H. *Tetrahedron Letters* **1999**, *40*, 2247.
- [408] Bielawski, C. W.; Grubbs, R. H. *Angewandte Chemie-International Edition* **2000**, *39*, 2903.
- [409] Weskamp, T.; Schattenmann, W. C.; Spiegler, M.; Herrmann, W. A. *Angewandte Chemie-International Edition* **1998**, *37*, 2490.
- [410] Weskamp, T.; Kohl, F. J.; Herrmann, W. A. *Journal of Organometallic Chemistry* **1999**, *582*, 362.
- [411] Weskamp, T.; Kohl, F. J.; Hieringer, W.; Gleich, D.; Herrmann, W. A. *Angewandte Chemie-International Edition* **1999**, *38*, 2416.
- [412] Ackermann, L.; Furstner, A.; Weskamp, T.; Kohl, F. J.; Herrmann, W. A. *Tetrahedron Letters* **1999**, *40*, 4787.
- [413] Huang, J. K.; Stevens, E. D.; Nolan, S. P.; Petersen, J. L. *Journal of the American Chemical Society* **1999**, *121*, 2674.
- [414] Herrmann, W. A.; Kocher, C. *Angewandte Chemie-International Edition in English* **1997**, *36*, 2163.
- [415] Sanford, M. S.; Ulman, M.; Grubbs, R. H. *Journal of the American Chemical Society* **2001**, *123*, 749.
- [416] Sanford, M. S.; Love, J. A.; Grubbs, R. H. *Journal of the American Chemical Society* **2001**, *123*, 6543.
- [417] Adlhart, C.; Chen, P. *Journal of the American Chemical Society* **2004**, *126*, 3496.
- [418] Adhart, C.; Chen, P. *Angewandte Chemie-International Edition* **2002**, *41*, 4484.
- [419] Cavallo, L. *Journal of the American Chemical Society* **2002**, *124*, 8965.

- [420] Straub, B. F. *Angewandte Chemie-International Edition* **2005**, *44*, 5974.
- [421] Occhipinti, G.; Bjorsvik, H. R.; Jensen, V. R. *Journal of the American Chemical Society* **2006**, *128*, 6952.
- [422] Lord, R. L.; Wang, H. J.; Vieweger, M.; Baik, M. H. *Journal of Organometallic Chemistry* **2006**, *691*, 5505.
- [423] Ledoux, N.; Allaert, B.; Pattyn, S.; Vander Mierde, H.; Vercaemst, C.; Verpoort, F. *Chemistry-a European Journal* **2006**, *12*, 4654.
- [424] Sanford, M. S.; Love, J. A.; Grubbs, R. H. *Organometallics* **2001**, *20*, 5314.
- [425] Love, J. A.; Morgan, J. P.; Trnka, T. M.; Grubbs, R. H. *Angewandte Chemie-International Edition* **2002**, *41*, 4035.
- [426] Choi, T. L.; Grubbs, R. H. *Angewandte Chemie-International Edition* **2003**, *42*, 1743.
- [427] Harrity, J. P. A.; Visser, M. S.; Gleason, J. D.; Hoveyda, A. H. *Journal of the American Chemical Society* **1997**, *119*, 1488.
- [428] Harrity, J. P. A.; La, D. S.; Cefalo, D. R.; Visser, M. S.; Hoveyda, A. H. *Journal of the American Chemical Society* **1998**, *120*, 2343.
- [429] Kingsbury, J. S.; Harrity, J. P. A.; Bonitatebus, P. J.; Hoveyda, A. H. *Journal of the American Chemical Society* **1999**, *121*, 791.
- [430] Kingsbury, J. S.; Hoveyda, A. H. *Journal of the American Chemical Society* **2005**, *127*, 4510.
- [431] Van Berlo, B.; Houthoofd, K.; Sels, B. F.; Jacobs, P. A. *Advanced Synthesis & Catalysis* **2008**, *350*, 1949.
- [432] Wakamatsu, H.; Blechert, S. *Angewandte Chemie-International Edition* **2002**, *41*, 794.
- [433] Wakamatsu, H.; Blechert, S. *Angewandte Chemie-International Edition* **2002**, *41*, 2403.
- [434] Grela, K.; Harutyunyan, S.; Michrowska, A. *Angewandte Chemie-International Edition* **2002**, *41*, 4038.
- [435] Bieniek, M.; Michrowska, A.; Gulajski, L.; Grela, K. *Organometallics* **2007**, *26*, 1096.
- [436] Marciniec, B.; Maciejewski, H.; Gulinski, J.; Rzejak, L. *Journal of Organometallic Chemistry* **1989**, *362*, 273.
- [437] Fridman, R. A.; Nosakova, S. M.; Liberov, L. G.; Bashkirov, A. N. *Bulletin of the Academy of Sciences of the Ussr Division of Chemical Science* **1977**, *26*, 614.

- [438] Berglund, M.; Andersson, C.; Larsson, R. *Journal of Organometallic Chemistry* **1985**, *292*, C15.
- [439] Sworen, J. C.; Pawlow, J. H.; Case, W.; Lever, J.; Wagener, K. B. *Journal of Molecular Catalysis a-Chemical* **2003**, *194*, 69.
- [440] Lehman, S. E.; Schwendeman, J. E.; O'Donnell, P. M.; Wagener, K. B. *Inorganica Chimica Acta* **2003**, *345*, 190.
- [441] Courchay, F. C.; Sworen, J. C.; Ghiviriga, I.; Abboud, K. A.; Wagener, K. B. *Organometallics* **2006**, *25*, 6074.
- [442] Schmidt, B. *Journal of Molecular Catalysis a-Chemical* **2006**, *254*, 53.
- [443] Hong, S. H.; Sanders, D. P.; Lee, C. W.; Grubbs, R. H. *Journal of the American Chemical Society* **2005**, *127*, 17160.
- [444] Schmidt, B. *Journal of Organic Chemistry* **2004**, *69*, 7672.
- [445] Bourgeois, D.; Pancrazi, A.; Nolan, S. P.; Prunet, J. *Journal of Organometallic Chemistry* **2002**, *643*, 247.
- [446] Monsaert, S.; Drozdzak, R.; Verpoort, F. *Chimica Oggi-Chemistry Today* **2008**, *26*, 93.
- [447] Ledoux, N.; Allaert, B.; Schaubroeck, D.; Monsaert, S.; Drozdzak, R.; Van Der Voort, P.; Verpoort, F. *Journal of Organometallic Chemistry* **2006**, *691*, 5482.
- [448] Ledoux, N.; Drozdzak, R.; Allaert, B.; Linden, A.; Van Der Voort, P.; Verpoort, F. *Dalton Transactions* **2007**, 5201.
- [449] Ledoux, N.; Linden, A.; Allaert, B.; Mierde, H. V.; Verpoort, F. *Advanced Synthesis & Catalysis* **2007**, *349*, 1692.
- [450] Ledoux, N.; Allaert, B.; Verpoort, F. *European Journal of Inorganic Chemistry* **2007**, 5578.
- [451] Ledoux, N.; Allaert, B.; Linden, A.; Van der Voort, P.; Verpoort, F. *Organometallics* **2007**, *26*, 1052.
- [452] Allaert, B.; Dieltiens, N.; Ledoux, N.; Vercaemst, C.; Van der Voort, P.; Stevens, C. V.; Linden, A.; Verpoort, F. *Journal of Molecular Catalysis a-Chemical* **2006**, *260*, 221.
- [453] Vercaemst, C.; Ide, M.; Allaert, B.; Ledoux, N.; Verpoort, F.; Van der Voort, P. *Chemical Communications* **2007**, 2261.
- [454] Vercaemst, C.; Ide, M.; Wiper, P. V.; Jones, J. T. A.; Khimyak, Y. Z.; Verpoort, F.; Van der Voort, P. *Chemistry of Materials* **2009**, accepted.
- [455] Jones, M. D.; Duer, M. J.; Hermans, S.; Khimyak, Y. Z.; Johnson, B. F. G.; Thomas, J. M. *Angewandte Chemie-International Edition* **2002**, *41*, 4726.

- [456] Treuherz, B. A.; Khimyak, Y. Z. *Microporous and Mesoporous Materials* **2007**, *106*, 236.
- [457] Ravikovitch, P. I.; Neimark, A. V. *Langmuir* **2002**, *18*, 9830.
- [458] Van Der Voort, P.; Ravikovitch, P. I.; De Jong, K. P.; Benjelloun, M.; Van Bavel, E.; Janssen, A. H.; Neimark, A. V.; Weckhuysen, B. M.; Vansant, E. F. *Journal of Physical Chemistry B* **2002**, *106*, 5873.
- [459] Neimark, A. V.; Ravikovitch, P. I. *Microporous and Mesoporous Materials* **2001**, *44*, 697.
- [460] Ravikovitch, P. I.; Neimark, A. V. *Langmuir* **2006**, *22*, 11171.
- [461] Pedersen, J. S. *Advances in Colloid and Interface Science* **1997**, *70*, 171.
- [462] Hudson, S.; Tanner, D. A.; Redington, W.; Magner, E.; Hodnett, K.; Nakahara, S. *Physical Chemistry Chemical Physics* **2006**, *8*, 3467.
- [463] Li, Z.; Chen, D. H.; Tu, B.; Zhao, D. Y. *Microporous and Mesoporous Materials* **2007**, *105*, 34.
- [464] Ruthstein, S.; Schmidt, J.; Kesselman, E.; Talmon, Y.; Goldfarb, D. *Journal of the American Chemical Society* **2006**, *128*, 3366.
- [465] Vercaemst, C.; Friedrich, H.; de Jongh, P. E.; Neimark, A. V.; Goderis, B.; Verpoort, F.; Van Der Voort, P. *Journal of Physical Chemistry C* **2009**, *113*, 5556.
- [466] Grun, M.; Lauer, I.; Unger, K. K. *Advanced Materials* **1997**, *9*, 254.
- [467] Vercaemst, C.; Ide, M.; Friedrich, H.; de Jong, K. P.; Verpoort, F.; Van der Voort, P. *Journal of Materials Chemistry* **2009**, DOI: 10.1039/b913961c.
- [468] Vercaemst, C.; Jones, J. T. A.; Khimyak, Y. Z.; Martins, J. C.; Verpoort, F.; Van der Voort, P. *Physical Chemistry Chemical Physics* **2008**, *10*, 5349.
- [469] Jaladi, H.; Katiyar, A.; Thiel, S. W.; Gulants, V. V.; Pinto, N. G. *Chemical Engineering Science* **2009**, *64*, 1474.
- [470] Hartono, S. B.; Qiao, S. Z.; Jack, K.; Ladewig, B. P.; Hao, Z. P.; Lu, G. Q. *Langmuir* **2009**, *25*, 6413.
- [471] Zhou, Z. Y.; Zhu, S. M.; Zhang, D. *Journal of Materials Chemistry* **2007**, *17*, 2428.
- [472] Lettow, J. S.; Han, Y. J.; Schmidt-Winkel, P.; Yang, P. D.; Zhao, D. Y.; Stucky, G. D.; Ying, J. Y. *Langmuir* **2000**, *16*, 8291.
- [473] Schmidt-Winkel, P.; Lukens, W. W.; Zhao, D. Y.; Yang, P. D.; Chmelka, B. F.; Stucky, G. D. *Journal of the American Chemical Society* **1999**, *121*, 254.

- [474] Sun, J. M.; Zhang, H.; Ma, D.; Chen, Y. Y.; Bao, X. H.; Klein-Hoffmann, A.; Pfander, N.; Su, D. S. *Chemical Communications* **2005**, 5343.
- [475] Lettow, J. S.; Han, Y. J.; Schmidt-Winkel, P.; Yang, P. D.; Zhao, D. Y.; Stucky, G. D.; Ying, J. Y. *Langmuir* **2000**, *16*, 8291.
- [476] Burleigh, M. C.; Markowitz, M. A.; Wong, E. M.; Lin, J.-S.; Gaber, B. P. *Chemistry of Materials* **2001**, *13*, 4411.
- [477] Zhou, X. F.; Qiao, S. Z.; Hao, N.; Wang, X. L.; Yu, C. Z.; Wang, L. Z.; Zhao, D. Y.; Lu, G. Q. *Chemistry of Materials* **2007**, *19*, 1870.
- [478] Vercaemst, C.; de Jongh, P. E.; Meeldijk, J. D.; Goderis, B.; Verpoort, F.; Van Der Voort, P. *Chemical Communications* **2009**, 4052.
- [479] Alami, E.; Beinert, G.; Marie, P.; Zana, R. *Langmuir* **1993**, *9*, 1465.
- [480] Hamoudi, S.; Royer, S.; Kaliaguine, S. *Microporous and Mesoporous Materials* **2004**, *71*, 17.
- [481] Yang, Q. H.; Kapoor, M. P.; Shirokura, N.; Ohashi, M.; Inagaki, S.; Kondo, J. N.; Domen, K. *Journal of Materials Chemistry* **2005**, *15*, 666.
- [482] Li, C. M.; Yang, H.; Shi, X.; Liu, R.; Yang, Q. H. *Microporous and Mesoporous Materials* **2007**, *98*, 220.
- [483] Bennett, M. A.; Huang, T. N.; Matheson, T. W.; Smith, A. K. *Inorganic Syntheses* **1982**, *21*, 74.
- [484] Neimark, A. V.; Ravikovitch, P. I.; Grun, M.; Schuth, F.; Unger, K. K. *Journal of Colloid and Interface Science* **1998**, *207*, 159.
- [485] Kremer, J. R.; Mastronarde, D. N.; McIntosh, J. R. *Journal of Structural Biology* **1996**, *116*, 71.
- [486] Frangakis, A. S.; Hegerl, R. *Journal of Structural Biology* **2001**, *135*, 239.
- [487] Bras, W.; Dolbnya, I. P.; Detollenaere, D.; van Tol, R.; Malfois, M.; Greaves, G. N.; Ryan, A. J.; Heeley, E. *Journal of Applied Crystallography* **2003**, *36*, 791.
- [488] Huang, T. C.; Toraya, H.; Blanton, T. N.; Wu, Y. *Journal of Applied Crystallography* **1993**, *26*, 180.
- [489] Clauss, J.; Schmidrohr, K.; Adam, A.; Boeffel, C.; Spiess, H. W. *Macromolecules* **1992**, *25*, 5208.

Scientific Publications

Prior to Ph.D. research

“Simple multivariate approach for the monitoring of vinylation reactions using FT-Raman spectroscopy”

D. A. A. Hutsebaut, C. Vercaemst, C. Hugelier and F. Verpoort, Applied Spectroscopy 2002, 56, 1314-1319. [IF: 2.062]

“Active Ru catalysts in carbene chemistry: A kinetic study of carbene formation and an evaluation of selective cyclopropanation” J. Van Craenenbroeck, K. Van Isterdael, C. Vercaemst and F. Verpoort, New Journal of Chemistry 2005, 29, 942-947. [IF: 2.942]

During Ph.D. research

“Synthesis and activity for ROMP of bidentate Schiff base substituted second generation Grubbs catalysts”

B. Allaert, N. Dieltiens, N. Ledoux, C. Vercaemst, P. Van der Voort, C. V. Stevens, A. Linden and F. Verpoort, Journal of Molecular Catalysis a-Chemical 2006, 260, 221-226. [IF: 2.814]

“N,N'-dialkyl- and N-alkyl-N-mesityl-substituted N-heterocyclic carbenes as ligands in Grubbs catalysts”

N. Ledoux, B. Allaert, S. Pattyn, H. Vander Mierde, C. Vercaemst and F. Verpoort, Chemistry-a European Journal 2006, 12, 4654-4661. [IF: 5.454]

“Qualitative FT-Raman investigation of the ring opening metathesis polymerization of dicyclopentadiene”

D. Schaubroeck, S. Brughmans, C. Vercaemst, J. Schaubroeck and F. Verpoort, Journal of Molecular Catalysis a-Chemical 2006, 254, 180-185. [IF: 2.814]

“Ultra-fast hydrothermal synthesis of diastereoselective pure ethenylene-bridged periodic mesoporous organosilicas”

C. Vercaemst, M. Ide, B. Allaert, N. Ledoux, F. Verpoort and P. Van der Voort, Chemical Communications 2007, 2261-2263. [IF: 5.34]

“Ordered mesoporous materials at the beginning of the third millennium: new strategies to create hybrid and non-siliceous variants”

P. Van der Voort, C. Vercaemst, D. Schaubroeck and F. Verpoort, Physical Chemistry Chemical Physics 2008, 10, 347-360. [IF: 4.064]

“Spectroscopic evidence of thermally induced metamorphosis in ethenylene-bridged periodic mesoporous organosilicas”

C. Vercaemst, J. T. A. Jones, Y. Z. Khimyak, J. C. Martins, F. Verpoort and P. Van Der Voort, Physical Chemistry Chemical Physics 2008, 10, 5349-5352. [IF: 4.064]

“Periodic Mesoporous Organosilicas Consisting of 3D Hexagonally Ordered Inter-connected Globular Pores”

C. Vercaemst, H. Friedrich, P. E. de Jongh, A. V. Neimark, B. Goderis, F. Verpoort and P. Van Der Voort, Journal of Physical Chemistry C 2009, 113, 5556-5562. [IF: 3.396]

“Ethenylene-bridged periodic mesoporous organosilicas with ultra-large mesopores”

C. Vercaemst, B. Goderis, P. E. de Jongh, J. D. Meeldijk, F. Verpoort and P. Van Der Voort, Chemical Communications 2009, 4052-4054. [IF: 5.34]

“Ethenylene-bridged periodic mesoporous organosilicas: from E to Z”

C. Vercaemst, M. Ide, P. V. Wiper, J. T. A. Jones, Y. Z. Khimyak, F. Verpoort and P. Van Der Voort, Chemistry of Materials 2009, accepted. [IF: 5.046]

“Isomeric periodic mesoporous organosilicas with controllable properties”

C. Vercaemst, M. Ide, H. Friedrich, K. P. de Jong, F. Verpoort and P. Van Der Voort, Journal of Materials Chemistry 2009, accepted. [IF: 4.646]